Improved Modeling for Fluid Flow through Porous Media

by

© Tareq Uz Zaman

A thesis submitted to the School of Graduate Studies
in partial fulfillment of the requirements for the degree of

Master of Engineering (Oil and Gas Engineering)

Department of Process Engineering (Oil and Gas Program)
Faculty of Engineering and Applied Sciences
Memorial University of Newfoundland

May 2018

St. John's, Newfoundland and Labrador, Canada

this work is dedicated to my loving and
supporting parents, wife, and two daughters

Abstract

Petroleum production is one of the most important technological challenges in the current world. Modeling and simulation of porous media flow is crucial to overcome this challenge. Recent years have seen interest in investigation of the effects of history of rock, fluid, and flow properties on flow through porous media. This study concentrates on the development of numerical models using a 'memory' based diffusivity equation to investigate the effects of history on porous media flow. In addition, this study focusses on developing a generalized model for fluid flow in packed beds and porous media.

The first part of the thesis solves a memory-based fractional diffusion equation numerically using the Caputo, Riemann-Liouville (RL), and Grünwald-Letnikov (GL) definitions for fractional-order derivatives on uniform meshes in both space and time. To validate the numerical models, the equation is solved analytically using the Caputo, and Riemann-Liouville definitions, for Dirichlet boundary conditions and a given initial condition. Numerical and analytical solutions are compared, and it is found that the discretization method used in the numerical model is consistent, but less than first order accurate in time. The effect of the fractional order on the resulting error is significant. Numerical solutions found using the Caputo, Riemann-Liouville, and Grünwald-Letnikov definitions are compared in the second part. It is found that the largest pressure values are found from Caputo definition and the lowest from Riemann-Liouville definition. It is also found that differences among the solutions increase with increasing fractional order, α.

In the third part of the thesis, the memory-based fractional diffusion equation is solved using graded meshes in time and uniform meshes in space. The computational procedure of the simulator is sequential and iterative over each time step. The Riemann-Liouville definition for the fractional-order derivative has been used, and the L1 algorithm for discretization on a non-uniform mesh is derived. A second-order finite difference method is used to solve the fractional diffusion equation. The solution scheme is analogous to Implicit Pressure and Explicit Saturation Method (IMPES). Numerical solutions are compared to analytical solutions for different values of the fractional order in the linear case and compared to manufactured solutions in non-linear cases. Comparisons are

made for different initial, boundary, and flow conditions. The error results affirm that the discretization method used in the numerical model is consistent, second-order accurate in space, and first-order accurate in time.

The fourth part of the thesis compares the numerical models developed using uniform and graded meshes. It is found that the non-uniform mesh grading in time used in this study provides more accurate numerical solutions compared to uniform mesh grading. In this part, the value of the fractional order in the mathematical model used in this paper is computed to fit different experimental data for one-dimensional flow measurements through a porous layer with constant pressure gradient. These data were collected from the literature. The value of the fractional order and the relaxation time are found to be 0.05 and 730 seconds, respectively. From the error analysis, the optimum number of time steps in unit time for this value of fractional order and for different number of grids in unit length is determined. The optimum number of steps in unit time is required to minimize the discretization and truncation error. The model can be used to investigate the effect of memory on fluid flow through porous media.

Different models developed for different purposes incorporating memory are found in the literature. In the fifth part of this theses, a general mathematical model has been proposed that can be simplified to derive all these models. The model considers both time and space memory. The model is generalized in the sense that all other established memory-based models can be derived from this model. The model can be used to develop a small-scale single-phase memory-based reservoir simulator.

In the last part of the thesis, a generalized semi-empirical equation is proposed that portrays the flow of fluid in packed beds and porous media. The new model calculates total pressure loss from viscous energy loss, local loss, and loss due to turbulence following the way of compact model development from asymptotic solutions. Non-spherical particle diameter is redefined to more accurately represent the wall surface area within the pore space. The model gives a new expression for a modified Reynolds number for fluid flow through porous media. The most significant new finding is that it portrays all the flow regimes that occur in porous media. The viscous term is dominant at very low flow rates, and turbulence and inertial loss occur at very high flow rates

while the viscous and inertial loss occur in-between, which is the central flow regime for porous media. This new equation can also be used for modeling the physical properties of random porous media. The model provides an innovative way to calculate tortuosity of porous media, diameter of equivalent volume spheres, and the head-loss coefficient.

Acknowledgement

First, I want to express my gratitude to Dr. M. Enamul Hossain for giving me the great opportunity of working in his research group. This opportunity has opened a new door in my life. I am grateful to him for his invaluable guidance and support during this work. My sincere appreciation goes to him for the patience and encouragement he showed to me from time to time. He taught me a lot about how to write a good review article, a good scientific article, and a good thesis. For last two years, he always taught me the true attitude to research and how to work efficiently. Above all, I always found him beside in any problem I faced during this critical period in Canada.

I must next recognize my co-supervisor Dr. Scott MacLachlan for guiding me in this journey. I consider myself fortunate for having the opportunity to work under his co-supervision. I am thankful to him for his deep insight and many insightful conversations. I learned a lot from him. He is a great teacher and mentor. He devoted many hours to teaching and discussing the insights of my research. Without his input and guidance, this work would have not been accomplished.

I would like to thank my co-supervisor Dr. Syed Imtiaz for being my mentor in this course of study. I would knock on his door without any appointment. He was very kind always. He would patiently listen to my research work that I would discuss with him. I am grateful to him for his review of the thesis paper, and his constructive remarks and guidance in improving the quality of the research.

Financial support from Natural Sciences and Engineering Research Council of Canada (NSERC), Research & Development Corporation of Newfoundland and Labrador (RDC), and Statoil Canada Ltd. is gratefully acknowledged.

I am grateful to my parents who brought me in this beautiful world and incessantly pray for me. They always want to see me as a good academician. I am currently in this position for their continuous inspiration for study and research. I am also grateful to my younger brother for his continuous support to our family in my absence.

I am most grateful to my best friend- my wife who was very patient to pass this hard time while I was not beside her. She took the responsibility of the most difficult job – taking care and raising our twin lovely girls who were premature during their birth. Moreover, she understood me, and always supported me psychologically during my tough time of living alone. Without her sacrifice, it was impossible for me to start and finish this M. Eng. program.

Last but mostly, I would like to acknowledge my dearest twin girls, Rameen and Raida, who were deprived of their father's caress and endearment during this period. Often, Raida asks her mother why I don't go home where her neighbour friend's father comes home at every evening. Sometimes, she asks me to show her my hand, finger, and leg in video chat. Probably she wants to make sure that her father is not only a picture, he has real existence. She has many plans to do when her father will return. Rameen, who can not express herself like Raida, converses with her father in her own words. Possibly she also has some questions and plans like Raida. Her staring at me in video chat tells me that she is also waiting for the days when she can continuously stay with me, likewise she was always with me before my coming to Canada. It would not be fair if I don't acknowledge them.

Table of Contents

List of Tables

List of Figures

List of Symbols

a	Proportionality constant between $\lim_{u\to 0}\frac{\Delta p}{L}$ and u
a_b	Surface area per unit bulk volume, cm^{-1}
a_v	Surface area per unit grain volume, cm^{-1}
A	Cross-sectional area of the sand layer, cm^2
$A(n)$	Weight of the fractional derivative of order n
A_p	Surface area of a single particle, cm^2
A_{sp}	Surface area of the equivalent-volume sphere, cm^2
b	Proportionality constant between $\lim_{u\to\infty}\frac{\Delta p}{L}$ and ρu^2
B_{ob}	Oil formation volume factor at p_b, fraction
c_o	Oil compressibility, atm^{-1}
c_R	Rock compressibility, atm^{-1}
c_t	Total compressibility of the system, atm^{-1}
d_e	Newly defined diameter of the equivalent-volume sphere, cm
d_p	Diameter of the solid particles, cm
D	Pipe diameter, cm
E	Mittag-Leffler function
Ei	Exponential integral function
f_f	Fanning friction factor
g	Gravitational constant, cms^{-2}
g_c	Unit conversion factor, $g.cms^{-2}dyn^{-1}$
H	Thickness, cm
k	Permeability of the medium, darcy
K_L	Head loss coefficient
L	Length in the x-direction, cm
ΔL	Pipe length, cm
N_x	Number of grid-points in space
N_t	Number of time steps

p	Pressure, atm
p_o	Initial pressure, atm
p_b	Bubble point pressure, atm
Δp	Pressure loss, $gcm^{-1}s^{-2}$
$\hat{q}$	Source term, $gcm^{-3}s^{-1}$
$\tilde{q}$	Strength of source, $gcm^{-3}s^{-1}$
Q	Volumetric flow rate, cm^3/sec
Q_o	Oil production rate, cm^3/sec
r_e	An arbitrary distance from center of wellbore, cm
r_H	Hydraulic radius, cm
r_w	Radius of wellbore, cm
t	Time at which pressure is calculated, sec
Δt	Length of time step, sec
T_f	Final time, sec
u	Volumetric flux, $cm^3/cm^2/s$
Δx	Length of space step, cm
u_t	Mean tortuous velocity, cms^{-1}
v	Fluid velocity through hollow pipe, cms^{-1}
V_p	Volume of a single (non-spherical) particle, cm^3
w	Fitting parameter for the proposed model
x	Point in space at which pressure is calculated, cm

Greek Letters

α	Fractional order of differentiation
β	Proportionality constant between N_t and N_x^2
Γ	Gamma function
λ	Fitting parameter to define the diameter of a particle of arbitrary shape
μ	Fluid dynamic viscosity, cp
ρ	Fluid density, gcm^{-3}

ρ_f	Fluid density, gcm^{-3}
ρ_v	Variation of the mass of fluid per unit volume in the porous medium
τ	Tortuosity
T	Relaxation time
ϕ	Porosity of the fluid media, fraction
φ_p	Particle shape factor (sphericity)
ω	Constant mesh grading

Chapter 1

Introduction

1.1 General

Reservoir modeling is a critical component in the development, planning, and production management of oil and gas fields. The ultimate goal of reservoir modeling is to aid the decision-making process throughout all stages of field life. Few models in the literature combine Darcy and non-Darcy flow, and none use transitions between various flow regimes within porous media and fracture networks. The models in the literature that combine Darcy and non-Darcy flow do not combine them following the way of compact model development.

In conventional reservoir models, the effect of history of rock, fluid, and flow properties on flow phenomena are not considered. However, in recent literature, some mathematical models are found that are based on the fact that fluid flow phenomena through porous media depend on their past (Caputo, 2000; Hossain *et al.*, 2008; Iaffaldano *et al.*, 2005). When a complex fluid flows through porous media, there is a change in both rock and fluid properties due to chemical reactions, mineral precipitation, etc., and, therefore, permeability and viscosity change over time. The phenomenon that rock and fluid properties change over time is represented by the term 'memory'. To quantify the effect of history, 'memory' is incorporated in the mathematical model. Two types of memory, time memory and space memory, are found in literature. Space memory considers the previous space that the fluids have passed through (Caputo, 2003).

Memory is incorporated in mathematical reservoir models using fractional-order derivatives in the model. The definition of fractional-order derivatives provides a natural way to include history. History of pressure, pressure gradients, or any other parameters can be taken into consideration using fractional-order derivatives of that parameter. To consider time memory, fractional-order

derivatives in time are used, and to consider space memory, fractional-order derivatives in space are used.

Once fractional-order derivatives come into the model to incorporate memory, the equation becomes complicated and highly non-linear. The equation becomes very difficult to even numerically solve. Unlike integer-order derivatives, fractional-order derivatives do not have a single definition. Different definitions produce different equations for same model. It is also difficult to discretize the model applying suitable finite-difference approximations. Developing new schemes and algorithms to handle the fractional-order diffusivity equation is a great challenge.

Conventional mathematical models of fluid flow through porous media do not consider the effect of memory. Currently, all reservoir simulators are based on conventional modelling. Development of memory-based reservoir simulators is necessary to investigate the effects of memory. Incorporation of memory in terms of fractional-order derivatives considering all the previous data, in calculation of data at the current step. This increases the computational load by many folds. Though memory-based models are assumed to increase accuracy, they will not be attractive if the computational load is too high. Therefore, it is a great challenge to reduce the computational load. The greatest challenge is to develop a reservoir simulator based on the memory-based approach.

1.2 Knowledge Gap

Hossain et al. (2008) developed a new porous media diffusivity equation through inclusion of fractional order derivative to account for the rock and fluid memories, but the numerical solution of the equation is not available yet. Also, other fractional-order diffusion equations developed to model fluid flow through porous media are not solved, using the Caputo, Riemann-Liouville, and Grünwald-Letnikov definitions for the fractional-order derivatives. In addition, the value of the fractional order for the Hossain et al. (2008) model has not been computed yet.

Currently, no reservoir simulator uses a fractional-order diffusion equation to consider memory. It is important to have a simulator based on this new approach to improve accuracy. Such a simulator,

if it can be developed, would answer many questions regarding memory, and take away the confusion of the research community.

Fluid flow models are generally developed for specific flow phenomenon. Developing a general equation instead of developing separate mathematical equations for each specific case is worthwhile. The general equation can be simplified easily for different cases, but it is a bigger challenge to develop a general mathematical model that will represent fluid flow for all type of rocks, fluids and flow phenomena. There are few models that consider all the flow regimes relevant to porous media flow. In addition, many models don't consider all types of pressure losses that occur during fluid flow.

1.3 Objectives

The main objectives of this study are:

i) To develop a numerical model to solve a memory-based diffusion equation using finite-difference approximations, uniform meshes, and utilizing Caputo, Riemann-Liouville, and Grünwald-Letnikov definitions for the fractional-order derivative.
ii) To compare the numerical solutions found from the application of Caputo, Riemann-Liouville, and Grünwald-Letnikov definitions for the fractional-order derivative.
iii) To develop an efficient numerical model to solve a memory-based diffusion equation using finite-differences approximation, non-uniform meshes in time, uniform meshes in space, and utilizing the Riemann-Liouville definition for the fractional-order derivative.
iv) To develop a small-scale memory-based reservoir simulator so that the effects of memory can be investigated.
v) To develop a generalized memory-based mathematical model from which other memory-based models can be derived.
vi) To develop a generalized semi-empirical equation that portrays the flow of fluid in packed beds and porous media.

1.4 Organization of the Thesis

This thesis consists of nine chapters and is written in "manuscript" format. The rest of the thesis is organized as follows:

Chapter 2 presents a literature review on modeling of fluid flow through porous media with specific focus on memory and fractional-order derivatives.

A numerical model has been developed using uniform meshes and the Riemann-Liouville definition for the fractional-order derivative to solve the model of Hossain et al. (2008) in Chapter 3. The model is validated comparing with an analytical solution for a specific case of the model. This chapter is written to submit as a journal article.

Numerical models have been developed using uniform meshes and the Caputo, and the Grünwald-Letnikov definitions for the fractional-order derivative to solve the model of Hossain et al. (2008) in Chapter 4. These models are compared with the model developed in Chapter 3. This chapter is written for submission as a journal article.

In Chapter 5, the model of Hossain et al. (2008) is solved numerically using graded meshes in time and the Riemann-Liouville definition for the fractional-order derivative. The L1 algorithm is derived for the applied graded meshes. The numerical model is validated. This chapter has also been prepared for submission as a journal article.

Chapter 6 compares the numerical models developed using uniform and graded meshes. In addition, experimental data is collected from the literature and the value of the fractional order and the relaxation time have been computed from the data. Optimal spatial and time steps in unit space and time have been computed for this value of fractional order by analyzing the error in an analytical solution. This chapter is written to submit as a journal article.

A generalized memory-based mathematical model has been proposed in Chapter 7. Different fractional-order diffusion equations can be derived from this model.

Chapter 8 proposes a generalized conventional model and dimensionless number for fluid flow in packed beds and porous media. A generalized semi-empirical equation is proposed that portrays the flow of fluid in packed beds and porous media. A new expression for the modified Reynolds number has been derived from the model. Novel ways to calculate tortuosity of the porous media, the diameter of the equivalent volume sphere and the head-loss coefficient are proposed. This chapter is written to submit as a journal article.

Chapter 9 summarizes the outcomes of the present study and presents some recommendations for future studies.

Bibliography

1. Caputo, M. (2000). Models of Flux in Pous Media with Memory. *Water Resources Research, 36*, 693-705.
2. Caputo, M. (2003). Diffusion with space memory modelled with distributed order space fractional differential equations. *Annals of Geophysics, 46(2)*, 223-234.
3. Hossain, M.E., Mousavizadegan, S.H., and Islam, M.R. (2008). A new porous media diffusivity equation with the inclusion of rock and fluid memories: *SPE-114287-MS, Society of Petroleum Engineers*.
4. Iaffaldano, G., Caputo, M., and Martino, S. (2005). Experimental and theoretical memory diffusion of water in sand. *Hydrology and Earth System Sciences, 10*, 93-100.

Chapter 2

Literature Review

2.1 Introduction

Much theoretical, numerical and observational work has been published focused on fluid flow through porous media. This research has placed memory and fractional derivatives in a central role for accurate modeling of fluid flow through porous media. Models that do not consider the effects of the history of the rock and fluid cannot accurately represent the characteristics of fluid flow. Properties of both the rock and fluid change with time while fluid flows through porous media. Pores of the medium might be enlarged, due to chemical reactions between the medium and the fluid, or can be diminished or even closed, due to deposition of solid particles carried by the fluid or by the precipitation of minerals from the fluid. Consideration of both space and time memory is required to capture this continuous alteration of rock and fluid properties. Some models consider only time memory, a few consider space memory, and classical models consider neither of these memories. However, for accurate mathematical representation of flow, both types of memory should be considered. Inclusion of time and space memory would give a path to formulate a generalized mathematical model. The generalized model could represent almost all types of flow phenomena that occur in porous media. Histories of the pressure and its gradient, as well as space memory, can be included in mathematical models using fractional-order derivatives. Use of fractional-order derivatives in modeling makes the model able to capture history but causes higher computational loads. Fractional diffusion models should be used where consideration of the effect of history is needed to justify the computational load.

The idea of including memory in subsurface flow modeling is comparatively new. In this perspective, all materials are assumed to have memory, so the history of the rock and fluid is considered to affect their present and future characteristics. Incorporation of memory includes this natural phenomenon in the governing equations and improves the prediction accuracy. Memory

incorporation makes the governing equations intricate and solving the equations becomes more challenging. This paper reviews different existing subsurface flow models and addresses the necessity of memory incorporation, problems that arise due to including memory, and the impact of considering memory in subsurface flow modeling.

2.2 Conventional Modeling Approach in Porous Media Flow

The principles of conservation of mass, energy, and linear and angular momentum, along with the equation of state and constitutive equation, describe the flow of fluids. Equations of state relate pressure, volume, and temperature (Landel *et al.*, 1986). Velocity and stress fields of the flows can be predicted by solving the conservation laws together with the constitutive model and equations of state using a suitable method (Carreau *et al.*, 1997; Keunings, 2003, and 2004; Hulsen, 1990).

Different constitutive models and equations of state are used depending on the type of fluid and flow. No constitutive equation can be used for all purposes. There is also no constitutive equation that can completely describe the behavior of complex fluids in general flow situations (Owens *et al.*, 2002; Larson, 1988). Modeling of flows of complex fluids is difficult, so several assumptions, such as laminar, incompressible, steady-state, and isothermal flow, are usually made to make the representation easier.

There are three different types of modeling depending on the scale of interest to represent the physics of fluid flow in porous media. The first is called continuum modeling. It is based on the continuum description of the porous medium that is associated with macroscopic semi-empirical equations such as the Ergun Equation, Darcy's law, or the Carman-Kozeny equation (Balhoff *et al.*, 2004). The second is pore-scale modeling or microscale modeling, which is based on the microscopic description of the pore geometry and on the physical laws of flow and transport within the pores. The third is multiple continua or hybrid modeling, which combines pore-scale and continuum-scale behavior.

The continuum approach is simple, with apparently no computational cost and does not account for the detailed physics at the pore level. Time-dependent transient effects cannot be modelled

with this approach. On the other hand, a detailed understanding of the physical processes occurring at the pore scale and a complete description of the morphology of the pore space are required for pore scale modeling. This is very complex and requires a lot of computation.

Different statistical (Adler *et al.*, 1990; Roberts, 1997; Yeong *et al.*, 1998) and process-based (Bakke *et al.*, 1997; Øren *et al.*, 1998, and 2002) techniques have been developed to describe the geometry of the pore space. Pore space can also be imaged directly using micro CT tomography (Dunsmuir *et al.*, 1991; Spanne *et al.*, 1994). Two approaches can be applied to model flow at the pore scale. Flow can be simulated directly in a three-dimensional pore-space image by solving the Navier-Stokes equations or by using the Lattice-Boltzman techniques (Gunstensen *et al.*, 1991, and 1993; Grunau *et al.*, 1993; Ferreol *et al.*, 1995; Van Katz *et al.*, 1999; Pan *et al.*, 2004) or by the smoothed particle hydrodynamics (SPH) method (Tartakovsky *et al.*, 2005). This is called direct modeling. Direct modeling becomes cumbersome and computationally expensive for capillary controlled flow with multiple phases. The Lattice-Boltzman and smoothed particle hydrodynamics methods are Lagrangian, particle-based approaches. Another approach is to describe the pore space as a network of pores connected by throats with some idealized geometry (Øren *et al.*, 2002; Delerue *et al.*, 2002). Then a series of flow steps in each pore or throat are combined to simulate flow in the medium. This is called pore-network modeling and has been the most common pore-scale modeling method.

2.2.1 Continuum Modeling

This approach treats the porous medium as a continuum and does not consider the intricacies and fine details of the microscopic pore structure. Darcy's law, the Blake-Kozeny-Carman and Ergun Equations are some examples of continuum modeling techniques. The commonly used equations of these three continuum models are given in Table 2.1.

The simplest model to describe the flow in porous media is Darcy's law that relates the pressure gradient in the direction of flow to the volumetric flux of fluid through the medium, permeability, and fluid viscosity. It is an empirical relation, yet it can be derived from the capillary bundle model using the Navier-Stokes Equations. Since Darcy's law contains only a viscous term and no inertial

Table 2.1: Commonly used equations for continuum model.

Model	Equation
Darcy	$\frac{\Delta P}{L} = \frac{\mu u}{K}$
Blake-Kozeny-Carman	$\frac{\Delta P}{L} = \frac{72C'\mu u(1-\phi)^2}{D_p^2\phi^3}$
Ergun	$\frac{\Delta P}{L} = \frac{150\mu u}{D_p^2}\frac{(1-\phi)^2}{\phi^3} + \frac{1.75\rho u^2}{D_p}\frac{(1-\phi)}{\phi^3}$

term, it is applicable only to laminar flow at low Reynolds numbers. The law cannot be applied when the flow becomes slow due to interaction between the fluid and the pore walls. The Darcy model only considers viscous Newtonian effects and does not consider boundary effects and heat transfer. Hence, Darcy's law is applicable to only isothermal, laminar, purely viscous, and incompressible Newtonian flow. Darcy's law has been modified and various generalizations to include nonlinearities have been made to represent more complex phenomena, such as non-Newtonian and multiphase flow (Shenoy, 1993; Schowalter *et al.*, 1978).

The Blake-Kozeny-Carman (BKC) model is one of the most popular models to represent flow through porous media. This model incorporates a number of equations that are developed under various conditions and assumptions. These equations associate the pressure drop across a granular packed bed to the volumetric flux of fluid through the fluid viscosity, the bed porosity, and the granule diameter. Macroscopic properties of random porous media, such as permeability, can be modelled from this family of equations. These relations are based on the capillary bundle concept with various level of sophistication. The BKC model is applicable to laminar flow through packed beds at low Reynolds numbers. The model has been extended to incorporate transitional and turbulent flow conditions (Kozicki *et al.*, 1988; Chapuis *et al.*, 2003).

The Ergun Equation is a widely used semi-empirical relation to model flow through porous medium. It correlates the pressure drop along a packed bed to the volumetric flux. Unlike the Darcy and Blake-Kozeny-Carman models, the Ergun Equation contains both viscous and inertial terms.

At low flow rates, the viscous term becomes dominant, while at high flow rates the inertial term becomes dominant. Therefore, the Ergun model can represent larger range of flow regimes compared to the Darcy or BKC models (Jones *et al.*, 1976; Plessis *et al.*, 1994; Stevenson, 2003).

The continuum approach can describe the complex characteristics of flow through porous media using a few simple averaging terms, and the computational cost of simulating continuum models is very low. Nonetheless, this approach ignores the physics of flow at pore level. Most of these continuum models have been modified to describe non-Newtonian behavior. To apply continuum models for non-Newtonian fluid, an effective viscosity, which will have the dimensions and physical significance of Newtonian viscosity, is defined so that the model can represent the non-Newtonian fluid flow (Pearson *et al.*, 2002). However, continuum models have had limited success in predicting the flow of complex fluids in porous media. Non-Newtonian continuum models fail to incorporate time-dependent effects and to model yield-stress.

2.2.2 Pore-Scale Modeling

Research on pore-scale modeling started its journey with the classical papers of Irvin Fatt on pore-network modeling in the 1950s (Fatt, 1956a; Fatt, 1956b; Fatt, 1956c). Pore-scale modeling is important to understand the physics of flow through porous media. It helps to predict the petrophysical properties and, thus, supplement and replace laboratory experiments. Pore-scale modeling has become popular due to advances in image resolution and computational power.

Pore-scale modeling has significant advantages, yet there are also limitations. Different pore-scale models that are used for same physical problem should be consistent. Many industrial processes involve multiple physical processes on which pore-scale models do not focus. Upscaling the pore-scale results is crucial to improve field-scale models. The question of how the available data from image resolution, and detailed and complicated physics based models can be employed to calculate simple and static properties is yet to be answered (Joekar-Niasar *et al.*, 2012).

2.2.2.1 Direct Modeling

The most prevalent approach to model fluid flow directly in porous media is the lattice Boltzmann method (Dunsmuir *et al.*, 1991; Chen and Doolen, 1998; Kang *et al.*, 2006; Manwart *et al.*, 2002; Porter *et al.*, 2009; Schaap *et al.*, 2007; Pan *et al.*, 2004; Hao and Cheng, 2010; Boek and Venturoli, 2010). It is a particle-based technique that is used for computational modeling of single and multiphase fluid flows in complex geometries. The method is based upon the Boltzmann equation, which considers the fluid to be composed of particles, and simulates the motion and collision of particles. The rules governing the motion and collision are established such that the averaged motion of a particle can be shown to be consistent with the governing Navier–Stokes Equations. Writing code for the lattice Boltzmann method is relatively easy. However, the method is not naturally computationally efficient, even with the use of parallel computing. Capillary controlled displacement on large samples is very difficult to capture accurately. Hence, relative permeability cannot be predicted reliably by this method. However, recent studies show that relative permeability can be computed using pore-space images with advanced computer technologies (Pan *et al.*, 2004; Hao and Cheng, 2010; Boek and Venturoli, 2010; Ramstad *et al.*, 2011). The method is suitable to compute permeability, dispersion coefficients, and effective reaction rates for single phase flow.

Another direct modeling technique is the level-set method that is developed to study capillary-controlled displacement. In this method, it is easy to follow changing topology. Hence, the method can handle complex boundaries very easily. Computational load is also high for this method. However, it gives insights into imbibition processes and fracture-matrix interactions (Sussman *et al.*, 1994; Prodanovic *et al.*, 2010).

General models for fluid flow can be developed for different physical phenomena, non-Newtonian rheology, and thermal effects by applying density-functional modelling techniques (Demianov *et al.*, 2011). These techniques have been successfully applied in the case of simple geometries. However, for complicated geometries, such as realistic porous media, the method has not been effective.

2.2.2.2 Pore-Scale Network Modeling

Quantitative description of the geometry of pore structure and solution of the governing equations of motion are required to quantify the macroscopic transport properties of pore space from their microscopic properties. Pore-scale network modeling follows these two steps. It combines computational resources with the physics of flow and pore-space structure.

In this modeling, the porous space is characterised by a network of flow channels. Larger voids are represented by pores that are interconnected by narrower regions called throats. The process to construct a completely realistic pore network is very complicated. There are two types of methods to generate pore-scale networks (Al-Raoush *et al.*, 2003). In the first type, an equivalent network is formed using pore- and throat-size distributions, coordination number, and size correlation between adjacent pores. The model is tuned to match experimental data by adjusting the coordination number, and pore- and throat- size distributions. The solution is not unique in this case. In another approach, pore space is constructed with the help of measured porosity and correlation functions (eg. Vogel and Roth, 1997; Bakke and Øren, 1997; Liang *et al.*, 1999; Okabe and Blunt, 2003), or by non-destructive three-dimensional imaging using microtomography or magnetic resonance (eg. Baldwin *et al.*, 1996; Rintoul *et al.*, 1996).

Two main types of pore network models are generally used to study fluid flow in porous media. One type is quasi-static displacement models, and another is dynamic displacement models. In the quasi-static models, the capillary force dominates. The static position of all fluid-fluid interfaces is determined using capillary pressure on the network. The dynamic aspects of pressure propagation and interface dynamics are ignored. The pores and throats change their configuration one at a time. Quasi-static models are extensions of percolation models. These models do not work in case of fracture flows, near-wellbore flows, and flows involving polymers, gels, and foams. However, the effects of viscous forces are modelled in addition to the capillary effect in dynamic displacement models. In dynamic models, a specified inflow rate for one of the fluids is imposed and the subsequent transient pressure response and the associated interface positions are calculated. In these models, a given volume of invading fluid is injected during a time step and Poiseuille flow is assumed in the throats. At each time step, the element pressures are computed and the displacement decisions are taken based on pressure difference rules.

2.2.3 High Velocity Fluid Flow Modeling

Darcy's model describes the fluid flow through porous media where the flow rate is low. At low flow rates, viscous force is dominant. With the increase of flow rate, inertial forces become significant. Darcy's law can no longer model the fluid flow in the case of high velocity. At high flow rates, the relationship between pressure gradient and superficial fluid velocity becomes non-linear. Forchheimer (1901) corrected the Darcy equation adding a second order of the velocity term to represent the microscopic inertial effect. In addition, Darcy's law does not consider the shearing effect between the fluid and the pore walls. In this regard, Brinkman (1947) modified the Darcy's equation adding the second-order derivatives of the velocity. Darcy (1856), Forchheimer (1901), and Brinkman (1947) equations and their assumptions are tabulated in Table 2.2.

Table 2.2: High velocity fluid flow models.

Author	Model Equation	Assumptions
Darcy (1856)	$\frac{\Delta P}{L} = \frac{\mu u}{K}$	• the solid is rigid, deformation of the solid is negligible • steady flow • negligible viscous effects within the fluid
Forchheimer (1901)	$-\frac{\partial p}{\partial x} = \frac{\mu u}{k} + \beta \rho u^2$	• the solid is rigid, deformation of the solid is negligible • significant inertial forces • negligible viscous effects within the fluid
Brinkman (1947)	$-\frac{\partial p}{\partial x} = \frac{\mu u}{k} - \mu(\frac{\partial^2 u}{\partial y^2} + \frac{\partial^2 u}{\partial z^2})$	• the solid is rigid, deformation of the solid is negligible • steady flow • viscous effects within the fluid are not negligible

2.3 Inclusion of Memory in Porous Media Flow Modeling

It is difficult to determine the pore-size distribution, the surface areas, and the tortuosity of a porous media. Through CT scanning, images have been used to determine the distribution of pore sizes (Xu *et al.*, 1999; Kamath *et al.*, 1998) and residual saturation (Hilpert *et al.*, 2000), but this is very costly. It is also not possible to scan a complete reservoir or rock samples taken from every part of

a reservoir. There are many ways to describe the pore spaces (Øren *et al.*, 1998; Patzek, 2001; Dixit *et al.*, 1998, 1999, and 2000; Blunt *et al.*, 1990, and 1991), but, in all cases, the geometric parameters are tuned to match available experimental data. So, these models do not represent the exact structure that exists in a reservoir. They are developed in such a way so that their predictions match given experimental results. It is even more difficult to observe the detailed processes that occur during fluid flow at the pore level in complex heterogeneous porous media through experiment.

Since each model, even at the pore level, is developed to match experimental data, it is rather good to infer the detailed structure and flow processes at pore level from macro level observation and from data obtained in idealized model experiments. Here, memory can be used to tune the continuum model to represent the medium and flow more accurately.

2.3.1 Fundamentals of Memory

Different authors have defined memory in different ways. According to Zhang, memory is a function of time and space, and forward time events depend on previous time events (Zhang, 2003). Zavala-Sanchez *et al.* showed that the system 'remembers' its initial state, which is defined as memory effects for the effective transport coefficients (Zavala-Sanchez *et al.*, 2009). Hossain and Abu-Khamsin (2012) defined memory as the effect of past events on the present and future course of developments. We define memory in the following comprehensive way.

When all affecting parameters (pressure, temperature etc.) excluding time remain unchanged, rock, fluid, and flow characteristics are conventionally assumed to remain constant. However, we think that they are changed, since time is not constant here. They depend on time and are changed with time. So, rock, fluid, and flow properties at the present depend on their past, and the past must be considered to determine the present behaviour. Future behaviour can also be predicted from the past. Here, past is one of our keys to modelling the present and future.

Conventional continuum approaches model only the physical processes of flow and consider only pressure and temperature to affect rock, fluid, and flow characteristics. Chemical and biological

processes that occur in the reservoir and change the rock, fluid, and flow behavior are not considered. However, these processes occur even in the simplest to model reservoirs.

Reactive transport modeling considers chemical microenvironments, mineral–fluid reaction rates, thermal– mechanical–chemical processes, and change in rock, fluid, and flow characteristics with the processes (Steefel *et al.*, 2005), but is very difficult to model, very complex, and has very high computational costs.

Different models are developed to represent different types of reservoir, fluid, and different flow characteristics. It would be nice if there were a general model that would act as a platform to represent all cases and, yet, had low computational cost. The general model that we are thinking about will follow the continuum approach and catch conventional physical processes explicitly. Chemical and biological processes, effects of time, reservoir heterogeneity, and all the other properties that may affect the flow phenomenon, will be included implicitly by using a memory function.

Here, we are defining memory as a function that will describe how the present depends on past; that will be used to evaluate the present and predict the future characteristics of an object from its past, and/or to tune the model so that the model can represent all the processes that were not considered explicitly in the model and can characterize the rock, fluid, and flow accurately and completely as well.

2.3.2 Modeling with Memory

Memory has been implicitly or explicitly included in various models of porous media flow. Memory comes into the model to serve different purposes, e.g. for better representation of flow in disordered or fractal media, to incorporate the effects of history or rock, fluid, and flow, etc.

Giona and Roman (1992a, and 1992b) derived a fractional diffusion equation containing an explicit reference to the history of the diffusion process by using fractional calculus. They did not

include memory directly in their model. Memory is implicitly included in their equation, since a fractional derivative has been used.

Metzler *et al.* (1994, and 1997) obtained a more general fractional model equation in which they used Fox's H -function. Giona and Roman (1992a, and 1992b) and Metzler *et al.* (1994) constructed an integrodifferential equation to express the memory effect via the integral term. Their work gives good results for homogeneous fractal media, where conductivity is identical in every diffusion path. They, however, failed to predict precisely the motion of a particle in inhomogeneous fractal media.

Park *et al.* (1998) set up a governing equation describing the diffusion phenomena in disordered media addressing a memory effect and non-locality, in which they formulated permeability as a function of space and time. Tian and Tong (2006) incorporated memory in their flow models of fluids by applying fractional derivatives.

Hossain and Islam (2006) described the memory of fluid as one of the most important and most neglected feature in fluid-flow models. They reviewed fluid-flow models with memory, addressed the intangible problems of memory, and identified the effects of considering memory.

Hossain *et al.* (2007) introduced a stress-strain model incorporating memory with viscous stresses. They obtained the variation of shear stress as a function of strain rate for a fluid in a sample oil reservoir to identify the effects of fluid memory. They showed the memory effects in space with pressure gradient change. Their computation indicates that the effect of memory causes a nonlinear and chaotic behavior for stress-strain relation. They claim that the model can be used in reservoir simulation and rheological study, well test analysis, and surfactant and foam selection for enhanced oil recovery. In a subsequent study (2009), they solved the model numerically.

Hossain *et al.* (2008) introduced a new model for fluid flow incorporating fluid and rock memory. The model was derived by introducing the Caputo fractional derivative to the classic Darcy law to account for the variation of fluid and formation properties with time. They modelled variable permeability and viscosity over time using fractional order derivative. They claim that their model

can be used in any crude oil flow through porous media. Furthermore, they proposed an explicit finite- difference scheme to solve the resulting nonlinear integro-differential equation.

Hossain and Islam (2009) developed a comprehensive material balance equation (MBE) including continuous variation of rock and fluid properties with time, due to changes of pressure and temperature. Memory effects of fluids and rock in terms of continuous time functions are included in their formulation. The developed MBE is highly non-linear, with a number of coefficients that are inherently non-linear. They solved the developed MBE numerically with a newly developed non-linear solver. The authors claim that the proposed MBE can be applied to fractured formations with dynamic features. Furthermore, an improvement of 5% in oil recovery was observed from the new MBE over the conventional MBE. However, the proposed MBE requires accurate rock and fluid compressibility data obtained from laboratory measurements or from reliable correlations.

Kolomietz (2014) applied kinetic theory to a nuclear Fermi liquid treating the nuclear collective dynamics in terms of the particle density, current density, pressure, etc. He studied the influence of Fermi-surface distortion, relaxation processes, and memory effects on the nuclear dynamics. He concluded that the memory kernel depends on the relaxation time and provided a connection between both limiting cases of the classical liquid dynamics (short relaxation time limit) and the quantum Fermi-liquid dynamics (long relaxation time limit). The research showed that memory effects lead to an important consequence of hindrance of the collective motion and, in particular, to nuclear fission.

Hristov (2015) applied the integral-balance method to diffusion models with fading memories with weakly singular kernels. They expressed the memory as Volterra integrals and time-fractional Riemann-Liouville derivatives.

Hassan *et al.* (2015a) investigated the effect of reservoir heterogeneity on the pressure distribution using a memory-based diffusivity equation. They claim that the memory-based diffusivity equation can be used to model the flow of fluid through heterogeneous reservoirs.

Hassan *et al.* (2015b) introduced memory to model variable rock and fluid properties with time. They used fractional derivatives as a memory formalism to account for the non-local aspects of fluid flow behavior through porous media. They investigated the effects of different parameters such as composite pseudopermeability, fluid velocity, and viscosity on the pressure response of the reservoir. They showed that there is an effect of memory on reservoir rock and fluid parameters and that it ultimately affects the pressure response of the reservoir. They concluded that the pseudo-permeability, fluid velocity, and memory decreases with distance, up to a certain extent of the reservoir, and then becomes constant toward the boundary of the reservoir. It was also concluded that the effects of these parameters increase with time around the wellbore and decrease toward the outer boundary. They solved the Integro-differential equation numerically in time and space domains for different dependent rock and fluid properties.

Rammay *et al.* (2015a) conducted a study to compare the variations of PVT properties using Darcy and memory-based diffusivity equations. Variable compressibility, formation volume factors, and viscosity of oil were obtained by solving both equations numerically using MATLAB. They obtained different variations of compressibility, formation volume factor, and viscosity of oil from the Darcy and memory-based diffusivity equations. They consider that memory has an effect on these PVT data and that the memory-based diffusivity equation is more rigorous than the Darcy diffusivity equation, due to the incorporation of the memory formalism term as a fractional order in the diffusivity equation. They conclude that viscosity and compressibility changes are more sensitive to pore pressure as compared to formation volume factor. They suggest using memory-based models in order to accurately predict the PVT properties for more rigorous and representative convergence in reservoir simulators.

Rammay *et al.* (2015b) found different porosity and permeability variations from Darcy and memory-based diffusivity equations. They observed that memory has an effect on porosity and permeability. They concluded that permeability change is more sensitive to pressure as compared to porosity change. They found differences between these two models, and they believe this difference can be significant enough during the convergence process in reservoir simulators. They also think that to accurately predict the rock properties for more rigorous and representative convergence in reservoir simulators, memory-based diffusivity equations should be used.

2.3.3 Experimental Investigation to Capture Memory

Many researchers believe that flow history has an effect on fluid flow through porous media. For example, when a complex fluid flows through porous media, there is a change in permeability due to chemical reactions, mineral precipitation, etc. and, therefore, permeability diminishes over time. This phenomenon shows that the effect of fluid pressure at the boundary on the flow of fluid through the medium is delayed, and the flow occurs as if the medium has a memory (Caputo, 2000). Experiments are conducted to justify this.

Memory phenomena have already been shown qualitatively by Elias and Hajash (1992) for diffusion of fluids in porous media, revealing a good fit with the flux rate observed in five laboratory experiments on diffusion of water in sand. Caputo (2000) validated his generalized memory-based theory, accounting for the non-local aspects of fluid transport. Iaffaldano *et al.* (2005) carried out an experimental study to capture the memory effect in the diffusion process of water in a porous media and proved that permeability of sand layers could decrease due to rearrangement of grains and subsequent compaction. De Espi´ındola *et al.* (2005) used the fractional derivative model (i.e., a measure of memory) to identify the dynamic properties of viscoelastic materials and experimentally validated their findings. Cloot and Botha (2006) used the generalized classical Darcy law, and a non-integer order derivative of the piezometric head for groundwater flow. Numerical solutions of their equation for various fractional orders of the derivatives were compared with experimental data to observe the behavior of fractional derivatives in a modified Darcy's law. Di Giuseppe *et al.* (2010) modified the constitutive equations by introducing a memory formalism operating on both the pressure gradient–flux and the pressure–density variations and used fractional-order derivatives to represent the memory formalism. Supported by laboratory experiments, a good agreement has been shown between the theoretical and observed flows over time.

2.3.4 Memory and Fractional Derivatives

Rock, fluid and flow properties depend on their history, and memory functions describe how they do depend on their history. So, the present condition of rock, fluid, and flow can be conveyed as

the convolution of the memory function and their history. To accomplish this, fractional derivatives can help better than conventional derivatives since fractional derivatives of a function can be expressed via a convolution of two functions. Moreover, it acts as conventional derivative when the order of derivative is a non-negative integer. Therefore, fractional derivatives can be used to describe natural phenomena like conventional derivatives and, in addition, to represent the effects of history.

Convolution systems are linear, causal, and time-invariant. Since the fractional derivatives of a function is a convolution of two functions, to describe a system using fractional derivatives, the system is required to be linear, causal, and time-invariant. Here, the question arises: are the systems demonstrating flow through porous media, representing change in rock and flow behavior with time linear, causal, and time-invariant? This is a subject of research, whether the systems are actually convolution systems, but when fractional derivatives are used to mathematically describe a system, the assumption comes implicitly that the system is linear, causal, and time-invariant. Here, the system of flow through porous media, changes in rock and flow behavior with time are assumed to be linear, causal, and time-invariant.

2.4 Fractional Calculus

In classical calculus, powers of the differentiation operator are integers. Differentiation and integration do not have similar definitions. In fractional calculus, powers of the differentiation operator can be real or complex numbers. Here, differentiation and integration are not treated in different ways, rather, they are generalized.

2.4.1 History of Fractional Calculus

Calculus was built from infinitesimal analysis, first by Isaac Newton during the 17th century (Boyer et al., 1970). Gottfried Wilhelm von Leibniz again, independently, made the same discovery during the period 1673-1676. Leibniz first introduced the idea of a symbolic method and used the symbol $d^n y/dx^n = D^n y$ for the n-th derivative, where n is a non-negative integer (Boyer et al., 1970).

Leibniz asked Guillaume François Antoine, Marquis de l'Hôpital in a letter, 'Can the meaning of derivatives with integer order be generalized to derivatives with non-integer orders?' L'Hôpital replied by another question to Leibnitz, 'What if the order will be ½?'. On September 30, 1695 Leibnitz replied in a letter, 'You can see by that, sir, that one can express by an infinite series a quantity such as $d^{1/2}\bar{x}\bar{y}$ or $d^{1:2}\bar{x}\bar{y}$. Although infinite series and geometry are distant relations, infinite series admits only the use of exponents which are positive and negative integers, and does not, as yet, know the use of fractional exponents.' Later, in this letter, he continues prophetically, 'Thus it follows that $d^{1/2}x$ will be equal to $x\sqrt{dx:x}$. This is an apparent paradox from which, one day, useful consequences will be drawn.' This date, September 30, 1695, can be said to be the exact birthday of fractional calculus (Machado et al., 2010; Leibniz et al., 1965; Ross, 1977). Leibniz mentions derivatives of 'general order' in a letter to Johann Bernoulli in the same year (Leibniz, 1695; Ross, 1977).

In 1697, in a letter to John Wallis (1616-1703), Leibniz discusses Wallis's infinite product for $\pi/2$ and states that differential calculus might have been used to achieve this result. He uses the notation $d^{1/2}y$ to denote the derivative of order $1/2$ (Leibniz, 1697; Ross, 1977).

In 1730 Leonhard Euler wrote, "When n is a positive integer, and if p should be a function of x, the ratio $\mathrm{d^n p}$ to $\mathrm{dx^n}$ can always be expressed algebraically, so that if $\mathrm{n} = 2$ and $\mathrm{p} = \mathrm{x^3}$, then $\mathrm{d^2(x^3)}$ to $\mathrm{d(x^2)}$ is $6\mathrm{x}$ to 1. Now it is asked what kind of ratio can then be made if n be a fraction. The difficulty in this case can easily be understood. For if n is a positive integer $\mathrm{d^n}$ can be found by continued differentiation. Such a way, however, is not evident if n is a fraction. But yet with the help of interpolation which I have already explained in this dissertation, one may be able to expedite the matter." (Euler, 1738; Ross, 1977). Fractional calculus attracted Euler's attention, and according to him, the result of the evaluation of $\mathrm{d^n y/dx^n}$ of the power function $\mathrm{x^m}$ has a meaning for non-integer m.

In 1772, Joseph-Louis Lagrange developed the law of exponents (indices) for differential operators of integer order. The law is that $\frac{d^m}{dx^m}.\frac{d^n}{dx^n}y = \frac{d^{m+n}}{dx^{m+n}}y$. This is an indirect contribution to fractional calculus. Mathematicians were interested in finding an analogous rule that would hold true for

arbitrary m and n (Ross, 1977). Pierre-Simon Laplace (1820) defined fractional derivatives by means of an integral.

In 1819, Sylvestre François Lacroix first mentioned a derivative of arbitrary order in a text of 700 pages in which he devoted less than two pages to this topic. Writing the n-th derivative of $y = x^m$ as $d^n y/dx^n = (m!/(m-n)!)x^{m-n}$, where n is a positive integer and $m \geq n$, he generalized the factorial using the gamma function and got $d^n y/dx^n = (\Gamma(m+1)/\Gamma(m-n+1))x^{m-n}$, where m and n may be fractional numbers. In particular, he calculated the derivative of order $1/2$ of x by putting $y = x$ and $n = 1/2$ and found $(d^{\frac{1}{2}}y/dx^{\frac{1}{2}}) = (\Gamma(2)/\Gamma(3/2))x^{1/2} = 2\sqrt{x}/\sqrt{\pi}$. Lacroix's method did not give any information about the application of a derivative of arbitrary order (Ross, 1977; Lacroix, 1819).

After Lacroix, Jean-Baptiste Joseph Fourier made mention of derivatives of arbitrary order. He obtained the integral representation for $f(x)$ as, $f(x) = \frac{1}{2\pi}\int_{-\infty}^{+\infty} f(\alpha)d\alpha \int_{-\infty}^{+\infty} \cos[p(x-\alpha) + n\pi/2]dp$.

For integer values of n, $(d^n/dx^n)cosp(x-\alpha) = p^n cos[p(x-\alpha) + n\pi/2]$. Fourier replaced formally n with u, where u is arbitrary, and obtained, $(d^u/dx^u)f(x) = (1/2\pi)\int_{-\infty}^{+\infty} f(\alpha)d\alpha \int_{-\infty}^{+\infty} p^u \cos[p(x-\alpha) + u\pi/2]dp$. In this way, he defined a fractional operation. According to Fourier, 'The number u which appears in the above will be regarded as any quantity whatsoever, positive or negative.' (Fourier, 1822; Ross, 1977).

The first use of fractional operations was made by Niels Henrik Abel in 1823. To solve an integral equation that arises in the formulation of the tautochrone (isochrone) problem, he used fractional calculus. This problem is about the determination of the shape of a frictionless plane curve through the origin in a vertical plane along which a particle of mass m can fall in a time which is independent of the starting position (Debnath, 1995). In this problem, the constant time of slide is given by $k = \int_0^x (x-t)^{-\frac{1}{2}} f(t)dt$. The function $f(t)$ in the integrand is unknown and needs to be determined. Abel wrote the right side of the equation as $\sqrt{\pi}(d^{-\frac{1}{2}}/dx^{-\frac{1}{2}})f(x)$. He then operated on

both sides with $(d^{\frac{1}{2}}/dx^{\frac{1}{2}})$ and obtained $(d^{\frac{1}{2}}/dx^{\frac{1}{2}})k = \sqrt{\pi}f(x)$. So now $f(x)$ can be determined from the fractional derivative of order ½ of the constant k. The derivative of a constant function may not always be equal to zero. This is an elegant solution according to mathematicians (Abel, 1881).

In 1832, Joseph Liouville published three large memoirs. He formally extended the formula for the derivative of integer order m, $D^m e^{ax} = a^m e^{ax}$ to derivatives of arbitrary order υ, $D^\upsilon e^{ax} = a^\upsilon e^{ax}$. Arbitrary derivatives of a function $f(x)$ which can be expanded in a series, $f(x) = \sum_{n=0}^{\infty} c_n e^{a_n x}$ was assumed to be found by the formula, $D^\upsilon f(x) = \sum_{n=0}^{\infty} c_n a_n^\upsilon e^{a_n x}$. This formula is referred to as Liouville's first formula for fractional derivatives. Here, υ can be any number-rational, irrational, or complex. But υ cannot have a value for which the series does not converge. Liouville knew this restriction, and he formulated a second definition. He started with a definite integral, $I = \int_0^\infty u^{a-1}e^{-xu}du, a > 0, u > 0$ to reach his second definition. This integral is related to the Euler integral of the second kind (the gamma function). Plugging in $xu = t$ gives $I = \int_0^\infty (t^{a-1}e^{-t})dt/x^a = \Gamma(a)/x^a$ or, $x^{-a} = (1/\Gamma(a))I$. Then, he operated on both sides with D^υ and got $D^\upsilon x^{-a} = (1/\Gamma(a))D^\upsilon \int_0^\infty u^{a-1}e^{-xu}du$. Applying Liouville's basic assumption, the arbitrary derivative was written as, $D^\upsilon x^{-a} = ((-1)^\upsilon/\Gamma(a)) \int_0^\infty u^{a+\upsilon-1}e^{-xu}du$. Finally, Liouville's second definition of a fractional derivative became, $D^\upsilon x^{-a} = ((-1)^\upsilon \Gamma(a + \upsilon)/\Gamma(a))x^{-a-\upsilon}$. He successfully applied both formulas to problems in potential theory. The second definition has also limitation. It can't be applied to all functions. However, it is useful for functions of the type x^{-a}.

2.4.2 Physical Meanings of Fractional Derivatives

Fractional derivatives are used extensively to model natural phenomena and to better fit experimental results, but their physical meanings are not yet well and lucidly understood. Some authors have tried to understand the physical meaning of fractional derivatives. Glöckle and Nonnenmacher (1994) found the fractional relaxation equation to be a special type of non-Markovian process. Schiessel and Blumen (1993) and Heymans and Bauwens (1994) showed that

fractional differential or integral equations are not mathematical artifacts, but rather they arise naturally when expressing the rheological behavior of a fractal model. Podlubny (2002) recently suggested physical and geometric interpretations of operations of fractional integration and differentiation. J. A. Tenreiro Machado, in 2003, presented a probabilistic interpretation of fractional-order derivatives, based on the Grunwald–Letnikov definition of fractional-order differentiation.

Interpretation of initial conditions is another problem arising in modeling with fractional derivatives. Though initial conditions for the Caputo derivatives are expressed in terms of initial values of integer-order derivatives, Riemann-Liouville fractional derivatives require initial conditions expressed in terms of initial values of fractional derivatives of the unknown function (Podlubny 1999, Samko *et al.* 1993). Heymans and Podlubny (2006) showed that it is possible to attribute physical meaning to initial conditions expressed in terms of Riemann Liouville fractional derivatives, and the corresponding quantities can be obtained from measurements. They suggested to consider the "inseparable twin" of the function and relate them via a basic physical law, and measure the function's initial values by measuring the corresponding values of its twin to express initial conditions in terms of fractional derivatives of the function. They also demonstrated that, in many instances of practical significance, zero initial conditions, which are used frequently in practice, appear in a natural way. Though in many cases it is possible to explain the physical meaning of initial conditions expressed in terms of fractional derivatives, the definite and general meaning of this language is still difficult to understand.

2.5 Application of Fractional Derivatives in Modeling

It is not a completely novel idea to use fractional calculus for describing dynamical processes in complex media mathematically. Fractional calculus has been applied mostly in electrochemistry to study AC response of rough electrodes. Oldham made significant contributions regarding the mathematical developments of fractional calculus in electrochemistry. Fractional derivatives were applied to model rheological properties of solids, frequency-independent quality factor Fennoscandian uplift, heat diffusion, and in other fields of research (Zhang, 2003; Bagley, 1986; Caputo, 1967; Körnig *et al.*, 1989; Lemehaute, 1983; Hossain *et al.*, 2011; Al-Mutairi *et al.*, 2013;

Zaslavsky, 2002; Hilfer, 2000; Metzler *et al.*, 2004). It was introduced to model sub/super-diffusion transport in the absence and presence of an external field (Barkai *et al.*, 2000; Metzler *et al.*, 1999), tumor invasion (Iomin *et al.*, 2004; Iomin, 2005, and 2006;), and studies related to the dynamics of interfaces between nanoparticles and substrate (Chow, 2005). Using fractional derivatives, one can consider memory of a property by definition (Park *et al.*, 2000). Even though it seems to be more complicated, this approach can be applicable for all time and all distance regimes.

2.5.1 Fluid Modeling with Fractional Derivatives

Fractional calculus has been proven to be a successful tool to extensively describe the constitutive relationships of viscoelastic fluids. Generally, development of fractional-order derivative models of non-Newtonian fluids is initiated by replacing the time derivative of an integer order of a classical differential equation by the Riemann–Liouville or Caputo fractional calculus operators.

Sloninsky (1967) modified the Kelvin-Voigt model by introducing fractional derivatives to describe the relaxation processes in polymers. Bagley and Torvik (1983) showed that models of viscoelastic materials developed using fractional differential equations of order 1/2 are in harmony with molecular theory. Friedrich (1991) established relaxation and retardation functions for the four-parameter Maxwell model. Material functions (complex moduli) of the modified Maxwell model were developed and compared with experimental results by Li and Jiang (1994). Bagley and Torvik (1986) generalized the standard solid model or Zener model using fractional differential equations. They determined the material functions and calculated the parameter range for thermodynamic admissibility. Friedrich (1992) and Glöckle (1991) generalized the models further, respectively. The two models were compared with respect to their usefulness and thermodynamic compatibility by Friedrich (1993). Junqi and Ciqun (1996), Wenchang *et al.* (2002), and Mingyu and Wenchang (2001, 2002) analyzed various problems of rheology using fractional calculus. They found the fractional calculus approach to be more appropriate for viscoelastic fluids. Song and Jiang (1998) obtained a very good fit with experimental data for viscoelastic glue fluids by applying fractional calculus. Fractional derivatives can describe

viscoelastic behavior quite flexibly (Schiessel *et al.*, 1995; Palade *et al.*, 1999; Rossihin *et al.*, 2001).

2.5.2 Applications in Ground-Water Flow

Botha and Cloot (2006) generalised the classical Darcy law regarding the water flow as a function of a non-integer order derivative of the piezometric head. In Darcy's law, the Darcy velocity at a given point and a given time was considered to be dependent on the piezometric head and/or its derivatives at that point or in the direct neighbourhood around that point at that time. They tried to catch the effect of the global spatial distribution of piezometric field and also its past history on the Darcy velocity at the point of consideration at a given time. The information relative to the direct neighbourhood of the specific point under consideration was regarded to have greater influence on the fluid flow than the information dealing with events taking place far away from that point by assigning a weighting factor. To take the effect of history into account, as it is not possible to know the history from time, the behaviour of the fluid particles situated at different but larger distances from the considered point was taken as an image of the behaviour of the fluid particles present at that point for different times in the past. To give more importance to contemporary history than the far past, a weighting factor contained in the integral model acts as a time filter. According to their work, the effect of the geometry of the flow was implicitly included in the model through the integral character of the equation. Then, the generalised Darcy law and the law of conservation of mass were combined to derive a new equation for groundwater flow. Numerical solutions of this equation for various fractional orders of the derivatives were compared with experimental data and Barker's generalised radial flow model, for which a fractal dimension for the flow is assumed. It was found that Cloot and Botha's model and Barker's model had much in common.

In the same line of ideas with Cloot and Botha (2006), Atangana (2014) derived a new equation for groundwater flow by combining the law of conservation of mass and generalized Darcy law regarding the water flow as a function of a noninteger order derivative of the piezometric head. They examined an approximate solution of the generalized groundwater flow equation via the

Frobenius method. The results obtained from his investigation showed better prediction compared to conventional groundwater flow equation.

2.5.3 Applications in Flow Modeling in Petroleum Reservoir

Generally, fractional derivatives are introduced in the flow model of viscoelastic fluids through porous media. Fractional calculus is also used to describe fractal geometry, fractional dimension, and flow through fractals.

Le Mehaute (1984) shows how the fractional derivative must be introduced to describe an irreversible process in a fractal media that involves coupling relations between space and time. He proposed a fractional constitutive equation for describing transfer processes in fractal media. He developed a kinetic equation to describe irreversible phenomena using fractional derivatives. He incorporated the interfacial characteristics into the fractional derivative in space-time. His idea of representing the temporal anomalies in the transfer processes by a convolutional constitutive equation between fluxes and driving forces is interesting, though it cannot be applied to the more general problem of diffusion on fractals.

Giona and Roman (1992) formulated a diffusion equation on fractals for a one-dimensional system in a very simple way within the framework of fractional calculus. Their approach is aimed at describing the average behaviour of the physical quantities on fractals only. They developed a one-parameter family of general fractional-differential diffusion equations, which reproduce the asymptotic behaviour of fractional Brownian motion and the standard model. They solved the fractional equation in one dimension and compared with exact results for fractional Brownian motion and the one-dimensional version of the standard diffusion equation on fractals.

Roman and Giona (1992) generalized their previously developed fractional diffusion equation in isotropic and homogenous fractal structures for d - dimensional Euclidean systems. They obtained the asymptotic behaviour of the probability density function exactly and derived analytical expressions for the scattering and relaxation functions.

Giona and Roman (1992a, and 1992b) considered the ‘standard’ diffusion equation on a fractal to be correct and represented the equation in terms of fractional derivatives. Their research shows that a fractional diffusion equation represents the ‘standard’ diffusion equation on a fractal accurately and more generally. Though they did not consider fractional derivatives as a tool to model independently diffusion on random fractal structures, their research shows that one can use fractional derivatives to model flow in fractal media accurately and generally. Their developed model contains the limitations of the ‘standard’ diffusion equation inherently, because they considered the ‘standard’ diffusion equation to be correct.

Park *et al.* (2000) introduced fractional calculus in the flow equation for fluid in a fractal reservoir. They proposed a general mathematical formula for the analysis of pressure behaviour that is applicable for the whole spatio-temporal domain in the fractal reservoir. The model captures the history and nonlocality of transport. They derived a new general constant-flow-rate solution, which is applicable to whole spatio-temporal ranges, using the Fox H-function. They find that the fractional calculus approach agrees with real fractal reservoirs, particularly that the described pressure behavior of the early-time stages is more accurate. However, they considered compressibility and density to be independent of the position of the media. Additional analysis for various field data and numerical studies is still required.

Tong *et al.* (2004) established relaxation models of non-Newtonian viscoelastic fluids with fractional derivatives in fractal reservoirs. They studied flow characteristics by using the integral transform, the discrete Laplace transform of sequential fractional derivatives and the generalized Mittag-Leffler function. They obtained exact solutions for arbitrary fractional-order derivatives and also long-time and short-time asymptotic solutions for an infinite reservoir. The pressure transient behavior of non-Newtonian viscoelastic fluid flow through an infinite fractal reservoir was studied by using Stehfest's inversion method for the numerical Laplace transform. Their research shows that the clearer the viscoelastic characteristics of the fluid, the more the fluid is sensitive to the order of the fractional derivative.

Tian *et al.* (2006) introduced fractional derivatives into the study of non-Newtonian fluids in porous media and fractal reservoirs. They studied the flow by using the finite integral transform,

the discrete Laplace transform of sequential fractional derivatives, and the generalized Mittag-Leffler function. They obtained exact solutions for arbitrary fractional-order derivatives. The long-time and short-time asymptotic solutions for an infinite reservoir were also obtained. The pressure transient behavior of fluids flowing through an infinite fractal reservoir was studied using Stehfest's inversion method for the numerical Laplace transform. They showed that the order of the fractional derivative affects the whole pressure behavior, particularly that the effect of pressure behavior at the early-time stage is larger.

Shan *et al.* (2009) established relaxation models of non-Newtonian viscoelastic fluids in dual porous media. They studied the flow characteristics using the Hankel transform, the discrete Laplace transform of sequential fractional derivatives, and the generalized Mittag-Leffler function. They obtained exact solutions for arbitrary fractional-order derivatives and also showed results of long-time and short-time asymptotic solutions for an infinite reservoir. The pressure transient behavior of non-Newtonian viscoelastic fluid flow through an infinite dual porous media was studied using Stehfest's inversion method for the numerical Laplace transform. Their research shows that the characteristics of the fluid flow are appreciably affected by the order of the fractional derivative.

Suzuki *et al.* (2010) employed fractional advection-dispersion equations (fADE) to describe non-Fickian mass transport in fractured rock masses. The fractional time derivative in fADE was responsible for the variance of travel time in the tracer responses, resulting in the non-Fickian transport. Their research supports that fADE can be used for characterizing complex fluid flow in geothermal reservoirs.

2.6 Discussions and Future Directions

Due to difficulty in describing pore space, difficulty in observing detailed processes occurring in the pore space, and the high cost of CT scanning, a general mathematical model is required that would act as a platform to represent different types of flow of different fluids in different reservoirs, would have low computational time, and would capture the majority of the processes occurring in a reservoir. Memory functions and fractional derivatives come to the model to capture

the effects of history and the effects of other processes within the reservoir that are not captured explicitly. This development of general models could be an exciting research topic for future researchers.

2.7 Conclusions

Memory, an important characteristic of rock and fluids, has been reviewed and defined. Models that incorporate memory have been reviewed. Fractional derivatives and their physical meaning have been studied, and their application in incorporating memory is discussed. Finally, the necessity of a general memory-based model is realized and recommended.

Bibliography

1. Abel, Niels H. (1881). Solution de quelques problémés à l'aide d'intégrales définies, in *Oeuvres Complétes* Christiania (Grondahl), 1, 16-18.
2. Adler, P.M., Jacquin, C.G., Quiblier, J.A. (1990). Flow in simulated porous media. *International Journal Multiphase Flow*. *16*, 691–712.
3. Al-Mutairi, S.M., Abu-khamsin, S.A., Hossain, M.E. (2013). A Novel Approach to Handle Continuous Wettability Alteration during Immiscible CO2 Flooding Process, in: Abu Dhabi Int. Pet. Conf. Exhib., Society of Petroleum Engineers. doi:10.2118/160638-MS.
4. Al-Raoush, R., Thompson, K. E., and Willson, C. S. (2003). Comparison of network generation techniques for unconsolidated porous media systems. *Soil Science Society of America Journal*, *67*, 1687–1700.
5. Atangana, A., and Vermeulen, P. D. (2014). Analytical solutions of a space-time fractional derivative of groundwater flow equation. *Abstract and Applied Analysis, 2014*, Article ID 381753.
6. Bagley, R.L., Torvik, P.T. (1983). A theoretical basis for the application of fractional calculus to viscoelasticity. *Journal of Rheology, 27*(3), 201–210.
7. Bagley, R.L., Torvik, P.T. (1986). On the fractional calculus model of viscoelastic behavior. *Journal of Rheology, 30*(1), 133–155.
8. Bakke, S., Øren, P.E. (1997). 3D pore-scale modeling of sandstones and flow simulations in the pore networks. *SPE Journal, 2*, 136–49.
9. Baldwin, C. A., Sederman, A. J., Mantle, M. D., Alexander, P., and Gladden, L. F. (1996). Determination and characterization of the structure of a pore space from 3d volume images. *Journal of Colloid and Interface Science*, 181, 79–92.
10. Balhoff M.T., Thompson, K.E. (2004). Modeling the steady flow of yield-stress fluids in packed beds. *AIChE Journal*, *50* (12), 3034–3048.
11. Barkai, E., Metzler, R., Klafter, J. (2000). From continuous time random walks to the fractional Fokker-Planck equation. *Physical Review E. 6*(1), 132–138. doi:10.1103/PhysRevE.61.132.

12. Blunt, M., King, P. (1990). Macroscopic parameters from simulations of pore scale flow. *Physical Review A, 42*(8), 4780–7.
13. Blunt, M., King, P. (1991). Relative permeabilities from two- and three dimensional pore-scale network modelling. *Transport of Porous Media, 6*, 407-33.
14. Boek, E.S., Venturoli, M. (2010). Lattice-Boltzmann studies of fluid flow in porous media with realistic rock geometries. *Computer and Mathematics with Applications, 59*(7), 2305–14.
15. Botha, J. F., and Cloot, A. H. (2006). A generalised groundwater flow equation using the concept of non-integer order derivatives, *Water SA*, *32*(1), 1–7.
16. Boyer, Carl, B. (1970). The History of the Calculus, *The Two-Year College Mathematics Journa*l*, 1*(1), 60-86.
17. Butzer, P.L., Westphal, U. (2000). An introduction to fractional calculus. In: Hilfer R (ed.) *Applications of fractional calculus in physics*. Singapore: World Scientific Publishing Co. Pte Ltd.
18. Caputo, M. (1967). Linear Models of Dissipation whose Q is almost Frequency Independent--II, *Geophysical Journal International, 13,* 529–539. doi:10.1111/j.1365-246X.1967.tb02303.x.
19. Caputo, M. (2000). Models of Flux in Pous Media with Memory. *Water Resources Research, 36*, 693-705.
20. Carreau P.J., Kee, D. D., Chhabra, R.P. (1997). *Rheology of Polymeric Systems*. Hanser Publishers.
21. Chapuis, R.P., Aubertin M. (2003). On the use of the Kozeny-Carman equation to predict the hydraulic conductivity of soils. *Canadian Geotechnical Journal, 40*(3), 616-28.
22. Chen, S., Doolen, G.D. (1998). Lattice Boltzmann method for fluid flows. *Annual Review of Fluid Mechanics, 30*, 329–64.
23. Chow, T.S. (2005). Fractional dynamics of interfaces between soft-nanoparticles and rough substrates, *Physics Letter A., 342*, 148–155. doi:10.1016/j.physleta.2005.05.045.
24. De Espi´ındola, J.J., Da Silva Neto, J.M., and Lopes, E.M.O. (2005). A Generalized Fractional Derivative Approach to Viscoelastic Material Properties Measurement. *Applied Mathematics and Computation*, *164*(2), 493–506.
25. Debnath, L., (1995), *Integral Transforms and Their Applications* (Boca Raton: CRC Press).

26. Delerue J. F., and Perrier. E. (2002). Dxsoil, a library for 3d image analysis in soil science. *Computational Geosciences, 28*(9), 1041–1050.
27. Demianov, A., Dinariev, O., Evseev, N. (2011). Density functional modelling in multiphase compositional hydrodynamics. *Canadian Journal of Chemical Engineering, 89*, 207.
28. Di Giuseppe, E., Moroni, M. and Caputo, M. (2010). Flux in Porous Media with Memory: Models and Experiments. *Transport in Porous Media*, 83, 479–500.
29. Dixit, A.B., McDougall, S.R., Sorbie, K.S. (1998). A pore-level investigation of relative-permeability hysteresis in water-wet systems. *SPE Journal, 3*, 115-23.
30. Dixit, A.B., McDougall, S.R., Sorbie, K.S., Buckley, J.S. (1999). Pore-scale modeling of wettability effects and their influence on oil recovery. *SPE Reservoir Evaluation Eng, 2*, 25–36.
31. Dixit, A.B., Buckley, J.S., McDougall, S.R., Sorbie, K.S. (2000). Empirical measures of wettability in porous media and the relationship between them derived from pore-scale modeling. *Transport in Porous Media, 40*(1), 27–54.
32. Du Plessis, J.P. (1994). Analytical quantification of coefficients in the Ergun equation for fluid friction in a packed bed. *Transport in Porous Media, 16*(2), 189-207.
33. Dunsmuir, J. H., Ferguson, S. R., D'Amico, K. L. and Stokes, J. P. (1991). X-ray microtomography: a new tool for the characterization of porous media. *Paper SPE 22860, Proceedings of the 66th SPE Annual Technical Conference and Exhibition, Dallas, TX, 6-9 October*, 1991.
34. Elias, B.P., and Hajash, Jr., A. (1992). Changes in quartz solubility and porosity due to effective stress: An experimental investigation of pressure solution, *Geology*, 20, 451-454.
35. Euler, Leonhard. (1738). De progressionibus transcendentibus, sev quarum termini generales algebraice dari nequent Commentarii Academiae Scientiarum Imperialis Scientiarum Petropolitanae 5, 55.
36. Fatt, I. (1956a). The network model of porous media I. Capillary pressure characteristics, *AIME*, *207*, 144-159.
37. Fatt, I. (1956b). The network model of porous media II. Dynamic properties of a single size tube network, *Trans AIME*, *207*, 160-163.
38. Fatt, I. (1956c). The network model of porous media III. Dynamic properties of networks with tube radius distribution, *Trans AIME*, *207*, 164-181.

39. Ferreol, B., and Rothman, D. H. (1995). Lattice-Boltzmann simulations of flow through Fontainebleau porous media. *Transport in Porous Media*, 20(1-2), 3–20, 1995.
40. Fourier, Joseph B J. (1822) *La Théorie Analytique de la Chaleur*, (English Translation by A. Freeman, Dover Publication, 1995).
41. Friedrich Chr. (1991). Relaxation and retardation functions of the Maxwell model with fractional derivatives. *Rheologica Acta, 30*, 151–158.
42. Friedrich, C., Braun H. (1992). Generalised Cole-Cole behavior and its rheological relevance. *Rheologica Acta. 31*, 309–322.
43. Friedrich, C. (1993). Mechanical stress relaxation in polymers: fractional integral model versus fractional differential model. *Journal of Non-Newtonian Fluid Mechanics, 46*, 307–314.
44. Giona, M., and Roman, H. E. (1992a). Fractional Diffusion Equation for Transport Phenomena in Random Media, *Physica A*, 185, 87-97.
45. Giona, M., and Roman, H. E. (1992b). Fractional Diffusion Equation on Fractals: One Dimensional Case and Asymptotic Behaviour. *Journal of Physics A: Mathematical and General, 25*, 2093-05.
46. Glöckle, W.G., Nonnenmacher, T.F. (1994). Fractional relaxation and the time-temperature superposition principle. *Rheologica Acta, 33*, 337–343.
47. Glöckle, W.G., Nonnenmacher, T.F. (1991). Fractional integral operators and Fox functions in the theory of viscoelasticity in the theory of viscoelasticity. *Macromolecules, 24*, 6426–6434.
48. Grunau, D., Chen, S., and Eggert. K. (1993). A lattice boltzmann model for multiphase fluid flows. *Physics of Fluids A - Fluid Dynamics*, 5(10), 2557–2562.
49. Gunstensen, A. K., and Rothman, D. H., Zaleski, S., and Zanetti G. (1991). Lattice boltzmann model of immiscible fluids. *Physical Review A*, 43(8), 4320–4327.
50. Gunstensen, A.K., Rothman, D.H. (1993). Lattice-Boltzmann studies of immiscible two-phase flow through porous media. *Journal of Geophysical Research, 98*(B4), 6431–6441.
51. Hao, L., Cheng, P. (2010). Pore-scale simulations on relative permeabilities of porous media by lattice Boltzmann method. *International Journal of Heat and Mass Transfer, 53*(9–10), 1908–13.

52. Hassan, A.M., Hossain, M.E. and Rammay, M.H. (2015a). Investigation of Reservoir Heterogeneity Using Memory-Based Diffusivity Equation. *Journal of Nature Science and Sustainable Technology, 9*(4), 713-723.
53. Hassan, A.M., Hossain, M.E. and Rammay, M.H., (2015b). Memory-based Diffusivity Equation: A Comprehensive Study on Variable Rock and Fluid Properties. *Journal of Nature Science and Sustainable Technology, 9*(4), 2015.
54. Heymans N, Bauwens J-C. (1994). Fractal rheological models and fractional differential equations for viscoelastic behavior. *Rheologica Acta, 33*, 210–219.
55. Heymans, N., and Podlubny, I. (2006). Physical interpretation of initial conditions for fractional differential equations with Riemann Liouville fractional derivatives. *Rheologica Acta*, 45, (5), 765-772.
56. Hilpert, M., McBride, J.F., Miller, C.T. (2000). Investigation of the residual-funicular nonwetting-phase-saturation relation. *Advances in Water Resources*, 24(2), 157-177.
57. Hilpert, M., Miller, C.T. (2001). Pore-morphology-based simulation of drainage in totally wetting porous media. *Advances in Water Resources, 24*, 243-55.
58. Hossain, M.E., Islam, M.R. (2006). Fluid properties with memory a critical review and some additions, in: Proceedings of 36th *International Conference on Computers and Industrial Engineering* CIE–00778, Taipei, Taiwan, 20–23.
59. Hossain, M. E., Mousavizadegan, S. H., Ketata, C., and Islam, M. R. (2007). A novel memory based stress-strain model for reservoir characterization. *Journal of Nature Science and Sustainable Technology,* 1, 653–678.
60. Hossain, M. E., Mousavizadegan, S. H., and Islam, M. R. (2009). Effects of Memory on the Complex Rock-Fluid Properties of a Reservoir Stress-Strain Model. *Petroleum Science and Technology, 27*(10), 1109–1123.
61. Hossain, M.E., and Islam, M.R., A (2009). Comprehensive Material Balance Equation with the Inclusion of Memory During Rock Fluid Deformation. *Advances in Sustainable Petroleum Engineering Science, 1*(2), 141–162.
62. Hossain, M.E., Abu-khamsin, S. (2011). Use of the Memory Concept to Investigate the Temperature Profile during a Thermal EOR Process, SPE 149094, in: *SPE/DGS Saudi Arab. Sect. Tech. Symp. Exhib., Society of Petroleum Engineers*, 2011.

63. Hossain, M.E. and Abu-Khamsin, S.A. (2012a). Utilization of Memory Concept to Develop Heat Transfer Dimensionless Numbers for Porous Media Undergoing Thermal Flooding with Equal Rock-Fluid Temperatures. *Journal of Porous Media. 15*(10), 937 – 953.
64. Hossain, M.E., Mousavizadegan, S.H., and Islam, M.R. (2008). A new porous media diffusivity equation with the inclusion of rock and fluid memories: *SPE-114287-MS, Society of Petroleum Engineers*.
65. Hristov, J. (2015). Diffusion models with weakly singular kernels in the fading memories: How the integral-balance method can be applied?, *Thermal Science, 19*(3): 947-957.
66. Hulsen. M.A. (1990). A numerical method for solving steady 2D and axisymmetrical viscoelastic flow problems with an application to inertia effects in contraction flows. Faculty of Mechanical Engineering and Marine Technology, MEMT report no. 11, Delft University of Technology.
67. Iaffaldano, G., Caputo, M., and Martino, S. (2005). Experimental and theoretical memory diffusion of water in sand. *Hydrology and Earth System Sciences*, 10, 93-100.
68. Iomin, A., Dorfman, S., and Dorfman, L. (2004). On tumor development: fractional transport approach. http://arxiv.org/abs/q-bio/0406001.
69. Iomin, A. (2005). Superdiffusion of cancer on a comb structure, *Journal of Physics: Conference Series, 7*, 57–67. doi:10.1088/1742 6596/7/1/005.
70. Iomin, A. (2006). Toy model of fractional transport of cancer cells due to self-entrapping, *Physical Review E. 73*. doi:10.1103/PhysRevE.73.061918.
71. Joekar-Niasar, V., Dijke M. I. J. V., and Hassanizadeh S. M. (2012). Pore-Scale Modeling of Multiphase Flow and Transport: Achievements and Perspectives. *Transport in Porous Media*, 94:461–464, DOI 10.1007/s11242-012-0047-4.
72. Jones, W.M. (1976). The flow of dilute aqueous solutions of macromolecules in various geometries: IV. the Ergun and Jones equations for flow through consolidated beds. *Journal of Physics D: Applied Physics, 9*(5), 771-2.
73. Junqi, H., Ciqun, L. (1996). Analysis of general second-order fluid flow in double cylinder rheometer. *Science China (Ser. A) 26*(10), 912–920.
74. Kamath, J., Xu, B., Lee, S.H., Yortsos, Y.C. (1998). Use of pore network models to interpret laboratory experiments on vugular rocks. *Journal of Petroleum Science and Engineering, 20*, 109-115.

75. Kang, Q., Lichtner, P.C., Zhang, D. (2006). Lattice Boltzmann pore-scale model for multicomponent reactive transport in porous media. *Journal of Geophysical Research, 111*:B05203.
76. Keunings, R. (2003). Finite element methods for integral viscoelastic fluids. *Rheology Reviews*,167–195.
77. Keunings, R. (2004). Micro-macro methods for the multi-scale simulation of viscoelastic flow using molecular models of kinetic theory. *Rheology Reviews*, pages 67–98.
78. Kolomietz, V.M. (2014). Memory effects in nuclear Fermi-liquid, *Physical Review C-Nuclear Physics*, 45, 609–627.
79. Körnig, M., Müller, G. (1989). Rheological models and interpretation of postglacial uplift, *Geophysical Journal International, 98*, 243–253. doi:10.1111/j.1365-246X.1989.tb03349.x.
80. Kozicki, W., Tiu, C. (1988). A unified model for non-Newtonian flow in packed beds and porous media. *Rheologica Acta, 27*(1), 31-8.
81. Lacroix, S. F. (1819). *Traité du Calcul Différentiel et du Calcul Intégral Paris* (Courcier) 3, second edition, 409-410.
82. Landel, R. F., Peng, S. T. J. (1986). Equations of State and Constitutive Equations. *Journal of Rheology*, 30(4), 741-766.
83. Laplace, P. S. (1820). *Théorie Analytique des Probabilités Paris* (Courcier).
84. Larson, R.G. (1988). *Constitutive Equations for Polymer Melts and Solutions*. Butterworth Publishers,.
85. Leibniz, G W. (1695a). Letter from Hanover, Germany to G.F.A. L'Hospital, September 30, 1695, in Mathematische Schriften 1849, reprinted 1962, Hildesheim, Germany (Olms Verlag) 2, 301-302.
86. Leibniz, G W. (1695b). Letter from Hanover, Germany to Johann Bernoulli, December 28, 1695, ibid., 3.1, 226.
87. Leibniz, G W. (1697). Letter from Hanover, Germany to John Wallis, May 28, 1697, ibid., 4, 25.
88. Lemehaute, A., Crepy, G. (1983). Introduction to transfer and motion in fractal media: The geometry of kinetics. *Solid State Ionics*. 9-10, 17–30. doi:10.1016/0167- 2738(83)90207-2.

89. Liang, Z.R., Philippi, P.C., Fernandes, C.P., Magnani, F.S. (1999). Prediction of permeability from the skeleton of three-dimensional pore structure. *SPE Reservoir Evaluation Eng, 2*, 161–8.

90. Li, J., Jiang, T.Q. (1994). Constitutive equation for viscoelastic fluids via fractional derivative. In: Siginer DA, Yanovsky YG (eds) Advances in Structured and Heterogeneous Continua. Allerton Press, Inc., New York.

91. Liouville, J. (1832). Mémoire sur l'integration de l'équation $(mx^2 + nx + p)\frac{d^2y}{dx^2} + (qx + r)\frac{dy}{dx} + sy = 0$ à l'aide des différentielles à indices quelconques Journal d 1'Ecole Polytechnique 13, cahier 21, 163-186.

92. Machado, J. A. T. (2003). A probabilistic interpretation of the fractional order differentiation, *Fractional Calculus and Applied Analysis, 6* (1), 73-80.

93. Machado, J. T., Kiryakova, V., Mainardi, F. (2010). A poster about the old history of fractional calculus. *Fractional Calculus and Applied Analysis,* 13 (4), 447–454.

94. Manwart, C., Aaltosalmi, U., Koponen, A., Hilfer, R., Timonen, J. (2002). Lattice-Boltzmann and finite-difference simulations for the permeability for three-dimensional porous media. *Physical Revies E*, 66, 16702–13.

95. Mehaute, A. L. 1984. Transfer processes in fractal media. *Journal of Statistical Physics* 36, 665–676.

96. Metzler, R., Glockle, W. G., and Nonnenmacher, T. F. (1994). Fractional Model Equation for Anomalous Diffusion. *Physica A*, 211, 13-24.

97. Metzler, R., and T. F. Nonnenmacher. (1997). Fractional Diffusion: Exact Representations of Spectral Functions. *Journal of Physics A: Mathematical and General, 30*, 1089-93.

98. Metzler, R., Barkai, E., Klafter, J. (1999). Anomalous Diffusion and Relaxation Close to Thermal Equilibrium: A Fractional Fokker-Planck Equation Approach, *Physical Review Letters*, 82, 3563–3567. doi:10.1103/PhysRevLett.82.3563.

99. Metzler, R., Klafter, J. (2004). The restaurant at the end of the random walk: recent developments in the description of anomalous transport by fractional dynamics, *Journal of Physics A: Mathematical and General, 37*, R161–R208. doi:10.1088/0305-4470/37/31/R01.

100. Mingyu, X., Wenchang, T. (2001). Theoretical analysis of the velocity field stress field and vortex sheet of generalized second order fluid with fractional anomalous diffusion. *Science China (Ser. A)* 31(7), 626–638.
101. Mingyu, X., Wenchang, T. (2002). The expression of generalized fractional element networks and generalized solution for the constitutive equation of viscoelastic materials. *Science China (Ser. A)* 32(8), 673–681.
102. Okabe, H. and Blunt, M. J. (2003). Multiple-point statistics to generate geologically realistic pore-scale representations. Proceedings of the society of core analysts annual meeting, SCA2003-A33, 22-25 September, PAU, FRANCE.
103. Øren, P. E., Bakke, S., and Arntzen, O. J. (1998). Extending predictive capabilities to network models. *SPE Journal*, 3(4), 324–336.
104. Øren, P. E., and Bakke, S. (2002). Process based reconstruction of sandstones and prediction of transport properties. *Transport in Porous Media*, 46(2-3), 311– 343.
105. Owens, R.G., Phillips, T.N. *Computational Rheology*. Imperial College Press, 2002.
106. Palade, L.I., Attane, P., Huilgol, R.R., and Mena, B. (1999). Anomalous stability behavior of a properly invariant constitutive equation which generalizes fractional derivative models. *International Journal of Engineering Science,* 37, 315N329.
107. Pan, C., Hilpert, M., Miller, C.T. (2004). Lattice-Boltzmann simulation of two-phase flow in porous media. *Water Resources Research*, 40, W01501.
108. Park, H. W., Jang I. S., and Kang, J. M. (1998). An analytic approach for pressure transients of fractally fractured reservoirs with variable apertures. *In Situ,* 22:321–337.
109. Park, H.W., Choe, J., Kang, J.M. (2000). Pressure behavior of transport in fractal porous media using a fractional calculus approach. *Energy Sources,* 22(10), 881–890. doi:10.1080/00908310051128237.
110. Patzek, T.W. (2001). Verification of a complete pore network simulator of drainage and imbibition. *SPE Journal*, 6(2), 144–56.
111. Pearson, J.R.A., Tardy, P.M.J. (2002). Models for flow of non-Newtonian and complex fluids through porous media. *Journal of Non-Newton Fluid Mechanics*, 102(2), 447-73.
112. Pilotti, M. (2000). Reconstruction of clastic porous media. *Transport in Porous Media*, 41(3), 359–64.
113. Podlubny, I. (1999). *Fractional Differential Equations*. Academic Press, San Diego

114. Podlubny, I. (2002). Geometric and physical interpretation of fractional integration and fractional differentiation. *Fractional Calculus and Applied Analysis,* 5, 367– 386.

115. Porter, M.L., Schaap, M.G., Wildenschild, D. (2009). Lattice-Boltzmann simulations of the capillary pressure–saturation–interfacial area relationship for porous media. *Advances in Water Resources*, 32(11), 1632–40.

116. Prodanovic, M., Bryant, S.L., Karpyn, Z.T. (2010). Investigating matrix/fracture transfer via a level set method for drainage and imbibition. *SPE Journal*, 15(1), 125–36.

117. Rammay, M.H., Hassan, A.M., and Hossain, M.E. (2015a). A Comparative Study of PVT Properties Variations Using Darcy and Memory-based Diffusivity Equation. *Journal Nature Science and Sustainable Technology, 1*0(1), 2016.

118. Rammay, M.H., Hassan, A.M., and Hossain, M.E., (2015b). A Comparative Study of Porosity and Permeability Variations Using Darcy and Memory-based Diffusivity Equations. *Journal Nature Science and Sustainable Technology*, *10*(1), 2016.

119. Ramstad, T., Idowu, N., Nardi, C., Øren, P-E. (2011). Relative permeability calculations from two-phase flow simulations directly on digital images of porous rocks. *Transport in Porous Media*; doi:http://dx.doi.org/10.1007/s11242-011-9877-8.

120. Rintoul, M. D., Torquato, S., Yeong, C., Kaene, D. T., Erramili, S., Jun, Y. N., Dabbs, D. M., and Aksay, I. A. (1996). Structure and transport properties of a porous magnetic gel via x-ray microtomography. *Physical Review E*, 54, 2663–2669.

121. Roberts, A. P. (1997). Statistical reconstruction of three-dimesional porous media from two-dimensional images. *Physical Review E*, 56(3):3203–3212.

122. Roman, H. E., and Giona, M. (1992). Fractional diffusion equation on fractals: Three-dimensional case and scattering function. *Journal of Physics A: Mathematical and General,* 30, 3463–3470.

123. Rossihin, Y.A., Shitikova, M.V. (2001). A new method for solving dynamic problems of fractional derivative viscoelasticity. *International Journal of Engineering Science,* 39, 149-176.

124. Ross, B. (1977). The development of fractional calculus 1695-1900. *Historia Mathematica* 4, 75-89.

125. Samko, S.G., Kilbas, A.A., Marichev, O.I. (1993). *Fractional Integrals and Derivatives: Theory and Applications*. Gordon and Breach, Amsterdam.

126. Schaap, M.G., Porter, M.L., Christensen, B.S.B., Wildenshild D. (2007). Comparison of pressure-saturation characteristics derived from computed tomography and lattice Boltzmann simulations. *Water Resources Research*, 43, W12S06.
127. Schiessel, H., Blumen, A. (1993). Hierarchical Analogues to Fractional Relaxation Equations. *Journal of Physics A: Mathematical and General, 26*, 5057-5069.
128. Schiessel, H., Metzler, R., Blumen, A., and Nonnenmacher, T.F. (1995). Generalized viscoelastic models: their fractional equations with solutions. *Journal of Physics A: Mathematical and General*, 28, 6567-6584.
129. Schowalter, W.R. (1978). *Mechanics of non-Newtonian fluids*. Pergamon Press Inc.
130. Shan, L., Tong, D., Xue, L. (2009). Unsteady flow of non-Newtonian visco-elastic fluid in dual porosity media with the fractional derivative. *Journal of Hydrodynamics. Ser. B 21*, 705–713, doi:10.1016/S1001-6058(08)60203-6.
131. Shenoy, A.V. (1993). Darcy-Forchheimer natural, forced and mixed convection heat transfer in non-Newtonian power-law fluid-saturated porous media. *Transport Porous Media*, *11*(3), 219-41.
132. Slonimsky, G.L. (1967). Laws of mechanical relaxation processes in polymer. *Journal of Polymer Science Part C, 16*, 1667–1672.
133. Song, D.Y., Jiang, T.Q. (1998). Study on the constitutive equation with fractional derivative for the vicoelastic fluids—modified Jeffreys model and its application. *Rheologica Acta, 27*, 512–517. doi:10.1007/s003970050138.
134. Spanne, P., Thovert, J. F., Jacquin, C. J., Lindquist, W. B., Jones, K. W., and Adler P. M. (1994). Synchrotron computed microtomography of porous media: topology and transports. *Physical Review Letters*, 73(14), 2001–2004.
135. Stevenson, P. (2003). Comment on "Physical insight into the Ergun and Wen & Yu equations for fluid flow in packed and fluidised beds", by R.K. Niven. *Chemical Engineering Science*, 58(23).
136. Steefel, C.I., DePaolo, D.J., Lichtner, P.C. (2005). Reactive transport modeling: An essential tool and a new research approach for the Earth sciences, *Earth and Planetary Science Letters*, 240, 539-558.
137. Sussman, M., Smereka, P., Osher, S. (1994). A level set approach for computing solutions to incompressible two-phase flow. *Journal of Computational Physics*, 114(1), 146–59.

138. Suzuki, A., Chiba, R., Okaze, T., Niibori, Y., Fomin, S., Chugunov, V., and Hashida, T. (2010). Characterizing non-Fickian transport in fractured rock masses using fractional derivative-based mathematical model, *Geothermal Resources Council Transactions, 34*, 1179-1184.

139. Tartakovsky, A.M., Meakin, P. (2005). A smoothed particle hydrodynamics model for miscible flow in threedimensional fractures and the two-dimensional Rayleigh–Taylor instability. *Journal of Computational Physics*, 207, 610–624.

140. Tian, Ji, Tong, D. (2006). The flow analysis of fluids in fractal reservoir with the fractional derivative. *Journal of Hydrodynamics, Ser. B*,18(3), 287-293.

141. Tong, D., Chen, Q. (1999). Generalized flow analysis of non-Newtonian visco-elastic fluid flow through fractal reservoir. *Applied Mathematics and Mechanics, 20*(12), 1367-1376.

142. Tong, D., Wang, R. (2004). The flow analysis of non-Newtonian visco-elastic fluids with the fractional derivative in fractal reservoir. *Science in China (Ser. G)*, 47(4): 424-441.

143. Van Kats, F. M., and Egberts, P. J. P. (1999). Simulation of three-phase displacement mechanisms using a 2D Lattice-Boltzmann model. *Transport in Porous Media*, 37(1):55–68.

144. Vogel, H.J., Roth, K. (2001). Quantitative morphology and network representation of soil pore structure. *Advances in Water Resources, 24*, 233–42.

145. Wenchang, T., Feng, X., Lan, W. (2002). The exact solution for unsteady Couette flow of generalized second order fluid. *Chinese Science Bulletin, 47*(16), 1226–1228.

146. Xu, B., Kamath, J., Yortsos, Y.C., Lee, S.H. (1999). Use of pore-network models to simulate laboratory corefloods in a heterogeneous carbonate sample. *SPE Journal, 4*, 179-186.

147. Yeong, C., Torquato, S. (1998). Reconstructing random media II. Three dimensional media from two-dimensional cuts. *Physical Review E, 58*, 224–33.

148. Zaslavsky, G. (2002). Chaos, fractional kinetics, and anomalous transport, *Physics Reports, 371*, 461–580. doi:10.1016/S0370-1573(02)00331-9.

149. Zavala-Sanchez, V., Dentz, M., and Sanchez-Vila, X. (2009). *Characterization of Mixing and Spreading in a Bounded Stratified Medium*. *Advances in Water Resources, 32*(5), 635–648.

150. Zhang, H.M. (2003). Driver memory, traffic viscosity and a viscous vehicular traffic flow model, *Transportation Research Part B Methodological, 37*, 27–41. doi:10.1016/S0191-2615(01)00043-1.

Chapter 3

Numerical Modeling of a Memory- based Diffusivity Equation Using the Riemann-Liouville Definition of the Fractional-Order Derivative and Uniform Meshes

Co-Authorship

Chapter 3 is prepared according to the Guidelines for Manuscript Format Theses in the Faculty of Engineering and Applied Science at Memorial University. This chapter has been prepared for submission as a journal article:

T. U. Zaman, S. MacLachlan, and M. E. Hossain (in preparation). "Numerical modeling of a memory-based radial diffusivity equation using the Riemann-Liouville definition of the fractional-order derivative and uniform meshes."

The research work presented in this chapter was conducted by Tareq Uz Zaman under the direction and supervision of M. Enamul Hossain, and the guidance and close supervision of Scott MacLachlan. The manuscript itself was written by Tareq Uz Zaman and reviewed by M. Enamul Hossain and Scott MacLachlan.

3.1 Abstract

Fractional order derivatives, that arise in the diffusion equation to incorporate memory make the equation complex and more challenging to solve analytically and numerically than the conventional diffusion equation. In this paper, a numerical model utilizing the Riemann-Liouville definition of the fractional-order derivative is developed for a time-fractional non-linear diffusion equation. Uniform meshes in both space and time have been used. The equation is also solved analytically for Dirichlet boundary conditions and for an initial condition to validate the numerical

model. Numerical and analytical solutions are compared, and it is found that the numerical and analytical solutions match with negligible error, calculated at a fixed final time for different numbers of time steps. The error results affirm that the discretization method used in the numerical model is consistent, but less than first order accurate in time. The effects of the fractional order on the error are significant, with increasing as the value of the fractional order is increased. The model can be used to investigate the effect of the fractional order on the solution of the diffusion equation.

Keywords: Memory, Numerical Modeling, Fractional diffusion equation, Riemann-Liouville definition, Uniform mesh.

3.2 Introduction

Modeling and simulation of porous media flow is important for development and recovery of petroleum resources. Numerous models and ways to look at subsurface flow phenomena have been developed over more than the past fifty years. Recent years have seen interest in investigation of the effects of history of rock, fluid, fluid flow, and its implication on flow through porous media, commonly referred as memory of rock, fluid, and fluid flow. Memory incorporation makes the governing equations intricate and solving these equations becomes more challenging.

The 'memory' idea is relatively new and growing in petroleum engineering. Zavala-Sanchez *et al.* (2009) showed that a system "remembers" its initial state, which defines memory effects for the effective transport coefficients. Hossain and Abu-Khamsin (2012) defined memory as the effect of past events on the present and future course of developments. Hossain (2006) considers the memory of the fluid as one of the most important and most neglected feature in fluid flow models. In this direction, Hossain *et al.* (2008) proposed the following diffusivity equation

$$\frac{\partial}{\partial x}\left[\frac{\rho k}{\mu} T^{\alpha} \frac{\partial^{\alpha}}{\partial t^{\alpha}}\left(\frac{\partial p}{\partial x}\right)\right] = \rho \phi c_t \frac{\partial p}{\partial t}, \tag{3.1}$$

where $p(x,t)$ is the pressure, $\rho(x,t)$ the fluid density, $\phi(x,t)$ the porosity of the fluid medium, $k(x,t)$ the permeability of the medium, $\mu(x,t)$ the dynamic viscosity of the fluid, $c_t(x,t)$ the total compressibility of the system, α the fractional order of differentiation and T the characteristic time.

The fractional-order derivative is introduced into the mathematical model when memory is incorporated. There is no simple physical or geometric interpretation of the fractional-order derivative. Fractional derivatives have been suggested because they have been shown in some cases to improve the 'fit' between measured physical data and numerical models. However, the discretization of fractional derivative gives some sensible physical meaning and relation to the physical world. The expression found after discretizing the fractional-order derivative term includes discrete history terms that tells that history can be incorporated using fractional-order derivatives.

Derivation of numerical solutions to fractional order differential equations is challenging because of their non-local behaviour. However, a number of studies on numerical approaches to the solution of fractional diffusion equations have appeared in the literature. Shen *et al.* (2005) proposed an explicit finite-difference approximation for a space-fractional diffusion equation. Tadjeran *et al.* (2006) used the Crank–Nicholson method combined with spatial extrapolation to obtain temporally and spatially second-order accurate numerical estimates for a fractional diffusion equation. Liu *et al.* (2011) developed a meshless approach using the L1 approximation for the time-fractional derivative and radial basis function (RBF) approximation for the spatial discretization. Sun and Wu (2006) constructed a finite-difference scheme for fractional diffusion-wave systems. Sweilam *et al.* (2012) applied the Crank-Nicolson finite-difference method to solve a time-fractional diffusion equation. A variational iteration method and the Adomian decomposition method were used by Monami *et al.* (2006) to solve linear fractional partial differential equations. Langlands and Henry (2005) discussed a fractional diffusion equation with Neumann boundary conditions. Cui (2009), Du *et al.* (2010) and Gao *et al.* (2011) presented high spatial accuracy schemes for fractional sub-diffusion and super-diffusion equations.

Instead of treating the fractional order derivative by its definition and discretizing the term that contains the fractional-order derivative, Hossain *et al.* (2008) considered the term as a parameter

and then solved the equation numerically in the way that an integer-order partial differential equation is solved. Hence their numerical solution is not accurate in the mathematical sense. The solution of this fractional-order diffusivity equation is important because it shows the way to solve other fractional-order diffusivity equations.

In this paper, the model of Hossain *et al.* (2008) is solved numerically using the Riemann-Liouville definition of the fractional-order derivative. The L1 algorithm (Oldham *et al.*, 1974) that uses the Riemann-Liouville definition for the fractional-order derivative is applied to discretize the diffusivity equation.

The mathematical model is discretized using uniform meshes in both space and time. For some positive numbers X, and T, and positive integers N_x, and N_t, the grid sizes in space and time are defined by $\Delta x = X/N_x$ and $\Delta t = T/N_t$ respectively. The grid points in the space interval $[0, X]$ are given by $x_i = i\Delta x, i = 0, 1, 2, \dots, N_x$, and the grid points in the time interval $[0, T]$ are labeled $t_n = n\Delta t, n = 0, 1, 2, \dots, N_t$. The value of the function p at the grid points is denoted by $p_i^n = p(x_i, t_n)$.

3.3 Discretization and Numerical Solution Algorithm for Riemann-Liouville Definition

Denoting $C_1(x,t) = \frac{\rho k}{\mu} T^\alpha$ and $C_2(x,t) = \rho\phi c_t$ in Eq. (3.1) gives

$$\frac{\partial}{\partial x}\left[C_1(x_i,t_n)\frac{\partial^\alpha}{\partial t^\alpha}\left(\frac{\partial p}{\partial x}\right)\right]_i^n = C_2(x_i,t_n)\frac{\partial p_i^n}{\partial t}. \tag{3.2}$$

Discretizing this using implicit Euler in time and centred differences in space, writing $F_{i\pm\frac{1}{2}}^n = \left[C_1\frac{\partial^\alpha}{\partial t^\alpha}\left(\frac{\partial p}{\partial x}\right)\right]_{i\pm\frac{1}{2}}^n$ gives

$$\frac{1}{\Delta x}\left(F_{i+\frac{1}{2}}^n - F_{i-\frac{1}{2}}^n\right) = C_2(x_i,t_n)\frac{p_i^n - p_i^{n-1}}{\Delta t}. \tag{3.3}$$

To represent the fractional derivative, we use the L1 algorithm (Oldham *et al.*, 1974), writing

$$\frac{\partial^\alpha u(x_i,t_n)}{\partial t^\alpha} = \frac{t_n^{-\alpha} n^\alpha}{\Gamma(2-\alpha)}\left[\frac{1-\alpha}{n^\alpha} u(x_i,0) + \sum_{j=0}^{n-1}\left\{u\left(x_i, t_n - \frac{j t_n}{n}\right) - u\left(x_i, t_n - \frac{(j+1)t_n}{n}\right)\right\}\{(j+1)^{1-\alpha} - j^{1-\alpha}\}\right] . \quad (3.4)$$

Using this, $F^n_{i+\frac{1}{2}}$ and $F^n_{i-\frac{1}{2}}$ can be written as

$$F^n_{i+\frac{1}{2}} = \frac{1}{\Delta x} C_1\left(x_{i+\frac{1}{2}}, t_n\right)\sigma_{\alpha,\Delta t}\left[\frac{1-\alpha}{n^\alpha}(p^0_{i+1} - p^0_i) + p^n_{i+1} - p^n_i - p^{n-1}_{i+1} + p^{n-1}_i + \sum_{j=1}^{n-1}\omega_j^{(\alpha)}(p^{n-j}_{i+1} - p^{n-j}_i - p^{n-j-1}_{i+1} + p^{n-j-1}_i)\right] , \quad (3.5)$$

$$F^n_{i-\frac{1}{2}} = \frac{1}{\Delta x} C_1\left(x_{i-\frac{1}{2}}, t_n\right)\sigma_{\alpha,\Delta t}\left[\frac{1-\alpha}{n^\alpha}(p^0_i - p^0_{i-1}) + p^n_i - p^n_{i-1} - p^{n-1}_i + p^{n-1}_{i-1} + \sum_{j=1}^{n-1}\omega_j^{(\alpha)}(p^{n-j}_i - p^{n-j}_{i-1} - p^{n-j-1}_i + p^{n-j-1}_{i-1})\right] , \quad (3.6)$$

where

$$\omega_j^{(\alpha)} = (j+1)^{1-\alpha} - j^{1-\alpha} , \quad (3.7)$$

$$\sigma_{\alpha,\Delta t} = \frac{1}{\Delta t^\alpha \Gamma(2-\alpha)} . \quad (3.8)$$

Substitution of Eq. (3.5) and (3.6) into Eq. (3.3), and rearrangement, gives

$$-C_1\left(x_{i-\frac{1}{2}}, t_n\right)p^n_{i-1} + \left[C_1\left(x_{i-\frac{1}{2}}, t_n\right) + C_1\left(x_{i+\frac{1}{2}}, t_n\right) + \frac{C_2(x_i,t_n)\Delta x^2}{\sigma_{\alpha,\Delta t}\Delta t}\right]p^n_i - C_1\left(x_{i+\frac{1}{2}}, t_n\right)p^n_{i+1} = \frac{C_2(x_i,t_n)\Delta x^2}{\sigma_{\alpha,\Delta t}\Delta t}p^{n-1}_i + C_1\left(x_{i+\frac{1}{2}}, t_n\right)G^n_i - C_1\left(x_{i-\frac{1}{2}}, t_n\right)H^n_i + C_1\left(x_{i+\frac{1}{2}}, t_n\right)\frac{1-\alpha}{n^\alpha}(p^0_{i+1} - p^0_i) - C_1\left(x_{i-\frac{1}{2}}, t_n\right)\frac{1-\alpha}{n^\alpha}(p^0_i - p^0_{i-1}) , \quad (3.9)$$

where

$$G_i^n = -p_{i+1}^{n-1} + p_i^{n-1} + \sum_{j=1}^{n-1} \omega_j^{(\alpha)} (p_{i+1}^{n-j} - p_i^{n-j} - p_{i+1}^{n-j-1} + p_i^{n-j-1}) \,, \tag{3.10}$$

$$H_i^n = -p_i^{n-1} + p_{i-1}^{n-1} + \sum_{j=1}^{n-1} \omega_j^{(\alpha)} (p_i^{n-j} - p_{i-1}^{n-j} - p_i^{n-j-1} + p_{i-1}^{n-j-1}) \,. \tag{3.11}$$

Fig. 3.1 shows the computational algorithm for the numerical model. Using the Riemann-Liouville definition of the fractional-order derivative, Eq. (3.9) is written for each grid-point and, then, the coupled system of equations is solved. Here a problem arises to solve the equation. The pressures, the solution of the equation, depend on the calculation of the density, permeability, viscosity, porosity, and compressibility, which themselves depend on these pressures.

To get rid of this dilemma an iterative scheme (fixed-point iteration) is used to update the density, permeability, viscosity, porosity, and compressibility. The approach is illustrated qualitatively by

$$A(\rho, k, \mu, \phi, c_t)^{n,z} \, p^{n,z+1} = RHS^{n,z}.$$

For each time step, and each inner iteration, the pressure, density, permeability, viscosity, porosity, and compressibility data are assumed known from the most recent computational value. At the start of a new time step, the most recent value is that from the solution at the previous time step, while during a given time step, it is that from the last iteration. The coefficients are updated using the new values of pressure as the pressures are updated and this process is continued. The iteration process terminates when the convergence criterion is satisfied. A MATLAB program has been written based on Eq. (3.9) to numerically solve Eq. (3.1).

3.4 Analytical Solution

To validate this algorithm, we consider the case where $C_1 = C_2 = 1$, and find the analytical solution of Eq. (3.1). For $C_1 = C_2 = 1$, the equation becomes linear. Initial and boundary conditions are taken as $p(x, 0) = sin(\pi x)$, and $p(0, t) = p(1, t) = 0$ respectively.

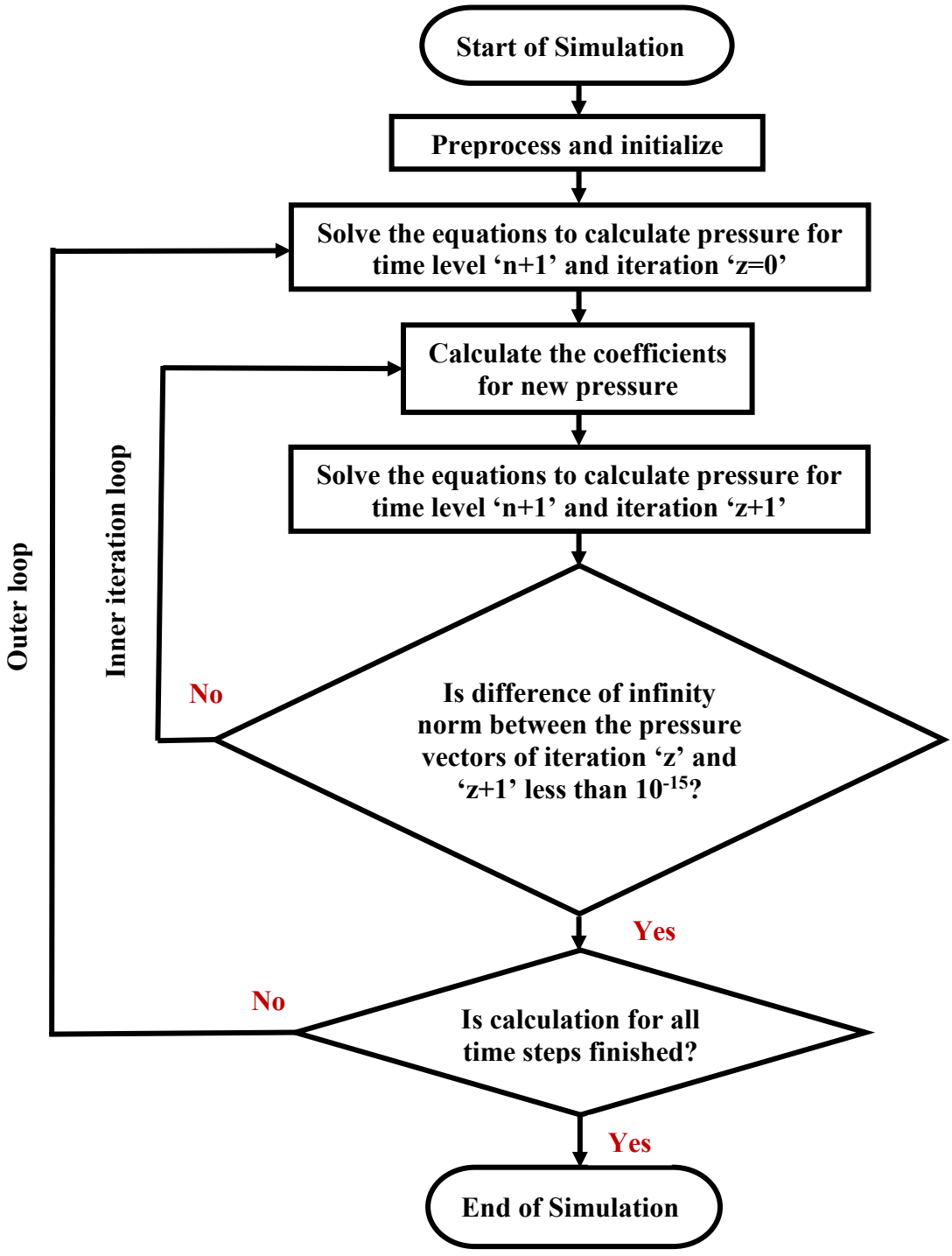

Figure 3.1: Computational algorithm to solve the numerical model.

Utilizing the Riemann-Liouville definition for the fractional-order derivative, the analytical solution of Eq. (3.1) is found as (details shown in Appendix, Eq. A 3.19)

$$p(x,t) = E_{1-\alpha}(-\pi^2 t^{1-\alpha}) sin(\pi x)\ , \tag{3.12}$$

where $E_{1-\alpha}(s)$ is the Mittag-Leffler function, and is defined for $(1-\alpha) > 0$ as

$$E_{1-\alpha}(s) = \sum_{k=0}^{\infty} \frac{s^k}{\Gamma((1-\alpha)k+1)}\ . \tag{3.13}$$

3.5 Results and Discussion

Finding analytical solution of Eq. (3.1) for initial and boundary conditions used in real field applications is very difficult. Numerical model can be helpful in this regard to find the solutions. However, it is required to validate the numerical model before using it to find the solutions. In this section, the validation of the developed numerical model has been checked. In addition, the order of temporal and spatial accuracies of the developed model have been investigated.

3.5.1 Validation of Numerical Models

Numerical solutions are compared with analytical solutions to validate the numerical models. The initial condition, $p(x,0) = sin(\pi x)$, and boundary conditions, $p(0,t) = 0, p(1,t) = 0$, are used for the numerical solution as they are used in the analytical solution. The solutions at 201 equally spaced time steps between $t = 0$ and $t = 1$ are shown in Fig. 3.2 and Fig. 3.3. Fig. 3.2 shows the solutions for $\alpha = 0$ and Fig. 3.3 shows the solutions for $\alpha = 0.25$. The analytical and numerical solutions match very well for $\alpha = 0$. For $\alpha = 0.25$, numerical solutions deviate slightly from the analytical solution for the chosen values of N_x and N_t.

Error values are also computed for different numbers of steps in space and time, and for different α values. Fig. 3.4 presents the change in error with number of time steps for $\alpha = 0, 0.1, 0.25, 0.50, 0.75,$ and 0.90, where the one-dimensional space is divided into 50, and 100

grid-points. In general, the error decreases linearly with the increase in number of time steps with good rate initially. With the increase of number of time steps, the error becomes smaller and the rate of change of the error decreases, until the error values reach a plateau before other errors start to dominate. The trend in error with the number of time steps implies that the numerical model is consistent. Order of temporal accuracies are computed for different values of fractional order, α, and are shown in Table 3.1. Table 3.1 shows that the numerical model is $(1-\alpha)$th-order accurate in time. For large values of α, increasingly many points in time are needed to achieve fixed accuracy. Also, notable in this figure is that the error increases with higher α values.

Fig. 3.4 also depicts that the error decreases with the increase of number of grid-points in space. At very small number of time steps, the differences between error found from 50 and 100 spatial grid-points is insignificant. However, at large numbers of time steps, the differences seen are substantial, reflect smaller spatial discretization error with $N_x = 100$.

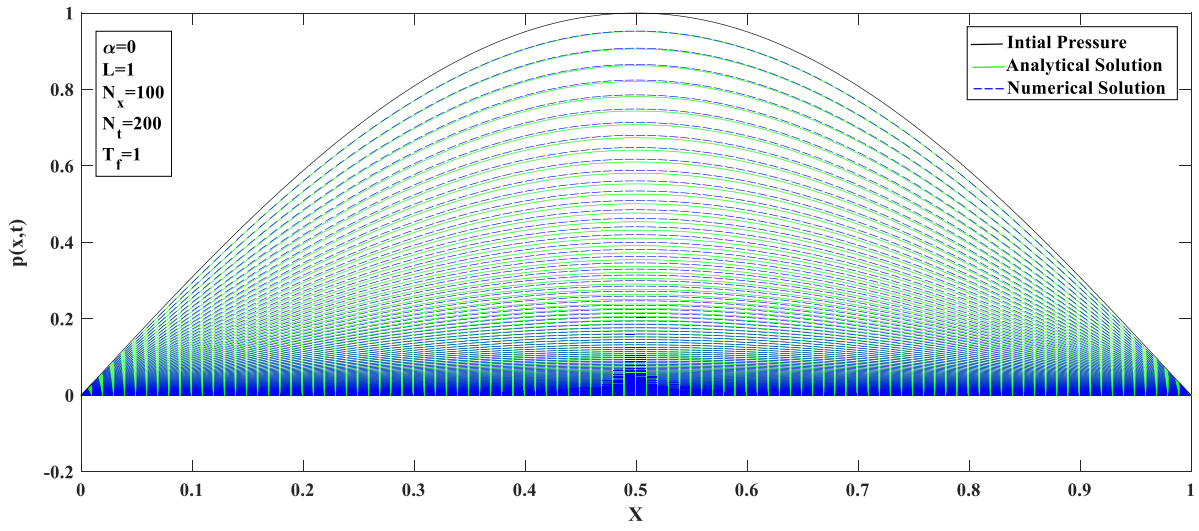

Figure 3.2: Comparison between analytical and numerical solutions for $\alpha = 0$ in RL case.

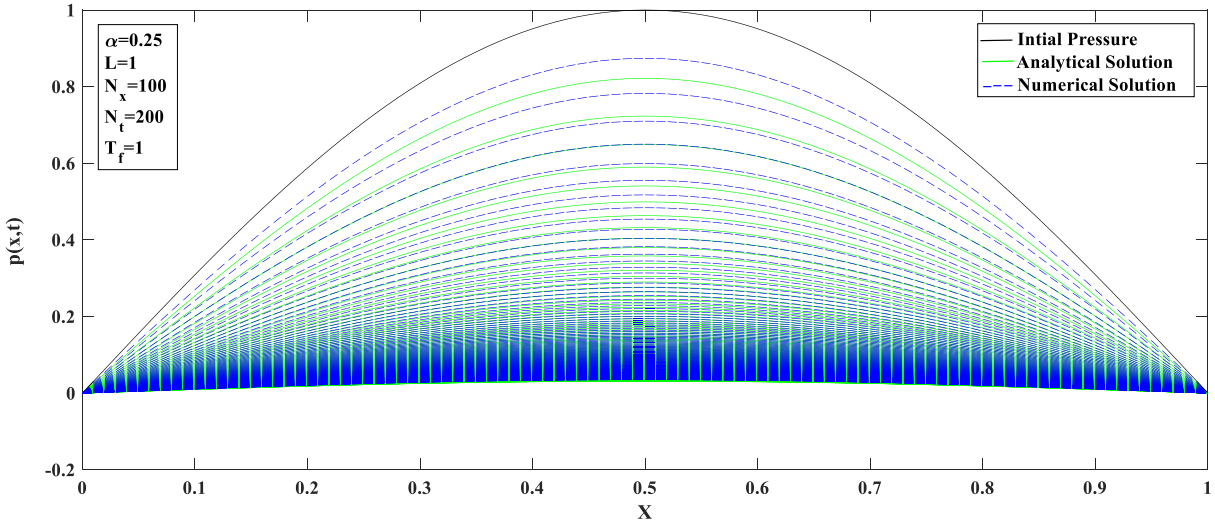

Figure 3.3: Comparison between analytical and numerical solutions for $\alpha = 0.25$ in RL case.

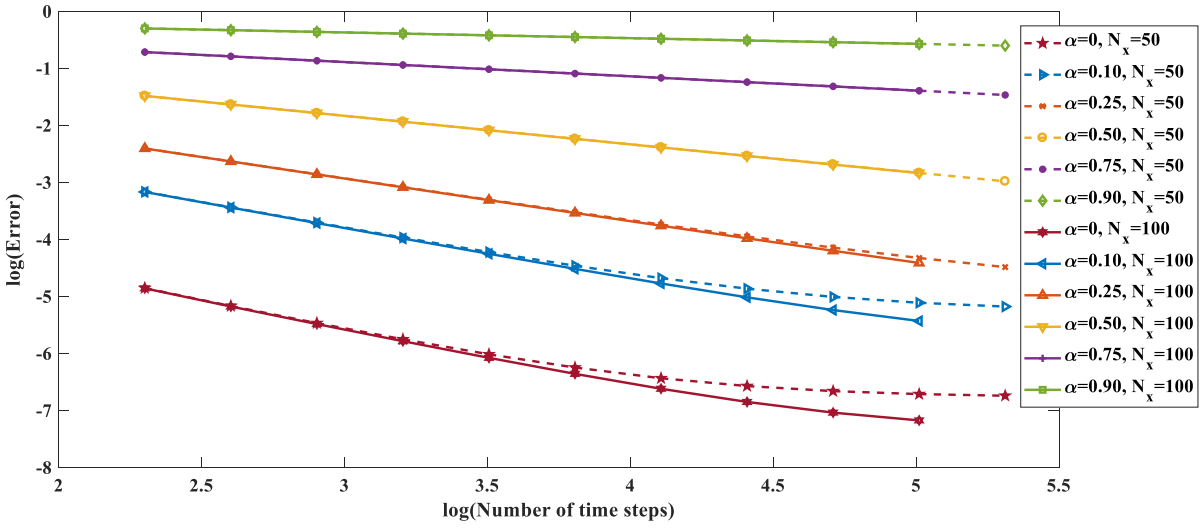

Figure 3.4 Comparison of the error values for different α and N_x.

Table 3.2 shows the error values found using different numbers of grid-points in space and different α values for 200 time steps. Here, the change in error with the change in number of grid-points in space is very small. Since the discretization is first-order in time (for $\alpha = 0$) and second-order in space (for $\alpha = 0$), the errors in this table are dominated by the temporal discretization error. Table 3.3 shows the error values using different numbers of time steps and different α values for 200 grid-points in space. Increasing the number of grid-points in space and/or number of time steps decreases the error. However, the rate of decrease in error is not the same in the two cases. The change observed in the error with changing in number of grid-points in space and time steps implies that the numerical model here is consistent. The tabulated values also show that the deviation of the numerical solution from the analytical solution increases with the increase in the value of α.

Table 3.4 shows the order of spatial accuracies computed for different values of fractional order, α. Order of accuracies for $N_t = 12800, 25600,$ and 51200 are calculated using the error values for $N_x = 10, 20,$ and 40. It is found from Table 3.4 that the numerical model here is second-order accurate in space for $\alpha = 0$.

Considering $\alpha = 0, \Delta x = 0.01,$ and $\Delta t = 0.0001$, the error value 5.6726×10^{-7} is achieved. We now consider the maximum values of length of time step needed to get the same error for $\Delta x = 0.00025$ and for different α values. It is found that the maximum values of length of time step, $\Delta t \leq 1\times10^{-7}$ for $\alpha = 0.1$, $\leq 1\times10^{-9}$ for $\alpha = 0.25$, and $\leq 1\times10^{-14}$ for $\alpha = 0.5$.

These results satisfy Theorem 2 provided by Gracia et al. (2017), that, if translated to our notation, states that the finite difference solution to the time-fractional heat equation is accurate to $O(h^2)$ in space, but only $O(t^{1-\alpha})$ in time.

Table 3.1 Order of temporal accuracy.

Value of fractional order, α	**Order of temporal accuracy**	
	$N_x = 50$	$N_x = 100$
0	0.9946	1.0256
0.10	0.8889	0.9042
0.25	0.7496	0.7535
0.50	0.5006	0.5009
0.75	0.2501	0.2502
0.90	0.1000	0.1000

Table 3.2 Error values for different number of spatial steps and α (No. of time steps = 200).

Total length of space = 1, Total time = 1, Number of time steps = 200			
No. of grid-points in space	**Absolute Error**		
	$\alpha = 0$	$\alpha = 0.25$	$\alpha = 0.50$
50	1.395695e-05	3.927319e-03	3.282228e-02
100	1.380472e-05	3.918687e-03	3.280845e-02
200	1.376672e-05	3.916529e-03	3.280499e-02
400	1.375721e-05	3.915990e-03	3.280413e-02
800	1.375481e-05	3.915855e-03	3.280391e-02
1600	1.375395e-05	3.915818e-03	3.280385e-02
3200	1.375051e-05	3.915796e-03	3.280383e-02
6400	1.373193e-05	3.915752e-03	3.280381e-02

Table 3.3 Error values for different number of time steps and α (No. of spatial steps = 200).

Total length of space = 1, Total time = 1, Number of spatial steps = 200			
No. of time steps	**Absolute Error**		
	$\alpha = 0$	$\alpha = 0.25$	$\alpha = 0.50$
200	1.376672e-05	3.916529e-03	3.280499e-02
400	6.594127e-06	2.319126e-03	2.317149e-02
800	3.230522e-06	1.374807e-03	1.637395e-02
1600	1.602791e-06	8.156872e-04	1.157351e-02
3200	8.022427e-07	4.843112e-04	8.181768e-03
6400	4.052734e-07	2.877807e-04	5.784659e-03

Table 3.4 Order of spatial accuracy.

N_t	Order of spatial accuracy		
	$\alpha = 0$	$\alpha = 0.10$	$\alpha = 0.25$
12800	1.8587	1.6168	0.9162
25600	1.9447	1.7756	1.1657
51200	1.9913	1.8758	1.3968
102400	2.0156	1.9347	1.5882

3.5.2 Significance of the Model and Sensitivity Analysis

It is difficult to interpret analytical solutions of the time fractional diffusion equation for some initial and boundary conditions. This model can help to numerically solve the equation for any initial and boundary conditions. The model also gives us an idea about the effect of the fractional order values on the solution. The solutions of Eq. (3.1) for different α values are shown in Fig. 3.5 considering $(\rho k/\mu)T^{\alpha} = 1$, and $\rho\phi c_t = 1$. Initial and boundary condition are taken as $p(x,0) = sin(\pi x)$, and $p(0,t) = p(1,t) = 0$ respectively. It is found that, with the increase of the α value, the numerical values of the solutions also increase within the range of $0 \leq \alpha < 1$. The equation gives different numerical solutions based on its fractional order while keeping the other parameters constant. Field data shall be used to determine the value of fractional order to accurately model flow phenomenon. From the value of fractional order, the dependence of flow phenomenon on history can be quantified.

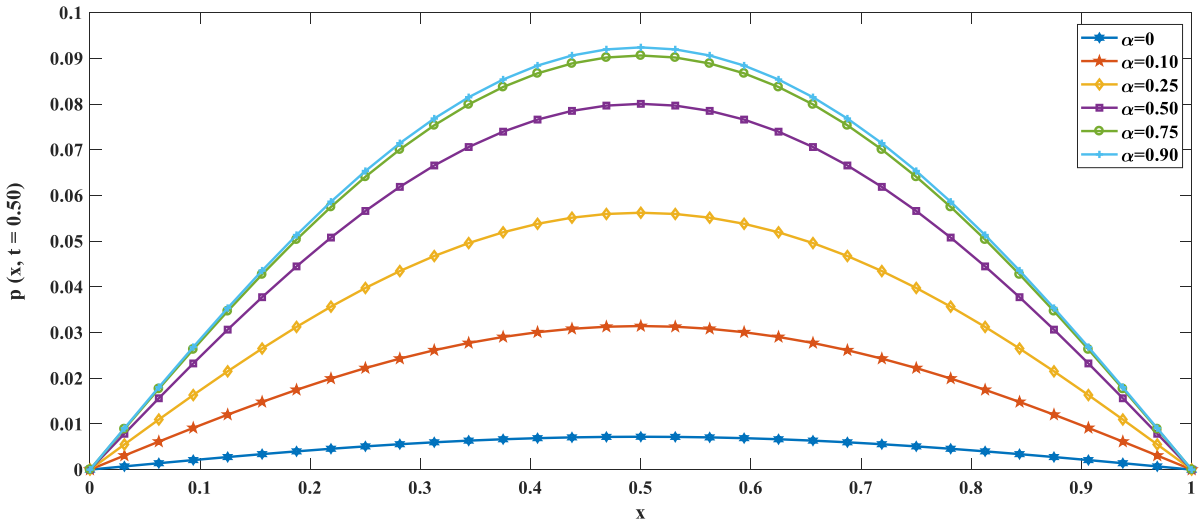

Figure 3.5 Solutions of the time fractional diffusion equation for different α values.

3.6 Conclusions

Numerical models are developed to solve a time-fractional diffusion equation applying the Riemann-Liouville definition for the fractional-order derivative. Uniform mesh spacing in both space and time has been used. The numerical model is validated comparing with an analytical solution. From the error analysis, it can be concluded that the numerical model is consistent, and $(1-\alpha)$th-order accurate in time. The differences among the analytical and numerical solutions increase with the increment of fractional order, α. It is also found that the solution of the diffusion equation increases in size with the increase of α value.

3.7 Acknowledgement

The authors would like to thank the Natural Sciences and Engineering Research Council of Canada (NSERC); Research & Development Corporation of Newfoundland and Labrador (RDC), funding no. 210992; and Statoil Canada Ltd., funding no. 211162 for providing financial support to accomplish this research under the Statoil Chair in Reservoir Engineering at the Memorial University of Newfoundland, St. John's, NL, Canada.

Bibliography

1. Cui, M. (2009). Compact finite difference method for the fractional diffusion equation. *Journal of Computational Physics, 228*, 7792–7804.
2. Du, R., Cao, W., Sun, Z.Z. (2010). A compact difference scheme for the fractional diffusion-wave equation. *Applied Mathematical Modelling, 34,* 2998–3007.
3. Gao, G.H., Sun, Z.Z. (2011). A compact finite difference scheme for the fractional sub-diffusion equations. *Journal of Computational Physics, 230*, 586–595.
4. Gracia, J. L., O'Riordan, E., Stynes, M. (2017). Convergence in positive time for a finite difference method applied to a fractional convection-diffusion problem. *Computational Methods in Applied Mathematics*. (forthcoming).
5. Hossain, M. E., Mousavizadegan, S. H., & Islam, M. R. (2008). A New Porous Media Diffusivity Equation with the Inclusion of Rock and Fluid Memories. *E-Library*, SPE– 114287.
6. Hossain, M. E. (2006). Fluid Properties With Memory – a Critical Review and Some Additions. *The 36th International Conference on Computers and Industrial Engineering June 20-23, 2006, Taipei, Taiwan*, (July), 13.
7. Hossain, M.E., & Abu-Khamsin, S.A. (2012). Utilization of Memory Concept to Develop Heat Transfer Dimensionless Numbers for Porous Media Undergoing Thermal Flooding with Equal Rock-Fluid Temperatures. *Journal of Porous Media. 15*(10), 937 – 953.
8. Langlands, T., Henry, B. (2005). The accuracy and stability of an implicit solution method for the fractional diffusion equation. *Journal of Computational Physics, 205*, 719–736.
9. Liu, Q., Gu, Y., Zhang, P., Liu, F., and Nie, Y. (2011). An implicit RBF meshless approach for time fractional diffusion equations. *Computational Mechanics, 48*, 1–12.
10. Momani, S., & Odibat, Z. (2006). Analytical approach to linear fractional partial differential equations arising in fluid mechanics. *Physics Letters A*, *355*(4–5), 271–279. http://doi.org/DOI 10.1016/j.physleta.2006.02.048
11. Murio, D. A. (2008). Implicit finite difference approximation for time fractional diffusion equations. *Computers and Mathematics with Applications*, *56*(4), 1138–1145. http://doi.org/10.1016/j.camwa.2008.02.015.
12. Oldham, K. B., Spanier, J. (1974). *The Fractional Calculus*, Academic Press, Inc., California.

13. Shen, S. (2004). Error analysis of an explicit finite difference approximation for the space fractional diffusion equation with insulated ends. *ANZIAM Journal*, *46*(August 2014), 1–10. http://doi.org/10.21914/anziamj.v46i0.995
14. Sun, Z.Z., Wu, X. (2006). A fully discrete difference scheme for a diffusion-wave system. *Applied Numerical Mathematics, 56*, 193–209.
15. Sweilam, N. H., Khader, M. M., & Mahdy, A. M. S. (2012). Crank-Nicolson finite difference method for solving time-fractional diffusion equation. *Journal of Fractional Calculus and Applications, 2*(2), 1–9.
16. Tadjeran, C., Meerschaert, M. M., & Scheffler, H.-P. (2006). A second-order accurate numerical approximation for the fractional diffusion equation. *Journal of Computational Physics*, *213*(1), 205–213. http://doi.org/10.1016/j.jcp.2005.08.008
17. Zavala-Sanchez, V., Dentz, M., and Sanchez-Vila, X. (2009). Characterization of Mixing and Spreading in a Bounded Stratified Medium. *Advances in Water Resources, 32*(5), 635–648.

Appendix

Analytical Solution

Considering unit value for all the coefficients of Hossain et al.'s equation, Eq. (3.1) can be written as

$$\frac{\partial}{\partial x}\left[\frac{\partial^{\alpha}}{\partial t^{\alpha}}\left(\frac{\partial p}{\partial x}\right)\right]=\frac{\partial p}{\partial t}\,. \tag{A 3.1}$$

Take, $p(x,t)=f(t)sin(\pi x)$ with $f(0)=1$.

This gives

$$p(x,0)=sin(\pi x)\,, \tag{A 3.2}$$

$$p(0,t)=0\,, \tag{A 3.3}$$

$$p(1,t)=0\,. \tag{A 3.4}$$

Then, $\frac{\partial f}{\partial t}sin(\pi x)=-\pi^{2}\left(\frac{\partial^{\alpha}}{\partial t^{\alpha}}f(t)\right)sin(\pi x)\,,$ (A 3.5)

$$or,\frac{\partial f}{\partial t}=-\pi^{2}\frac{\partial^{\alpha}f(t)}{\partial t^{\alpha}},\ \ [f(0)=1]\,. \tag{A 3.6}$$

Taking the Laplace Transform in time

$$\mathcal{L}\left[\frac{\partial f}{\partial t}\right]=sF(s)-f(0)=sF(s)-1\,. \tag{A 3.7}$$

For the Riemann-Liouville definition of the fractional order derivative,

$$\mathcal{L}\left[\frac{\partial^\alpha f}{\partial t^\alpha}\right] = s^\alpha F(s) - [D^{\alpha-1} f(t)]_{t=0}\,, \tag{A 3.8}$$

where $D^{\alpha-1} f(t)$ represents the derivative of $f(t)$ of order $\alpha - 1$.

Take $[D^{\alpha-1} f(t)]_{t=0} = c$. (A 3.9)

We get

$$sF(s) - 1 = -\pi^2 (s^\alpha F(s) - c)\,, \tag{A 3.10}$$

$$or, F(s) = \frac{1+\pi^2 c}{s+\pi^2 s^\alpha} = \frac{(1+\pi^2 c)s^{-\alpha}}{s^{1-\alpha}+\pi^2}\,. \tag{A 3.11}$$

It is known that

$$\mathcal{L}\left[x^{c_1-1} E_{c_2,c_1}(c_3 x^{c_2})\right] = \frac{s^{c_2-c_1}}{s^{c_2}-c_3}\,, \tag{A 3.12}$$

where E represents the generalized Mittag-Leffler function.

Comparing $\frac{s^{c_2-c_1}}{s^{c_2}-c_3}$ with $\frac{(1+\pi^2 c)s^{-\alpha}}{s^{1-\alpha}+\pi^2}$ we get $c_2 = 1-\alpha, c_1 = 1, c_3 = -\pi^2$.

Therefore, $f(t) = (1+\pi^2 c) E_{1-\alpha,1}(-\pi^2 t^{1-\alpha})$. (A 3.13)

Recognizing $D^{\alpha-1} f = I^{1-\alpha} f, \quad$ since $\alpha - 1 < 0$, (A 3.14)

where $I^{1-\alpha} f$ represents the integral of f of order $(1-\alpha)$, we have

$$I^{1-\alpha}\left(E_{1-\alpha}(\lambda t^{1-\alpha})\right) = \frac{1}{\lambda}(E_{1-\alpha}(\lambda t^{1-\alpha}) - 1) \tag{A 3.15}$$

$$or, D^{\alpha-1}f(t) = \frac{(1+\pi^2 c)}{-\pi^2}(E_{1-\alpha}(-\pi^2 t^{1-\alpha}) - 1) \quad \text{(A 3.16)}$$

$$or, [D^{\alpha-1}f(t)]_{t=0} = \frac{(1+\pi^2 c)}{-\pi^2}(E_{1-\alpha}(0) - 1) = c\ . \quad \text{(A 3.17)}$$

But $E_{1-\alpha}(0) = \frac{1}{\Gamma(1)} = 1$, Hence, $c = 0$.

Therefore, $f(t) = E_{1-\alpha}(-\pi^2 t^{1-\alpha})$. (A 3.18)

Therefore, the analytical solution of Eq. (A 3.1) is

$$p(x,t) = E_{1-\alpha}(-\pi^2 t^{1-\alpha}) sin(\pi x)\ . \quad \text{(A 3.19)}$$

Chapter 4

Comparison among Proposed Numerical Models Using the Riemann-Liouville, Caputo, and Grünwald-Letnikov Definitions of the Fractional-Order Derivative for a Memory- based Diffusivity Equation

Co-Authorship

Chapter 4 is prepared according to the Guidelines for Manuscript Format Theses in the Faculty of Engineering and Applied Science at Memorial University. This chapter has been prepared for submission as a journal article:

T. U. Zaman, S. MacLachlan, and M. E. Hossain (in preparation). "Comparison among numerical models of a memory- based radial diffusivity equation developed using the Riemann-Liouville, Caputo, and Grünwald-Letnikov definitions of the fractional-order derivative."

The research work presented in this chapter was conducted by Tareq Uz Zaman under the direction and supervision of M. Enamul Hossain, and the guidance and close supervision of Scott MacLachlan. The manuscript itself was written by Tareq Uz Zaman and reviewed by M. Enamul Hossain and Scott MacLachlan.

4.1 Abstract

Unlike the conventional diffusivity equation, memory- based diffusivity equations use fractional-order derivatives that make the equations complicated and difficult to solve, both analytically and numerically, compared to the conventional diffusivity equation. In this paper, a numerical model that utilizes the Caputo definition of the fractional-order derivative, is developed for a time-fractional non-linear diffusion equation. Analytical solution of the equation is derived for Dirichlet boundary conditions and for an initial condition to validate the numerical model. Numerical and

analytical solutions are compared and it is found that numerical and analytical solutions match with negligible error. Deviation of the numerical solution from the analytical solution gets larger with increases in the value of the fractional order, α. The time-fractional non-linear diffusion equation is also solved using the Grünwald-Letnikov definition of the fractional-order derivative. The Grünwald-Letnikov definition of the fractional-order derivative is itself a numerical algorithm, hence, validation by analytical solution is not required in this case. Numerical solutions found using the Caputo and Grünwald-Letnikov definitions are compared. They are also compared with the numerical solutions found from a numerical model that uses the Riemann-Liouville definition of the fractional-order derivative. It is found that the use of the Caputo definition gives the largest pressure values, and use of the Riemann-Liouville definition gives the lowest pressure values. Pressure values obtained using the Grünwald-Letnikov definition lie between those found from the application of the Caputo and Riemann-Liouville definitions.

Keywords: Memory, Numerical Modeling, Fractional diffusion equation, Caputo definition, Riemann-Liouville definition, Grünwald-Letnikov definition, Uniform mesh.

4.2 Introduction

Recent years have seen interest in the investigation of the effects of history of rock, fluid, and flow of fluid on flow through porous media. From this perspective, it is assumed that all materials have memory, and that memory affects the present and future characteristics of the materials. Incorporation of memory makes the governing equations intricate, and solving the equations becomes more challenging.

The ‘memory’ idea is relatively new and growing in petroleum engineering. Zhang (2003) defined memory as a function of time and space, where forward-time events depend on previous-time events. Hossain and Abu-Khamsin (2012) defined memory as the effect of past events on the present and future course of developments. Hossain *et al.* (2006) claim that the memory of the fluid is the most important and most neglected feature in considering fluid flow models. In this direction, Hossain *et al.* (2008) proposed the following diffusivity equation

$$\frac{\partial}{\partial x}\left[\frac{\rho k}{\mu} T^{\alpha} \frac{\partial^{\alpha}}{\partial t^{\alpha}}\left(\frac{\partial p}{\partial x}\right)\right] = \rho \phi c_t \frac{\partial p}{\partial t}, \tag{4.1}$$

where $p(x,t)$ is the pressure, $\rho(x,t)$ the fluid density, $\phi(x,t)$ the porosity of the fluid medium, $k(x,t)$ the permeability of the medium, $\mu(x,t)$ the dynamic viscosity of the fluid, $c_t(x,t)$ the total compressibility of the system, α the fractional order of differentiation and T the characteristic time.

Memory is incorporated in the mathematical model by the inclusion of a fractional-order derivative. Finding numerical solutions to fractional-order differential equations is challenging because of their non-local behaviour. However, a number of studies on numerical approaches to fractional diffusion equations have recently appeared in the literature. Sun *et al.* (2011) solved time-fractional diffusion equations by applying a semi-analytical finite-element method. Wang *et al.* (2011) solved a space-fractional advection diffusion equation by developing a fast characteristic difference method. Murillo and Yuste (2009) compared the solutions of the time-fractional anomalous diffusion equations utilizing three explicit difference methods, where all three methods were based on the Grünwald–Letnikov discretization. Based on the L1 discretization, Zhuang *et al.* (2006) constructed a finite-difference scheme and analyzed its stability and convergence using a maximum principle argument. Celik and Duman (2012) applied the Crank-Nicolson method with the Riesz fractional derivative to numerically solve a fractional diffusion equation. Lin and Xu (2007) combined the L1 approximation for the time-fractional part with spectral approximations for spatial derivatives.

The solution of a particular fractional-order diffusivity equation is important because it shows the way to solve other fractional-order diffusivity equations. While the physical meaning of a fractional-order differential equation is very difficult to understand, we can use its discrete solution to give some sensible physical interpretation.

In this paper, the model of Hossain *et al.* (2008) is solved numerically for two cases: a) for the Caputo definition of the fractional-order derivative, and b) for the Grünwald-Letnikov definition of the fractional-order derivative. An implicit finite-difference approximation for the computation of the Caputo fractional derivative given by Murio (2008) is used to discretize the Eq. (4.1) for

case (a). The G1 algorithm that uses the Grünwald-Letnikov definition for the fractional-order derivative is applied to discretize the diffusivity equation for case (b). The solutions found for case (a) and case (b) are compared with the numerical solutions found by Zaman et al. (2017) using the Riemann-Liouville definition of fractional order derivative.

The mathematical model is discretized using uniform meshes in both space and time. For some positive numbers X, and T, and positive integers N_x, and N_t, the grid sizes in space and time are defined by $\Delta x = X/N_x$ and $\Delta t = T/N_t$ respectively. The grid points in the space interval $[0, X]$ are given by $x_i = i\Delta x, i = 0, 1, 2, \dots, N_x$, and the grid points in the time interval $[0, T]$ are labeled $t_n = n\Delta t, n = 0, 1, 2, \dots, N_t$. The values of a function p at the grid points are denoted by $p_i^n = p(x_i, t_n)$.

4.3 Numerical Solutions for Different Approaches

4.3.1 For Caputo Definition

Writing $C_1(x,t) = \frac{\rho k}{\mu} T^\alpha$ and $C_2(x,t) = \rho\phi c_t$ in Eq. (4.1) and use of the Caputo definition for the fractional-order derivative gives

$$\frac{\partial}{\partial x}\left[C_1(x_i,t_n)\frac{{}^{c}\partial^\alpha}{{}^{c}\partial t^\alpha}\left(\frac{\partial p}{\partial x}\right)\right]_i^n = C_2(x_i,t_n)\frac{\partial p_i^n}{\partial t}, \tag{4.2}$$

where the left superscript, c in $\frac{{}^{c}\partial^\alpha}{{}^{c}\partial t^\alpha}\left(\frac{\partial p}{\partial x}\right)$ stands for the Caputo definition of the fractional-order derivative.

Discretization by implicit Euler in time and staggered finite differences in space, with $F_{i\pm\frac{1}{2}}^n = \left[C_1\frac{{}^{c}\partial^\alpha}{{}^{c}\partial t^\alpha}\left(\frac{\partial p}{\partial x}\right)\right]_{i\pm\frac{1}{2}}^n$ gives

$$\frac{1}{\Delta x}\left(F^n_{i+\frac{1}{2}} - F^n_{i-\frac{1}{2}}\right) = C_2(x_i, t_n)\frac{p_i^n - p_i^{n-1}}{\Delta t}\,. \tag{4.3}$$

Murio's (2008) approximation formula for the Caputo definition of the fractional-order derivative is

$$\frac{{}^C\partial^\alpha u(x_i,t_n)}{{}^C\partial t^\alpha} = \sigma_{\alpha,\Delta t}\sum_{j=1}^n \omega_j^{(\alpha)}(u_i^{n-j+1} - u_i^{n-j})\,, \tag{4.4}$$

where $\sigma_{\alpha,\Delta t} = \frac{1}{\Delta t^\alpha \Gamma(2-\alpha)}$ and $\omega_j^{(\alpha)} = j^{1-\alpha} - (j-1)^{1-\alpha}$. Applying Murio's formula, $F^n_{i+\frac{1}{2}}$ and $F^n_{i-\frac{1}{2}}$ can be written as

$$\begin{aligned} F^n_{i+\frac{1}{2}} = \frac{1}{\Delta x}C_1\left(x_{i+\frac{1}{2}}, t_n\right)\sigma_{\alpha,\Delta t}[&p_{i+1}^n - p_i^n - p_{i+1}^{n-1} + p_i^{n-1} \\ &+ \textstyle\sum_{j=2}^n \omega_j^{(\alpha)}\left(p_{i+1}^{n-j+1} - p_i^{n-j+1} - p_{i+1}^{n-j} + p_i^{n-j}\right)]\,, \end{aligned} \tag{4.5}$$

$$\begin{aligned} F^n_{i-\frac{1}{2}} = \frac{1}{\Delta x}C_1\left(x_{i-\frac{1}{2}}, t_n\right)\sigma_{\alpha,\Delta t}[&p_i^n - p_{i-1}^n - p_i^{n-1} + p_{i-1}^{n-1} \\ &+ \textstyle\sum_{j=2}^n \omega_j^{(\alpha)}\left(p_i^{n-j+1} - p_{i-1}^{n-j+1} - p_i^{n-j} + p_{i-1}^{n-j}\right)]\,. \end{aligned} \tag{4.6}$$

Substitution of Eq. (4.5) and (4.6) into Eq. (4.3) and rearrangement gives

$$\begin{aligned} &-C_1\left(x_{i-\frac{1}{2}}, t_n\right)p_{i-1}^n + \left[C_1\left(x_{i+\frac{1}{2}}, t_n\right) + C_1\left(x_{i-\frac{1}{2}}, t_n\right) + \frac{C_2(x_i,t_n)\Delta x^2}{\sigma_{\alpha,\Delta t}\Delta t}\right]p_i^n - \\ &C_1\left(x_{i+\frac{1}{2}}, t_n\right)p_{i+1}^n = \frac{C_2(x_i,t_n)\Delta x^2}{\sigma_{\alpha,\Delta t}\Delta t}p_i^{n-1} + C_1\left(x_{i+\frac{1}{2}}, t_n\right)G_i^n - C_1\left(x_{i-\frac{1}{2}}, t_n\right)H_i^n\,, \end{aligned} \tag{4.7}$$

where

$$G_i^n = -p_{i+1}^{n-1} + p_i^{n-1} + \textstyle\sum_{j=2}^n \omega_j^{(\alpha)}(p_{i+1}^{n-j+1} - p_i^{n-j+1} - p_{i+1}^{n-j} + p_i^{n-j})\,, \tag{4.8}$$

$$H_i^n = -p_i^{n-1} + p_{i-1}^{n-1} + \sum_{j=2}^{n} \omega_j^{(\alpha)} (p_i^{n-j+1} - p_{i-1}^{n-j+1} - p_i^{n-j} + p_{i-1}^{n-j}) \,. \tag{4.9}$$

4.3.2 For Grünwald-Letnikov Definition

Using the Grünwald-Letnikov definition of the fractional-order derivative, Eq. (4.2) can be written as

$$\frac{\partial}{\partial x}\left[C_1(x_i, t_n) \frac{{}^{GL}\partial^\alpha}{{}^{GL}\partial t^\alpha}\left(\frac{\partial p}{\partial x}\right)\right]_i^n = C_2(x_i, t_n) \frac{\partial p_i^n}{\partial t} \,, \tag{4.10}$$

where the left superscript, GL in $\frac{{}^{GL}\partial^\alpha}{{}^{GL}\partial t^\alpha}\left(\frac{\partial p}{\partial x}\right)$ stands for the Grünwald-Letnikov definition of the fractional-order derivative.

Again, discretizing using implicit Euler in time and staggered finite differences in space with $F_{i\pm\frac{1}{2}}^n = \left[C_1 \frac{{}^{GL}\partial^\alpha}{{}^{GL}\partial t^\alpha}\left(\frac{\partial p}{\partial x}\right)\right]_{i\pm\frac{1}{2}}^n$ gives

$$\frac{1}{\Delta x}\left(F_{i+\frac{1}{2}}^n - F_{i-\frac{1}{2}}^n\right) = C_2(x_i, t_n) \frac{p_i^n - p_i^{n-1}}{\Delta t} \,. \tag{4.11}$$

We now use the G1 algorithm (Oldham *et al.*, 1974) to approximate the fractional-order derivative as

$$\frac{{}^{GL}\partial^\alpha u(x_i, t_n)}{{}^{GL}\partial t^\alpha} = \frac{\Delta t^{-\alpha}}{\Gamma(-\alpha)} \sum_{j=0}^{n-1} \frac{\Gamma(j-\alpha)}{\Gamma(j+1)} u_i^{n-j} \,. \tag{4.12}$$

Applying the G1 algorithm, $F_{i+\frac{1}{2}}^n$ and $F_{i-\frac{1}{2}}^n$ can be written as

$$F_{i+\frac{1}{2}}^n = \frac{1}{\Delta x} C_1\left(x_{i+\frac{1}{2}}, t_n\right) \frac{\Delta t^{-\alpha}}{\Gamma(-\alpha)} \left[\Gamma(-\alpha)(p_{i+1}^n - p_i^n) + \sum_{j=1}^{n-1} \frac{\Gamma(j-\alpha)}{\Gamma(j+1)} (p_{i+1}^{n-j} - p_i^{n-j})\right], \tag{4.13}$$

$$F_{i-\frac{1}{2}}^{n} = \frac{1}{\Delta x} C_1\left(x_{i-\frac{1}{2}}, t_n\right) \frac{\Delta t^{-\alpha}}{\Gamma(-\alpha)} \left[\Gamma(-\alpha)(p_i^n - p_{i-1}^n) + \sum_{j=1}^{n-1} \frac{\Gamma(j-\alpha)}{\Gamma(j+1)} (p_i^{n-j} - p_{i-1}^{n-j})\right]. \quad (4.14)$$

Substitution of Eq. (4.13) and (4.14) into Eq. (4.11) and rearranging terms gives

$$-C_1\left(x_{i-\frac{1}{2}}, t_n\right) p_{i-1}^n + \left[C_1\left(x_{i-\frac{1}{2}}, t_n\right) + C_1\left(x_{i+\frac{1}{2}}, t_n\right) + \frac{C_2(x_i,t_n)\Delta x^2}{\Delta t^{1-\alpha}}\right] p_i^n -$$
$$C_1\left(x_{i+\frac{1}{2}}, t_n\right) p_{i+1}^n = \frac{C_2(x_i,t_n)\Delta x^2}{\Delta t^{1-\alpha}} p_i^{n-1} + C_1\left(x_{i+\frac{1}{2}}, t_n\right) \frac{1}{\Gamma(-\alpha)} G_i^n - C_1\left(x_{i-\frac{1}{2}}, t_n\right) \frac{1}{\Gamma(-\alpha)} H_i^n , \quad (4.15)$$

where

$$G_i^n = \sum_{j=1}^{n-1} \frac{\Gamma(j-\alpha)}{\Gamma(j+1)} (p_{i+1}^{n-j} - p_i^{n-j}) , \quad (4.16)$$

$$H_i^n = \sum_{j=1}^{n-1} \frac{\Gamma(j-\alpha)}{\Gamma(j+1)} (p_i^{n-j} - p_{i-1}^{n-j}) . \quad (4.17)$$

4.3.3 For Riemann-Liouville Definition

Zaman *et al.* (2017) developed the following numerical model using uniform meshes both in space and time to numerically solve Eq. (4.1) when the fractional-order derivative is taken using the Riemann-Liouville definition,

$$-C_1\left(x_{i-\frac{1}{2}}, t_n\right) p_{i-1}^n + \left[C_1\left(x_{i-\frac{1}{2}}, t_n\right) + C_1\left(x_{i+\frac{1}{2}}, t_n\right) + \frac{C_2(x_i,t_n)\Delta x^2}{\sigma_{\alpha,\Delta t}\Delta t}\right] p_i^n -$$
$$C_1\left(x_{i+\frac{1}{2}}, t_n\right) p_{i+1}^n = \frac{C_2(x_i,t_n)\Delta x^2}{\sigma_{\alpha,\Delta t}\Delta t} p_i^{n-1} + C_1\left(x_{i+\frac{1}{2}}, t_n\right) G_i^n - C_1\left(x_{i-\frac{1}{2}}, t_n\right) H_i^n +$$
$$C_1\left(x_{i+\frac{1}{2}}, t_n\right) \frac{1-\alpha}{n^\alpha} (p_{i+1}^0 - p_i^0) - C_1\left(x_{i-\frac{1}{2}}, t_n\right) \frac{1-\alpha}{n^\alpha} (p_i^0 - p_{i-1}^0) , \quad (4.18)$$

where

$$G_i^n = -p_{i+1}^{n-1} + p_i^{n-1} + \sum_{j=1}^{n-1} \omega_j^{(\alpha)} (p_{i+1}^{n-j} - p_i^{n-j} - p_{i+1}^{n-j-1} + p_i^{n-j-1})] , \quad (4.19)$$

$$H_i^n = -p_i^{n-1} + p_{i-1}^{n-1} + \sum_{j=1}^{n-1} \omega_j^{(\alpha)} (p_i^{n-j} - p_{i-1}^{n-j} - p_i^{n-j-1} + p_{i-1}^{n-j-1})] \, . \tag{4.20}$$

For the Caputo and Grünwald-Letnikov definitions of the fractional-order derivative, Eq. (4.7) and (4.15) are written for each grid-point, respectively and, then, the system of equations is solved. Here, solution of the system is complicated by its nonlinearity. The density, permeability, viscosity, porosity, and compressibility themselves depend on the pressure, the solution of the equation. To resolve this, an iterative scheme (fixed-point iteration) is used to update the density, permeability, viscosity, porosity, and compressibility. The approach is illustrated qualitatively by

$$A(\rho, k, \mu, \phi, c_t)^{n,z} \, p^{n,z+1} = RHS^{n,z}.$$

For each time step, and each iteration level, the pressure, density, permeability, viscosity, porosity, and compressibility data are assumed known from the most recent computational value. At the start of a new time step, the most recent value is that from the solution at the previous time step, while during a given time step it is that from the last iteration. The coefficients are updated using the new values of pressure as the pressures are updated and this process is continued. The iteration process terminates when the convergence criterion is satisfied. Two MATLAB programs have been written based on Eqs. (4.7), and (4.15) to numerically solve Eq. (4.1). MATLAB program written by Zaman *et al.* (2017) has been used to solve Eq. (4.18).

4.4 Analytical Solution

To validate this algorithm, we consider the case where $C_1 = C_2 = 1$, and find the analytical solution of Eq. (4.1). For $C_1 = C_2 = 1$, the equation becomes linear. Initial and boundary conditions are taken as $p(x, 0) = sin(\pi x)$, and $p(0, t) = p(1, t) = 0$ respectively.

Utilizing the Caputo definition for the fractional-order derivative, the analytical solution of Eq. (4.1) is found as to be

$$p(x, t) = sin(\pi x) \quad 0 < \alpha < 1 \, . \tag{4.21}$$

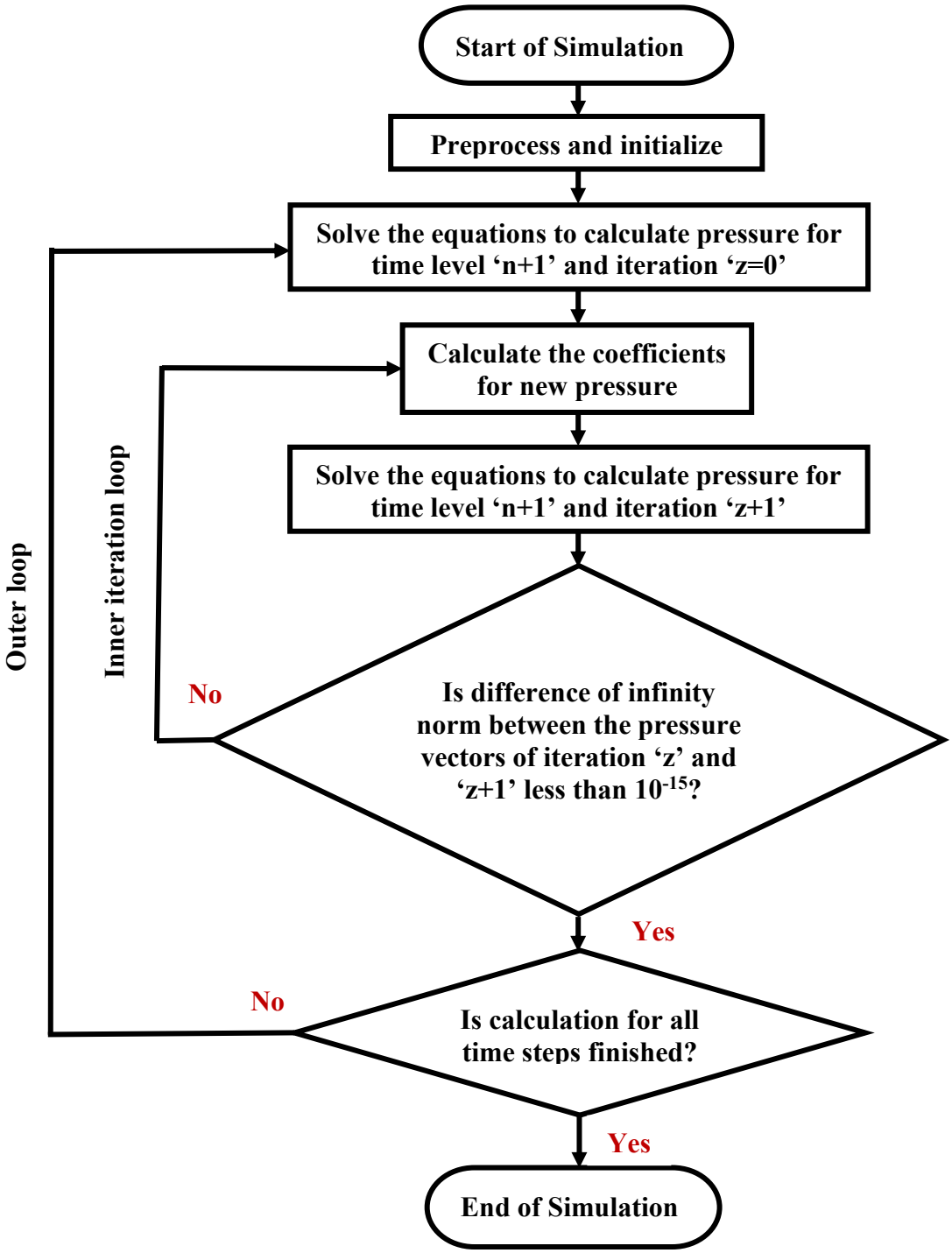

Figure 4.1 Computational algorithm to solve the numerical model.

For $\alpha = 0$, Caputo derivative does not coincide with the classical derivative. In this case, the analytical solution of Eq. (4.1) is not derived. Instead, we use the analytical solution of the equation $(\partial/\partial x)[(\partial^{\alpha}/\partial t^{\alpha})(\partial p(x,t)/\partial x)] - \pi^2\, sin(\pi x) = (\partial p/\partial t)$ with the same initial and boundary condition, and obtain

$$p(x,t) = sin(\pi x)\, e^{-\pi^2 t}\ . \tag{4.22}$$

4.5 Results and Discussion

4.5.1 Validation of Numerical Model

The numerical solutions are compared with the analytical solutions to validate the numerical models. The initial condition $p(x,0) = sin(\pi x)$ and boundary conditions $p(0,t) = 0, p(1,t) = 0$ are used for the numerical solution, as they are used in the analytical solution.

The analytical solution (Eq. 4.21) found using the Caputo definition is applicable for $0 < \alpha < 1$, while the numerical solution obtained for this definition is applicable for $0 \leq \alpha < 1$. The term '$-\pi^2\, sin(\pi x)$' is added to the right-hand side of Eq. 4.7 as a forcing function when comparing with the analytical solution (Eq. 4.22) of the modified equation in the case of $\alpha = 0$. MATLAB code was written to evaluate the numerical and analytical solutions. The solutions are shown and compared in Figs. 4.2, 4.3, 4.4, and 4.5 for $\alpha = 0, 0.25, 0.50$ and 0.75 respectively. The numerical solutions match very well with the analytical solutions. For $\alpha \neq 0$, the solution does not depend on time, hence only one curve is found for both analytical and numerical solutions. The fact that the solution derived using the Caputo definition is independent of time did not result from the choice of initial condition $p(x,0) = sin(\pi x)$. It is shown in Appendix that the solution of Eq. (4.2) for $C_1 = C_2 = 1$ is independent of α and t for any initial condition when the Caputo definition is used.

4.5.2 Comparison among the Solutions for the Riemann-Liouville, Caputo and Grünwald-Letnikov Definitions

The solutions found from the Caputo, Grünwald-Letnikov, and Riemann-Liouville definitions of the fractional-order derivative for $T_f = 0.0005$ are compared in Figs. 4.6, 4.7, and 4.8 for $\alpha = 0, 0.25$, and 0.50, respectively. Fig. 4.6 shows that, for $\alpha = 0$, all three definitions for the fractional-order derivative give same result. However, Fig. 4.7 and Fig. 4.8 show that, for $0 < \alpha < 1$, the Caputo definition gives the largest value (equal to the initial condition), the Riemann-Liouville definition gives the lowest value and the values given by the Grünwald-Letnikov definition lie in between. From the figures, it is also found that the differences among the three solutions increase with increase in the value of α.

Figs. 4.9, and 4.10 depicts the solutions found from the Caputo, Grünwald-Letnikov, and Riemann-Liouville definitions of the fractional-order derivative using $\alpha = 0.25$ for $T_f = 0.005$, and 0.05 respectively. It is found from Figs. 4.7, 4.9, and 4.10 that the differences among the three solutions increase as the time at which the solutions are obtained increases.

The reason behind the differences among the three solutions and the increment of the differences with α and time can be understood looking at the three different definitions of fractional-order derivatives. Eq. (24), (25), and (26) are the Grünwald-Letnikov, the Riemann-Liouville, and the Caputo definitions respectively.

$$\frac{\partial^\alpha u(x,t)}{\partial t^\alpha} \equiv \lim_{N\to\infty}\{\frac{(\frac{t}{N})^{-\alpha}}{\Gamma(-\alpha)}\sum_{j=0}^{N-1}\frac{\Gamma(j-\alpha)}{\Gamma(j+1)}u(x,t-j\frac{t}{N})\} \tag{23}$$

$$\frac{\partial^\alpha u(x,t)}{\partial t^\alpha} \equiv \frac{1}{\Gamma(q-\alpha)}\frac{\partial^q}{\partial t^q}\int_0^t (t-\tau)^{q-\alpha-1}u(x,\tau)d\tau \qquad (q-1<\alpha<q) \tag{24}$$

$$\frac{\partial^\alpha u(x,t)}{\partial t^\alpha} \equiv \frac{1}{\Gamma(q-\alpha)}\int_0^t (t-\tau)^{q-\alpha-1}\frac{\partial^q u(x,\tau)}{\partial t^q}d\tau \qquad (q-1<\alpha<q) \tag{25}$$

Riemann-Liouville definition takes the qth-order derivative of the integral of the product of $(t-\tau)^{q-\alpha-1}$ and u, whereas Caputo definition takes the integral of the product of $(t-\tau)^{q-\alpha-1}$ and qth-order derivative of u. Grünwald-Letnikov definition is also different from the other two definitions. The three definitions are not unique, and it is not possible to reach one definition from the other. Therefore, the differences among the solutions found from the Caputo, Grünwald-Letnikov, and Riemann-Liouville definitions of the fractional-order derivative increases with the increase of α and time.

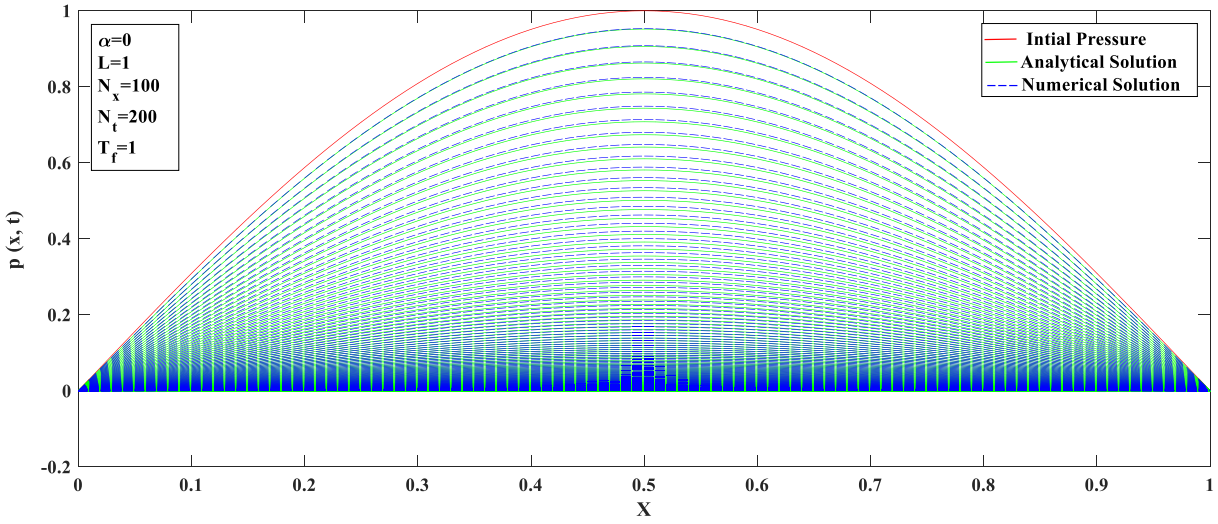

Figure 4.2 Comparison between analytical and numerical solution for $\alpha = 0$ in Caputo case.

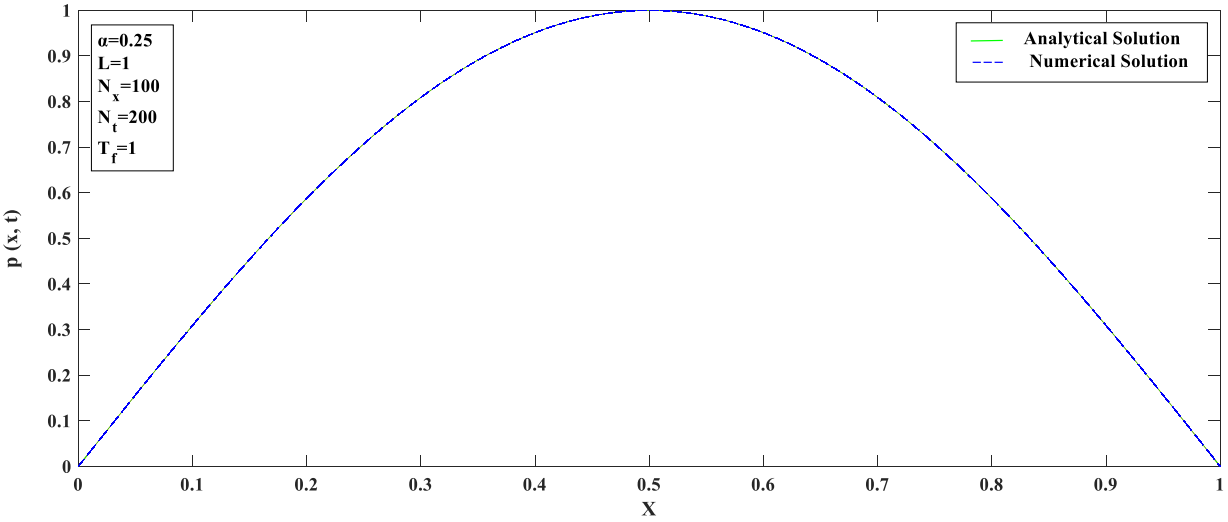

Figure 4.3 Comparison between analytical and numerical solution for $\alpha = 0.25$ in Caputo case.

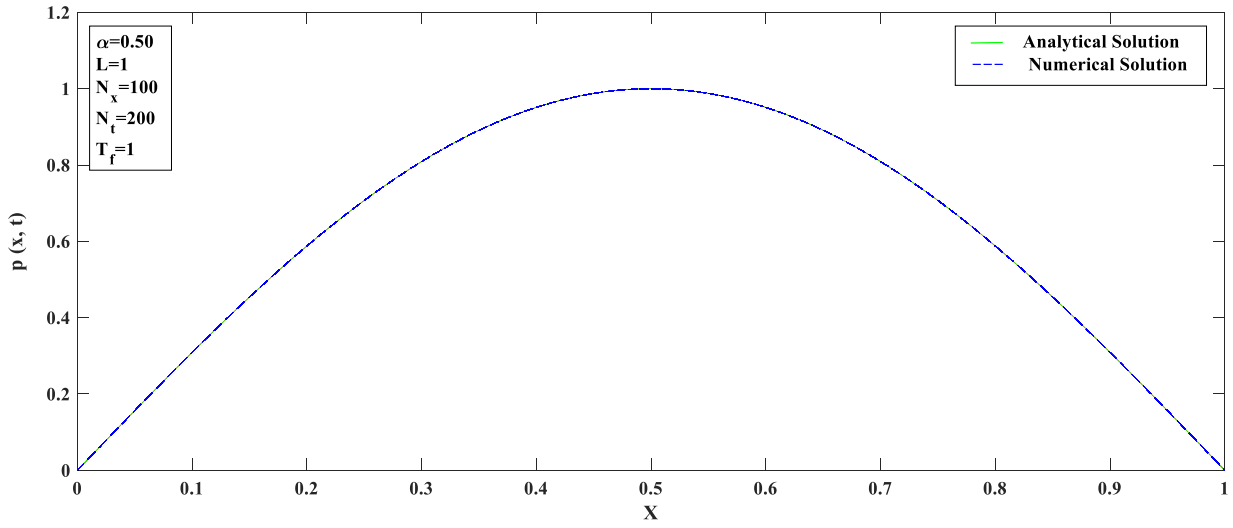

Figure 4.4 Comparison between analytical and numerical solution for $\alpha = 0.50$ in Caputo case.

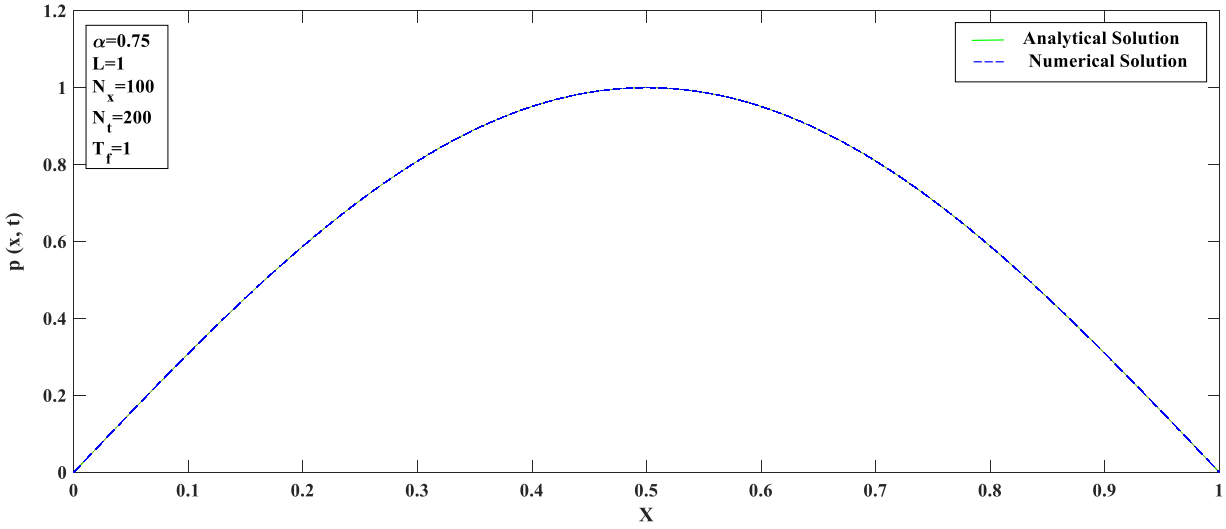

Figure 4.5 Comparison between analytical and numerical solution for $\alpha = 0.75$ in Caputo case.

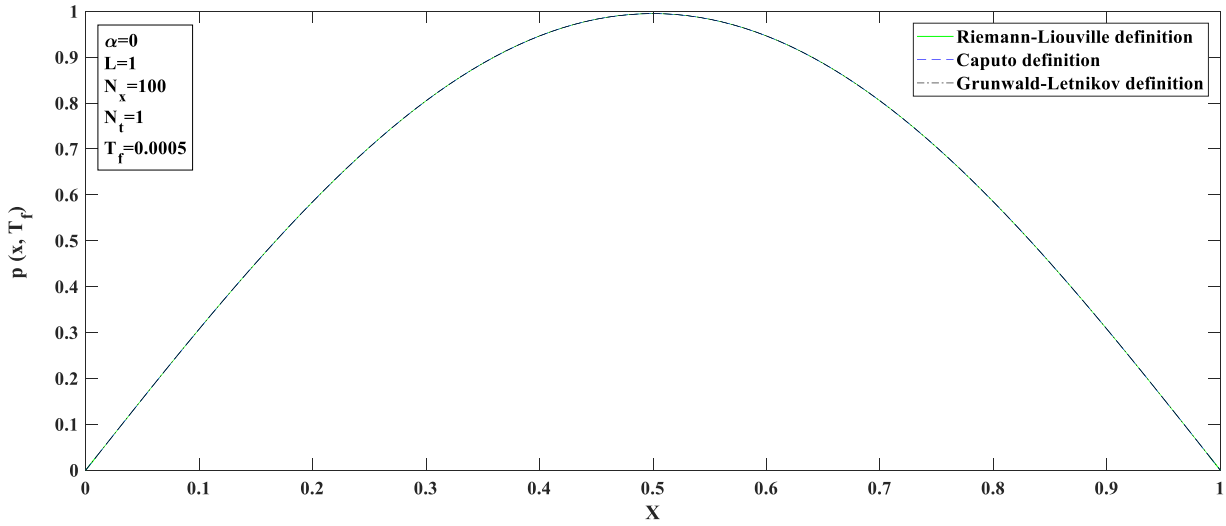

Figure 4.6 Comparison among three solutions for $\alpha = 0, L = 1, N_x = 100, N_t = 1, T_f = 0.0005$.

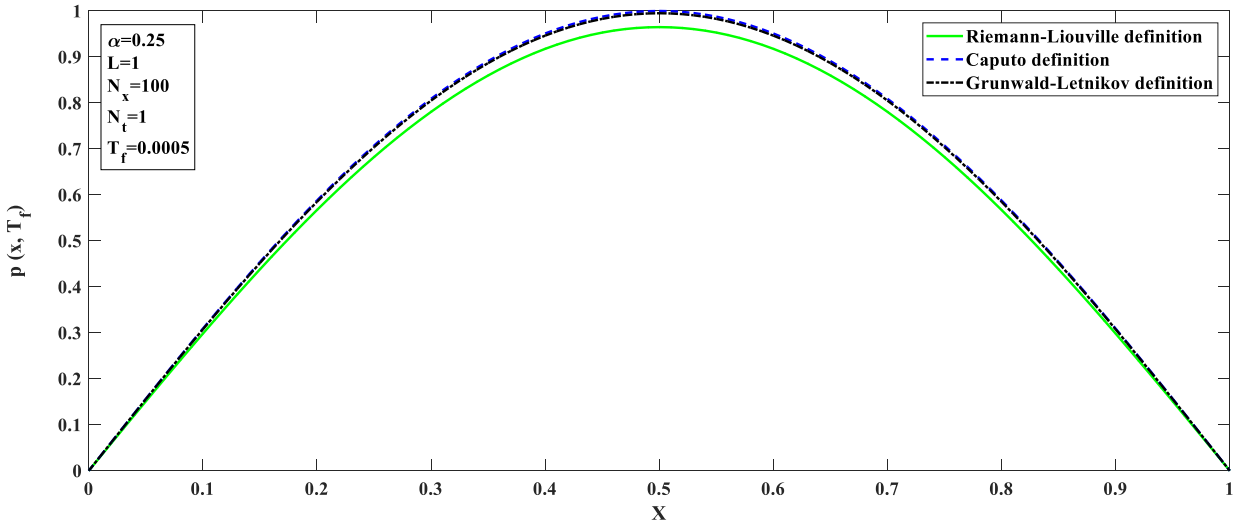

Figure 4.7 Comparison among three solutions for $\alpha = 0.25, L = 1, N_x = 100, N_t = 1,\ T_f = 0.0005$.

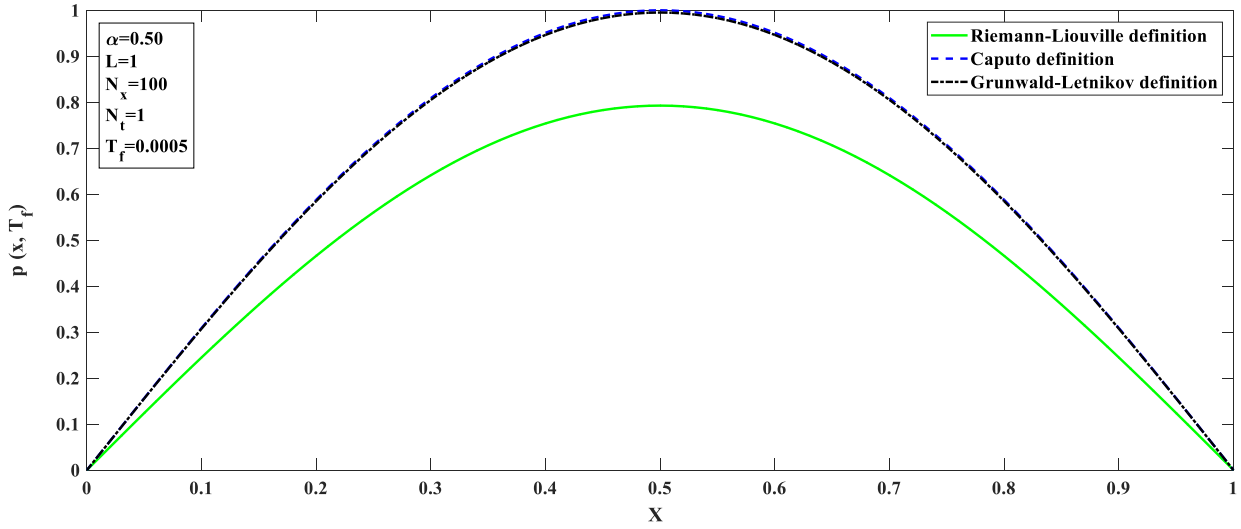

Figure 4.8 Comparison among three solutions for $\alpha = 0.50, L = 1, N_x = 100, N_t = 1,\ T_f = 0.0005$.

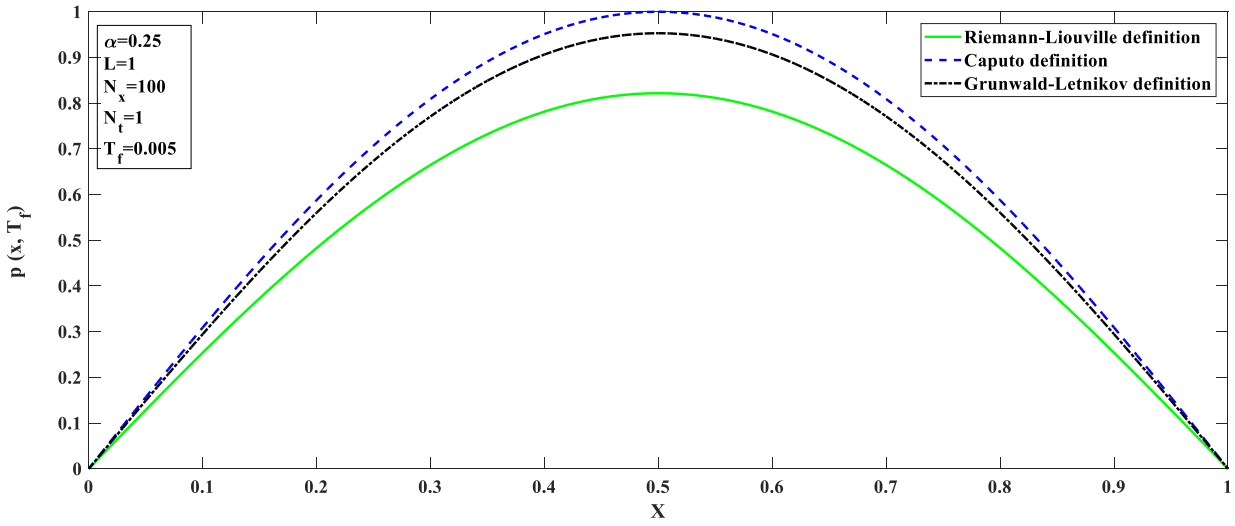

Figure 4.9 Comparison among three solutions for $\alpha = 0.25, L = 1, N_x = 100, N_t = 1,\ T_f = 0.005$.

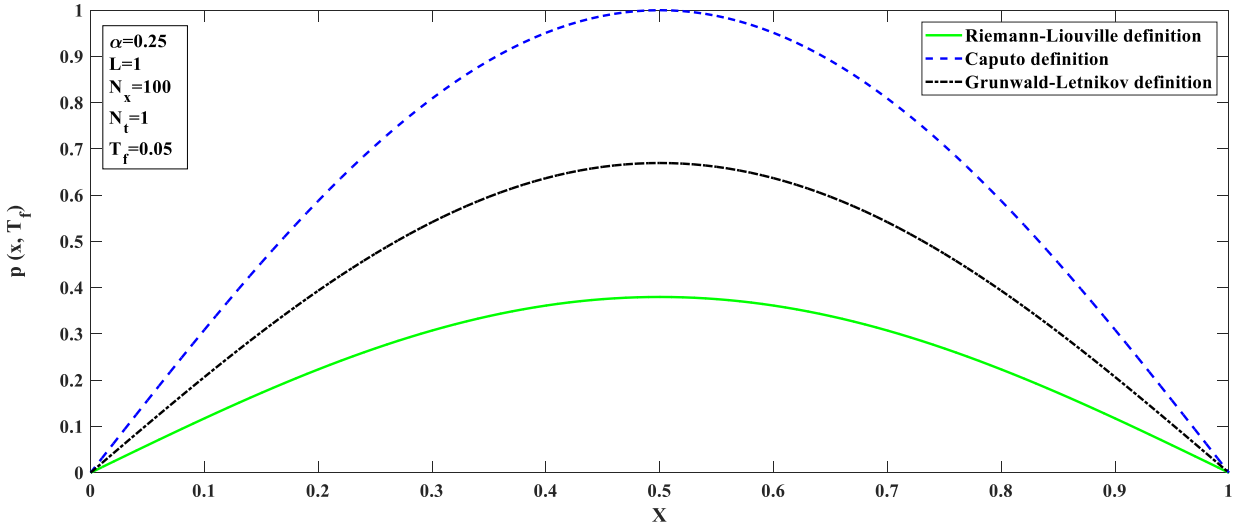

Figure 4.10 Comparison among three solutions for $\alpha = 0.25, L = 1, N_x = 100, N_t = 1,\ T_f = 0.05$.

4.6 Conclusions

Numerical models are developed to solve a time-fractional diffusion equation applying the Caputo, and Grünwald-Letnikov definitions for the fractional-order derivative. Uniform mesh grading in both space and time has been used. The numerical model developed using the Caputo definition is validated by comparing with the analytical solution. Numerical solutions found from the Caputo and Grünwald-Letnikov definitions are compared with the solutions found from the use of the Riemann-Liouville definition. It is found that Caputo definition gives the largest pressure values, and the Riemann-Liouville definition gives the lowest values. The pressure values found using the Grünwald-Letnikov definition lie between those found from the application of the Caputo and Riemann-Liouville definitions.

4.7 Acknowledgement

The authors would like to thank the Natural Sciences and Engineering Research Council of Canada (NSERC); Research & Development Corporation of Newfoundland and Labrador (RDC), funding no. 210992; and Statoil Canada Ltd., funding no. 211162 for providing financial support to accomplish this research under the Statoil Chair in Reservoir Engineering at the Memorial University of Newfoundland, St. John's, NL, Canada.

Bibliography

1. Çelik, C., & Duman, M. (2012). Crank-Nicolson method for the fractional diffusion equation with the Riesz fractional derivative. *Journal of Computational Physics*, *231*(4), 1743–1750. http://doi.org/10.1016/j.jcp.2011.11.008
2. Hossain, M. E. (2006). Fluid Properties With Memory – a Critical Review and Some Additions. *The 36th International Conference on Computers and Industrial Engineering June 20-23, 2006, Taipei, Taiwan*, (July), 13.
3. Hossain, M. E., Mousavizadegan, S. H., & Islam, M. R. (2008). A New Porous Media Diffusivity Equation with the Inclusion of Rock and Fluid Memories. *Society of Petroleum Engineers,* SPE-114287-MS.
4. Hossain, M.E., & Abu-Khamsin, S.A. (2012). Utilization of Memory Concept to Develop Heat Transfer Dimensionless Numbers for Porous Media Undergoing Thermal Flooding with Equal Rock-Fluid Temperatures. *Journal of Porous Media. 15*(10), 937 – 953.
5. Lin, X., Xu, C. (2007). Finite difference/spectral approximations for the time-fractional diffusion equation, *Journal of Computational Physics, 225*, 1533–1552.
6. Murillo, J.Q., Yuste, S.B. (2009). On three explicit difference schemes for fractional diffusion and diffusion-wave equations, *Physica Scripta, T136*, 014025, doi:10.1088/0031-8949/2009/T136/014025.
7. Murio, D.A., (2008). Implicit finite difference approximation for time fractional diffusion equations, *Computers and Mathematics with Applications, 56*, 1138–1145.
8. Oldham, K. B., Spanier, J. (1974). *The Fractional Calculus*, Academic Press, Inc., California.
9. Sun, H., Chen, W., & Sze, K. Y. (2013). A semi-discrete finite element method for a class of time-fractional diffusion equations. *Philosophical Transactions of the Royal Society. Series A*, *371*, 20120268. http://doi.org/10.1098/rsta.2012.0268
10. Wang, K.X., Wang, H. (2011). A fast characteristic finite difference method for fractional advection–diffusion equations. *Advances in Water Resources. 34* (2011) 810–816.
11. Zaman, T. U., MacLachlan, S., and Hossain, M. E. (2017). Numerical modelling of a memory-based radial diffusivity equation using the Riemann-Liouville definition of the fractional-order derivative and uniform meshes. (in preparation).
12. Zhang, H. M. (2003). Driver memory, traffic viscosity and a viscous vehicular traffic flow

model. *Transportation Research Part B: Methodological*, *37*(1), 27–41. http://doi.org/10.1016/S0191-2615(01)00043-1

13. Zhuang, P., Liu, F., (2006). Implicit difference approximation for the time fractional diffusion equation, *Journal of Applied Mathematics and Computing, 22*, 87–99.

Appendix

Analytical Solution for Caputo Definition

To find the analytical solution, we consider $C_1 = C_2 = 1$ in Eq. (4.2) giving

$$\frac{\partial}{\partial x}\left[\frac{{}^{C}\partial^{\alpha}}{{}^{C}\partial t^{\alpha}}\left(\frac{\partial p}{\partial x}\right)\right] = \frac{\partial p}{\partial t}\,, \tag{A 4.1}$$

with boundary conditions $p(0) = p(1) = 0$.

We write the solution in series form as

$$p(x,t) = \sum_{k=1}^{\infty} T_k\,(t) sin(k\pi x)\,, \tag{A 4.2}$$

noting that

$$\frac{\partial p}{\partial t}(x,t) = \sum_{k=1}^{\infty} T_k'(t)\, sin(k\pi x) = -\sum_{k=1}^{\infty} k^2\pi^2 \frac{\partial^{\alpha} T_k(t)}{\partial t^{\alpha}}\, sin(k\pi x) = \frac{\partial}{\partial x}\left[\frac{{}^{C}\partial^{\alpha}}{{}^{C}\partial t^{\alpha}}\left(\frac{\partial p}{\partial x}\right)\right]. \tag{A 4.3}$$

To be a solution, we require that

$$T_k'(t) = -k^2\pi^2 \frac{{}^{C}\partial^{\alpha} T_k(t)}{{}^{C}\partial t^{\alpha}}\,, \tag{A 4.4}$$

$$\text{and } T_k(0) = \beta_k\,, \tag{A 4.5}$$

where β_k comes from the sine series expansion of the initial data, $p(x,0) = \sum_{k=1}^{\infty} \beta_k\, sin(k\pi x)$.

Taking Laplace transforms, we have

$$\mathcal{L}[T_k'(t)] = s\hat{T}_k(s) - \beta_k\,. \tag{A 4.6}$$

For the Caputo definition of the fractional-order derivative,

$$\mathcal{L}\left[\frac{{}^{C}\partial^{\alpha}T_k(t)}{{}^{C}\partial t^{\alpha}}\right] = s^{\alpha}\hat{T}_k(s) - s^{\alpha-1}\beta_k \ . \tag{A 4.7}$$

Therefore,

$$s\hat{T}_k(s) - \beta_k = -k^2\pi^2(s^{\alpha}\hat{T}_k(s) - s^{\alpha-1}\beta_k) \tag{A 4.8}$$

$$or, (s + k^2\pi^2 s^{\alpha})\hat{T}_k(s) = \beta_k(1 + k^2\pi^2 s^{\alpha-1}) \ , \tag{A 4.9}$$

$$or, \hat{T}_k(s) = \beta_k \frac{(1+k^2\pi^2 s^{\alpha-1})}{(s+k^2\pi^2 s^{\alpha})} = \frac{\beta_k}{s} \ . \tag{A 4.10}$$

We get

$$T_k(t) = \beta_k \ , \tag{A 4.11}$$

giving $p(x,t) = p(x,0)$. (A 4.12)

Eq. (A 4.12) is the general analytical solution of Eq. (A 4.1) for any initial condition while using the Caputo definition of fractional order derivative. The analytical solution found in this case is independent of α and t.

Chapter 5

Numerical Approximation of a Time-Fractional Diffusion Equation Using the Riemann-Liouville Definition of the Fractional Derivative and Graded Meshes

Co-Authorship

Chapter 5 is prepared according to the Guidelines for Manuscript Format Theses in the Faculty of Engineering and Applied Science at Memorial University. This chapter has been prepared for submission as a journal article:

T. U. Zaman, S. MacLachlan, and M. E. Hossain (in preparation). "Numerical approximation of a time-fractional diffusion equation using the Riemann-Liouville definition of the fractional derivative and graded meshes."

The research work presented in this chapter was conducted by Tareq Uz Zaman under the direction and supervision of M. Enamul Hossain, and the guidance and close supervision of Scott MacLachlan. The manuscript itself was written by Tareq Uz Zaman and reviewed by M. Enamul Hossain and Scott MacLachlan.

5.1 Abstract

A time-fractional non-linear diffusion equation is numerically solved by applying the finite-difference method. The Riemann-Liouville definition for the fractional-order derivative has been used. A graded mesh in time is adapted to the problem and the L1 algorithm is derived for graded meshes. The fractional diffusion equation is discretized using a uniform mesh in space and a graded mesh in time. To validate the numerical model, numerical solutions are compared to analytical solutions in the linear case and compared to manufactured solutions in non-linear cases. Comparisons are made for different boundary conditions, and errors are analyzed. The error results

affirm that the discretization method used in the numerical model is consistent, second-order accurate in space, and first-order accurate in time. The developed numerical solutions can be used to investigate the effects of memory on fluid flow through porous media. The developed numerical model, and the written code are initial steps to develop a memory-based reservoir simulator.

Keywords: Memory, Numerical Modeling, Fractional diffusion equation, Riemann-Liouville definition, Graded mesh.

5.2 Introduction

Numerous models have been developed over more than the past fifty years for simulations of porous media flow that are crucial to overcoming the challenges associated with petroleum production. The continuum approach, the simplest among the common approaches, is based on semi-empirical equations such as Darcy's law, the Blake-Kozeny-Carman, or Ergun equations (Sochi, 2010). Several continuum models are also based in their derivation on the capillary bundle concept. Another approach is pore-scale network modeling that is a compromise between the two extremes of continuum and numerical approaches (Sochi, 2010). This approach takes the microscopic description of the pore geometry with affordable computational resources into consideration. However, these approaches do not consider the effects of history of the rock, fluid, and flow on fluid flow phenomena.

The effects of history are incorporated in fluid flow models by the inclusion of 'memory'. The parameter 'memory' represents the effects of history of both the rock and fluid. According to Zhang (2003), memory is a function of time and space, where forward time events depend on previous time events. The 'memory' idea is relatively new and growing in petroleum engineering. Hossain *et al.* (2006) considered the memory of the fluid as the most important and most neglected feature in fluid flow models. In this direction, Hossain *et al.* (2008) proposed the following diffusivity equation

$$\frac{\partial}{\partial x}\left[\frac{\rho k}{\mu} T^{\alpha} \frac{\partial^{\alpha}}{\partial t^{\alpha}}\left(\frac{\partial p}{\partial x}\right)\right] = \rho \phi c_t \frac{\partial p}{\partial t}, \tag{5.1}$$

where $p(x,t)$ is the pressure, $\rho(x,t)$ the fluid density, $\phi(x,t)$ the porosity of the fluid medium, $k(x,t)$ the permeability of the medium, $\mu(x,t)$ the dynamic viscosity of the fluid, $c_t(x,t)$ the total compressibility of the system, α the fractional order of differentiation and T the characteristic time.

Memory is incorporated in the mathematical model with the aid of fractional-order derivatives. Derivation of numerical solutions to fractional-order differential equation is challenging because of their non-local behaviour. However, a number of studies on the numerical approaches to fractional diffusion equations have recently appeared in the literature. Different numerical methods have been applied to solve fractional differential equations (Gorenflo *et al.* (2002), Lynch *et al.* (2003), Meerschaert *et al.* (2004), Yuste *et al.* (2005), Yuste (2006), Sun *et al.* (2006), Chen *et al.* (2007), Podlubny *et al.* (2009), Cui (2009), Brunner *et al.* (2010), Skovranek *et al.* (2010), Mustapha *et al.* (2011)). Finite difference methods are convenient among these methods. However, constant time steps are used in almost all cases. Very few cases use variable time steps.

Instead of treating the fractional-order derivative by its definition and discretizing the term that contains the fractional-order derivative, Hossain *et al.* (2008) considered the term as a parameter and then solved the Eq. (5.1) numerically in the way that an integer-order partial differential equation would be solved. Hence, their numerical solution is not accurate in the mathematical sense. The solution of a fractional-order diffusivity equation is important, because it shows the way to solve other fractional order diffusivity equations.

Zaman *et al.* (2017) solved Eq. (5.1) numerically using uniform meshes. However, Stynes *et al.* (2017) defined a graded mesh for a time-fractional diffusion equation and showed that the graded mesh gives better performance for time-fractional equations. Their definition of a graded mesh has been adapted for the time derivative in this work.

In this paper, the fractional order diffusivity equation (Eq. (5.1)) is solved numerically using the Riemann-Liouville definition for the fractional-order derivative. The L1 algorithm for graded meshes using the Riemann-Liouville definition for fractional-order derivatives is derived and applied to discretize the diffusivity equation.

Eq. (5.1) is discretized using a uniform mesh in space and graded meshes in time. For some positive numbers X, and T, and positive integers N_x, and N_t, the grid sizes in space and time are defined by $\Delta x = X/N_x$ and $\Delta t_n = t_n - t_{n-1}$ respectively. The grid points in the space interval $[0, X]$ are the numbers $x_i = i\Delta x, i = 0, 1, 2, \dots, N_x$, and the grid points in the time interval $[0, T]$ are labeled $t_n = T(n/N)^{\omega}, n = 0, 1, 2, \dots, N_t$, where the constant mesh grading $\omega \geq 1$ is adapted from Stynes *et al.* (2017). For our case, $\omega = (1+\alpha)/(1-\alpha)$ relate to Stynes *et al.* (2017). The values of a function p at the grid points are denoted by $p_i^n = p(x_i, t_n)$.

5.3 L1 Algorithm for Non-Uniform Mesh Grading

The L1 algorithm is derived for non-uniform mesh grading using the Riemann-Liouville definition for fractional-order derivatives.

From its definition, the Riemann-Liouville fractional derivative for $\alpha \geq 0$ is given by

$$\left[\frac{d^{\alpha} f}{d(x-a)^{\alpha}}\right]_{R-L} \equiv \frac{d^{\alpha}}{dx^{\alpha}}\left[\frac{d^{\alpha-n} f}{d(x-a)^{\alpha-n}}\right]_{R-L} \equiv \frac{d^{n}}{dx^{n}}\left[\frac{1}{\Gamma(n-\alpha)}\int_a^x \frac{f(y)dy}{(x-y)^{\alpha-n+1}}\right], \qquad n > \alpha\,. \tag{5.2}$$

Applying the Leibniz rule for differentiating integrals, Eq. (5.2) is identical to

$$\left[\frac{d^{\alpha} f}{d(x-a)^{\alpha}}\right]_{R-L} \equiv \sum_{k=0}^{n-1} \frac{(x-a)^{k-\alpha} f^{(k)}(a)}{\Gamma(k-\alpha+1)} + \frac{1}{\Gamma(n-\alpha)}\int_a^x \frac{f^{(n)}(y)dy}{(x-y)^{\alpha-n+1}}, \qquad n > \alpha\,. \tag{5.3}$$

Now, setting $a = 0$ and $n = 1$, restricting $0 \leq \alpha < 1$ yields

$$\frac{d^{\alpha} f}{dx^{\alpha}} \equiv \frac{x^{-\alpha} f(0)}{\Gamma(1-\alpha)} + \frac{1}{\Gamma(1-\alpha)}\int_0^x \frac{df(y)}{dy}\frac{dy}{(x-y)^{\alpha}}\,. \tag{5.4}$$

Eq. (5.4) can be written as

$$\frac{d^{\alpha} f}{dx^{\alpha}} \equiv \frac{1}{\Gamma(1-\alpha)}\left[\frac{f(0)}{x^{\alpha}} + \sum_{J=0}^{N-1}\int_{x_j}^{x_{j+1}} \frac{df(y)}{dy}\frac{dy}{(x-y)^{\alpha}}\right]. \tag{5.5}$$

The L1 algorithm utilizes the approximations

$$\int_{x_j}^{x_{j+1}} \frac{df(y)}{dy}\frac{dy}{(x-y)^{\alpha}} \equiv \frac{f(x_{j+1})-f(x_j)}{x_{j+1}-x_j}\int_{x_j}^{x_{j+1}} \frac{dy}{(x-y)^{\alpha}} \equiv \frac{1}{1-\alpha}\frac{f(x_{j+1})-f(x_j)}{x_{j+1}-x_j}\left[\left(x-x_j\right)^{1-\alpha} - (x-x_{j+1})^{1-\alpha}\right]. \quad (5.6)$$

Substitution of Eq. (5.6) into Eq. (5.5) gives

$$\left[\frac{d^{\alpha}f}{dx^{\alpha}}\right]_{L1} \equiv \frac{1}{\Gamma(1-\alpha)}\left[\frac{f(0)}{x^{\alpha}} + \sum_{J=0}^{N-1}\frac{1}{1-\alpha}\frac{f(x_{j+1})-f(x_j)}{x_{j+1}-x_j}\left[\left(x-x_j\right)^{1-\alpha} - \left(x-x_{j+1}\right)^{1-\alpha}\right]\right]. \quad (5.7)$$

Eq. (5.7) can be written as

$$\left[\frac{d^{\alpha}f}{dx^{\alpha}}\right]_{L1} \equiv \frac{1}{\Gamma(2-\alpha)}\left[\frac{(1-\alpha)f(0)}{x^{\alpha}} + \sum_{J=0}^{N-1}\frac{f(x_{j+1})-f(x_j)}{x_{j+1}-x_j}\left[\left(x-x_j\right)^{1-\alpha} - \left(x-x_{j+1}\right)^{1-\alpha}\right]\right]. \quad (5.8)$$

Eq. (5.8) is the L1 algorithm for non-uniform mesh spacing for the Riemann-Liouville definition of the fractional-order derivative.

5.4 Numerical Solution for Riemann-Liouville Definition

Writing $C_1(x,t) = \frac{\rho k}{\mu}T^{\alpha}$ and $C_2(x,t) = \rho\phi c_t$ in Eq. (5.1) gives

$$\frac{\partial}{\partial x}\left[C_1(x_i,t_n)\frac{\partial^{\alpha}}{\partial t^{\alpha}}\left(\frac{\partial p}{\partial x}\right)\right]_i^n = C_2(x_i,t_n)\frac{\partial p_i^n}{\partial t}. \quad (5.9)$$

Discretizing this using implicit Euler in time and staggered finite differences in space with $F_{i\pm\frac{1}{2}}^n = \left[C_1\frac{\partial^{\alpha}}{\partial t^{\alpha}}\left(\frac{\partial p}{\partial x}\right)\right]_{i\pm\frac{1}{2}}^n$ gives

$$\frac{1}{\Delta x}\left(F_{i+\frac{1}{2}}^n - F_{i-\frac{1}{2}}^n\right) = C_2(x_i,t_n)\frac{p_i^n - p_i^{n-1}}{t_n - t_{n-1}}. \quad (5.10)$$

Using the L1 algorithm derived in Eq. (5.8), $F^n_{i+\frac{1}{2}}$ and $F^n_{i-\frac{1}{2}}$ can be written as

$$F^n_{i+\frac{1}{2}} = \frac{1}{\Delta x \Gamma(2-\alpha)} C_1\left(x_{i+\frac{1}{2}}, t_n\right)\left[\frac{(1-\alpha)}{(t_n)^\alpha}(p^0_{i+1} - p^0_i)\right.$$
$$+(t_n - t_{n-1})^{-\alpha}(p^n_{i+1} - p^n_i) - (t_n - t_{n-1})^{-\alpha}(p^{n-1}_{i+1} - p^{n-1}_i)$$
$$\left.+\sum_{J=0}^{n-2}\frac{\left[(t_n - t_j)^{1-\alpha} - (t_n - t_{j+1})^{1-\alpha}\right]}{(t_{j+1} - t_j)}(p^{j+1}_{i+1} - p^{j+1}_i - p^j_{i+1} + p^j_i)\right], \tag{5.11}$$

$$F^n_{i-\frac{1}{2}} = \frac{1}{\Delta x \Gamma(2-\alpha)} C_1\left(x_{i-\frac{1}{2}}, t_n\right)\left[\frac{(1-\alpha)}{(t_n)^\alpha}(p^0_i - p^0_{i-1})\right.$$
$$+(t_n - t_{n-1})^{-\alpha}(p^n_i - p^n_{i-1}) - (t_n - t_{n-1})^{-\alpha}(p^{n-1}_i - p^{n-1}_{i-1})$$
$$\left.+\sum_{J=0}^{n-2}\frac{\left[(t_n - t_j)^{1-\alpha} - (t_n - t_{j+1})^{1-\alpha}\right]}{(t_{j+1} - t_j)}(p^{j+1}_i - p^{j+1}_{i-1} - p^j_i + p^j_{i-1})\right]. \tag{5.12}$$

Substitution of Eqs. (5.11) and (5.12) into Eq. (5.10), rearranging terms,

$$-C_1\left(x_{i-\frac{1}{2}}, t_n\right)p^n_{i-1} + \left[C_1\left(x_{i-\frac{1}{2}}, t_n\right) + C_1\left(x_{i+\frac{1}{2}}, t_n\right) + C_2(x_i, t_n)\Delta x^2\Gamma(2-\alpha)(t_n - t_{n-1})^{\alpha-1}\right]p^n_i - C_1\left(x_{i+\frac{1}{2}}, t_n\right)p^n_{i+1} = C_2(x_i, t_n)\Delta x^2\Gamma(2-\alpha)(t_n - t_{n-1})^{\alpha-1}p^{n-1}_i +$$
$$C_1\left(x_{i+\frac{1}{2}}, t_n\right)(t_n - t_{n-1})^\alpha G^n_i - C_1\left(x_{i-\frac{1}{2}}, t_n\right)(t_n - t_{n-1})^\alpha H^n_i + C_1\left(x_{i+\frac{1}{2}}, t_n\right)\frac{(1-\alpha)}{(t_n)^\alpha}(t_n -$$
$$t_{n-1})^\alpha(p^0_{i+1} - p^0_i) + C_1\left(x_{i-\frac{1}{2}}, t_n\right)\frac{(1-\alpha)}{(t_n)^\alpha}(t_n - t_{n-1})^\alpha(p^0_i - p^0_{i-1}), \tag{5.13}$$

where

$$G^n_i = -(t_n - t_{n-1})^{-\alpha}(p^{n-1}_{i+1} - p^{n-1}_i)$$
$$+\sum_{J=0}^{n-2}\frac{\left[(t_n - t_j)^{1-\alpha} - (t_n - t_{j+1})^{1-\alpha}\right]}{(t_{j+1} - t_j)}(p^{j+1}_{i+1} - p^{j+1}_i - p^j_{i+1} + p^j_i), \tag{5.14}$$

$$H^n_i = -(t_n - t_{n-1})^{-\alpha}(p^{n-1}_i - p^{n-1}_{i-1})$$

$$+\sum_{J=0}^{n-2}\frac{\left[(t_n-t_j)^{1-\alpha}-(t_n-t_{j+1})^{1-\alpha}\right]}{(t_{j+1}-t_j)}(p_i^{j+1}-p_{i-1}^{j+1}-p_i^j+p_{i-1}^j)\,. \tag{5.15}$$

Fig. 5.1 shows the computational algorithm to solve the numerical model. Eq. (5.13) is written for each grid-point and, then, the system of equations is solved. Note, however, that the equation is nonlinear: the pressures depend on the density, permeability, viscosity, porosity, and compressibility which, themselves, depend on these pressures. Thus, an iterative scheme is used to update the density, permeability, viscosity, porosity, and compressibility. The approach is illustrated qualitatively by

$$A(\rho,k,\mu,\phi,c_t)^{n,z}\,p^{n,z+1}=RHS^{n,z}.$$

For each time step, and each iteration level, the pressure, density, permeability, viscosity, porosity, and compressibility data are assumed known from the most recent computational value. At the start of a new time step, the most recent value is that from the previous time step, while during a given time step it is that from the last iteration. The coefficients are updated using the new values of pressure as the pressures are solved and this process is continued. The iteration process terminates when the convergence criterion is satisfied. A MATLAB program has been written based on Eq. (5.13) to numerically solve Eq. (5.1).

5.5 Analytical Solution for Linear Case

To find the analytical solution, $C_1=C_2=1$ is considered in Eq. (5.9). For $C_1=C_2=1$ the equation becomes linear. The initial condition is taken to be $p(x,0)=x(1-x)$ and the boundary conditions are taken as $p(0,t)=p(1,t)=0$. The Riemann-Liouville definition for fractional-order derivative is utilized. The analytical solution is found to be (details shown in Appendix, Eq. A 5.31)

$$p(x,t)=\sum_{k=1}^{\infty}\frac{4}{k^3\pi^3}[1-(-1)^k]E_{1-\alpha}(-k^2\pi^2t^{1-\alpha})\,sin(k\pi x)\,, \tag{5.16}$$

where $E_{1-\alpha}(s)$ is the Mittag-Leffler function, and is defined for $(1-\alpha)>0$ as

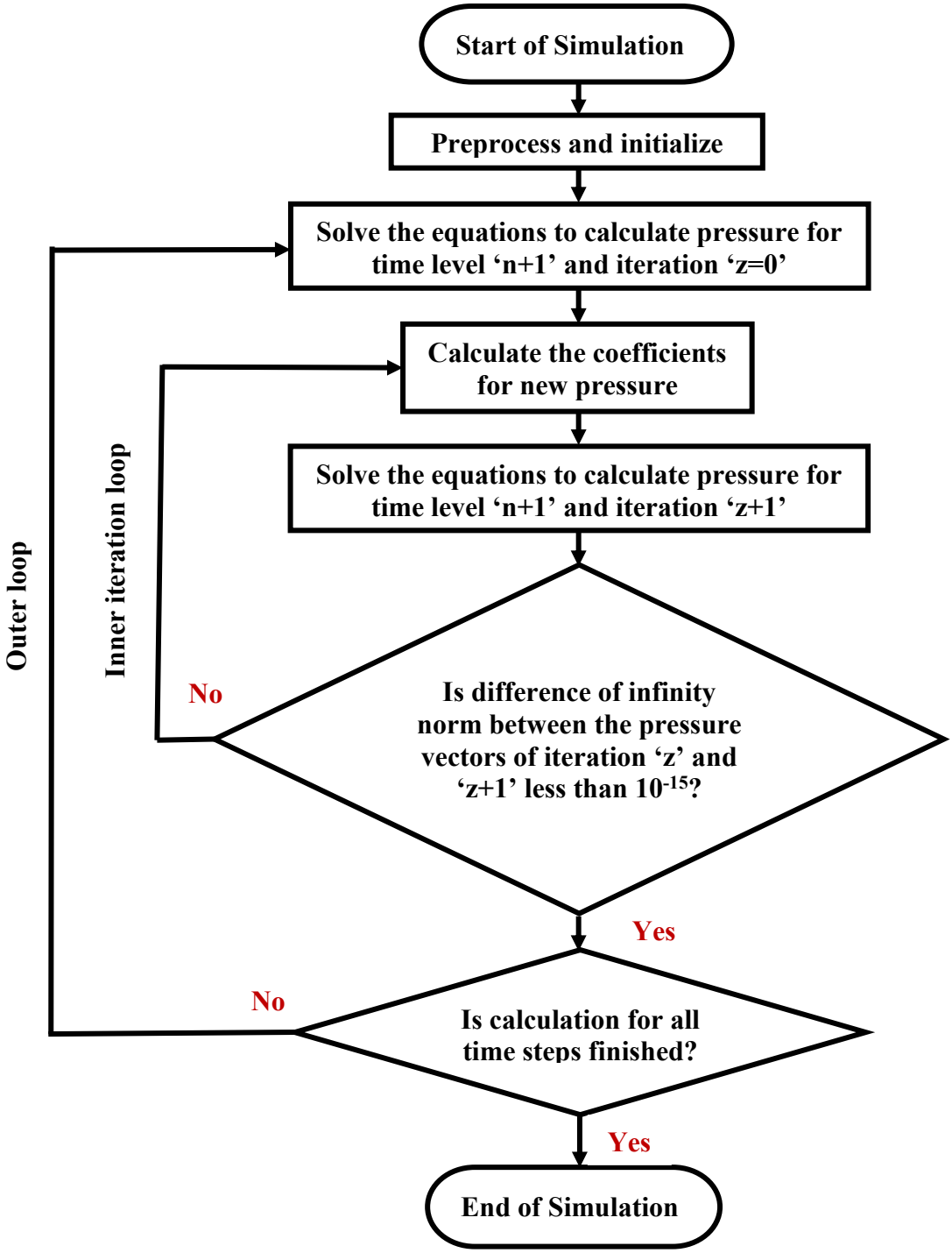

Figure 5.1 Computational algorithm to solve the numerical model.

$$E_{1-\alpha}(s) = \sum_{k=0}^{\infty} \frac{s^k}{\Gamma((1-\alpha)k+1)}. \quad (5.17)$$

5.6 Manufactured Solution for Non-Linear Case

Eq. (5.9) becomes non-linear when C_1 and/or C_2 are not constant. To find a manufactured solution, non-linearity in the equation is included considering just one among $\rho, \phi, c_{t,}$ or μ as variable at a time, while others are kept constant. The variable is expressed in terms of pressure. The true expressions of ρ, ϕ, μ are simplified, and non-linearity is introduced into the equation by considering the simplified terms. For each non-linear term, a manufactured solution is obtained by adding a forcing function to Eq. (5.1).

5.6.1 Inclusion of Density, ρ

5.6.1.1 Case $\alpha = 0$

Taking $\rho = 50 + \frac{p}{1000} - (\frac{p}{1000})^2$, unit values for $\phi, c_{t,}$ μ, and k, and $\alpha = 0$, Eq. (5.1) becomes

$$\frac{\partial}{\partial x}\left[\rho \frac{\partial p}{\partial x}\right] = \rho \frac{\partial p}{\partial t}. \quad (5.18)$$

The initial condition, and boundary conditions are taken to be $p(x,0) = sin(\pi x)$ and $p(0,t) = p(1,t) = 0$, respectively. The solution is then taken to be $p(x,t) = e^{-\pi^2 t} sin(\pi x)$, and Eq. (5.18) is modified to the following (details shown in Appendix)

$$\frac{\partial}{\partial x}\left[\rho \frac{\partial p}{\partial x}\right] = \rho \frac{\partial p}{\partial t} + \frac{1}{10^3}\pi^2 e^{-2\pi^2 t}\, cos^2(\pi x) - \frac{2}{10^6}\pi^2 e^{-3\pi^2 t}\, sin(\pi x)\, cos^2(\pi x). \quad (5.19)$$

5.6.1.2 Case $\alpha \neq 0$

In this case, considering unit values for $\phi, c_{t,}$ μ, k, and T, $\alpha \neq 0$, and $\rho = 50 + \frac{p}{1000} - (\frac{p}{1000})^2$, Eq. (5.1) becomes

$$\frac{\partial}{\partial x}\left[\rho\frac{\partial^{\alpha}}{\partial t^{\alpha}}\left(\frac{\partial p}{\partial x}\right)\right]=\rho\frac{\partial p}{\partial t}\,. \tag{5.20}$$

Taking the initial condition, $p(x,0)=sin(\pi x)$ and boundary conditions, $p(0,t)=p(1,t)=0$, the solution is fixed to be $p(x,t)=e^{-\pi t}sin(\pi x)$. The following modified equation gives this solution (details shown in Appendix)

$$\frac{\partial}{\partial x}\left[\rho\frac{\partial^{\alpha}}{\partial t^{\alpha}}\left(\frac{\partial p}{\partial x}\right)\right]=\rho\frac{\partial p}{\partial t}+\pi t^{-\alpha}E_{1,1-\alpha}(-\pi t)\left[\frac{1}{10^{3}}\pi e^{-\pi t}\,cos^{2}(\pi x)-\right.$$
$$\left.\frac{2}{10^{6}}\pi e^{-2\pi t}\,sin(\pi x)\,cos^{2}(\pi x)-50\pi\,sin(\pi x)-\frac{1}{10^{3}}\pi e^{-\pi t}\,sin^{2}(\pi x)+\frac{1}{10^{6}}\pi e^{-2\pi t}sin^{3}(\pi x)\right]+$$
$$50\pi e^{-\pi t}\,sin(\pi x)+\frac{1}{10^{3}}\pi e^{-2\pi t}\,sin^{2}(\pi x)-\frac{1}{10^{6}}\pi e^{-3\pi t}sin^{3}(\pi x)\,. \tag{5.21}$$

5.6.2 Inclusion of Porosity, ϕ

5.6.2.1 Case $\alpha = 0$

Taking $\phi=0.25+10^{-9}p$, unit values for $\rho, c_{t,}\ \mu, k$, and $\alpha=0$, Eq. (5.1) becomes

$$\frac{\partial^{2}p}{\partial x^{2}}=\phi\frac{\partial p}{\partial t}\,. \tag{5.22}$$

Eq. (5.22) is modified to provide the solution $p(x,t)=e^{-\pi^{2}t}sin(\pi x)$ for initial condition $p(x,0)=sin(\pi x)$ and boundary conditions $p(0,t)=p(1,t)=0$, giving (details shown in Appendix)

$$\frac{\partial^{2}p}{\partial x^{2}}=\phi\frac{\partial p}{\partial t}-0.75\pi^{2}e^{-\pi^{2}t}\,sin(\pi x)+10^{-9}\pi^{2}e^{-2\pi^{2}t}\,sin^{2}(\pi x)\,. \tag{5.23}$$

5.6.2.2 Case $\alpha \neq 0$

Considering unit values for $\rho, c_{t,}\ \mu, k$, and T, $\alpha\neq 0$ and $\phi=0.25+10^{-9}p$, Eq. (5.1) becomes

$$\frac{\partial}{\partial x}\left[\frac{\partial^{\alpha}}{\partial t^{\alpha}}\left(\frac{\partial p}{\partial x}\right)\right] = \phi\frac{\partial p}{\partial t}. \tag{5.24}$$

For initial condition $p(x,0) = sin(\pi x)$ and boundary conditions $p(0,t) = p(1,t) = 0$, the following equation gives the solution $p(x,t) = e^{-\pi t}sin(\pi x)$ (details shown in Appendix)

$$\frac{\partial}{\partial x}\left[\frac{\partial^{\alpha}}{\partial t^{\alpha}}\left(\frac{\partial p}{\partial x}\right)\right] = \phi\frac{\partial p}{\partial t} - \pi^2\, sin(\pi x)\, t^{-\alpha}E_{1,1-\alpha}(-\pi t) + [\pi e^{-\pi t}sin(\pi x)][0.25 + 10^{-9}e^{-\pi t}\, sin(\pi x)]\,. \tag{5.25}$$

5.6.3 Inclusion of viscosity, μ

5.6.3.1 Case $\alpha = 0$

Taking $k = 10^{-7}$, $\mu = (10^{-4}p)^{10^{-3}p}$, unit values for ρ, ϕ, c_t and $\alpha = 0$, Eq. (5.1) becomes

$$\frac{\partial}{\partial x}\left[\frac{10^{-7}}{(10^{-4}p)^{10^{-3}p}}\frac{\partial p}{\partial x}\right] = \frac{\partial p}{\partial t}\,. \tag{5.26}$$

Taking initial and boundary conditions to be $p(x,0) = sin(\pi x)$ and $p(0,t) = p(1,t) = 0$ respectively, the equation that gives the solution $p(x,t) = e^{-\pi^2 t}sin(\pi x)$ is (details shown in Appendix)

$$\frac{\partial}{\partial x}\left[\frac{10^{-7}}{(10^{-4}p)^{10^{-3}p}}\frac{\partial p}{\partial x}\right] = \frac{\partial p}{\partial t} + -10^{-7}\pi e^{-\pi^2 t}\, cos(\pi x)\frac{10^{-3}\pi e^{-\pi^2 t}\, cos(\pi x)\, ln\left(10^{-4}e^{-\pi^2 t}\, sin(\pi x)\right) + 10^{-3}\pi e^{-\pi^2 t}\, cos(\pi x)}{\left(10^{-4}e^{-\pi^2 t}\, sin(\pi x)\right)^{10^{-3}e^{-\pi^2 t}\, sin(\pi x)}} - 10^{-7}\pi^2 e^{-\pi^2 t}\, sin(\pi x)\frac{1}{\left(10^{-4}e^{-\pi^2 t}\, sin(\pi x)\right)^{10^{-3}e^{-\pi^2 t}\, sin(\pi x)}} + \pi^2 e^{-\pi^2 t}\, sin(\pi x). \tag{5.27}$$

5.6.3.2 Case $\alpha \neq 0$

Considering unit values for ρ, ϕ, c_t, T and $\alpha \neq 0$, with $k = 10^{-7}$, $\mu = (10^{-4}p)^{10^{-3}p}$, Eq. (5.1) becomes

$$\frac{\partial}{\partial x}\left[\frac{10^{-7}}{(10^{-4}p)^{10^{-3}p}}\frac{\partial^{\alpha}}{\partial t^{\alpha}}\left(\frac{\partial p}{\partial x}\right)\right] = \frac{\partial p}{\partial t}\,. \tag{5.28}$$

For Initial condition $p(x,0) = sin(\pi x)$ and boundary conditions $p(0,t) = p(1,t) = 0$, the solution is taken to be $p(x,t) = e^{-\pi t} sin(\pi x)$. The following equation gives this as its solution (details shown in Appendix)

$$\frac{\partial}{\partial x}\left[\eta\frac{\partial^{\alpha}}{\partial t^{\alpha}}\left(\frac{\partial p}{\partial x}\right)\right] = \frac{\partial p}{\partial t} + \pi t^{-\alpha} E_{1,1-\alpha}(-\pi t)\left[cos(\pi x)\frac{\partial \eta}{\partial x} - \pi\, sin(\pi x)\,\eta\right] + \pi e^{-\pi t}\, sin(\pi x)\,, \tag{5.29}$$

where

$$\eta = \frac{10^{-7}}{(10^{-4}p)^{10^{-3}p}} T^{\alpha}\,. \tag{5.30}$$

5.7 Analytical Solution and Numerical Approximation for Linear Case in Cylindrical Co-ordinates

For $\alpha = 0$, Eq. (5.1) becomes $(\partial/\partial x)[\rho k(\partial p/\partial x)/\mu] = \rho\phi c_t(\partial p/\partial t)$, which in cylindrical co-ordinate system converts to

$$\frac{1}{r}\frac{\partial}{\partial r}\left(r\frac{\rho k}{\mu}\frac{\partial p}{\partial r}\right) = \rho\phi c_t\frac{\partial p}{\partial t}\,. \tag{5.31}$$

For initial condition $p(r,0) = p_o, 0 \leq r < \infty$, and boundary conditions $p(r,t) = p_o$ as $r \to \infty, t \geq 0$, and $r(\partial p/\partial r) = Q\mu/(2\pi kh)$ as $r \to 0, t > 0$, the analytical solution can be written as

$$p(r,t) = p_o + \frac{Q\mu}{4\pi kH} Ei\left(-\frac{\phi\mu c_t r^2}{4kt}\right), \quad t > 0\,, \tag{5.32}$$

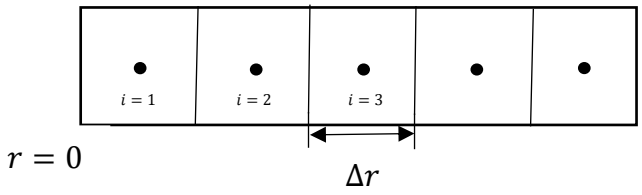

Figure 5.2 Discretization in space.

where $Ei(s)$ is the exponential integral, and is defined as

$$Ei(s) = \int_s^\infty \frac{e^{-w}}{w} dw \, . \tag{5.33}$$

Fig. 5.2 shows the space discretization for Eq. (5.31) where the pressure is calculated at the center of each grid cell. Time is non-uniformly discretized according to the definition of adapted graded mesh above. Discretization of Eq. (5.31) gives

$$-\frac{\Delta t}{\left(i-\frac{1}{2}\right)\Delta r^2}(i-1)C_1\left(r_{i-\frac{1}{2}},t_n\right)p_{i-1}^n + \frac{\Delta t}{\left(i-\frac{1}{2}\right)\Delta r^2}\left[(i-1)C_1\left(r_{i-\frac{1}{2}},t_n\right) + iC_1\left(r_{i+\frac{1}{2}},t_n\right) + \frac{\left(i-\frac{1}{2}\right)\Delta r^2}{\Delta t}C_2(r_i,t_n)\right]p_i^n - \frac{\Delta t}{\left(i-\frac{1}{2}\right)\Delta r^2}iC_1\left(r_{i+\frac{1}{2}},t_n\right)p_{i+1}^n = C_2(r_i,t_n)p_i^{n-1} \, . \tag{5.34}$$

5.8 Results and Discussion

It is necessary to validate the numerical model before using it to find the solutions. In this section, the validation of the developed numerical model has been checked. In addition, the order of temporal and spatial accuracies of the developed model have been investigated.

5.8.1 Validation of the Model

To validate the numerical model, numerical solutions are compared with analytical solutions for the linear case. Eq. (5.17) gives the analytical solution for initial condition $p(x,0) = x(1-x)$ and boundary conditions $p(0,t) = p(1,t) = 0$. Errors are calculated for different numbers of steps in

space and time, and different α values. Figure 5.3 shows the variation of error with number of time steps for $\alpha = 0, 0.1, 0.25$ and 0.50, where the one-dimensional space is divided into 50, and 100 grid-points. As the number of time steps is increased, the error decreases linearly at first. However, for higher numbers of time steps, the rate of change in error decreases and, at some point, the error values reach a plateau before spatial discretization error starts to dominate. The change in error with the number of time steps implies that the numerical model is consistent. The figure shows that the numerical model gives the least error for $\alpha = 0$. With increases in α, the model gives larger errors.

Figure 5.3 also shows that the error decreases with increase in the number of grid-points. At very small numbers of time steps, the differences between error found from 50 and 100 grid-points is insignificant. However, at large number of time steps, the differences are substantial indicating the plateau behaviour is due to the spatial discretization error.

Table 5.1 shows the order of temporal accuracies computed for different values of fractional order, α. It is found that the numerical model is first-order accurate in time. Order of spatial accuracies calculated for different values of fractional order, α, and number of time steps, N_t, are tabulated in Table 5.2. Here, the order of spatial accuracies for $N_t = 12800$, and 25600 are calculated using the error values for $N_x = 10, 20$, and 40. Table 5.2 shows that the order of spatial accuracy of the discretization method approaches 'two', when large value of number of time steps, N_t is used. Therefore, it can be concluded that the numerical model developed using graded meshes is second-order accurate in space.

Error values found using different numbers of grid-points in space and different α values are presented in Table 5.3. It is observed that increases in the number of grid-points in space reduces the error, but that the rate of decrease in the error is not the same as with increasing the number of time steps. The tabulated values also show that the deviation of the numerical solution from the analytical solution increases with the increase in the value of α.

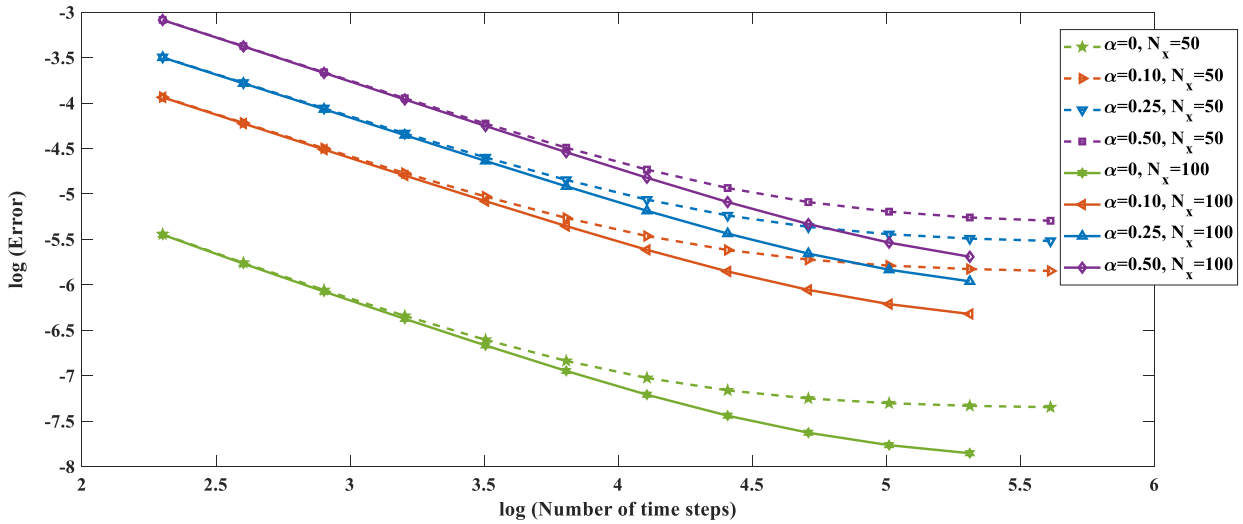

Figure 5.3 Error for different α and N_x.

Table 5.1: Order of temporal accuracy.

Value of fractional order, α	**Order of temporal accuracy**		
	$N_x = 50$	$N_x = 100$	$N_x = 200$
0	0.9946	1.0256	1.0337
0.10	0.9273	0.9524	0.9589
0.25	0.9274	0.9465	0.9515
0.50	0.9555	0.9683	0.9716

Table 5.2: Order of spatial accuracy.

N_t	**Order of spatial accuracy**			
	$\alpha = 0$	$\alpha = 0.10$	$\alpha = 0.25$	$\alpha = 0.50$
12800	1.8581	1.7712	1.7071	1.5971
25600	1.9441	1.8770	1.8389	1.7722

Table 5.3: Error values for different number of grid-points in space for 200 time steps.

Total length of space = 1, Total time = 1, Number of time steps = 200			
No. of grid-points in space	**Absolute Error**		
	$\boldsymbol{\alpha = 0}$	$\boldsymbol{\alpha = 0.25}$	$\boldsymbol{\alpha = 0.50}$
50	3.601062e-06	3.198723e-04	8.245439e-04
100	3.561788e-06	3.177042e-04	8.210083e-04
200	3.551982e-06	3.171656e-04	8.201315e-04
400	3.549531e-06	3.171175e-04	8.200890e-04
800	3.548915e-06	3.189707e-04	8.238759e-04
1600	3.548733e-06	2.889448e-04	7.631701e-04
3200	3.548448e-06	2.889438e-04	7.631672e-04
6400	3.546670e-06	2.889509e-04	7.631698e-04

Numerical solutions of the modified equations are compared with the manufactured solutions for different numbers of space and time steps, and varying α values to validate the numerical model. Code for the numerical solution is modified to include the expression for the pressure-dependent parameters and the source term arising when the equation is modified to obtain that solution. Tables 5.4, 5.5, and 5.6 shows the error found incorporating ρ, ϕ and k/μ in terms of pressure in Eq. (5.1). Numerical values of the errors in these tables give the same conclusions that were made from the linear case.

Table 5.4: Error values incorporating $\rho = 50 + \frac{p}{1000} - (\frac{p}{1000})^2$, and $N_x = 50$.

$\boldsymbol{\rho = 50 + \frac{p}{1000} - (\frac{p}{1000})^2, N_x = 50}$					
$\boldsymbol{N_t}$	**Absolute Error**				
	α=0	**α=0.25**	**α=0.50**	**α=0.75**	**α=0.90**
200	1.3953×10^{-5}	4.7073×10^{-4}	1.0435×10^{-3}	5.2555×10^{-3}	2.7103×10^{-2}
400	6.7659×10^{-6}	2.3965×10^{-4}	4.7512×10^{-4}	2.2868×10^{-3}	1.2867×10^{-2}
800	3.3952×10^{-6}	1.2804×10^{-4}	2.2341×10^{-4}	9.7888×10^{-4}	6.0437×10^{-3}
1600	1.7639×10^{-6}	7.3516×10^{-5}	1.1020×10^{-4}	4.0512×10^{-4}	2.8057×10^{-3}
3200	9.6166×10^{-7}	4.6701×10^{-5}	5.8808×10^{-5}	1.5552×10^{-4}	1.2780×10^{-3}
6400	5.6383×10^{-7}	3.3463×10^{-5}	3.5473×10^{-5}	6.2953×10^{-5}	5.6052×10^{-4}
12800	3.6574×10^{-7}	2.6915×10^{-5}	2.4999×10^{-5}	5.5179×10^{-5}	2.2607×10^{-4}
25600	2.6690×10^{-7}	2.3676×10^{-5}	2.0436×10^{-5}		

Table 5.5: Error values incorporating $\phi = 0.25 + 10^{-9}p$, and $N_x = 50$.

$\phi = 0.25 + 10^{-9}p, N_x = 50$					
N_t	Absolute Error				
	α=0	α=0.25	α=0.50	α=0.75	α=0.90
200	4.5922×10^{-7}	1.4289×10^{-4}	5.4423×10^{-4}	4.5573×10^{-3}	2.6355×10^{-2}
400	2.3824×10^{-7}	7.4488×10^{-5}	2.3158×10^{-4}	1.9675×10^{-3}	1.2538×10^{-2}
800	1.2980×10^{-7}	4.3647×10^{-5}	1.0624×10^{-4}	8.5457×10^{-4}	5.9554×10^{-3}
1600	7.6082×10^{-8}	2.9244×10^{-5}	5.4672×10^{-5}	3.7673×10^{-4}	2.8512×10^{-3}
3200	4.9348×10^{-8}	2.2351×10^{-5}	3.2845×10^{-5}	1.7140×10^{-4}	1.3938×10^{-3}
6400	3.6011×10^{-8}	1.8997×10^{-5}	2.3340×10^{-5}	8.2905×10^{-5}	7.1017×10^{-4}
12800	2.9351×10^{-8}	1.7348×10^{-5}	1.9087×10^{-5}	4.4677×10^{-5}	3.9022×10^{-4}
25600	2.6022×10^{-8}	1.6532×10^{-5}	1.7138×10^{-5}	2.8094×10^{-5}	2.3997×10^{-4}
51200	2.4359×10^{-8}	1.6127×10^{-5}	1.6227×10^{-5}	2.0866×10^{-5}	1.6991×10^{-4}

Table 5.6: Error values incorporating $\frac{k}{\mu} = \frac{10^{-7}}{(10^{-4}p)^{10^{-3}p}}$, and $N_x = 50$.

$\frac{k}{\mu} = \frac{10^{-7}}{(10^{-4}p)^{10^{-3}p}}, N_x = 50$					
N_t	Absolute Error				
	α=0	α=0.25	α=0.50	α=0.75	α=0.90
200	2.4470×10^{-2}	6.7009×10^{-3}	8.6624×10^{-3}	1.6384×10^{-2}	4.0056×10^{-2}
400	1.2286×10^{-2}	3.3550×10^{-3}	4.3401×10^{-3}	8.2286×10^{-3}	2.0266×10^{-2}
800	6.1555×10^{-3}	1.6786×10^{-3}	2.1722×10^{-3}	4.1234×10^{-3}	1.0193×10^{-2}
1600	3.0809×10^{-3}	8.3949×10^{-4}	1.0865×10^{-3}	2.0639×10^{-3}	5.1115×10^{-3}
3200	1.5413×10^{-3}	4.1975×10^{-4}	5.4328×10^{-4}	1.0323×10^{-3}	2.5594×10^{-3}
6400	7.7082×10^{-4}	2.0982×10^{-4}	2.7154×10^{-4}	5.1615×10^{-4}	1.2805×10^{-3}
12800	3.8546×10^{-4}	1.0484×10^{-4}	1.3565×10^{-4}	2.5795×10^{-4}	6.4032×10^{-4}
25600	1.9274×10^{-4}	5.2356×10^{-5}	6.7699×10^{-5}	1.2882×10^{-4}	3.2006×10^{-4}
51200	9.6375×10^{-5}	2.6109×10^{-5}	3.3721×10^{-5}	6.4251×10^{-5}	1.5988×10^{-4}

The numerical model for the memory-based radial diffusivity equation is developed following the way that the model is developed for the linear case. The memory-based radial diffusivity equation converts to the standard radial diffusivity equation for $\alpha = 0$. The numerical solution for $\alpha = 0$ is compared to the analytical solution of the radial diffusivity equation for initial condition $p(r, 0) = p_o, 0 \leq r < \infty$, and boundary conditions $p(r, t) = p_o$ as $r \to \infty, t \geq 0$, and $r(\partial p/\partial r) = Q\mu/(2\pi kh)$ as $r \to 0, t > 0$. The parameters used in the calculation are shown in Table 5.7. Analytical and numerical solutions at distances of r_w and r_e are tabulated in Tables 5.8 and 5.9,

respectively. From these tables, it is seen that the numerical solution is very close to the analytical solution. The difference between analytical and numerical solution is about 0.18 at $r = r_w$. The differences between analytical and numerical solutions are negligible at the distance of r_e from the center of wellbore. Pressure profiles generated from the numerical simulation for this case is shown in Fig. 5.4.

Table 5.7: Parameters for a reservoir.

Item	Description	Value	
		In British unit system	In Darcy Unit System
Q_o	Oil production rate	300 STB/D	552.04 cm^3/sec
μ	Oil viscosity	1.06 cp	1.06 cp
k	Permeability	300 md	0.3 darcy
H	Thickness	100 ft	3048 cm
c_o	Oil compressibility	0.00001 psi^{-1}	1.46959×10^{-4} atm^{-1}
c_R	Rock compressibility	0.000004 psi^{-1}	5.87838×10^{-5} atm^{-1}
c_t	Total compressibility, $(c_o + c_R)$	0.000014 psi^{-1}	2.05743×10^{-4} atm^{-1}
ϕ	Porosity	0.2 (fraction)	0.2 (fraction)
p_o	Initial pressure	3600 psia	244.9656 atm
p_b	Bubble point pressure	2000 psia	136.092 atm
B_{ob}	Oil formation volume factor at p_b	1.063 (fraction)	1.063 (fraction)
r_w	Radius of wellbore	0.1875 ft	5.715 cm
r_e	An arbitrary distance from center of wellbore	28.0176 ft	853.98 cm
L	Length in the x-direction	8100 ft	246888 cm

Table 5.8: The pressure comparison at $r = r_w$.

Time (days)	Time (Seconds)	p (analytical solution) (psia)	p_h (numerical solution) (psia)	$p_h - p$ (psia)
0.1	8640	3588.08	3588.26	0.18
0.2	17280	3587.54	3587.72	0.18
0.3	25920	3587.22	3587.40	0.18
0.4	34560	3587.00	3587.18	0.18
0.5	43200	3586.82	3587.00	0.18
0.6	51840	3586.68	3586.86	0.18
0.7	60480	3586.56	3586.74	0.18
0.8	69120	3586.45	3586.64	0.19
0.9	77760	3586.36	3586.54	0.18
1.0	86400	3586.28	3586.46	0.18

Table 5.9: The pressure comparison at $r = r_e$.

Time (days)	Time (Seconds)	p (analytical solution) (psia)	p_h (numerical solution) (psia)	$p_h - p$ (psia)
0.1	8640	3595.9205103	3595.9196454	-0.0008649
0.2	17280	3595.3779089	3595.3781949	0.0002860
0.3	25920	3595.0605074	3595.0611771	0.0006697
0.4	34560	3594.8353075	3594.8361691	0.0008616
0.5	43200	3594.6606288	3594.6616056	0.0009768
0.6	51840	3594.5179060	3594.5189595	0.0010535
0.7	60480	3594.3972355	3594.3983439	0.0011084
0.8	69120	3594.2927060	3594.2938555	0.0011495
0.9	77760	3594.2005045	3594.2016859	0.0011814
1.0	86400	3594.1180274	3594.1192344	0.0012070

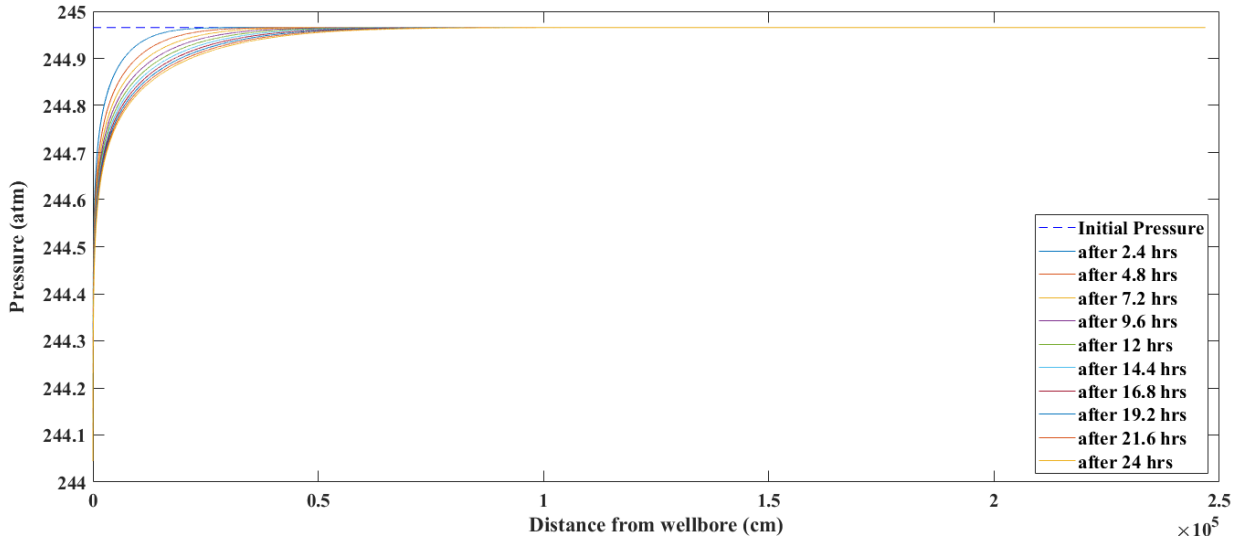

Figure 5.4 Pressure profile from numerical simulation for the radial case.

5.8.2 Significance of the Model and Sensitivity Analysis

Finding analytical solutions of the time-fractional diffusion equation is not always convenient. This model can be helpful to numerically solve the equation for any initial and boundary conditions. In addition, the model can be used to observe the effects of the fractional order on the

solutions. The solutions of Eq. (5.1) for different α values are shown in Fig. 5.5. Here, $(\rho k/\mu)T^{\alpha} = 1$, and $\rho\phi c_t = 1$ has been considered. The initial condition is taken as $p(x,0) = x(1-x)$ and boundary condition is taken as $p(0,t) = p(1,t) = 0$. The numerical values of the solutions get higher as the value of fractional order increases within $0 \leq \alpha < 1$. The equation can give different numerical solutions based on its fractional order while keeping the other parameters constant. Field data can be used to determine the value of the fractional order that will accurately represent true flow phenomenon. The fractional order value provides information about the dependence of the fluid flow phenomenon through that porous media on its history.

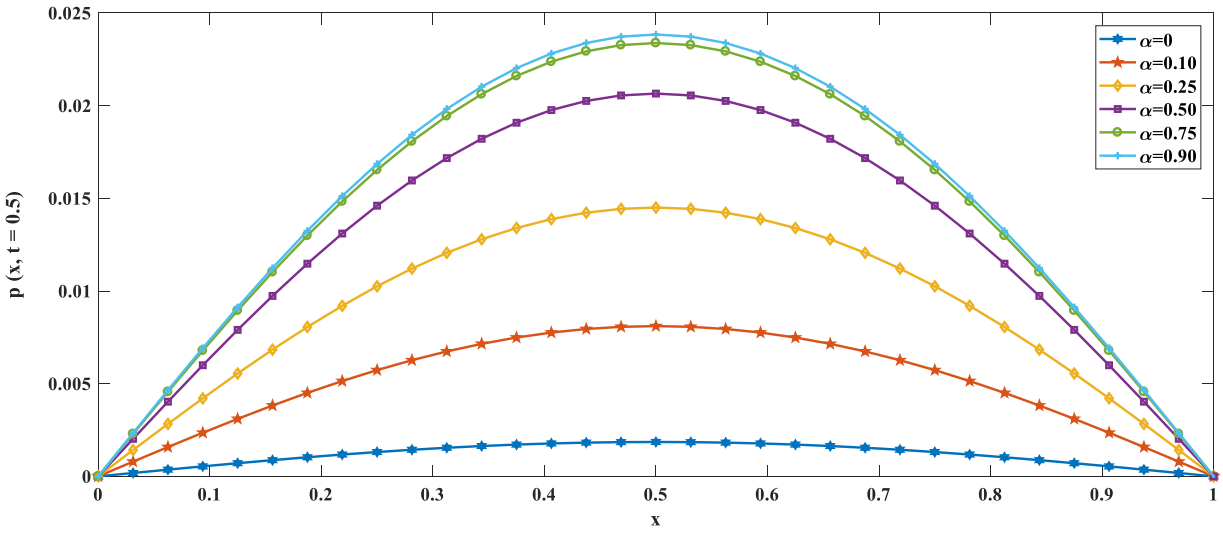

Figure 5.5 Solutions of the time fractional diffusion equation for different α values.

5.9 Conclusions

A numerical model is developed to solve a time-fractional non-linear diffusion equation applying the Riemann-Liouville definition for the fractional-order derivative. The L1 algorithm is derived for an adapted graded mesh. The numerical model is validated, comparing with analytical solutions in the linear case and with manufactured solutions in the non-linear cases of the equation. From the error analysis, it can be concluded that the numerical model is consistent, second-order accurate

in space, and first-order accurate in time. The model can be used to investigate the effect of memory on fluid flow through porous media.

5.10 Acknowledgement

The authors would like to thank the Natural Sciences and Engineering Research Council of Canada (NSERC); Research & Development Corporation of Newfoundland and Labrador (RDC), funding no. 210992; and Statoil Canada Ltd., funding no. 211162 for providing financial support to accomplish this research under the Statoil Chair in Reservoir Engineering at the Memorial University of Newfoundland, St. John's, NL, Canada.

Bibliography

1. Brunner, H., Ling, L., & Yamamoto, M. (2010). Numerical simulations of 2D fractional subdiffusion problems. *Journal of Computational Physics*, *229*(18), 6613–6622. http://doi.org/10.1016/j.jcp.2010.05.015
2. Chen, C. M., Liu, F., Turner, I., & Anh, V. (2007). A Fourier method for the fractional diffusion equation describing sub-diffusion. *Journal of Computational Physics*, *227*(2), 886–897. http://doi.org/10.1016/j.jcp.2007.05.012
3. Cui, M. (2009). Compact finite difference method for the fractional diffusion equation. *Journal of Computational Physics*, *228*(20), 7792–7804. http://doi.org/10.1016/j.jcp.2009.07.021
4. Gorenflo, R., Mainardi, F., Moretti, D., & Paradisi, P. (2002). Time fractional diffusion: A discrete random walk approach. *Nonlinear Dynamics*, *29*(1–4), 129–143. http://doi.org/10.1023/A:1016547232119
5. Hossain, M. E., Mousavizadegan, S. H., & Islam, M. R. (2008). A New Porous Media Diffusivity Equation with the Inclusion of Rock and Fluid Memories. *Society of Petroleum Engineers,* SPE-114287-MS.
6. Lynch, V. E., Carreras, B. A., del-Castillo-Negrete, D., Ferreira-Mejias, K. M., & Hicks, H. R. (2003). Numerical methods for the solution of partial differential equations of fractional order. *Journal of Computational Physics*, *192*(2), 406–421. http://doi.org/10.1016/j.jcp.2003.07.008
7. ME Hossain, M. I. (2006). Fluid Properties With Memory – a Critical Review and Some Additions. *The 36th International Conference on Computers and Industrial Engineering June 20-23, 2006, Taipei, Taiwan*, (July), 13.
8. Meerschaert, M. M., & Tadjeran, C. (2004). Finite difference approximations for fractional advection-dispersion flow equations. *Journal of Computational and Applied Mathematics*, *172*(1), 65–77. http://doi.org/10.1016/j.cam.2004.01.033
9. Murio, D. A. (2008). Implicit finite difference approximation for time fractional diffusion equations. *Computers and Mathematics with Applications*, *56*(4), 1138–1145. http://doi.org/10.1016/j.camwa.2008.02.015
10. Mustapha, K., & McLean, W. (2011). Piecewise-linear, discontinuous Galerkin method for a

fractional diffusion equation. *Numerical Algorithms*, *56*(2), 159–184. http://doi.org/10.1007/s11075-010-9379-8

11. Podlubny, I., Chechkin, A., Skovranek, T., Chen, Y., & Vinagre Jara, B. M. (2009). Matrix approach to discrete fractional calculus II: Partial fractional differential equations. *Journal of Computational Physics*, *228*(8), 3137–3153. http://doi.org/10.1016/j.jcp.2009.01.014
12. Shen, S. (2004). Error analysis of an explicit finite difference approximation for the space fractional diffusion equation with insulated ends. *ANZIAM Journal*, *46*(August 2014), 1–10. http://doi.org/10.21914/anziamj.v46i0.995
13. Skovranek, T., Verbickij, V. V., Tarte, Y., Podlubny, I. (2010). Discretization of fractional-order operators and fractional differential equations on a non-equidistant mesh. *Proceedings of FDA10, The 4th IFAC Workshop Fractional Differentiation and its Applications, Badajoz, 18*.
14. Sochi, T. (2010). Non-Newtonian flow in porous media. *Polymer*, *51*(22), 5007–5023. http://doi.org/10.1016/j.polymer.2010.07.047
15. Stynes, M., O'Riordan, E., & Gracia, J. E. L. (2017). Error analysis of a finite difference method on graded meshes for a time-fractional diffusion equation, *SIAM Journal of Numerical Analysis, 55*(2), 1057–1079.
16. Sun, Q. Y., & Schatten, H. (2006). Regulation of dynamic events by microfilaments during oocyte maturation and fertilization. *Reproduction*, *131*(2), 193–205. http://doi.org/10.1016/j.apnum.2005.03.003
17. Yuste, S. B. (2006). Weighted average finite difference methods for fractional diffusion equations. *Journal of Computational Physics*, *216*(1), 264–274. http://doi.org/10.1016/j.jcp.2005.12.006
18. Yuste, S. B., & Acedo, L. (2005). Neumann-Type Stability Analysis for Fractional, *42*(5), 1862–1874.
19. Zaman, T. U., MacLachlan, S., and Hossain, M. E. (2017). Numerical modelling of a memory-based radial diffusivity equation using the Riemann-Liouville definition of the fractional-order derivative and uniform meshes. (in preparation).
20. Zhang, H. M. (2003). Driver memory, traffic viscosity and a viscous vehicular traffic flow model. *Transportation Research Part B: Methodological*, *37*(1), 27–41. http://doi.org/10.1016/S0191-2615(01)00043-1

Appendix

Analytical Solution for Linear Case

To find the analytical solution, we consider $C_1 = C_2 = 1$ in Eq. (5.9) giving

$$\frac{\partial}{\partial x}\left[\frac{\partial^\alpha}{\partial t^\alpha}\left(\frac{\partial p}{\partial x}\right)\right] = \frac{\partial p}{\partial t}\,, \tag{A 5.1}$$

with boundary conditions $p(0) = p(1) = 0$.

We write the solution in series form as

$$p(x,t) = \sum_{k=1}^{\infty} T_k\,(t) sin(k\pi x)\,, \tag{A 5.2}$$

noting that

$$\frac{\partial p}{\partial t}\,(x,t) = \sum_{k=1}^{\infty} T_k'(t)\, sin(k\pi x) = -\sum_{k=1}^{\infty} k^2\pi^2\, \frac{\partial^\alpha T_k(t)}{\partial t^\alpha}\, sin(k\pi x) = \frac{\partial}{\partial x}[\frac{\partial^\alpha}{\partial t^\alpha}\,(\frac{\partial p}{\partial x})]\,. \tag{A 5.3}$$

To be a solution, we require that

$$T_k'(t) = -k^2\pi^2\, \frac{\partial^\alpha T_k(t)}{\partial t^\alpha}\,, \tag{A 5.4}$$

$$\text{and } T_k(0) = \beta_k\,, \tag{A 5.5}$$

where β_k comes from the sine series expansion of the initial data, $p(x,0) = \sum_{k=1}^{\infty} \beta_k\, sin(k\pi x)$.

Taking Laplace transforms, we have

$$\mathcal{L}[T_k'(t)] = s\hat{T}_k(s) - \beta_k\,. \tag{A 5.6}$$

For the Riemann-Liouville definition of the fractional-order derivative,

$$\mathcal{L}\left[\frac{\partial^{\alpha}T_k(t)}{\partial t^{\alpha}}\right] = s^{\alpha}\hat{T}_k(s) - [D^{\alpha-1}T_k(t)]_{t=0}\,. \tag{A 5.7}$$

Therefore,

$$s\hat{T}_k(s) - \beta_k = -k^2\pi^2(s^{\alpha}\hat{T}_k(s) - c_k) \quad \text{where } c_k = [D^{\alpha-1}T_k(t)]_{t=0} \tag{A 5.8}$$

$$or, (s + k^2\pi^2 s^{\alpha})\hat{T}_k(s) = \beta_k + k^2\pi^2 c_k\,, \tag{A 5.9}$$

$$or, \hat{T}_k(s) = \frac{\beta_k + k^2\pi^2 c_k}{s + k^2\pi^2 s^{\alpha}} = \frac{(\beta_k + k^2\pi^2 c_k)s^{-\alpha}}{s^{1-\alpha} + k^2\pi^2}\,. \tag{A 5.10}$$

This gives

$$T_k(t) = (\beta_k + k^2\pi^2 c_k)E_{1-\alpha}(-k^2\pi^2 t^{1-\alpha})\,, \tag{A 5.11}$$

where $E_{1-\alpha}(v)$ is the Mittag-Leffler function, and is defined for $(1-\alpha) > 0$ as

$$E_{1-\alpha}(v) = \sum_{k=0}^{\infty} \frac{v^k}{\Gamma((1-\alpha)k+1)}\,, \tag{A 5.12}$$

since $\mathcal{L}[E_{1-\alpha}(-k^2\pi^2 t^{1-\alpha})] = \frac{s^{-\alpha}}{s^{1-\alpha} + k^2\pi^2}\,.$ (A 5.13)

Now,

$$D^{\alpha-1}[(\beta_k + k^2\pi^2 c_k)E_{1-\alpha}(-k^2\pi^2 t^{1-\alpha})] = \frac{\beta_k + k^2\pi^2 c_k}{-k^2\pi^2}(E_{1-\alpha}(-k^2\pi^2 t^{1-\alpha}) - 1)\,, \tag{A 5.14}$$

which forces $D^{\alpha-1}[T_k(t)]_{t=0} = 0$ as $E_{1-\alpha}(0) = 1\,,$ (A 5.15)

giving $c_k = 0, T_k(t) = \beta_k E_{1-\alpha}(-k^2\pi^2 t^{1-\alpha})$, (A 5.16)

and $p(x,t) = \sum_{k=1}^{\infty} \beta_k E_{1-\alpha}(-k^2\pi^2 t^{1-\alpha}) \, sin(k\pi x)$. (A 5.17)

Eq. (A 5.17) is the general analytical solution of Eq. (A 5.1) for any initial condition.

Now, taking the initial condition considered above,

$p_0(x) = x(1-x)$, (A 5.18)

We write this as

$p_0(x) sin(m\pi x) \equiv \sum_{k=1}^{\infty} \beta_k \, sin(k\pi x) \, sin(m\pi x)$, (A 5.19)

$or, \int_0^1 p_0(x) sin(m\pi x) dx \equiv \int_0^1 \sum_{k=1}^{\infty} \beta_k \, sin(k\pi x) \, sin(m\pi x) \, dx$. (A 5.20)

Interchanging summation and integration and expanding, we get,

$\int_0^1 p_0(x) sin(m\pi x) dx \equiv \int_0^1 \beta_1 \, sin(\pi x) \, sin(m\pi x) \, dx + \int_0^1 \beta_2 \, sin(2\pi x) \, sin(m\pi x) \, dx + \cdots + \int_0^1 \beta_k \, sin(k\pi x) \, sin(m\pi x) \, dx + \cdots$ (A 5.21)

If $k \neq m$,

$\int_0^1 \beta_k \, sin(k\pi x) \, sin(m\pi x) \, dx = 0$, (A 5.22)

while, if $k = m$,

$\int_0^1 \beta_k \, sin(k\pi x) \, sin(m\pi x) \, dx \neq 0$. (A 5.23)

So, we get, $\int_0^1 p_0(x)sin(k\pi x)dx = \int_0^1 \beta_k \, sin^2(k\pi x)\, dx$. (A 5.24)

Solving for β_k gives

$$\beta_k = \frac{\int_0^1 p_0(x)sin(k\pi x)dx}{\int_0^1 sin^2(k\pi x)dx} . \quad \text{(A 5.25)}$$

Now,

$$\int_0^1 x(1-x)\, sin(k\pi x)\, dx = [-\frac{1}{k\pi}(x-x^2)\, cos(k\pi x) + \frac{1}{k^2\pi^2}(1-2x)\, sin(k\pi x) - \frac{2}{k^3\pi^3} cos(k\pi x)]_0^1 \quad \text{(A 5.26)}$$

$$= -\frac{1}{k^2\pi^2} sin(k\pi) - \frac{2}{k^3\pi^3} cos(k\pi) + \frac{2}{k^3\pi^3} = \frac{2}{k^3\pi^3} - \frac{2}{k^3\pi^3}(-1)^k , \quad \text{(A 5.27)}$$

and

$$\int_0^1 sin^2(k\pi x)\, dx = \frac{1}{2}\int_0^1 \{1 - cos(2k\pi x)\}\, dx = \frac{1}{2} . \quad \text{(A 5.28)}$$

Hence,

$$\beta_k = \frac{\frac{2}{k^3\pi^3} - \frac{2}{k^3\pi^3}(-1)^k}{\frac{1}{2}} , \quad \text{(A 5.29)}$$

$$or, \beta_k = 2[\frac{2}{k^3\pi^3} - \frac{2}{k^3\pi^3}(-1)^k] = \frac{4}{k^3\pi^3}[1-(-1)^k] . \quad \text{(A 5.30)}$$

This gives

$$p(x,t) = \sum_{k=1}^{\infty} \frac{4}{k^3\pi^3}[1-(-1)^k] E_{1-\alpha}(-k^2\pi^2 t^{1-\alpha})\, sin(k\pi x) . \quad \text{(A 5.31)}$$

Manufactured Solutions for the Nonlinear case

Inclusion of Density, ρ

Case $\alpha = 0$

Taking $\rho = 50 + \frac{p}{1000} - (\frac{p}{1000})^2$, unit values for $\phi, c_{t,}\ \mu$, and k, and $\alpha = 0$, Eq. (5.1) becomes

$$\frac{\partial}{\partial x}\left[\rho \frac{\partial p}{\partial x}\right] = \rho \frac{\partial p}{\partial t}\ . \tag{A 5.32}$$

Let the analytical solution of the equation

$$\frac{\partial}{\partial x}\left[\rho \frac{\partial p}{\partial x}\right] = \rho \frac{\partial p}{\partial t} + f(x,t) \tag{A 5.33}$$

be $p(x,t) = e^{-\pi^2 t} sin(\pi x)$, giving (A 5.34)

$$\rho = 50 + \frac{1}{1000} e^{-\pi^2 t} sin(\pi x) - \frac{1}{10^6} e^{-2\pi^2 t} sin^2(\pi x)\ . \tag{A 5.35}$$

Note $p(x,t)$ as given satisfies the initial condition $p(x,0) = sin(\pi x)$, and the boundary conditions $p(0,t) = p(1,t) = 0$.

Now,

$$\frac{\partial}{\partial x}\left(\rho \frac{\partial p}{\partial x}\right) = \frac{\partial \rho}{\partial x}\frac{\partial p}{\partial x} + \rho \frac{\partial^2 p}{\partial x^2} \tag{A 5.36}$$

$$\text{gives } \frac{\partial}{\partial x}\left(\rho \frac{\partial p}{\partial x}\right) = [\frac{1}{10^3}\pi e^{-\pi^2 t} cos(\pi x) - \frac{2}{10^6}\pi e^{-2\pi^2 t} sin(\pi x) cos(\pi x)]\left[\pi e^{-\pi^2 t} cos(\pi x)\right]$$
$$+[50 + \frac{1}{10^3} e^{-\pi^2 t} sin(\pi x) - \frac{1}{10^6} e^{-2\pi^2 t} sin^2(\pi x)][-\pi^2 e^{-\pi^2 t} sin(\pi x)]\ , \tag{A 5.37}$$

$$or, \frac{\partial}{\partial x}\left(\rho \frac{\partial p}{\partial x}\right) = \frac{1}{10^3}\pi^2 e^{-2\pi^2 t}\, cos^2(\pi x) - \frac{2}{10^6}\pi^2 e^{-3\pi^2 t}\, sin(\pi x)\, cos^2(\pi x) - 50\pi^2 e^{-\pi^2 t}\, sin(\pi x) - \frac{1}{10^3}\pi^2 e^{-2\pi^2 t}\, sin^2(\pi x) + \frac{1}{10^6}\pi^2 e^{-3\pi^2 t}\, sin^3(\pi x)\,. \quad \text{(A 5.38)}$$

From direct calculation,

$$\rho \frac{\partial p}{\partial t} = \left[50 + \frac{1}{10^3} e^{-\pi^2 t}\, sin(\pi x) - \frac{1}{10^6} e^{-2\pi^2 t} sin^2(\pi x)\right]\left[-\pi^2 e^{-\pi^2 t}\, sin(\pi x)\right], \quad \text{(A 5.39)}$$

$$or, \rho \frac{\partial p}{\partial t} = -50\pi^2 e^{-\pi^2 t}\, sin(\pi x) - \frac{1}{10^3}\pi^2 e^{-2\pi^2 t}\, sin^2(\pi x) + \frac{1}{10^6}\pi^2 e^{-3\pi^2 t}\, sin^3(\pi x)\,. \quad \text{(A 5.40)}$$

Therefore, defining

$$f(x,t) = \frac{\partial}{\partial x}\left(\rho \frac{\partial p}{\partial x}\right) - \rho \frac{\partial p}{\partial t} \quad \text{(A 5.41)}$$

gives $f(x,t) = \frac{1}{10^3}\pi^2 e^{-2\pi^2 t}\, cos^2(\pi x) - \frac{2}{10^6}\pi^2 e^{-3\pi^2 t}\, sin(\pi x)\, cos^2(\pi x)\,.$ (A 5.42)

Case $\alpha \neq 0$

Consider unit values for $\phi, c_{t,}\ \mu, k$, and T, $\alpha \neq 0$ and $\rho = 50 + \frac{p}{1000} - (\frac{p}{1000})^2$. For these values, Eq. (5.1) becomes

$$\frac{\partial}{\partial x}\left[\rho \frac{\partial^\alpha}{\partial t^\alpha}\left(\frac{\partial p}{\partial x}\right)\right] = \rho \frac{\partial p}{\partial t}\,. \quad \text{(A 5.43)}$$

Let the analytical solution of the equation

$$\frac{\partial}{\partial x}\left[\rho \frac{\partial^\alpha}{\partial t^\alpha}\left(\frac{\partial p}{\partial x}\right)\right] = \rho \frac{\partial p}{\partial t} + f(x,t) \quad \text{(A 5.44)}$$

be $p(x,t) = e^{-\pi t} sin(\pi x)$. With this, (A 5.45)

$$\rho = 50 + \frac{1}{10^3} e^{-\pi t} sin(\pi x) - \frac{1}{10^6} e^{-2\pi t} sin^2(\pi x) \, . \tag{A 5.46}$$

Note that $p(x,t)$ satisfies the initial condition $p(x,0) = sin(\pi x)$, and the boundary conditions $p(0,t) = p(1,t) = 0$.

Now,

$$\frac{\partial}{\partial x}\left[\rho \frac{\partial^\alpha}{\partial t^\alpha}\left(\frac{\partial p}{\partial x}\right)\right] = \frac{\partial}{\partial x}\left[\rho \frac{\partial^\alpha}{\partial t^\alpha}(\pi e^{-\pi t} cos(\pi x))\right] . \tag{A 5.47}$$

Using the Riemann-Liouville definition of the fractional order derivative, $\frac{\partial^\alpha}{\partial t^\alpha}\left(e^{\lambda t}\right) = t^{-\alpha} E_{1,1-\alpha}(-\pi t)$, we get

$$\frac{\partial}{\partial x}\left[\rho \frac{\partial^\alpha}{\partial t^\alpha}\left(\frac{\partial p}{\partial x}\right)\right] = \frac{\partial}{\partial x}\left[\rho\pi \, cos(\pi x) \, t^{-\alpha} E_{1,1-\alpha}(-\pi t)\right] , \tag{A 5.48}$$

$$or, \frac{\partial}{\partial x}\left[\rho \frac{\partial^\alpha}{\partial t^\alpha}\left(\frac{\partial p}{\partial x}\right)\right] = \pi t^{-\alpha} E_{1,1-\alpha}(-\pi t)\left[cos(\pi x)\frac{\partial \rho}{\partial x} + \rho(-\pi sin(\pi x))\right] . \tag{A 5.49}$$

$$\begin{aligned} \text{Thus, } \frac{\partial}{\partial x}\left[\rho \frac{\partial^\alpha}{\partial t^\alpha}\left(\frac{\partial p}{\partial x}\right)\right] = \pi t^{-\alpha} E_{1,1-\alpha}(-\pi t)\Big[cos(\pi x)\Big\{&\frac{1}{10^3}\pi e^{-\pi t} cos(\pi x) - \\ &\frac{2}{10^6}\pi e^{-2\pi t} sin(\pi x) cos(\pi x)\Big\} - \pi \, sin(\pi x)\Big\{50 + \frac{1}{10^3} e^{-\pi t} sin(\pi x) - \\ &\frac{1}{10^6} e^{-2\pi t} sin^2(\pi x)\Big\}\Big] , \end{aligned} \tag{A5.50}$$

$$\begin{aligned} or, \frac{\partial}{\partial x}\left[\rho \frac{\partial^\alpha}{\partial t^\alpha}\left(\frac{\partial p}{\partial x}\right)\right] = \pi t^{-\alpha} E_{1,1-\alpha}(-\pi t)\Big[&\frac{1}{10^3}\pi e^{-\pi t} cos^2(\pi x) - \\ &\frac{2}{10^6}\pi e^{-2\pi t} sin(\pi x) cos^2(\pi x) - 50\pi \, sin(\pi x) - \frac{1}{10^3}\pi e^{-\pi t} sin^2(\pi x) + \frac{1}{10^6}\pi e^{-2\pi t} sin^3(\pi x)\Big]. \end{aligned} \tag{A 5.51}$$

Furthermore,

$$\rho \frac{\partial p}{\partial t} = \left[50 + \frac{1}{10^3} e^{-\pi t} sin(\pi x) - \frac{1}{10^6} e^{-2\pi t} sin^2(\pi x)\right][-\pi e^{-\pi t} sin(\pi x)] , \tag{A 5.52}$$

$$or,\ \rho\frac{\partial p}{\partial t} = \left[-50\pi e^{-\pi t}\, sin(\pi x) - \frac{1}{10^3}\pi e^{-2\pi t}\, sin^2(\pi x) + \frac{1}{10^6}\pi e^{-3\pi t} sin^3(\pi x)\right]. \quad \text{(A 5.53)}$$

Thus, defining

$$f(x,t) = \frac{\partial}{\partial x}\left[\rho\frac{\partial^\alpha}{\partial t^\alpha}\left(\frac{\partial p}{\partial x}\right)\right] - \rho\frac{\partial p}{\partial t} \quad \text{(A 5.54)}$$

gives $f(x,t) = \pi t^{-\alpha} E_{1,1-\alpha}(-\pi t)\left[\frac{1}{10^3}\pi e^{-\pi t}\, cos^2(\pi x) - \frac{2}{10^6}\pi e^{-2\pi t}\, sin(\pi x)\, cos^2(\pi x) - 50\pi\, sin(\pi x) - \frac{1}{10^3}\pi e^{-\pi t}\, sin^2(\pi x) + \frac{1}{10^6}\pi e^{-2\pi t} sin^3(\pi x)\right] + 50\pi e^{-\pi t}\, sin(\pi x) + \frac{1}{10^3}\pi e^{-2\pi t}\, sin^2(\pi x) - \frac{1}{10^6}\pi e^{-3\pi t} sin^3(\pi x)$. (A 5.55)

Inclusion of Porosity, ϕ

Case $\alpha = 0$

Taking $\phi = 0.25 + 10^{-9}p$, unit values for $\rho, c_{t,}\ \mu$, and k, and $\alpha = 0$, Eq. (5.1) becomes

$$\frac{\partial^2 p}{\partial x^2} = \phi\frac{\partial p}{\partial t}\,. \quad \text{(A 5.56)}$$

Let the analytical solution of the equation

$$\frac{\partial^2 p}{\partial x^2} = \phi\frac{\partial p}{\partial t} + f(x,t) \quad \text{(A 5.57)}$$

be $p(x,t) = e^{-\pi^2 t} sin(\pi x)$, giving (A 5.58)

$$\phi = 0.25 + 10^{-9} e^{-\pi^2 t} sin(\pi x)\,. \quad \text{(A 5.59)}$$

Note $p(x,t)$ as given satisfies the initial condition $p(x,0) = sin(\pi x)$, and the boundary conditions $p(0,t) = p(1,t) = 0$.

Now,

$$\frac{\partial^2 p}{\partial x^2} = -\pi^2 e^{-\pi^2 t} sin(\pi x) \, . \tag{A 5.60}$$

From direct calculation,

$$\phi \frac{\partial p}{\partial t} = (0.25 + 10^{-9} p)[-\pi^2 e^{-\pi^2 t} sin(\pi x)] \, , \tag{A 5.61}$$

$$or, \ \phi \frac{\partial p}{\partial t} = [0.25 + 10^{-9} e^{-\pi^2 t} \, sin(\pi x)][-\pi^2 e^{-\pi^2 t} sin(\pi x)] \, , \tag{A 5.62}$$

$$or, \ \phi \frac{\partial p}{\partial t} = -0.25\pi^2 e^{-\pi^2 t} \, sin(\pi x) - 10^{-9} \pi^2 e^{-2\pi^2 t} \, sin^2(\pi x) \, . \tag{A 5.63}$$

Therefore, defining

$$f(x,t) = \frac{\partial^2 p}{\partial x^2} - \phi \frac{\partial p}{\partial t} \tag{A 5.64}$$

$$\text{gives } f(x,t) = -0.75\pi^2 e^{-\pi^2 t} \, sin(\pi x) + 10^{-9} \pi^2 e^{-2\pi^2 t} \, sin^2(\pi x) \, . \tag{A 5.65}$$

Case $\alpha \neq 0$

Consider unit values for $\rho, c_t, \ \mu, \ k$, and T, $\alpha \neq 0$ and $\phi = 0.25 + 10^{-9} p$. For these values, Eq. (5.1) becomes

$$\frac{\partial}{\partial x}\left[\frac{\partial^\alpha}{\partial t^\alpha}\left(\frac{\partial p}{\partial x}\right)\right] = \phi \frac{\partial p}{\partial t} \, . \tag{A 5.66}$$

Let the analytical solution of the equation

$$\frac{\partial}{\partial x}\left[\frac{\partial^\alpha}{\partial t^\alpha}\left(\frac{\partial p}{\partial x}\right)\right] = \phi \frac{\partial p}{\partial t} + f(x,t) \tag{A 5.67}$$

be $p(x,t) = e^{-\pi t} sin(\pi x)$. With this, (A 5.68)

$$\phi = 0.25 + 10^{-9} e^{-\pi t} sin(\pi x) \, . \tag{A 5.69}$$

Note that $p(x,t)$ satisfies the initial condition $p(x,0) = sin(\pi x)$, and the boundary conditions $p(0,t) = p(1,t) = 0$.

Now,

$$\frac{\partial}{\partial x}\left[\frac{\partial^\alpha}{\partial t^\alpha}\left(\frac{\partial p}{\partial x}\right)\right] = \frac{\partial}{\partial x}\left[\frac{\partial^\alpha}{\partial t^\alpha}(\pi e^{-\pi t} cos(\pi x))\right] \tag{A 5.70}$$

$$\text{gives } \frac{\partial}{\partial x}\left[\frac{\partial^\alpha}{\partial t^\alpha}\left(\frac{\partial p}{\partial x}\right)\right] = \frac{\partial}{\partial x}\left[\pi \, cos(\pi x) \, t^{-\alpha} E_{1,1-\alpha}(-\pi t)\right] , \tag{A 5.71}$$

$$or, \; \frac{\partial}{\partial x}\left[\frac{\partial^\alpha}{\partial t^\alpha}\left(\frac{\partial p}{\partial x}\right)\right] = -\pi^2 \, sin(\pi x) \, t^{-\alpha} E_{1,1-\alpha}(-\pi t) \, . \tag{A 5.72}$$

Furthermore,

$$\phi \frac{\partial p}{\partial t} = [0.25 + 10^{-9} e^{-\pi t} \, sin(\pi x)][-\pi e^{-\pi t} sin(\pi x)] \, . \tag{A 5.73}$$

Thus, defining

$$f(x,t) = \frac{\partial}{\partial x}\left[\frac{\partial^\alpha}{\partial t^\alpha}\left(\frac{\partial p}{\partial x}\right)\right] - \phi \frac{\partial p}{\partial t} \tag{A 5.74}$$

$$\text{gives } f(x,t) = -\pi^2 \, sin(\pi x) \, t^{-\alpha} E_{1,1-\alpha}(-\pi t) + [\pi e^{-\pi t} sin(\pi x)][0.25 + 10^{-9} e^{-\pi t} \, sin(\pi x)] \, . \tag{A 5.75}$$

Inclusion of μ

Case $\alpha = 0$

Taking $k = 10^{-7}$, $\mu = (10^{-4}p)^{10^{-3}p}$, unit values for ρ, ϕ, c_t and $\alpha = 0$, Eq. (5.1) becomes

$$\frac{\partial}{\partial x}\left[\frac{10^{-7}}{(10^{-4}p)^{10^{-3}p}}\frac{\partial p}{\partial x}\right] = \frac{\partial p}{\partial t} \ . \tag{A 5.76}$$

Let the analytical solution of the equation

$$\frac{\partial}{\partial x}\left[\frac{10^{-7}}{(10^{-4}p)^{10^{-3}p}}\frac{\partial p}{\partial x}\right] = \frac{\partial p}{\partial t} + f(x,t) \tag{A 5.77}$$

be $p(x,t) = e^{-\pi^2 t} sin(\pi x)$. (A 5.78)

Note $p(x,t)$ as given satisfies the initial condition $p(x,0) = sin(\pi x)$, and the boundary conditions $p(0,t) = p(1,t) = 0$.

Now, defining

$$f(x,t) = \frac{\partial}{\partial x}\left[\frac{10^{-7}}{(10^{-4}p)^{10^{-3}p}}\frac{\partial p}{\partial x}\right] - \frac{\partial p}{\partial t} \tag{A 5.79}$$

gives $f(x,t) =$

$$-10^{-7}\pi e^{-\pi^2 t}\, cos(\pi x)\frac{10^{-3}\pi e^{-\pi^2 t}\, cos(\pi x)\, ln\left(10^{-4}e^{-\pi^2 t}\, sin(\pi x)\right) + 10^{-3}\pi e^{-\pi^2 t}\, cos(\pi x)}{\left(10^{-4}e^{-\pi^2 t}\, sin(\pi x)\right)^{10^{-3}e^{-\pi^2 t}\, sin(\pi x)}} -$$

$$10^{-7}\pi^2 e^{-\pi^2 t}\, sin(\pi x)\frac{1}{\left(10^{-4}e^{-\pi^2 t}\, sin(\pi x)\right)^{10^{-3}e^{-\pi^2 t}\, sin(\pi x)}} + \pi^2 e^{-\pi^2 t}\, sin(\pi x) \ . \tag{A 5.80}$$

Case $\alpha \neq 0$

Consider unit values for ρ, ϕ, c_t, T and $\alpha \neq 0$, $k = 10^{-7}$, $\mu = (10^{-4}p)^{10^{-3}p}$, and $\eta = (k/\mu)T^{\alpha}$. For these values, Eq. (5.1) becomes

$$\frac{\partial}{\partial x}\left[\eta \frac{\partial^{\alpha}}{\partial t^{\alpha}}\left(\frac{\partial p}{\partial x}\right)\right] = \frac{\partial p}{\partial t}\,. \tag{A 5.81}$$

Let the analytical solution of the equation

$$\frac{\partial}{\partial x}\left[\eta \frac{\partial^{\alpha}}{\partial t^{\alpha}}\left(\frac{\partial p}{\partial x}\right)\right] = \frac{\partial p}{\partial t} + f(x,t) \tag{A 5.82}$$

be $p(x,t) = e^{-\pi t} sin(\pi x)$. (A 5.83)

Note that $p(x,t)$ satisfies the initial condition $p(x,0) = sin(\pi x)$, and the boundary conditions $p(0,t) = p(1,t) = 0$.

Now,

$$\frac{\partial}{\partial x}\left[\eta \frac{\partial^{\alpha}}{\partial t^{\alpha}}\left(\frac{\partial p}{\partial x}\right)\right] = \frac{\partial}{\partial x}\left[\eta \frac{\partial^{\alpha}}{\partial t^{\alpha}}\left(\pi e^{-\pi t}\, cos(\pi x)\right)\right] \tag{A 5.84}$$

$$\text{gives } \frac{\partial}{\partial x}\left[\eta \frac{\partial^{\alpha}}{\partial t^{\alpha}}\left(\frac{\partial p}{\partial x}\right)\right] = \frac{\partial}{\partial x}\left[\eta\pi\, cos(\pi x)\, t^{-\alpha} E_{1,1-\alpha}(-\pi t)\right], \tag{A 5.85}$$

$$or, \frac{\partial}{\partial x}\left[\eta \frac{\partial^{\alpha}}{\partial t^{\alpha}}\left(\frac{\partial p}{\partial x}\right)\right] = \pi t^{-\alpha} E_{1,1-\alpha}(-\pi t)\left[cos(\pi x)\frac{\partial \eta}{\partial x} + \eta(-\pi sin(\pi x))\right], \tag{A 5.86}$$

$$or, \frac{\partial}{\partial x}\left[\eta \frac{\partial^{\alpha}}{\partial t^{\alpha}}\left(\frac{\partial p}{\partial x}\right)\right] = \pi t^{-\alpha} E_{1,1-\alpha}(-\pi t)\left[cos(\pi x)\frac{\partial \eta}{\partial x} - \pi sin(\pi x)\eta\right]. \tag{A 5.87}$$

Furthermore,

$$\frac{\partial p}{\partial t} = -\pi e^{-\pi t}\, sin(\pi x)\,. \tag{A 5.88}$$

Thus, defining

$$f(x,t) = \frac{\partial}{\partial x}\left[\eta \frac{\partial^{\alpha}}{\partial t^{\alpha}}\left(\frac{\partial p}{\partial x}\right)\right] - \frac{\partial p}{\partial t} \tag{A 5.89}$$

gives $f(x,t) = \pi t^{-\alpha} E_{1,1-\alpha}(-\pi t)\left[cos(\pi x)\frac{\partial \eta}{\partial x} - \pi\, sin(\pi x)\,\eta\right] + \pi e^{-\pi t}\, sin(\pi x),$ (A 5.90)

where

$$\frac{\partial \eta}{\partial x} = -10^{-7} T^{\alpha} \frac{10^{-3}\pi e^{-\pi t}\, cos(\pi x)\, ln\left(10^{-4} e^{-\pi t}\, sin(\pi x)\right) + 10^{-3}\pi e^{-\pi t}\, cos(\pi x)}{\left(10^{-4} e^{-\pi t}\, sin(\pi x)\right)^{10^{-3} e^{-\pi t}\, sin(\pi x)}}. \quad \text{(A 5.91)}$$

Chapter 6

Comparison among Numerical Models of a Memory- based Diffusivity Equation Developed Using Uniform and Graded Meshes, and Determination of 'α' value

Co-Authorship

Chapter 6 is prepared according to the Guidelines for Manuscript Format Theses in the Faculty of Engineering and Applied Science at Memorial University. This chapter has been prepared for submission as a journal article:

T. U. Zaman, S. MacLachlan, and M. E. Hossain (in preparation). "Comparison among numerical models of a memory- based radial diffusivity equation developed using uniform and graded meshes."

The research work presented in this chapter was conducted by Tareq Uz Zaman under the direction and supervision of M. Enamul Hossain, and the guidance and close supervision of Scott MacLachlan. The manuscript itself was written by Tareq Uz Zaman and reviewed by M. Enamul Hossain and Scott MacLachlan.

6.1 Abstract

Two different numerical models developed for a memory-based radial diffusivity equation utilizing uniform and graded meshes have been studied and compared. Numerical solutions obtained from these numerical models are compared with analytical solutions for Dirichlet boundary conditions and two different initial conditions to calculate and compare errors. It is found that the numerical model developed using graded meshes gives smaller error than that using uniform meshes. Experimental data regarding one-dimensional flow measurements through a

porous layer with constant pressure gradient are collected from the literature. The value of the fractional order in the diffusivity equation in this paper is computed to fit the experimental data by the mathematical model. A reasonable value of the fractional order is found to be 0.05. Optimal numbers of time steps in unit time for this value of fractional order and for different numbers of grid-points in unit length are found by error analysis, where the optimal number of steps in unit time is required to minimize the temporal discretization error. The comparison between uniform and graded meshes shows that utilization of graded meshes to develop the numerical model for the time-fractional diffusion equation is advantageous compared to the utilization of uniform meshes.

Keywords: Memory, Numerical Modeling, Fractional diffusion equation, Riemann-Liouville definition, Uniform mesh, Graded mesh.

6.2 Introduction

Reservoir modeling is a critical component in the development, planning, and production management of oil and gas fields. The ultimate goal of reservoir modeling is to aid in the decision-making process throughout all stages of field life. Numerous mathematical models have been developed for different types of reservoirs and fluids over more than the past fifty years modelling various flow regimes and properties. In recent years, researchers have started to investigate the effects of the history of the rock, fluid, and flow, that is also known as memory, on flow through porous media. The recent literature on the mathematical modeling of rock/fluid interactions in porous media shows that many researchers are developing models with memory (Caputo, 1998; Caputo, 2000; Hossain *et al.*, 2012a; Hossain *et al.*, 2012b; Hossain *et al.*, 2015).

Several definitions of memory are found in the literature. Zhang (2003) defined memory as a function of time and space, where forward time events depend on previous time events. Christensen (2003) defined memory to be when the history of the deformation and fractures of a solid under stress is used to determine the propagation of a fracture within a solid. Zavala-Sanchez *et al.* (2009) showed that the system "remembers" its initial state, which was defined as memory effects for the effective transport coefficients. Hossain *et al.* (2012a) defined memory as the effect

of past events on the present and future course of developments. In this direction, Hossain *et al.* (2008) proposed the following diffusivity equation

$$\frac{\partial}{\partial x}\left[\frac{\rho k}{\mu} T^{\alpha} \frac{\partial^{\alpha}}{\partial t^{\alpha}}\left(\frac{\partial p}{\partial x}\right)\right] = \rho \phi c_t \frac{\partial p}{\partial t}, \tag{6.1}$$

where $p(x,t)$ is the pressure, $\rho(x,t)$ the fluid density, $\phi(x,t)$ the porosity of the fluid medium, $k(x,t)$ the permeability of the medium, $\mu(x,t)$ the dynamic viscosity of the fluid, $c_t(x,t)$ the total compressibility of the system, α the fractional order of differentiation and T the characteristic time.

The fractional-order derivative is required to be included in the diffusion equation in order to incorporate memory. However, inclusion of the fractional-order derivative makes the diffusion equation difficult to solve analytically and numerically. The non-local behavior of the fractional-order differential equation makes the equation challenging to solve numerically. However, numerous studies on numerical approaches to fractional diffusion equations are found in the literature. Various powerful methods have been proposed for numerical solution of fractional differential equations. Many authors have applied finite-difference methods (Abu-Saman, 2007; Chen *et al.*, 2007; Chen *et al.*, 2009; Chen *et al.*, 2010; Cui *et al.*, 2009; Du *et al.*, 2010; Gao *et al.*, 2011; Langlands *et al.*, 2005; Liu *et al.*, 2006; Liu *et al.*, 2011; Lynch *et al.*, 2003; Meerschaert *et al.*, 2004; Murillo *et al.*, 2009; Sun *et al.*, 2006; Tadjeran *et al.*, 2006; Wang *et al.*, 2011; Yuste *et al.*, 2005; Zhuang *et al.*, 2006; Zhuang *et al.*, 2008), while others have applied finite-element methods (Deng, 2008; Roop, 2006). Gorenflo *et al.* (2002) used random walk approaches, and Li *et al.* (2009, 2010) used a spectral method. A decomposition method was applied by El-Sayed *et al.* (2010), and Odibat (2006). Momani *et al.* (2007), and Yildirim (2010) utilized a homotopy perturbation method; Kumar *et al.* (2006) used an integral equation method; Jiang *et al.* (2010) applied a reproducing kernel method; and a variational iteration method was applied by Odibat *et al.* (2009) to solve a fractional differential equation. Zhuang *et al.* (2006) introduced a difference scheme that is based on the L1 approximation for Caputo time-fractional derivatives. Murillo *et al.* (2011) developed an explicit finite difference schemes. These authors also showed stability conditions by means of fractional von-Neumann analysis techniques. An implicit finite difference scheme using the L1 formula was constructed by Sun *et al.* (2006).

Zaman *et al.* (2017a) developed a numerical model for Eq. (6.1) using uniform meshes in both space and time, and the Riemann-Liouville definition of the fractional-order derivative. However, Stynes *et al.* (2017) defined a graded mesh and theoretically showed that their graded mesh gives better performance for the time-fractional equation. Zaman *et al.* (2017b) adapted their definition of graded mesh for Eq. (6.1) and solved the equation utilizing this definition of a graded mesh in time. In this paper, the numerical models developed by Zaman *et al.* (2017a, 2017b) for Eq. (6.1) utilizing uniform and graded meshes are studied and compared. The value of fractional order, α has been calculated for different experimental data collected from literature. The relationship between the optimal number of steps in unit time and number of grid-points in unit length is found for different values of α.

The mathematical model (Eq. (6.1)) is discretized using a finite-difference method. For some positive value X, and integer N_x, the grid size in space is defined by $\Delta x = X/N_x$. The grid points in the space interval $[0, X]$ are given by $x_i = i\Delta x, i = 0,1,2, \dots, N_x$. In case of uniform mesh in time, for some positive value T, and integer N_t, the grid size is defined by $\Delta t = T/N_t$. The grid points in the time interval $[0, T]$ are labeled $t_n = n\Delta t, n = 0, 1, 2, \dots, N_t$. For the graded mesh, the local grid size is defined by $\Delta t_n = t_n - t_{n-1}$. The grid points in the time interval $[0, T]$ are labeled $t_n = T(n/N)^{\omega}, n = 0, 1, 2, \dots, N$ where the constant mesh grading $\omega \geq 1$ is adapted from Stynes *et al.* (2017). In the notation of Eq. (6.1), $\omega = (1 + \alpha)/(1 - \alpha)$ matches that recommended in Stynes *et al.* (2017). The values of a function p at the grid points are denoted by $p_i^n = p(x_i, t_n)$ for both uniform and graded meshes.

6.3 Numerical Model for Uniform Mesh in Time

Zaman *et al.* (2017a) developed the following numerical model for Eq. (6.1) using uniform meshes in both space and time.

$$-C_1\left(x_{i-\frac{1}{2}},t_n\right)p_{i-1}^n+\left[C_1\left(x_{i-\frac{1}{2}},t_n\right)+C_1\left(x_{i+\frac{1}{2}},t_n\right)+\frac{C_2(x_i,t_n)\Delta x^2}{\sigma_{\alpha,\Delta t}\Delta t}\right]p_i^n-$$
$$C_1\left(x_{i+\frac{1}{2}},t_n\right)p_{i+1}^n=\frac{C_2(x_i,t_n)\Delta x^2}{\sigma_{\alpha,\Delta t}\Delta t}p_i^{n-1}+C_1\left(x_{i+\frac{1}{2}},t_n\right)G_i^n-C_1\left(x_{i-\frac{1}{2}},t_n\right)H_i^n+$$
$$C_1\left(x_{i+\frac{1}{2}},t_n\right)\frac{1-\alpha}{n^\alpha}(p_{i+1}^0-p_i^0)-C_1\left(x_{i-\frac{1}{2}},t_n\right)\frac{1-\alpha}{n^\alpha}(p_i^0-p_{i-1}^0)\,, \tag{6.2}$$

where

$$G_i^n=-p_{i+1}^{n-1}+p_i^{n-1}+\sum_{j=1}^{n-1}\omega_j^{(\alpha)}(p_{i+1}^{n-j}-p_i^{n-j}-p_{i+1}^{n-j-1}+p_i^{n-j-1})]\,, \tag{6.3}$$

$$H_i^n=-p_i^{n-1}+p_{i-1}^{n-1}+\sum_{j=1}^{n-1}\omega_j^{(\alpha)}(p_i^{n-j}-p_{i-1}^{n-j}-p_i^{n-j-1}+p_{i-1}^{n-j-1})]\,, \tag{6.4}$$

and $C_1(x,t)=\frac{\rho k}{\mu}T^\alpha$, (6.5)

$$C_2=\rho\phi c_t\,. \tag{6.6}$$

6.4 Numerical Model for Graded Mesh in Time

The following numerical model is developed by Zaman *et al.* (2017b) for Eq. (6.1) using a uniform mesh in space and graded mesh in time,

$$-C_1\left(x_{i-\frac{1}{2}},t_n\right)p_{i-1}^n+\left[C_1\left(x_{i-\frac{1}{2}},t_n\right)+C_1\left(x_{i+\frac{1}{2}},t_n\right)+C_2(x_i,t_n)\Delta\mathrm{x}^2\Gamma(2-\alpha)(t_n-\right.$$
$$\left.t_{n-1})^{\alpha-1}\right]p_i^n-C_1\left(x_{i+\frac{1}{2}},t_n\right)p_{i+1}^n=C_2(x_i,t_n)\Delta\mathrm{x}^2\Gamma(2-\alpha)(t_n-t_{n-1})^{\alpha-1}p_i^{n-1}+$$
$$C_1\left(x_{i+\frac{1}{2}},t_n\right)(t_n-t_{n-1})^\alpha G_i^n-C_1\left(x_{i-\frac{1}{2}},t_n\right)(t_n-t_{n-1})^\alpha H_i^n+C_1\left(x_{i+\frac{1}{2}},t_n\right)\frac{(1-\alpha)}{(t_n)^\alpha}(t_n-$$
$$t_{n-1})^\alpha(p_{i+1}^0-p_i^0)+C_1\left(x_{i-\frac{1}{2}},t_n\right)\frac{(1-\alpha)}{(t_n)^\alpha}(t_n-t_{n-1})^\alpha(p_i^0-p_{i-1}^0)\,, \tag{6.7}$$

where

$$G_i^n = -(t_n - t_{n-1})^{-\alpha}(p_{i+1}^{n-1} - p_i^{n-1}) + \sum_{J=0}^{n-2} \frac{\left[(t_n - t_j)^{1-\alpha} - (t_n - t_{j+1})^{1-\alpha}\right]}{(t_{j+1} - t_j)} (p_{i+1}^{j+1} - p_i^{j+1} - p_{i+1}^{j} + p_i^{j}) , \quad (6.8)$$

$$H_i^n = -(t_n - t_{n-1})^{-\alpha}(p_i^{n-1} - p_{i-1}^{n-1}) + \sum_{J=0}^{n-2} \frac{\left[(t_n - t_j)^{1-\alpha} - (t_n - t_{j+1})^{1-\alpha}\right]}{(t_{j+1} - t_j)} (p_i^{j+1} - p_{i-1}^{j+1} - p_i^{j} + p_{i-1}^{j}) , \quad (6.9)$$

and C_1 and C_2 are defined by Eq. (6.5) and (6.6), respectively.

6.5 Analytical Solution

To find the analytical solution, Zaman *et al.* (2017a, 2017b) made Eq. (6.1) linear, by considering $C_1 = (\rho k/\mu)T^{\alpha} = 1$, and $C_2 = \rho\phi c_t = 1$. The Riemann-Liouville definition for the fractional-order derivative is utilized.

For the initial condition $p(x, 0) = sin(\pi x)$, and boundary conditions $p(0, t) = p(1, t) = 0$, the analytical solution of Eq. (6.1) is found as

$$p(x, t) = E_{1-\alpha}(-\pi^2 t^{1-\alpha}) sin(\pi x) . \quad (6.10)$$

For the initial condition $p(x, 0) = x(1 - x)$, and boundary conditions $p(0, t) = p(1, t) = 0$, the analytical solution of Eq. (6.1) becomes

$$p(x, t) = \sum_{k=1}^{\infty} \frac{4}{k^3\pi^3} [1 - (-1)^k] E_{1-\alpha}(-k^2\pi^2 t^{1-\alpha}) \, sin(k\pi x) . \quad (6.11)$$

6.6 Comparison of Errors found from Uniform and Graded Meshes

Figures 6.1 through 6.6 compare the errors found using uniform and graded meshes for different values of fractional order, α, and for different number of grid-points in space for the linear model problem presented above. Figs. 6.1 to 6.3 are for initial condition, $p(x, 0) = sin(\pi x)$, and Figs.

6.4 to 6.6 are for initial condition, $p(x,0) = x(1-x)$. It is found that in all cases, the graded mesh gives smaller errors than the uniform mesh, except when $\alpha = 0$, where the errors for the uniform and graded meshes are identical, since in this case, the graded mesh coincides with the uniform mesh. We note that, in the Figures 6.1 through 6.6, the shape of the error lines found for $\alpha = 0.75$ and a graded mesh are different from the other error lines, depicting that the error reaches a minimum value at $N_t = 6400$, and then starts to increase. It seems roundoff error starts to dominate beyond $N_t = 6400$. The size of the first-time step falls to about 10^{-26} for $N_t = 6400$. However, Fig. 6.7 shows that for $\alpha = 0.75$ in graded meshes, the size of the first-time step is smaller than 10^{-16} for $N_t = 200$. With a time-step that small, any numerical accuracy in the solution for $\alpha = 0.75$ should not be expected. This is true for that α and N_t, for which the size of the first-time step is smaller than 10^{-16}.

Tables 6.1, and 6.2 compare order of accuracies of the numerical models developed using uniform and graded meshes. The Tables show that the numerical model developed using uniform meshes is $(1-\alpha)$th-order accurate in time, and that developed using graded meshes is second-order accurate in space, and first-order accurate in time.

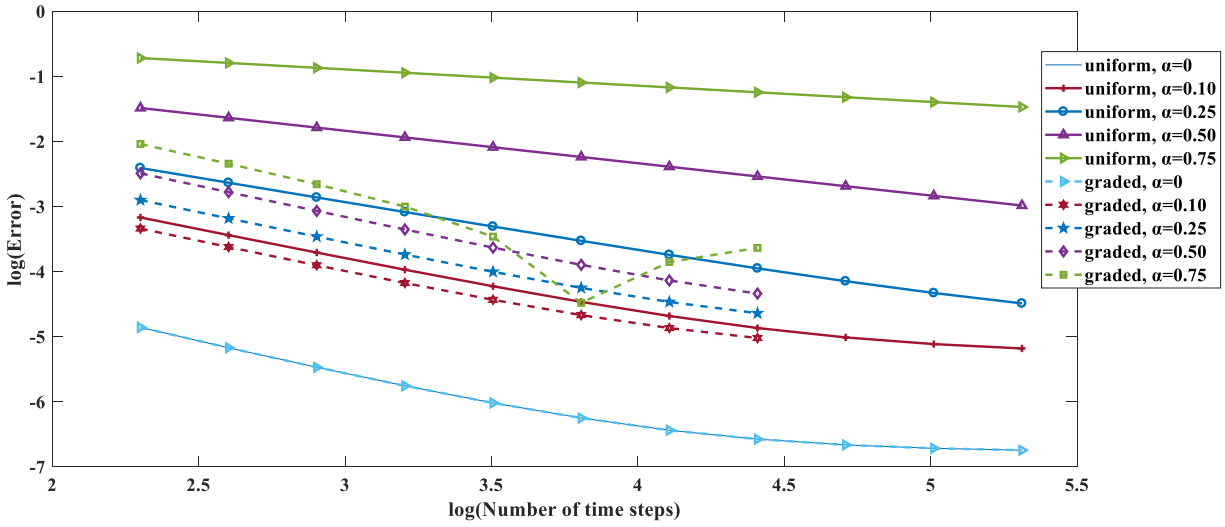

Figure 6.1 Comparison of the error values for uniform and graded meshes for initial condition $p(x,0) = sin(\pi x)$ $(N_x = 50)$.

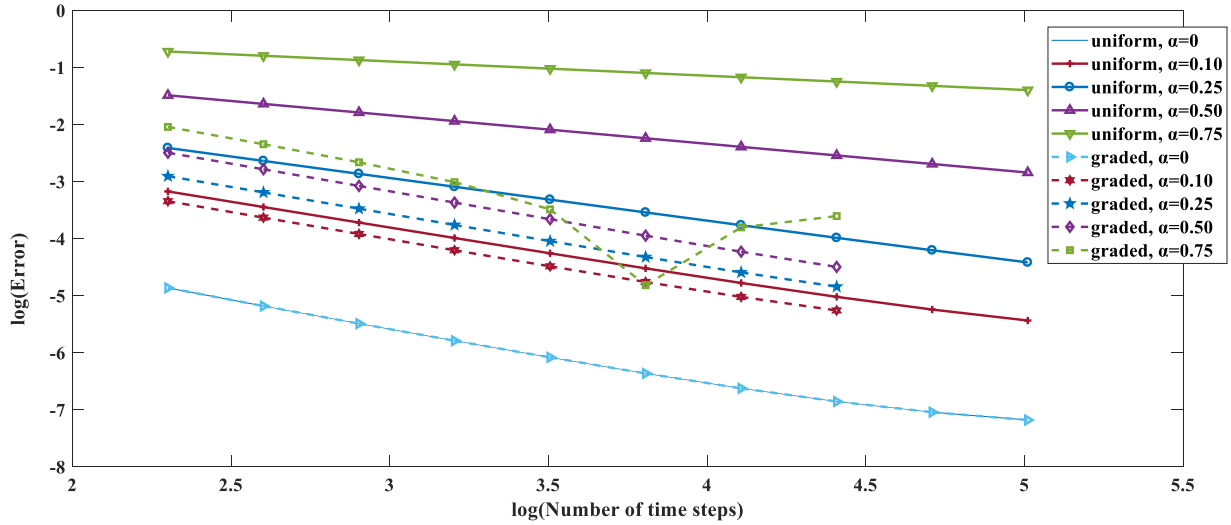

Figure 6.2 Comparison of the error values for uniform and graded meshes for initial condition $p(x,0) = sin(\pi x)$ $(N_x = 100)$.

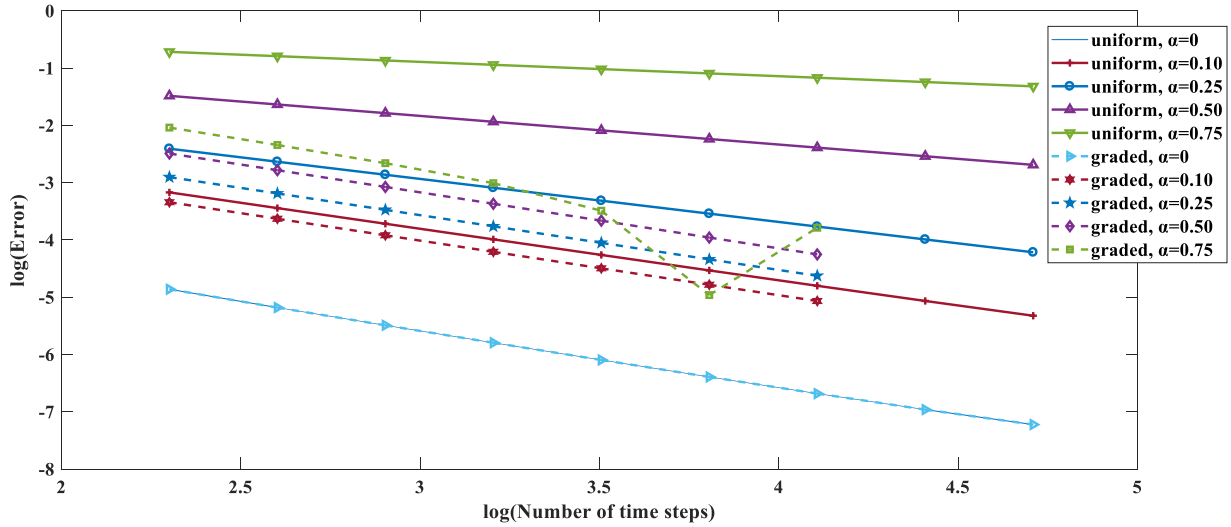

Figure 6.3 Comparison of the error values for uniform and graded meshes for initial condition $p(x,0) = sin(\pi x)$ $(N_x = 200)$.

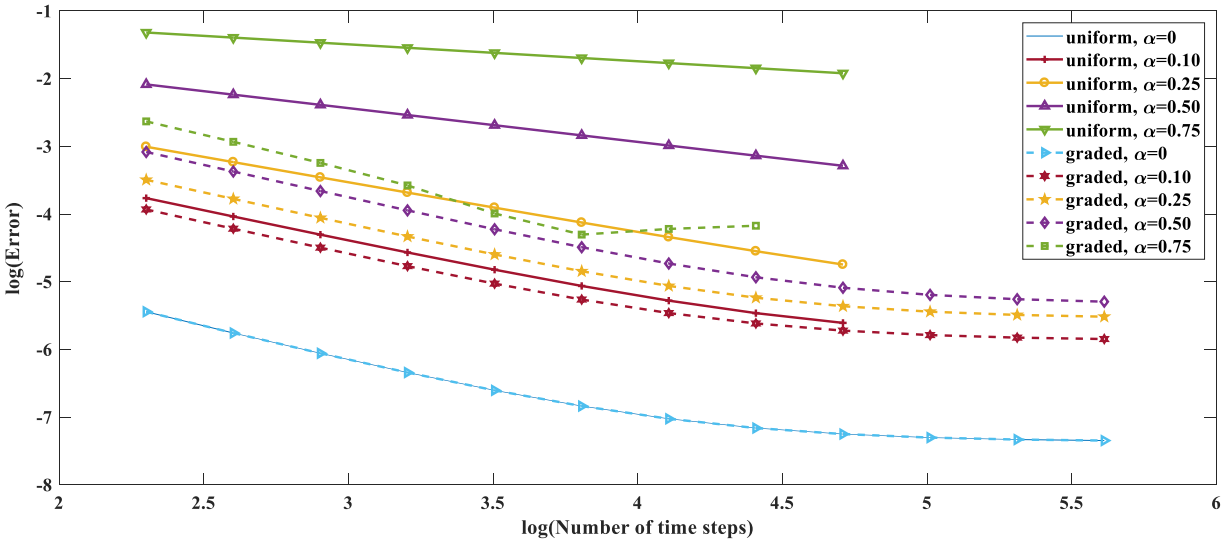

Figure 6.4 Comparison of the error values for uniform and graded meshes for initial condition $p(x,0) = x(1-x)$ ($N_x = 50$).

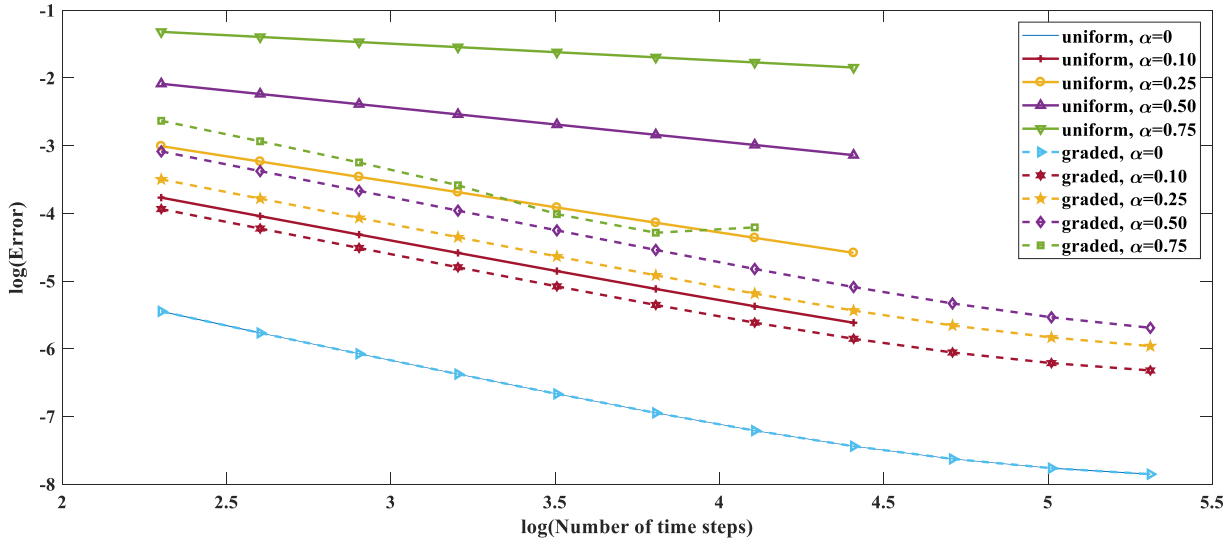

Figure 6.5 Comparison of the error values for uniform and graded meshes for initial condition $p(x,0) = x(1-x)$ ($N_x = 100$).

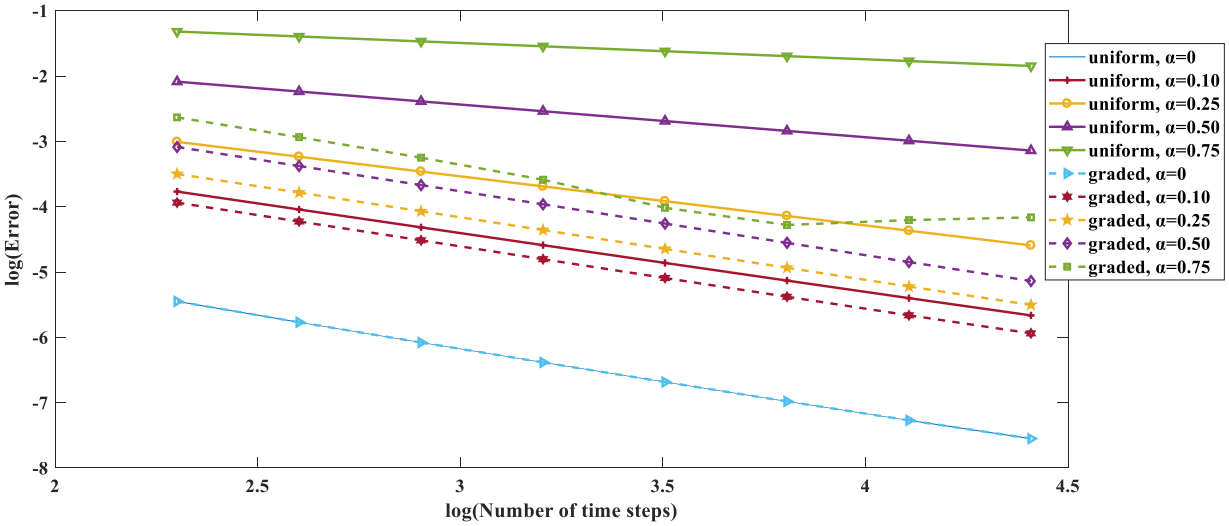

Figure 6.6 Comparison of the error values for uniform and graded meshes for initial condition $p(x,0) = x(1-x)$ ($N_x = 200$).

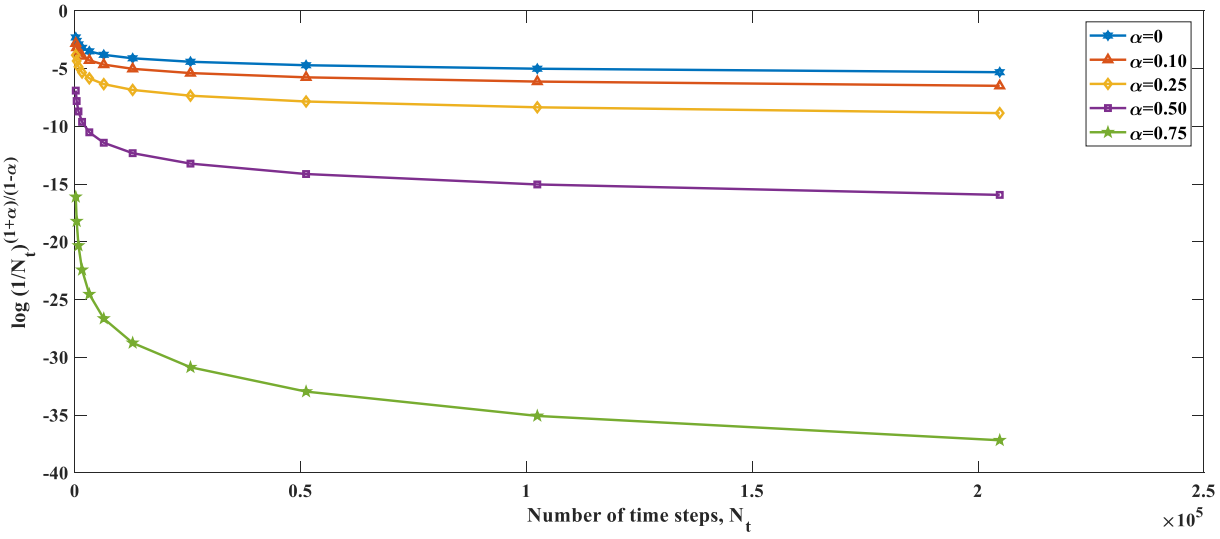

Figure 6.7 Minimum time-step size for graded mesh.

Table 6.1 Comparison of order of temporal accuracies for uniform and graded meshes for initial condition, $p(x,0) = sin(\pi x)$.

Value of fractional order, α	**Order of temporal accuracy**			
	$N_x = 50$		**$N_x = 100$**	
	Uniform mesh	**Graded mesh**	**Uniform mesh**	**Graded mesh**
0	0.9946	0.9946	1.0256	1.0256
0.10	0.8889	0.9270	0.9042	0.9522
0.25	0.7496	0.9269	0.7535	0.9462
0.50	0.5006	0.9551	0.5009	0.9681
0.75	0.2501	*1.0629*	0.2502	*1.0705*

Table 6.2 Comparison of order of temporal accuracies for uniform and graded meshes for initial condition, $p(x,0) = x(1-x)$.

Value of fractional order, α	**Order of temporal accuracy**					
	$N_x = 50$		**$N_x = 100$**		**$N_x = 200$**	
	Uniform mesh	**Graded mesh**	**Uniform mesh**	**Graded mesh**	**Uniform mesh**	**Graded mesh**
0	1.0195	0.9946	1.0256	1.0256	1.0337	1.0337
0.10	0.8890	0.9273	0.9044	0.9524	0.9083	0.9589
0.25	0.7497	0.9274	0.7536	0.9465	0.7546	0.9515
0.50	0.5006	0.9555	0.5009	0.9683	0.5010	0.9716
0.75	0.2501	*1.0464*	0.2502	*1.0535*	0.2502	*1.0552*

6.7 Determination of the Values of α and T from Experimental Data

Iaffaldano et al. (2005) designed an experiment to measure volumetric flux through a porous layer while keeping the pressure difference constant between the boundary surfaces. Fig. 6.8 shows the experimental device used in their study. Water-saturated sand is used in the cell for the medium. A cylinder-shaped metal box of height 11.6 cm with surface's inner diameter of 10.1 cm was used to keep the sand in. Dry sand and water were slowly and alternately filled in the empty cell to obtain the condition of saturation. The initial pressure value for water inside the cell is attained by keeping water-taps R and R_I switched on and R_U switched off, until the height of the water column, H, is obtained. After attaining the same pressure as the initial pressure through the medium, water-tap R_U is opened. This results in atmospheric pressure on the right boundary plane. Since the

pressure on the left boundary plane is atmospheric pressure plus the pressure due to the water column of height H, the pressure difference is the pressure due to the water column of height H, and water starts to flow through the porous medium and runs out from R_U. The height of the water column is always H because the surplus water from the water-tap R flows out from the output gate, U. Water flow at the right boundary surface was measured by storing water in a small container of known volume, and measuring the relative time interval.

Five different samples of sand were used as the porous layer. The authors presented their experimental results by plotting volumetric flux as a function of elapsed time. The plots that they presented in their article are redrawn here in Figs. 6.9 to 6.13. Their experimental results support that permeability may decrease due to rearrangement of the grains and consequent compaction, which was qualitatively shown by Elias and Hajash (1992).

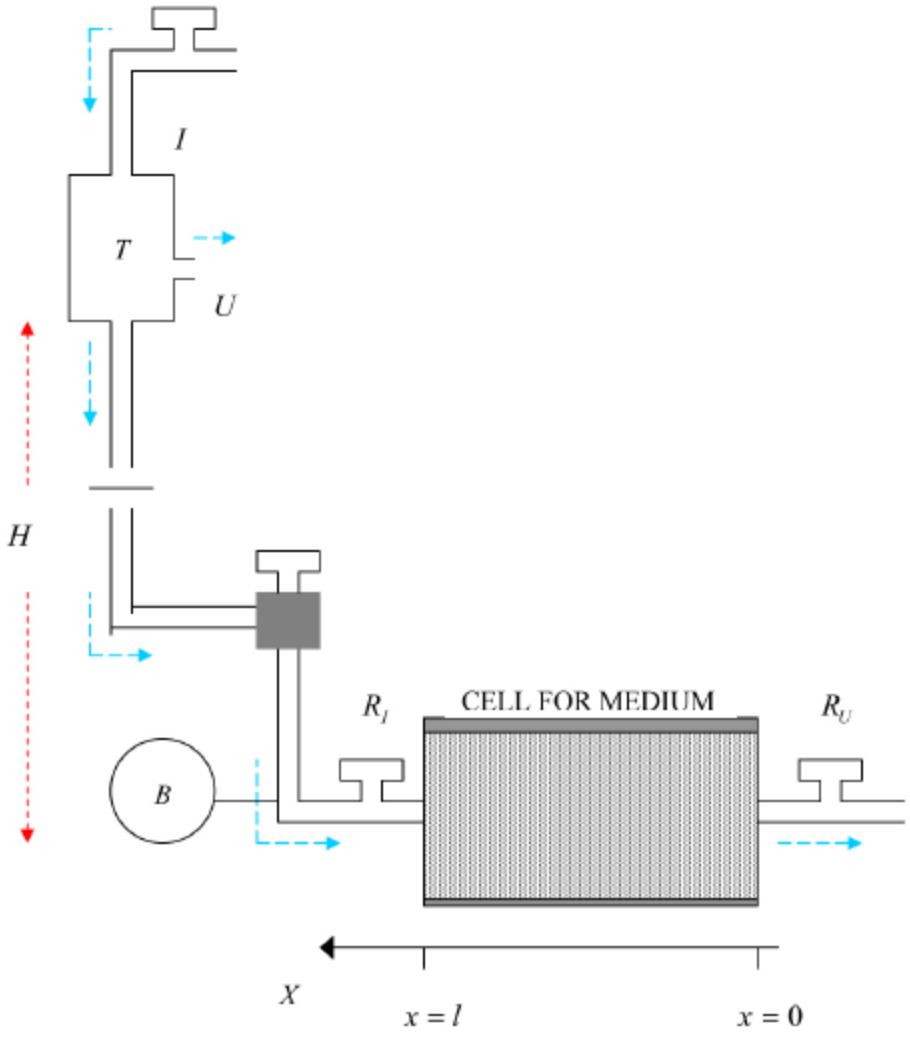

Figure 6.8 Experimental device used in experiment of Iaffaldano et al. (from Iaffaldano et al. (2005))

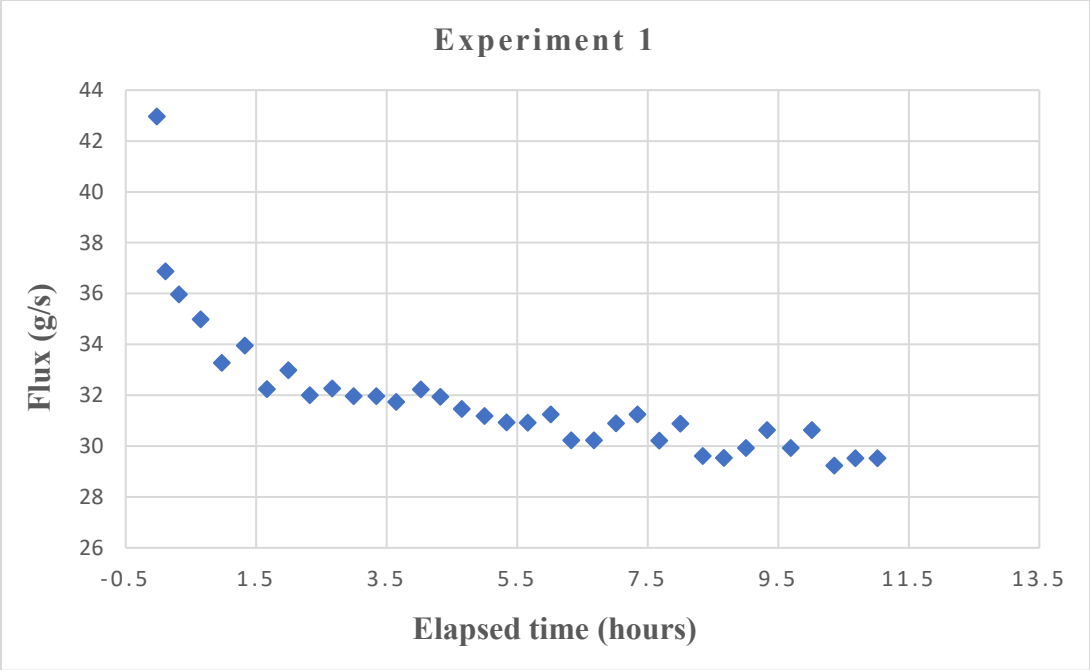

Figure 6.9 Flux results from first experiment. (Redrawn from Iaffaldano et al. (2005))

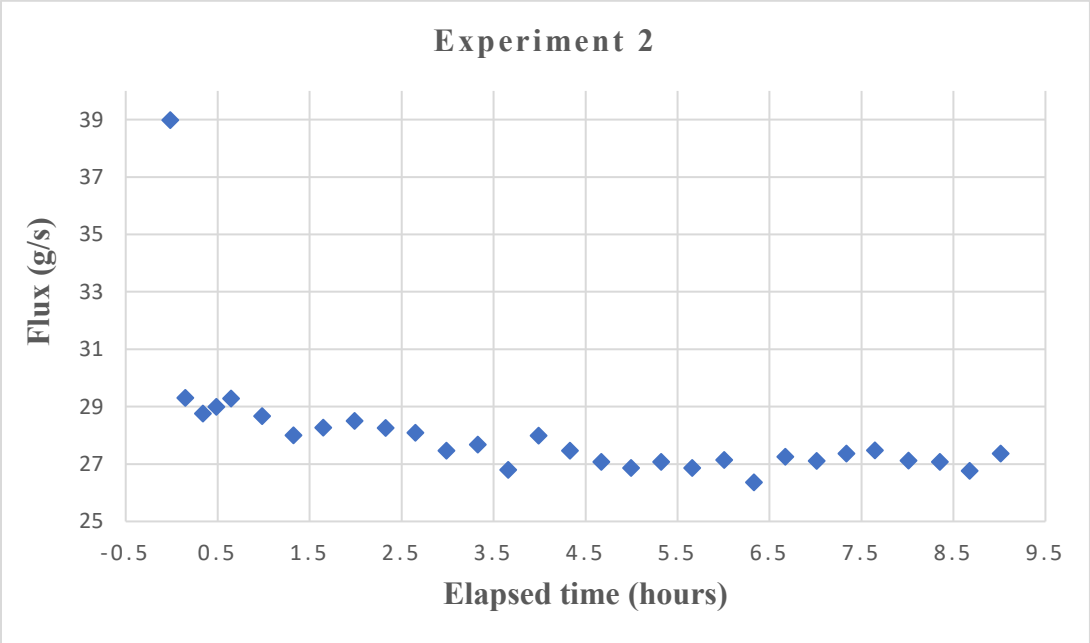

Figure 6.10 Flux results from second experiment. (Redrawn from Iaffaldano et al. (2005))

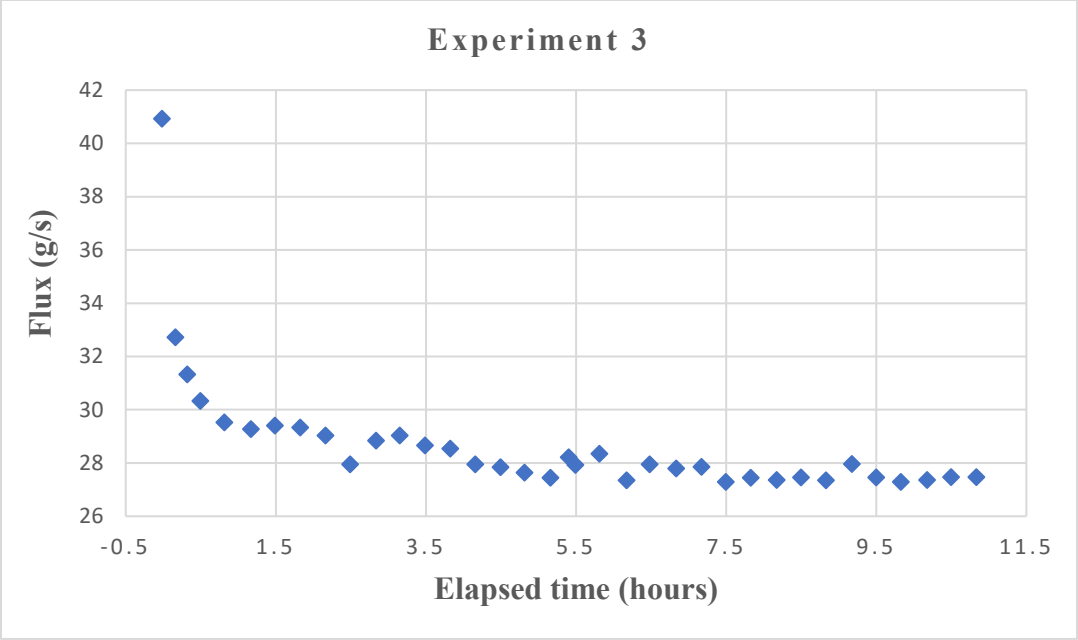

Figure 6.11 Flux results from third experiment. (Redrawn from Iaffaldano et al. (2005))

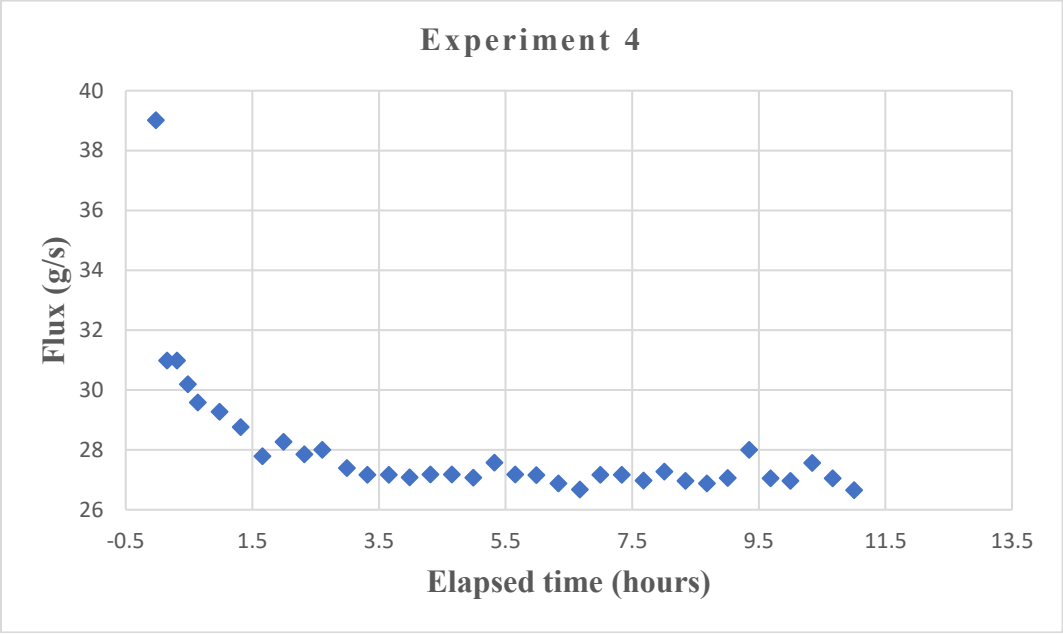

Figure 6.12 Flux results from fourth experiment. (Redrawn from Iaffaldano et al. (2005))

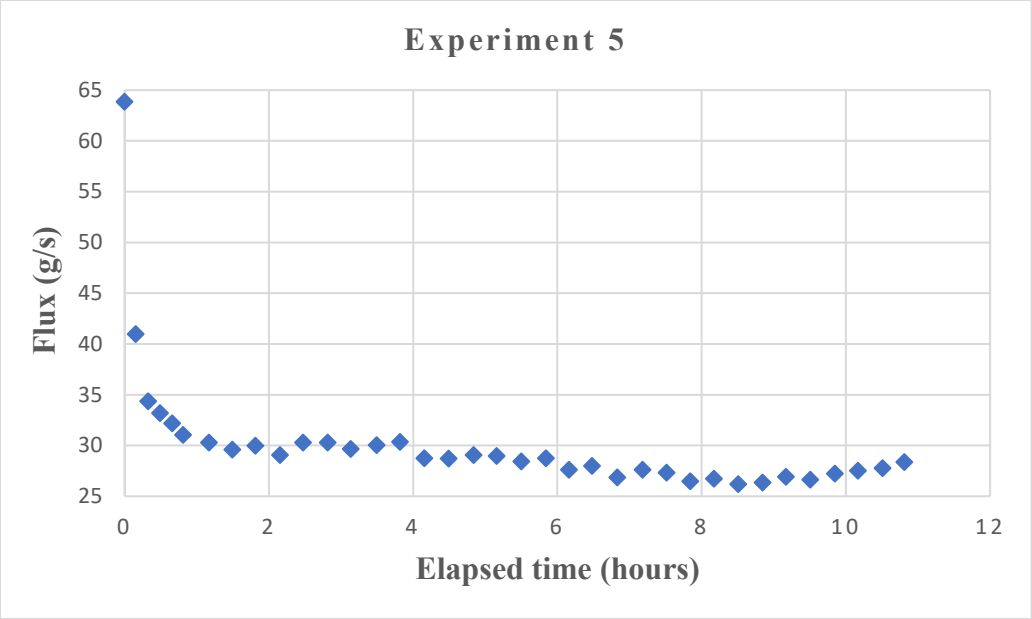

Figure 6.13 Flux results from the fifth experiment. (Redrawn from Iaffaldano et al. (2005))

Iaffaldano et al. (2005) used the empirical Fair and Hatch law (1993) to calculate the permeability, k (Bear, 1972), and found k=26 darcy. They used water of 19^{0}C as the fluid in all of their experiments. The density and viscosity of water at 19^{0}C are 0.998408 g/cc and 1.0266 cp, respectively. A pressure difference was maintained by exerting an additional pressure equivalent to 212 cm height of water column (0.20485 atm) at one end. The mass of dry sand used in each experiment was around 1550 g. The density of sand used was 2.4 gcm^{-3}. From this information, the porosity in the sand medium within the cylinder-shaped metal box can be calculated as 30.51%.

Hossain *et al.*'s (2008) diffusivity equation (Eq. 6.1) is based on the following equation that relates volumetric flux to pressure gradient,

$$u = -\frac{k}{\mu} T^{\alpha} \left[\frac{\partial^{\alpha}}{\partial t^{\alpha}} \left(\frac{\partial p}{\partial x}\right)\right] . \tag{6.12}$$

Using the Riemann-Liouville definition of the fractional-order derivative, Eq. (6.12) can be written as

$$u = -\frac{k}{\mu} T^{\alpha} \frac{1}{\Gamma(2-\alpha)} \left[\frac{(1-\alpha)\frac{\partial p}{\partial x}(t=0)}{(t_n)^{\alpha}} + \sum_{j=0}^{n-1} \frac{\frac{\partial p}{\partial x}(t=t_{j+1}) - \frac{\partial p}{\partial x}(t=t_j)}{t_{j+1}-t_j} \{(t_n - t_j)^{1-\alpha} - (t_n - t_{j+1})^{1-\alpha}\} \right]. \quad (6.13)$$

Since the pressure gradient is kept constant in the experiment, Eq. (6.13) can be written as

$$u = -\frac{k}{\mu} \frac{(1-\alpha)}{\Gamma(2-\alpha)} \frac{T^{\alpha}}{(t_n)^{\alpha}} \frac{\partial p}{\partial x}(t=0). \quad (6.14)$$

Substitution of the permeability, viscosity, and pressure gradient with their numerical values in Eq. (6.14) gives

$$u = (0.44726) \frac{(1-\alpha)}{\Gamma(2-\alpha)} \frac{T^{\alpha}}{(t_n)^{\alpha}}. \quad (6.15)$$

Taking the logarithm of both sides of Eq. (6.15), we obtain

$$log(u) = log\left(0.44726 \frac{(1-\alpha)}{\Gamma(2-\alpha)} T^{\alpha}\right) - \alpha log(t_n) \quad (6.16)$$

Eq. (6.16) can be written as,

$$log(u) = log(Z) - \alpha log(t_n), \quad (6.17)$$

where

$$Z = 0.44726 \frac{(1-\alpha)}{\Gamma(2-\alpha)} T^{\alpha}. \quad (6.18)$$

We calculate the values of α and Z with least-squares regression analysis using the data obtained from the experiments. Using the formula of least-square regression analysis, we get

$$-\alpha = \frac{N\sum_{j=1}^{N}(log(u)*log(t_n))_j - \sum_{j=1}^{N} log(u)_j \sum_{j=1}^{N} log(t_n)_j}{N\sum_{j=1}^{N}(log(t_n)_j)^2 - [\sum_{j=1}^{N} log(t_n)_j]^2}, \quad (6.19)$$

where N is the number of data points,

and $Z = 10^{\gamma}$, (6.20)

where

$$\gamma = \frac{\sum_{j=1}^{N} \log(u)_j [\sum_{j=1}^{N} \log(t_n)_j]^2 - \sum_{j=1}^{N} \log(t_n)_j \sum_{j=1}^{N} (\log(u)*\log(t_n))_j}{N\sum_{j=1}^{N}(\log(t_n)_j)^2 - [\sum_{j=1}^{N} \log(t_n)_j]^2}. \quad (6.21)$$

Eq. (6.18) gives,

$$T = [\frac{Z\Gamma(2-\alpha)}{0.44726(1-\alpha)}]^{(\frac{1}{\alpha})} . \quad (6.22)$$

Calculation for α and T gives the following values tabulated in Table 6.3. The average values of α and T are found to be around 0.05 and 730 seconds, respectively. Iaffaldano et al. (2005) calculated the value of fractional order in their model to be 0.53. The Caputo fractional derivative was used in their article, whereas we used the Riemann-Liouville fractional derivative. In addition, the mathematical models used in Iaffaldano et al.'s (2005) article and in this research work are not identical. Hence, the value of fractional order calculated in Iaffaldano et al.'s (2005) work is different from that calculated in this article.

Table 6.3 Computed values of α and T

Experiment No.	Fractional order, α	Relaxation time, T (seconds)
1	0.050348217	2020.30
2	0.023771495	0.40
3	0.038373096	55.10
4	0.034639443	14.50
5	0.075865421	1559.60

6.8 Simulated and Experimental Flux Values

Figs. 6.14 through 6.18 show the simulated flux values for $\alpha = 0.05$ and $T = 730$ seconds. The pressure values in each grid cell in each time step, that are required to calculate flux values, are computed using the numerical model that was developed using graded meshes. The length of grid cell was taken to be 0.02 cm. The length of n-th time step is calculated as, $\Delta t_n = t_n - t_{n-1}$, where $t_n = T(n/N)^{\omega}, n = 0,1,2, \ldots, N_t$, and $\omega = (1+\alpha)/(1-\alpha)$. Figs. 6.14 through 6.18 compare the simulated flux values with those obtained from the experiments. It is found that the simulated values are very close to experimental values. The figures also present the flux calculated from Darcy's law without the fractional derivative terms, showing the improved physical accuracy gained by including the memory term.

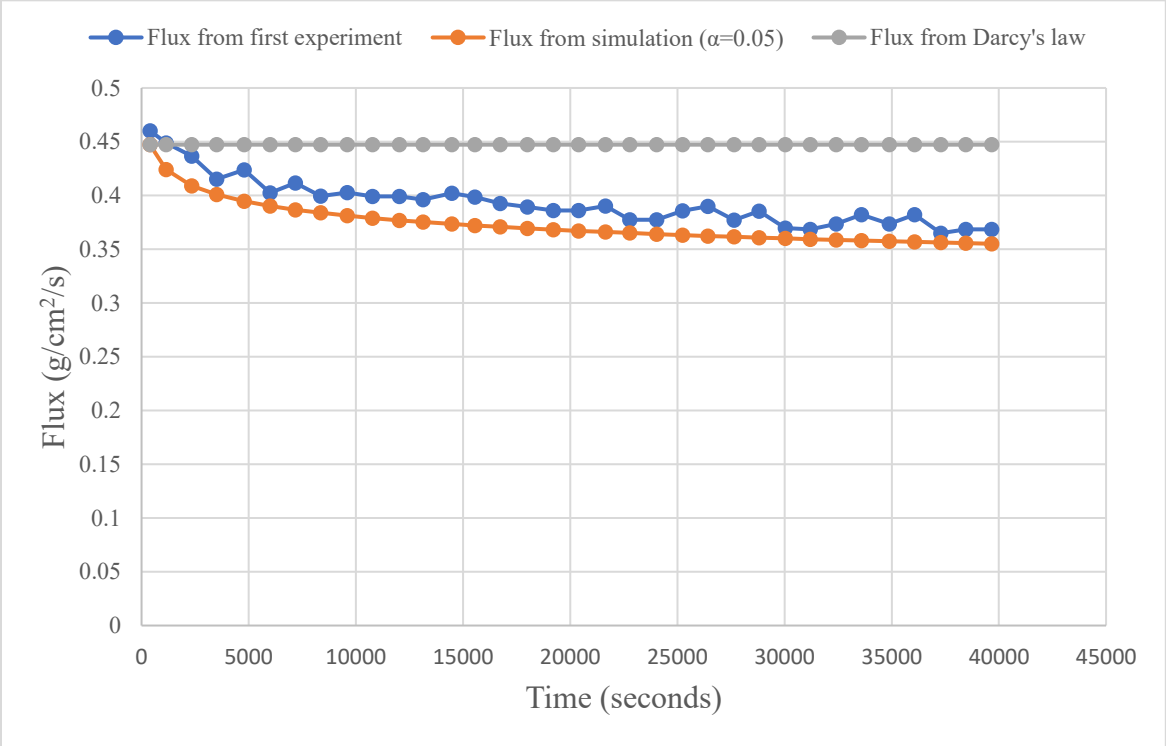

Figure 6.14 Flux values from the first experiment, simulation, and Darcy's law for $\alpha = 0.05$.

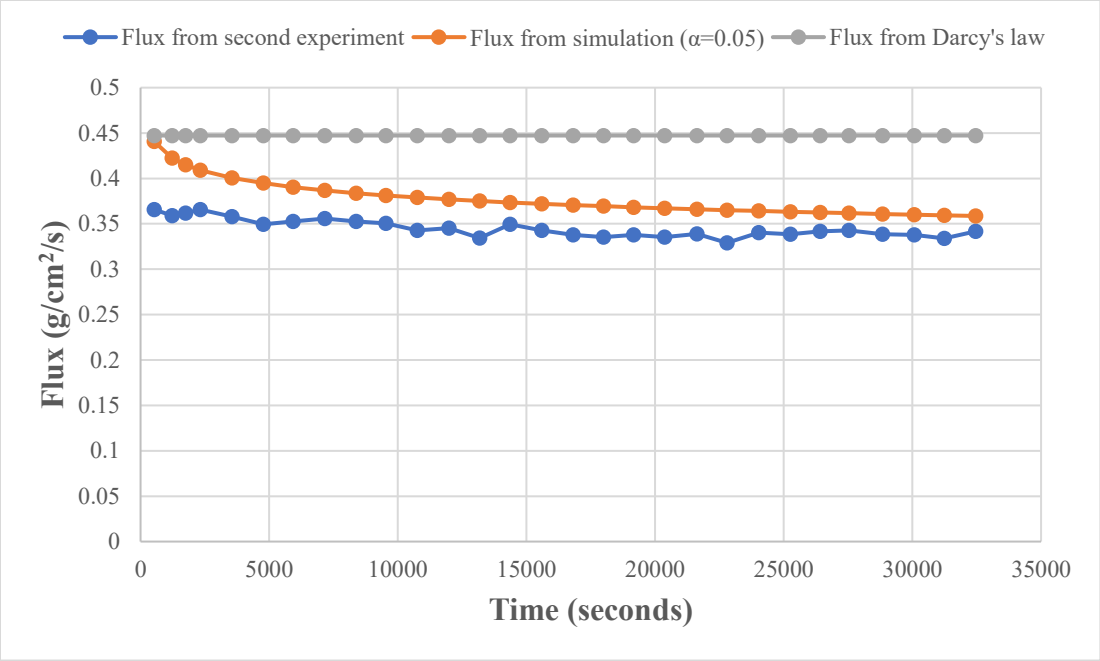

Figure 6.15 Flux values from the second experiment, simulation, and Darcy's law for $\alpha = 0.05$.

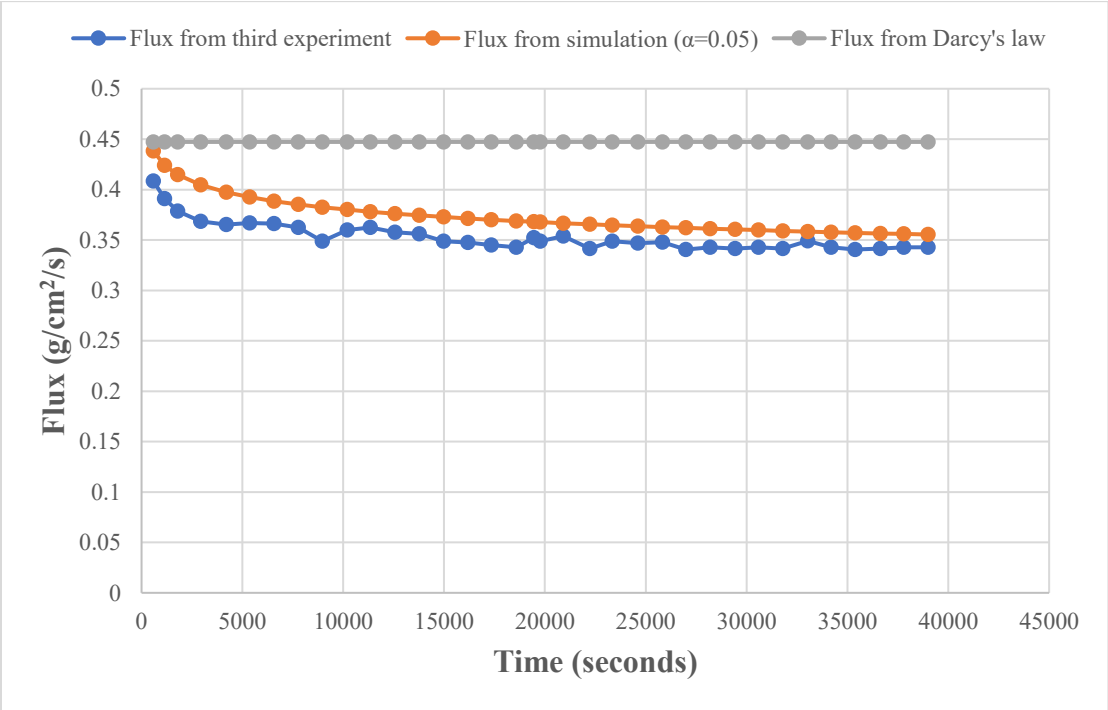

Figure 6.16 Flux values from the third experiment, simulation, and Darcy's law for $\alpha = 0.05$.

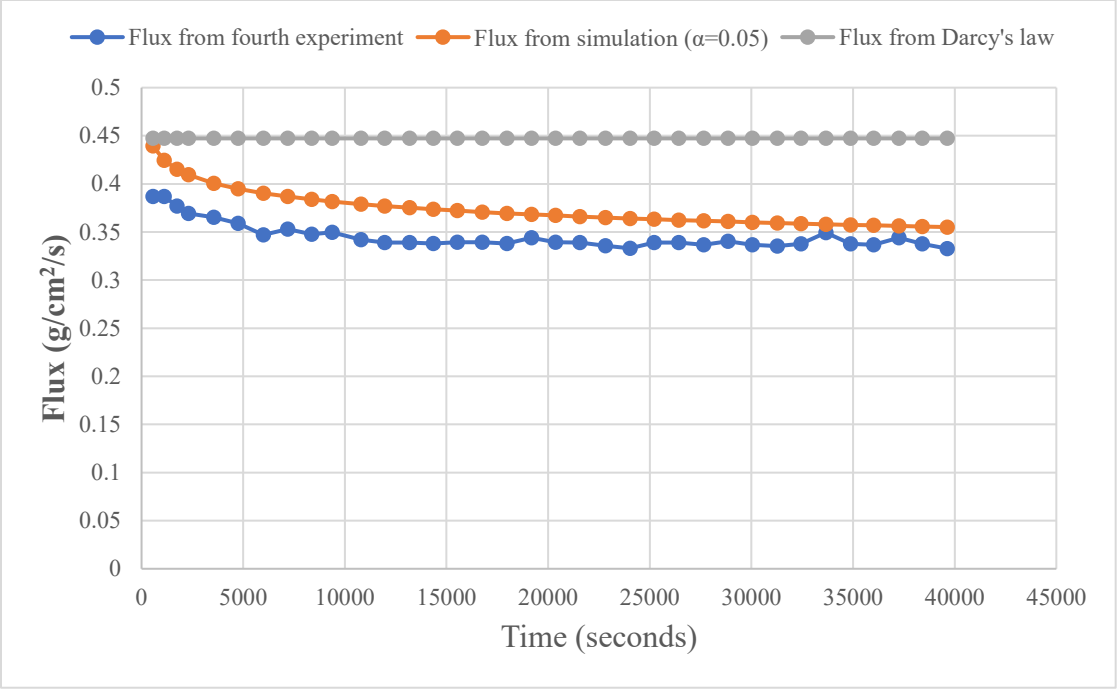

Figure 6.17 Flux values from the fourth experiment, simulation, and Darcy's law for $\alpha = 0.05$.

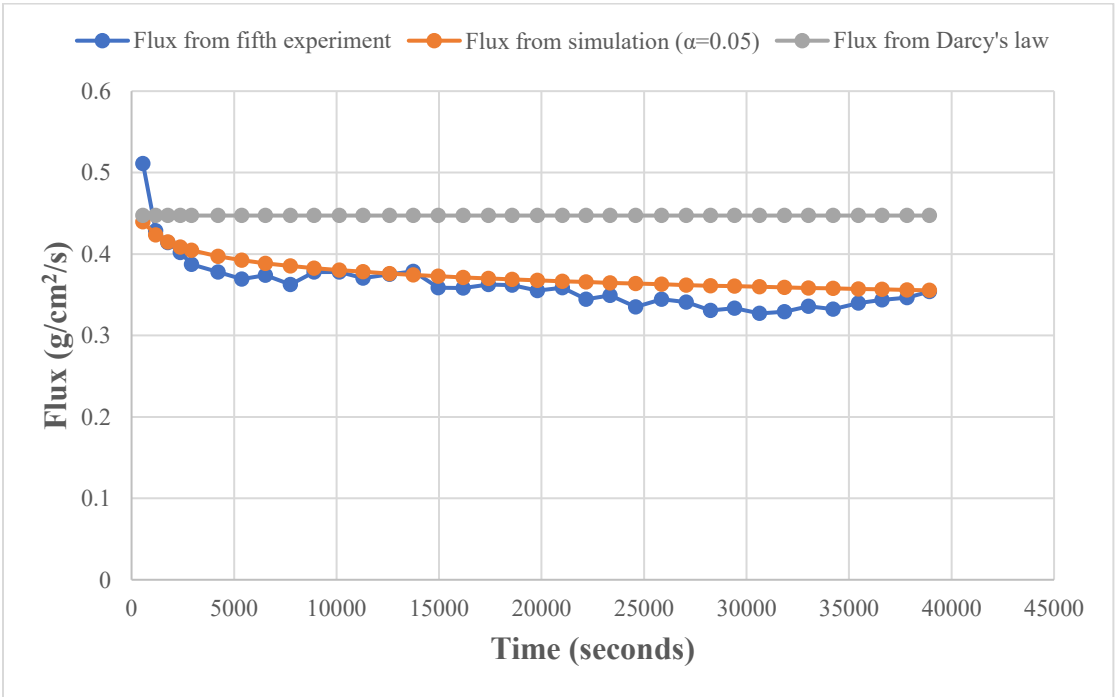

Figure 6.18 Flux values from the fifth experiment, simulation, and Darcy's law for $\alpha = 0.05$.

6.9 Optimum Number of Time Steps

The value of the fractional order, $\alpha \approx 0.05$, has been found in the previous section. In section 6.6, the closest value of α that we calculated error for is 0.10. Tables 6.4 and 6.5 show the error values computed using graded meshes for the initial conditions $p(x,0) = sin(\pi x)$ and $p(x,0) = x(1-x)$, respectively. The discretization method used in the numerical model is second-order accurate in space, and first-order accurate in time. Hence, the relationship between number of grid-points in space and number of steps in time should be written as $N_t = \beta N_x^2$. The best value of β, the proportionality constant between N_t and N_x^2, can be found looking at the computed error values.

For $N_x = 50$, the rate of change in error becomes insignificant beyond $N_t = 6400$. The optimal number of time steps in this case can be taken in the range of 3200-6400. Hence, the optimal value of β for $N_x = 50$ lies in the range of 1 to 3. Similarly, the optimal range of number of time steps in unit time for $N_x = 100$ is 6400-25600. Therefore, the ideal value of β for $N_x = 100$ is in the range of 1 to 3.

Table 6.4 Error values found using graded meshes for initial condition $p(x,0) = sin(\pi x)$.

Total length of space = 1, Total time = 1, $\alpha = 0.10$			
No. of time steps	$\boldsymbol{N_x = 50}$	$\boldsymbol{N_x = 100}$	$\boldsymbol{N_x = 200}$
200	4.604229e-04	4.563393e-04	4.553187e-04
400	2.392911e-04	2.352417e-04	2.342296e-04
800	1.255623e-04	1.215300e-04	1.205222e-04
1600	6.703984e-05	6.301615e-05	6.201050e-05
3200	3.695421e-05	3.293490e-05	3.193034e-05
6400	2.151257e-05	1.749547e-05	1.649146e-05
12800	1.360172e-05	9.585728e-06	8.582000e-06
25600	9.556525e-06	5.541100e-06	

Table 6.5 Error values found using graded meshes for initial condition $p(x,0) = x(1-x)$.

Total length of space = 1, Total time = 1, $\alpha = 0.10$			
No. of time steps	$N_x = 50$	$N_x = 100$	$N_x = 200$
200	1.167251e-04	1.156942e-04	1.154378e-04
400	6.065559e-05	5.963321e-05	5.937896e-05
800	3.182051e-05	3.080240e-05	3.054921e-05
1600	1.698451e-05	1.596855e-05	1.571590e-05
3200	9.358771e-06	8.343898e-06	8.091521e-06
6400	5.445493e-06	4.431169e-06	4.178929e-06
12800	3.441040e-06	2.426993e-06	2.174823e-06
25600	2.416238e-06	1.402331e-06	1.150195e-06
51200	1.893230e-06	8.793942e-07	
102400	1.626758e-06	6.129576e -07	

6.10 Conclusions

Error values calculated for two numerical models developed using uniform and graded meshes for a memory-based diffusivity equation have been compared. It has been found that the numerical model developed using graded meshes gives smaller errors compared to that using uniform meshes. The value of fractional order used in the mathematical model has been computed using experimental data collected from literature. The value of fractional order and relaxation time are found to be around 0.05 and 730 seconds respectively. Optimal number of time steps in unit time for this value of fractional order and for different number of grid-points in unit length has been estimated by error analysis. The range of the optimal number of steps in unit time is found to be 3200-6400 for $N_x = 50$ and 6400-25600 for $N_x = 100$. The study recommends utilizing graded meshes instead of uniform meshes for better accuracy.

6.11 Acknowledgement

The authors would like to thank the Natural Sciences and Engineering Research Council of Canada (NSERC); Research & Development Corporation of Newfoundland and Labrador (RDC), funding no. 210992; and Statoil Canada Ltd., funding no. 211162 for providing financial support to

accomplish this research under the Statoil Chair in Reservoir Engineering at the Memorial University of Newfoundland, St. John's, NL, Canada.

Bibliography

1. Abu-Saman A.M., and Assaf A.M. (2007). Stability and convergence of Crank–Nicolson method for fractional advection dispersion equation, *Advances in Applied Mathematical Analysis, 2*, 117–125.
2. Bear, J. (1972). *Dynamics of fluids in porous media*, Elsevier.
3. Caputo, M. (1998). Diffusion of Fluids in Porous Media with Memory. *Geothermics, 28*, 113–130.
4. Caputo, M. (2000). Models of Flux in Pous Media with Memory. *Water Resources Research, 36*, 693-705.
5. Chen, C., Liu, F., Turner, I., and Anh, V. (2007). A Fourier method for the fractional diffusion equation describing sub-diffusion, *Journal of Computational Physics, 227*, 886–897.
6. Chen, S., Liu, F., Zhuang, P., Anh, V. (2009). Finite difference approximations for the fractional Fokker-Planck equation, *Applied Mathematical Modellling, 33*, 256–273.
7. Chen, C., Liu, F., Turner, I., and Anh, V. (2010). Numerical schemes with high spatial accuracy for a variable-order anomalous subdiffusion equation, *SIAM Journal of Scientific Computation, 32*, 1740–1760.
8. Christensen R.M. (2003). *Theory of Viscoelasticity*, 2nd edition, Dover Publications, New York.
9. Cui, M. (2009). Compact finite difference method for the fractional diffusion equation. *Journal of Computational Physics, 228,* 7792–7804.
10. Deng, W. (2008). Finite element method for the space and time fractional Fokker-Planck equation. *SIAM Journal of Numerical Analysis, 47*, 204–226.
11. Du, R., Cao, W., and Sun, Z.Z. (2010). A compact difference scheme for the fractional diffusion-wave equation, *Applied Mathematical Modellling, 34*, 2998–3007.
12. Elias, B.P., and Hajash Jr., A. (1992). Changes in quartz solubility and porosity due to effective stress: An experimental investigation of pressure solution, *Geology, 20*, 451-454.
13. El-Sayed, A., Behiry, S., Raslan, W. (2010). Adomian's decomposition method for solving an intermediate fractional advection-dispersion equation. *Computer and Mathematics with Applications, 59*, 1759–1765.
14. Gao, G.H., Sun, Z.Z., (2011). A compact finite difference scheme for the fractional sub-diffusion equations, *Journal of Computational Physics, 230*, 586–595.

15. Gorenflo, R., Mainardi, F., Moretti, D., and Paradisi, P. (2002). Time fractional diffusion: A discrete random walk approach. *Nonlinear Dynamics, 29*, 129–143.
16. Hossain, M.E., Mousavizadegan, S.H. and Islam, M.R. (2008). A New Porous Media Diffusivity Equation with the Inclusion of Rock/Fluid Memories. *E-Library, SPE– 114287*.
17. Hossain, M.E., and Abu-Khamsin, S.A. (2012a). Utilization of Memory Concept to Develop Heat Transfer Dimensionless Numbers for Porous Media Undergoing Thermal Flooding with Equal Rock-Fluid Temperatures. *Journal of Porous Media, 15*(10), 937 – 953.
18. Hossain, M.E., and Abu-Khamsin, S.A. (2012b). Development of Dimensionless Numbers for Heat Transfer in Porous Media Using Memory Concept. *Journal of Porous Media, 15*(10), 957–973.
19. Hossain, M.E., Abu-Khamsin, S.A., and Al-Helali, A. (2015). A Mathematical Model for the Steam Flood with Equal Rock and Fluid Temperatures. *Journal of Porous Media, 18*(7), July, 731 – 744.
20. Iaffaldano, G., Caputo, M., and Martino, S. (2005). Experimental and theoretical memory diffusion of water in sand. *Hydrology and Earth System Sciences, 10*, 93-100.
21. Jiang, W., Lin, Y. (2010). Approximate solution of the fractional advection-dispersion equation, *Computer Physics Communications, 181*, 557–561.
22. Kumar, P., Agrawal, O.P. (2006). An approximate method for numerical solution of fractional differential equations. *Signal Process, 86*, 2602–2610.
23. Langlands, T., Henry, B., (2005). The accuracy and stability of an implicit solution method for the fractional diffusion equation. *Journal of Computational Physics, 205*, 719–736.
24. Li, X., Xu, C. (2009). A space-time spectral method for the time fractional diffusion equation. *SIAM Journal of Numerical Analysis, 47*, 2108–2131.
25. Li, X., Xu, C. (2010). Existence and uniqueness of the weak solution of the space-time fractional diffusion equation and a spectral method approximation. *Communications in Computional Physics, 8*, 1016–1051.
26. Liu, F., Zhuang, P., Anh, V., and Turner, I. (2006). A fractional-order implicit difference approximation for the space-time fractional diffusion equation, *ANZIAM Journal, 47*, C48–C68.
27. Liu, Q., Gu, Y., Zhang, P., Liu, F., and Y. Nie, An implicit RBF meshless approach for time fractional diffusion equations, *Computational Mechanics, 48*,1–12.

28. Lynch, V., Carreras, B., Castillo-Negrete, D., Ferreira-Mejias, K., and Hicks, H. (2003). Numerical methods for the solution of partial differential equations of fractional order, *Journal of Computational Physics, 192*, 406–421.
29. Meerschaert, M.M., and Tadjeran, C. (2004). Finite difference approximations for fractional advection-dispersion flow equations, *Journal of Computational and Applied Mathematics, 172*, 65–77.
30. Momani, S., Odibat, Z. (2007). Homotopy perturbation method for nonlinear partial differential equations of fractional order. *Physics Letter A, 365*, 345–350.
31. Murillo, J.Q., and Yuste, S.B. (2009). On three explicit difference schemes for fractional diffusion and diffusion-wave equations. *Physica Scripta*, doi:10.1088/0031-8949/2009/T136/014025.
32. Murillo, J.Q., Yuste, S.B. (2011). An explicit difference method for solving fractional diffusion and diffusion-wave equations in the Caputo form, *Journal of Computational and Nonlinear Dynamics, 6*, 021014.
33. Odibat, Z. (2006). Rectangular decomposition method for fractional diffusion-wave equations, *Applied Mathematics and Computation, 179*, 92–97.
34. Odibat, Z., Momani, S. (2009). The variational iteration method: An efficient scheme for handling fractional partial differential equations in fluid mechanics. *Computers and Mathematics with Applications, 58*, 2199–2208.
35. Roop, J.P. (2006). Computational aspects of FEM approximation of fractional advection dispersion equations on bounded domains in R2. *Journal of Computational and Applied Mathematics, 193*, 243–268.
36. Sun, Z.Z., and Wu, X. (2006). A fully discrete difference scheme for a diffusion-wave system. *Applied Numerical Mathematics, 56*, 193–209.
37. Stynes, M., O'riordan, E., & Gracia, J. E. L. (2017). Error analysis of a finite difference method on graded meshes for a time-fractional diffusion equation, *SIAM Journal of Numerical Analysis, 55*(2), 1057–1079.
38. Tadjeran, C., Meerschaert, M. M., Scheffler, H.P. (2006). A second-order accurate numerical approximation for the fractional diffusion equation, *Journal of Computational Physics, 213*, 205–213.
39. Wang, K.X., Wang, H. (2011). A fast characteristic finite difference method for fractional

advection–diffusion equations, *Advances in Water Resources, 34*, 810–816.

40. Yildirim, A. (2010). Analytical approach to Fokker-Planck equation with space- and time-fractional derivatives by means of the homotopy perturbation method, *Journal of King Saud University (Science)*, 22, 257–264.
41. Yuste, S.B., Acedo, L. (2005). An explicit finite difference method and a new von-Neumann-type stability analysis for fractional diffusion equations, *SIAM Journal of Numerical Analysis, 42*, 1862–1874.
42. Zaman, T. U., MacLachlan, S., and Hossain, M. E. (2017a). Numerical modelling of a memory- based radial diffusivity equation using the Riemann-Liouville definition of the fractional-order derivative and uniform meshes. (in preparation).
43. Zaman, T. U., MacLachlan, S., and Hossain, M. E. (2017b). Numerical approximation of a time-fractional diffusion equation using the Riemann-Liouville definition of the fractional derivative and graded meshes. (in preparation).
44. Zhang, H. M. (2003). Driver memory, traffic viscosity and a viscous vehicular traffic flow model. *Transportation Research Part B: Methodological*, *37*(1), 27–41. http://doi.org/10.1016/S0191-2615(01)00043-1
45. Zavala-Sanchez, V., Dentz, M., and Sanchez-Vila, X. (2009). Characterization of Mixing and Spreading in a Bounded Stratified Medium. *Advances in Water Resources, 32*(5), 635–648.
46. Zhuang, P., Liu, F. (2006). Implicit difference approximation for the time fractional diffusion equation, *Journal of Applied Mathematics and Computing, 22*, 87–99.
47. Zhuang, P., Liu, F., Anh, V., Turner, I. (2008). New solution and analytical techniques of the implicit numerical method for the anomalous subdiffusion equation, *SIAM Journal of Numerical Analysis, 46*, 1079–1095.

Chapter 7

A Generalized Memory- based Mathematical and Numerical Model for Flow through Porous Media

Co-Authorship

Chapter 7 is prepared according to the Guidelines for Manuscript Format Theses in the Faculty of Engineering and Applied Science at Memorial University. This chapter has been prepared for submission as a journal article:

T. U. Zaman, S. MacLachlan, and M. E. Hossain (in preparation). "A generalized memory-based mathematical and numerical model for flow through porous media."

The research work presented in this chapter was conducted by Tareq Uz Zaman under the direction and supervision of M. Enamul Hossain, and the guidance and close supervision of Scott MacLachlan. The manuscript itself was written by Tareq Uz Zaman and reviewed by M. Enamul Hossain and Scott MacLachlan.

7.1 Abstract

Modeling and simulation of porous media flow is crucial to overcome the technological challenges associated with petroleum production. Numerous models have been developed over more than the past fifty years. Continuum models are the simplest among all the models that are based on Darcy's law, relating the pressure gradient in the direction of flow to the volumetric flux of fluid, through the medium permeability and fluid viscosity. Another approach is pore-scale modeling, which takes the microscopic description of the pore geometry into consideration. These models cannot accurately represent the characteristics of fluid flow, however, as they do not consider the effects of history of the rock and fluid, though fluid flow depends on this history. This limitation can be

addressed by the inclusion of ‘memory’ in the fluid-flow model. The parameter ‘memory’ stands for the effects of history of the rock and fluid. This idea is relatively new and growing in petroleum engineering. Several models that incorporate memory have been developed for different purposes, but there is no general mathematical model developed yet that will represent fluid flow for all type of rocks, fluids and flow phenomena. In this paper, such a general mathematical model is proposed. The model is generalized and valid in the sense that all other established memory-based models can be derived from this model. Another strength of this model is its consideration of both time and space memory. The model can be used to develop a small-scale memory-based reservoir simulator.

Keywords: Porous medium, memory, mathematical modeling, numerical modelling, Riemann-Liouville definition, Caputo definition.

7.2 Introduction

Fluid flow through porous media is studied in many branches of science, e.g., petroleum engineering, chemical engineering, and hydrogeology. It is important because it is associated with some of the most important technological challenges such as groundwater management, reduction of concentration of greenhouse gases in the atmosphere, and petroleum production.

Terzaghi (1923 and 1936) developed the basic equations for fluid diffusion in porous media in addition to significant contributions from other researchers (Biot, 1941, 1956, 1956, and 1973; Biot *et al.*, 1957; Boley *et al.*, 1962; Nowacki, 1964; McNamee *et al.*, 1960; Booker, 1974; Rice *et al.*, 1976; Bell *et al.*, 1978; and Roeloffs, 1988). These authors formulated equations to represent the flow of fluid through elastic porous media and obtained solutions for the equations in many cases.

Generally, the empirical Darcy law is used to study diffusion problems in porous media. The law states that the fluid flux is proportional to the pressure gradient. Many authors extended Darcy’s law in different ways to accurately represent the fluid flow through porous media and obtained solutions in many interesting cases.

Different authors have modified Darcy's law by incorporating the memory concept (Caputo, 1999, 2000, and 2003; Caputo *et al.*, 2004; Hossain *et al.*, 2008). In this paper, we review the Caputo (1999, 2000, 2003), Caputo *et al.* (2004), and Hossain *et al.* (2008) models for fluid flow, modify Darcy law, and propose a general diffusivity equation. The modified Darcy law presented in this paper is more general than those existing in the literature.

7.2.1 Darcy Equation

Darcy (1856) presented his experimental results by the equation

$$Q = uA = \frac{kA}{L}(H + L - H_0)\,, \tag{7.1}$$

where u is the superficial fluid velocity, k is defined as the hydraulic conductivity, L is the height of the sand layer, A is the cross-sectional area of the sand layer, and H and H_0 are the height of liquid in manometer from the top and bottom of the sand layer, respectively.

The hydraulic conductivity, k, is, in fact, fluid dependent besides being affected by the solid matrix of the porous medium. The effects of fluid viscosity are not considered in Darcy's law. Darcy's law is said to be valid for incompressible and isothermal creeping flow of a Newtonian fluid through a relatively long, uniform, and isotropic porous medium of low hydraulic conductivity.

7.2.2 The Hazen-Darcy Equation

Hazen (1893) was the first to include the effect of viscosity indirectly in the Darcy equation. In his experiment, he altered the temperature of the water prior to entering the filter and observed the influence of water temperature on the hydraulic conductivity in the Darcy equation. The experiment was otherwise performed under isothermal conditions. He modified the Darcy equation in the form

$$u = \left(\frac{T+10}{60}\right) k_{50} \frac{\Delta P}{L}\,, \tag{7.2}$$

where T is the water temperature in degrees Fahrenheit, k_{50} is the reference hydraulic conductivity value measured with water flowing isothermally through the permeable medium at a temperature equal to 50^0F, and ΔP is the pressure difference. Here, the change in hydraulic conductivity with temperature actually mimics the hydraulic conductivity dependence on viscosity.

Fluid viscosity was incorporated directly as an individual component in the Darcy equation in 1918 by Krüger, in 1920 by Zunker, and in 1927 by Kozeny.

Ingham *et al.* (1998) refer to the equation

$$u = \left(\frac{K}{\mu}\right)\frac{\Delta P}{L}, \tag{7.3}$$

as the Hazen-Darcy equation to differentiate it from the original equation (Eq. (7.1)) proposed by Darcy. In this equation, K represents the permeability and μ is the dynamic fluid viscosity.

There is a lack of experimental work validating the Hazen-Darcy equation for non-isothermal flow, which is typical in a porous medium (Ingham *et al.*, 1998).

7.3 Memory- Based Modified Darcy's Laws

Permeability is considered constant with time in the classical form of Darcy's law. However, due to rock and fluid interaction during fluid flow, both rock and fluid properties change with time. Consideration of this variation is necessary to accurately represent fluid flow through the porous medium. Caputo (1999) modified Darcy's law by introducing a memory formalism to simulate the effect of a decrease of the permeability in time. He proposed the following equation for volumetric flux,

$$u = -\eta\rho\,\frac{c_{\partial^\alpha}}{c_{\partial t^\alpha}}\frac{\partial p}{\partial x}, \tag{7.4}$$

with $0 \leq \alpha < 1$. Here, p represents pressure, and $\frac{{}^{C}\partial^{\alpha}}{{}^{C}\partial t^{\alpha}}$ denotes the Caputo fractional derivative with respect to time t of order α and it is defined by

$$\frac{{}^{C}\partial^{\alpha} p(x,t)}{{}^{C}\partial t^{\alpha}} = \frac{1}{\Gamma(n-\alpha)} \int_0^t (t-s)^{n-\alpha-1} \frac{d^n p(s)}{ds^n} ds\,,\ n-1 < \alpha < n\,, \tag{7.5}$$

where Γ is the gamma function (Kilbas *et al.*, 2006, pp. 91, Eq. 2.4.1). η is defined in this model as the ratio of the pseudopermeability of the medium with memory to the fluid viscosity.

The term $\frac{\partial^{\alpha}}{\partial t^{\alpha}} \frac{\partial p}{\partial x}$ in the above equation includes the pressure gradient at the current time as well as all the pressure gradients of the previous time steps. Here, fluid flux does not depend only on the present pressure gradient, but on the history of the pressure gradient as well. This term arises in the equation to represent permeability variation with time depending on the previous pressure gradients. This equation uses two parameters, namely α and η, to describe the flow of the fluid, instead of the single parameter 'permeability' as in Hazen-Darcy equation. Eq. (7.4) infers that 'K' in Eq. (7.3) is not constant but varies with time.

Caputo (2000) introduced a memory formalism that operates on both of flow and pressure gradient to modify Darcy's law. He proposes that permeability changes with time depending on the previous pressure gradient and flow. To simulate the memory formalism, he proposed the following equation to substitute for the classical Darcy's law,

$$\left(\gamma + \varepsilon \frac{{}^{C}\partial^{n_1}}{{}^{C}\partial t^{n_1}}\right) u = \left(c + d \frac{{}^{C}\partial^{n_2}}{{}^{C}\partial t^{n_2}}\right) \frac{\partial p}{\partial x}\,, \tag{7.6}$$

where $0 \leq n_1 < 1$, $0 \leq n_2 < 1$, and $\frac{{}^{C}\partial^{n_1} p(x,t)}{{}^{C}\partial t^{n_1}}$ and $\frac{{}^{C}\partial^{n_2}}{{}^{C}\partial t^{n_2}}$ denote the Caputo fractional derivative with respect to time t of order n_1 and n_2, respectively, defined by Eq. (7.5).

Caputo (2000) also took into account the change in physical properties of the fluid due to its temperature variations and physical or chemical interactions with the matrix. He represented the

relation between the variation of the mass of fluid per unit volume, relative to its value in the undisturbed condition, and the pressure in the following form, to consider that the fluid and the matrix may be subject to changes in their physical properties,

$$\left(a + b\frac{{}_{C}\partial^{m_2}}{{}_{C}\partial t^{m_2}}\right)p = \left(\alpha + \beta\frac{{}_{C}\partial^{m_1}}{{}_{C}\partial t^{m_1}}\right)\rho_v \,, \tag{7.7}$$

where ρ_v is the variation of the mass of fluid per unit volume in the porous medium from the undisturbed condition, $0 \leq m_1 < 1$, and $0 \leq m_2 < 1$.

These memory formalisms imply the use of twelve free parameters, namely, $a, b, c, d, \alpha, \beta, \gamma, \varepsilon, m_1, m_2, n_1$ and n_2. A very large number of different models can be selected to describe diffusion with memory by assigning different values in these free parameters. Eq. (7.6) considers the history of the pressure gradient and fluid flux. Eq. (7.7) considers the history of pressure and the variation of the mass of fluid per unit volume, relative to its value in the undisturbed condition. Assigning appropriate values to twelve free parameters, one can consider or neglect the effect of any of these histories.

Hossain *et al.* (2008) proposed the following relationship between the fluid velocity and pressure gradient

$$u = -\eta\frac{{}_{C}\partial^{\alpha}}{{}_{C}\partial t^{\alpha}}\frac{\partial p}{\partial x}\,, \tag{7.8}$$

with $0 \leq \alpha < 1$. They defined η as

$$\eta = \frac{K}{\mu}T^{\alpha}\,. \tag{7.9}$$

The model proposed by Caputo (1999) and Hossain *et al.* (2008) look identical, but the models are different due to the dissimilar definitions of η used in them.

The above models consider only time memory, and do not incorporate space memory. To consider the observed deviations of the flow from those implied by the classic diffusion equation, Caputo (2003) introduced a space memory formalism in the classical Darcy's law as

$$q = -\left(\frac{\alpha}{b-a}\right)\int_a^b A(n)\frac{{}^{C}\partial^n p}{{}^{C}\partial x^n}dn - \beta\frac{\partial p}{\partial x}, \tag{7.10}$$

with $0 \leq n < 1$. $A(n)$ represents the weight of the fractional derivative of order n in the range $[a, b]$.

Here, the memory mechanism operates directly on the pressure rather than on the pressure gradient. This equation considers the pressure over all the space that the fluid has passed through. Space memory can be used flexibly to represent local phenomena, while time memory is more flexible to represent variations in space (Caputo, 2003).

Iaffaldano *et al.*'s (2005) experiment, in which they measured fluid flux through a porous layer with constant hydraulic pressure difference between the boundary surfaces, shows that fluid flux decreases over time, and that the volume of sand is decreased as well. Their experiment implies that mechanical compaction occurring during diffusion causes flux variations, and that mechanical compaction is caused by the permeability changes.

Giuseppe *et al.* (2010) conducted experiments to determine the flow rate through a uniformly packed column of porous media. They designed the experimental setup on purpose to determine the memory parameters appearing within Eqs. (7.6) and (7.7). They conclude that memory largely influences the experiment. Experimental data also show that mechanical compaction decreases permeability and, consequently, flux.

7.4 Memory- Based Modified Diffusion Equations

The mathematical model-

$$\frac{{}_C\partial^\gamma p(x,t)}{{}_C\partial t^\gamma} - \frac{\partial^2 p(x,t)}{\partial x^2} = \hat{q}(x,t) \tag{7.11}$$

where $\hat{q}(x,t)$ is a given source term, is known as a subdiffusion wave equation when $0 < \gamma < 1$ and as a diffusion wave equation when $1 < \gamma < 2$.

The dynamics of physical processes involving anomalous transport mechanisms can be represented by this model (Jin *et al.*, 2016). The subdiffusion equation can describe thermal diffusion in media with fractal geometry (Nigmatulin, 1986), and highly heterogeneous aquifers (Adams *et al.*, 1992, and Hatano *et al.*, 1998). The diffusion equation can model the propagation of mechanical waves in viscoelastic media (Mainardi, 1996).

Applying conservation of mass, we have

$$\frac{\partial}{\partial t}(\rho\phi) + \frac{\partial}{\partial x}(\rho u) = \tilde{q}\,, \tag{7.12}$$

where ρ is the density of the fluid, ϕ is porosity of the porous medium, and $\tilde{q}$ is the strength of the source.

Writing

$$\frac{\partial}{\partial t}(\rho\phi) = \rho\phi c_t \frac{\partial p}{\partial t}\,, \tag{7.13}$$

where c_t is the total compressibility, yields

$$\rho\phi c_t \frac{\partial p}{\partial t} - \frac{\partial}{\partial x}\left(\rho\eta \frac{{}_C\partial^\alpha}{{}_C\partial t^\alpha}\left(\frac{\partial p}{\partial x}\right)\right) = \tilde{q}\,. \tag{7.14}$$

Incorporation of Caputo's (1999) model (Eq. (7.4)) into Eq. (7.12) also gives the same diffusion Eq. (7.14) with a different definition of η.

7.5 Generalized Darcy's Law and Diffusion Equation

Caputo (1999, 2000, 2003), Caputo *et al.* (2004), and Hossain *et al.*'s (2008) models give the idea that permeability and fluid properties might depend on the history of flux, pressure gradient, and space memory. To account for the observed deviations of the flow from those implied by the classic diffusion equation, we propose the following equation to substitute for the classical Darcy's law

$$\left(e + f\,\frac{{}^{C}\partial^{\gamma-1}}{{}^{C}\partial t^{\gamma-1}}\right)u = -\left(a + b\,\frac{{}^{RL}\partial^{\alpha}}{{}^{RL}\partial t^{\alpha}}\right)\frac{\partial p}{\partial x} - \left(c + d\,\frac{{}^{RL}\partial^{\beta}}{{}^{RL}\partial x^{\beta}}\right)p\,, \tag{7.15}$$

with $0 \le \alpha < 1$, $0 \le \beta < 1$ and $0 \le \gamma < 2$.

Here, $\frac{{}^{RL}\partial^{\alpha}p(x,t)}{{}^{RL}\partial t^{\alpha}}$ and $\frac{{}^{RL}\partial^{\beta}}{{}^{RL}\partial t^{\beta}}\left(\frac{\partial p(x,t)}{\partial x}\right)$ denote the Riemann-Liouville fractional derivatives with respect to time t of order α and β, respectively, defined by (Kilbas *et al.*, 2006, pp. 70, Eq. 2.1.5)

$$\frac{{}^{RL}\partial^{\alpha}p(x,t)}{{}^{RL}\partial t^{\alpha}} = \frac{1}{\Gamma(n-\alpha)}\frac{d^{n}}{dt^{n}}\int_{0}^{t}(t-s)^{n-\alpha-1}p(s)ds\,,\ n-1 < \alpha < n\,, \tag{7.16}$$

$\frac{{}^{C}\partial^{\gamma-1}u(x,t)}{{}^{C}\partial t^{\gamma-1}}$ denotes the Caputo fractional derivative with respect to time t of order $(\gamma-1)$ and it is defined by Eq. (7.5).

Here, we have introduced the memory formalism on the fluid flux and pressure gradient. We have also incorporated space memory, operating on the pressure.

The Riemann-Liouville definition has been used for two fractional-order derivatives, and the Caputo definition has been used for another fractional-order derivative in Eq. (7.15). The definitions are selected based on the solutions allowed by the model for the fractional-order derivatives. Solutions of models having only one fractional derivative term and not mixed with the spatial derivatives can be derived via separation of variables and the Laplace transform. If the

Riemann-Liouville derivative is used there, the only solutions found are constant in time. If, on the other hand, the Caputo derivative is used, the solutions are found in terms of the Mittag-Leffler functions, and we get solutions for different time. The opposite happens when the model contains a first derivative in time and the fractional derivative mixed within the spatial derivatives. In this case, the Caputo derivative supports only a constant-in-time solution, while the Riemann-Liouville derivative gives solution in terms of the Mittag-Leffler functions.

To consider the relation between the variation of the mass of fluid per unit volume, relative to its value in the undisturbed condition, and the pressure, we take the equation from Caputo (2000),

$$\left(g + j\,\frac{{}^{C}\partial^{\delta}}{{}^{C}\partial t^{\delta}}\right)p = \left(l + m\,\frac{{}^{C}\partial^{\zeta}}{{}^{C}\partial t^{\zeta}}\right)\rho\ , \tag{7.17}$$

with $0 \le \delta < 1$, $0 \le \zeta < 1$.

This memory formalism implies the use of fifteen free parameters, namely, $a, b, c, d, e, f, g, j, l, m, \alpha, \beta, \gamma, \delta,$ and ζ. These parameters will allow a very large number of different models to selectively describe diffusion with memory by assigning different values in these free parameters. Eqs. (7.12), (7.15), and (7.17) must be solved collectively to find the pressure at different grid-points at different times. However, an analytical solution procedure would be very difficult.

To numerically solve Eq. (7.15), we simplify the equation considering $e = 0$ and $f = 1$ and we get

$$\frac{{}^{C}\partial^{\gamma-1}(u)}{{}^{C}\partial t^{\gamma-1}} = -\left(a + b\,\frac{{}^{RL}\partial^{\alpha}}{{}^{RL}\partial t^{\alpha}}\right)\frac{\partial p}{\partial x} - \left(c + d\,\frac{{}^{RL}\partial^{\beta}}{{}^{RL}\partial x^{\beta}}\right)p\ . \tag{7.18}$$

Rearranging Eq. (7.18) gives

$$u = -\frac{{}^{C}\partial^{1-\gamma}}{{}^{C}\partial t^{1-\gamma}}\left[\left(a + b\,\frac{{}^{RL}\partial^{\alpha}}{{}^{RL}\partial t^{\alpha}}\right)\frac{\partial p}{\partial x} + \left(c + d\,\frac{{}^{RL}\partial^{\beta}}{{}^{RL}\partial x^{\beta}}\right)p\right]\ . \tag{7.19}$$

Also, we consider Eq. (7.13), (and not Eq. (7.17)) and take ρ to be a constant. Substitution of Eq. (7.13) and (7.19) in Eq. (7.12) yields

$$\rho\phi c_t \frac{\partial p}{\partial t} - \frac{\partial}{\partial x}\left(\rho \frac{{}_C\partial^{1-\gamma}(u)}{{}_C\partial t^{1-\gamma}}\left[\left(a + b\frac{{}_{RL}\partial^{\alpha}}{{}_{RL}\partial t^{\alpha}}\right)\frac{\partial p}{\partial x} + \left(c + d\frac{{}_{RL}\partial^{\beta}}{{}_{RL}\partial x^{\beta}}\right)p\right]\right) = \tilde{q}\ . \tag{7.20}$$

Eq. (7.20) can be written as

$$w\frac{{}_C\partial^{\gamma}p(x,t)}{{}_C\partial t^{\gamma}} - \frac{\partial}{\partial x}\left[\left(a + b\frac{{}_{RL}\partial^{\alpha}}{{}_{RL}\partial t^{\alpha}}\right)\frac{\partial p}{\partial x} + \left(c + d\frac{{}_{RL}\partial^{\beta}}{{}_{RL}\partial x^{\beta}}\right)p\right] = \bar{q}\ , \tag{7.21}$$

where $w = \phi c_t$, and $\bar{q} = \frac{{}_C\partial^{\gamma-1}(\tilde{q})}{{}_C\partial t^{\gamma-1}}$.

If $a = c = d = 0,\ \alpha = 0, w = 1,$ and $b = 1,$ then this gives the time-fractional diffusion or subdiffusion equation. For $\gamma = 1,$ and $a = c = d = 0,$ this equation is converted to Caputo's (1999) and Hossain et al.'s (2008) diffusion Eq. (7.14).

Again, for $c = d = 0$, the generalized Darcy's law (Eq. (7.15)) converts to Eq. (7.6). For $\gamma = 1$, and $\alpha = 0$, Eq. (7.15) considers only space memory.

7.6 Conclusions

Models are generally developed for specific flow phenomenon. Developing a general equation instead of developing mathematical equation for each specific case is worthy, particularly when the general equation can be simplified easily for different cases. However, it is a bigger challenge to develop a general mathematical model that will represent fluid flow for all types of rocks, fluids, and flow phenomena. In this paper, an attempt has been made to meet this great challenge. A general memory-based mathematical model for flow through porous media is proposed. A small-scale memory-based reservoir simulator, that is called an 'emulator' by Islam et al. (2016), might be developed based on this generalized model. Numerical experiments using that emulator would give the value of different parameters used in the model for different types of rocks, fluids and

flow phenomenon. Though simulation based on this memory approach is at an initial stage, research is on going to overcome the challenges and to develop a small-scale emulator. This small-scale emulator will be the basis for a future complete emulator.

7.7 Acknowledgement

The authors would like to thank the Natural Sciences and Engineering Research Council of Canada (NSERC); Research & Development Corporation of Newfoundland and Labrador (RDC), funding no. 210992; and Statoil Canada Ltd., funding no. 211162 for providing financial support to accomplish this research under the Statoil Chair in Reservoir Engineering at the Memorial University of Newfoundland, St. John's, NL, Canada.

Bibliography

1. Adams, E. E., and Gelhar, L. W. (1992). Field study of dispersion in a heterogeneous aquifer: 2. Spatial moments analysis, *Water Resources Research, 28*, 3293–3307.
2. Bell, M.L., and Nur, A. (1978). Strength changes due to reservoir-induced pore pressure and stresses and application to Lake Oroville. *Journal of Geophysical Research, 83*, 4469-4483.
3. Biot, M.A. (1941). General theory of three dimensional consolidation. *Journal of Applied Physics, 12*, 155-164.
4. Biot, M.A. (1956). General solutions of the equations of elasticity and consolidation for a porous material. *Journal of Applied Mechanics, 78*, 91-96.
5. Biot, M.A. (1956). Thermoelasticity and irreversible thermodynamics. *Journal of Applied Physics, 27*, 240-253.
6. Biot, M.A. (1973). Non linear and semilinear rheology of porous media. *Journal of Geophysical research, 78*, 4924-4937.
7. Biot, M.A., and Willis, D.G. (1957). The elastic coefficients of the theory of consolidation. *Journal of Applied Mechanics, 24*, 594-601.
8. Boley, B.A., and Tolins, I.S. (1962). Transient coupled thermoelastic boundary value problem in the half space. *Journal of Applied Mechanics, 29*, 637-646.
9. Booker, J.R. (1974). Time dependent strain following faulting of a porous medium. *Journal of Geophysical Research, 79*, 2037-2044
10. Caputo, M. (1999). Diffusion of fluids in porous media with memory. *Geothermics, 28*, 113-130.
11. Caputo, M. (2000). Models of flux in porous media with memory. *Water Resources Research. 36*(3), 693-705.
12. Caputo, M. (2003). Diffusion with space memory modelled with distributed order space fractional differential equations, *Annals of Geophysics, 46*(2), 223-234.
13. Caputo, M., and Plastino, W., (2004). Diffusion in porous layers with memory. *Geophysical Journal International, 158*, 385-396.
14. Darcy, H. P. G. (1856). Les Fontaines Publiques de la Ville de Dijon. *Victor Dalmont, Paris*.
15. Giuseppe, E. D., Moroni, M., and Caputo, M. (2010). Flux in porous media with memory: Models and experiments, *Transport in Porous Media. 83*, 479-500.

16. Hatano, Y., and Hatano, N. (1998). Dispersive transport of ions in column experiments: An explanation of long-tailed profiles. *Water Resources Research. 34*, 1027–1033.
17. Hazen, A. (1893). Some physical properties of sand and gravels with special reference to their use in filtration. *Massachusetts State Board of Health, Twenty-fourth Annual Report*, 541.
18. Hossain, M.E., Mousavizadegan, S.H., and Islam, M.R. (2008). A new porous media diffusivity equation with the inclusion of rock and fluid memories. *Society of Petroleum Engineers*, SPE-114287-MS.
19. Iaffaldano, G., Caputo, M., and Martino, S. (2005). Experimental and theoretical memory diffusion of water in sand. *Hydrology and Earth System Sciences, 10*, 93-100.
20. Ingham, D.B., Pop, I. (Eds.) (1998). *Transport Phenomena in Porous Media*. Oxford: Pergamon press.
21. Islam, M.R., Hossain, M.E., Mousavizadeghan, S.H., Mustafiz, S. and Abou-kassem, J.H. (2016). *Advanced Petroleum Reservoir Simulation: Towards Developing Reservoir Emulators*. ISBN: 978-1-119-03851-1, 2nd Edition, John Wiley & Sons, Inc. Hoboken, New Jersey, and Scrivener Publishing LLC, Salem, Massachusetts, USA, 592 pp.
22. Jin, B., Lazarov, R., and Zhou, Z. (2016). Two fully discrete schemes for fractional diffusion and diffusion-wave equations with nonsmooth data. *SIAM Journal on Scientific Computing, 38*, A146– A170.
23. Kilbas, A. A., Srivastava, H. M., and Trujillo, J. J. (2006). *Theory and Applications of Fractional Differential Equations*. Amsterdam: Elsevier.
24. Kozeny, J. (1927). Ueber Grundwasserbewegung. *Wasserkraft und Wasserwirtschaft, 22*, 67.
25. Krüger, E. (1918). Die Grundwasserbewegung. *Internationale Mitteilungen fur Bodenkunde, 8*, 105.
26. Mainardi, F. (1996). Fractional relaxation-oscillation and fractional diffusion-wave phenomena. *Chaos, Solitons & Fractals, 7*, 1461–1477.
27. McNamee, J., and Gibson, R.E. (1960). Displacement functions and linear transforms applied to diffusion through porous elastic media. *Quarterly Journal of Mechanics Applied to Mathematics, 13*, 99-111.
28. Nigmatulin, Raoul R. (1986). The realization of the generalized transfer equation in a medium with fractal geometry. *Physica Status Solidi B, 133*, 425–430.

29. Nowacki, W. (1964). Green function for a thermoelastic medium 2. *In: Bulletin of the Academy of Polish Science, Series Science Mathematics, Astronomy, Physics, vol. 12*, 465-472.
30. Rice, J.R., Cleary, M.P. (1976). Some basic stress-diffusion solutions for fluid saturated elastic porous media with compressible constituents. *Review of Geophysics and Space Physics, 14*, 227-241.
31. Roeloffs, E.A. (1988). Fault stability changes induced beneath a reservoir with cyclic variations in water level. *Journal of Geophysical Research, 93*, 2107-2124.
32. Stynes, M., O'Riordan, E., and Gracia, J. L. (2017). Error analysis of a finite difference method on graded meshes for a time-fractional diffusion equation. *SIAM Journal on Numerical Analysis, 55*(2), 1057-1079.
33. Terzaghi, K. (1923). Die Berechnung der Durchlässigkeitsziffer des Tones aus dem Verlauf der Hydrodynamischen Spannungserscheinungen. *Sitzungsbericht Akademie Wissentschafliche, Mathematik-Naturwissenschaft, Wien, Kl., Abt. 2A*, 132, 105.
34. Terzaghi, K. (1936). The shearing resistance of saturated soils. *In: Proceedings International Conference on Soil Mechanics Foundation Engineering, Vol.1*, 54-55.
35. Zunker, F. (1920). Das allgemeine Grundwasserfliessgesetz, *Journal fur Gasbeleuchtung und Wasserversorgung*.

Chapter 8

A Generalized Model and Dimensionless Number for Fluid Flow in Packed Beds and Porous Media

Co-Authorship

Chapter 8 is prepared according to the Guidelines for Manuscript Format Theses in the Faculty of Engineering and Applied Science at Memorial University. This chapter has been prepared for submission as a journal article:

T. U. Zaman, M. E. Hossain, and S. MacLachlan (in preparation). "A generalized model and dimensionless number for fluid flow in packed beds and porous media."

The research work presented in this chapter was conducted by Tareq Uz Zaman under the direction and supervision of M. Enamul Hossain, and the guidance and close supervision of Scott MacLachlan. The manuscript itself was written by Tareq Uz Zaman and reviewed by M. Enamul Hossain and Scott MacLachlan.

8.1 Abstract

A generalized semi-empirical equation is proposed that portrays the flow of fluid in packed beds and porous media. The new model is based on the fact that flow regimes in porous media are not simply laminar and turbulent. In fact, the characteristic flow regime for porous media lies in-between. The proposed model calculates total pressure loss from viscous energy loss, local loss, and loss due to turbulence following the technique of compact model development from asymptotic solutions. It links the pressure drop along a porous medium to the superficial velocity. The non-spherical particle diameter is redefined to more accurately represent the wall surface area within the pore space. The model gives a new expression for the modified Reynolds number for

fluid flow through porous media. The generalized model is reduced for each flow regime. The most significant new finding is that the proposed model portrays all the flow regimes that occur in porous media. The viscous term is dominant at very low flow rates, turbulence and inertial loss occur at very high flow rates, while the viscous and inertial loss occur in-between, which is the central flow regime for porous media. The ratio of pressure gradient to superficial fluid velocity varies linearly with superficial fluid velocity in both cases of characteristic and turbulent flows, but the slopes in the two cases are different. This new equation is also used for modeling the physical properties of random porous media. The model provides an innovative way to calculate tortuosity of a porous media, the diameter of equivalent volume sphere, and the head-loss coefficient. The novelty of the new model is in the ability to describe any flow phenomenon for any type of fluid through packed beds and porous media.

Keywords: Packed beds, porous medium, superficial velocity, pressure drop, flow regime, tortuosity.

8.2 Introduction

Theoretical analysis and experimental investigation have been carried out for many years to study the pressure loss accompanying the flow of fluids through columns packed with granular material and underground porous media. Numerous factors come into consideration to determine the pressure drop in porous media; however, the effects of some factors are very difficult to quantify. Different authors have proposed different models making simplifying assumptions to correlate the factors. Some of the models are applicable only at low fluid flow rates, while others are useful at high fluid flow rates. There are also models that are proposed for both low and high fluid flow rates.

Pressure drop through a granular bed is known to be proportional to the velocity of fluid at low flow rates and to the square of the velocity at high flow rates. Osborne Reynolds (1900) first expressed the pressure gradient as sum of two terms. He expressed the terms as proportional to the first power of the fluid velocity and to the product of the density of the fluid with second power of its velocity, respectively, which is written as

$$\frac{\Delta p}{L} = au + b\rho u^2 \, . \tag{8.1}$$

Blake (1922) first successfully established the dependency of the pressure drop on porosity. He obtained two dimensionless groups, which are $[\{\Delta p g_c \, d_p \, \phi^3\}/\{\rho u^2 L \, (1-\phi)\}]$ and $\left[\{d_p \rho u\}/\{\mu(1-\phi)\}\right]$. Burke and Plummer (1928) found the viscous energy loss to be proportional to $[(1-\phi)/\phi^2]$ and kinetic loss to$[(1-\phi)/\phi^3]$. However, they did not combine these two losses to calculate the total pressure drop. Kozeny (1927) found the pressure loss to be proportional to $[(1-\phi)^2/\phi^3]$ which is different by a fraction of $[(1-\phi)/\phi]$ from the factor derived by Burke and Plummer (1928) for viscous flow. Leva et al. (1947) noted the pressure drop to be proportional to $[(1-\phi)^2/\phi^3]$ at lower flow rates. They also pointed out that the pressure drop is proportional to $[(1-\phi)/\phi^3]$ at higher flow rates. Carman (1937) showed that the method of Blake (1922) leads to the Kozeny (1927) equation at low fluid-flow rates and, due to this reason, the Kozeny (1927) equation is also referred to as the Blake-Kozeny equation or as the Kozeny-Carman equation. In addition, Carman (1937) showed that the method of Blake (1922) leads to the Burke and Plummer (1928) equation for turbulent flows. Hence, the Kozeny (1927) model serves the same purpose for porous media as the Hagen-Poiseuille equation does for circular pipes. Similarly, the Burke-Plummer (1928) model is used for turbulent flows in porous media, such as the Darcy-Weisbach equation for turbulent flow through a circular pipe. Models used for laminar and turbulent flows through circular pipes and porous media are tabulated in Table 8.1.

Ergun *et al.* (1949) first realized that both viscous and kinetic energy losses would contribute to total energy losses. They treated the total pressure losses as a sum of viscous and kinetic energy losses, where viscous energy losses are proportional to $[(1-\phi)^2/\phi^3]$ and kinetic energy losses are proportional to $[(1-\phi)/\phi^3]$. In the same direction, Ergun (1952) proposed an equation applicable for both laminar and turbulent flow, in which he added the Kozeny (1927) and Burke-Plummer (1928) equations to calculate the pressure drop. The Ergun (1952) equation is widely used by chemical engineers.

Table 8.1 Models used for different types of flow through different medium.

Author	Model Equation	Parameters	Type of flow	Type of Medium
Kozeny (1927)	$\Delta p = \frac{150\mu u(1-\phi)^2 L}{d_p^2 \phi^3}$	μ, ϕ, d_p, L	Laminar flow	Porous medium
Burke-Plummer (1928)	$\Delta p = \frac{1.75\rho u^2(1-\phi)L}{d_p \phi^3}$	ρ, ϕ, d_p, L	Turbulent flow	Porous medium
Hagen-Poiseuille	$\Delta p = \frac{32\mu L u}{D^2}$	μ, D, L	Laminar flow	Hollow cylindrical pipe
Darcy-Weisbach	$\Delta p = \frac{4 f_f \rho L u^2}{2D}$	f_f, ρ, D, L	Turbulent flow	Hollow cylindrical pipe
Ergun (1952)	$\Delta p = \frac{150\mu u(1-\phi)^2 L}{d_p^2 \phi^3} + \frac{1.75\rho u^2(1-\phi)L}{d_p \phi^3}$	ρ, μ, ϕ, d_p, L	Both laminar and turbulent flow	Porous medium

The Kozeny (1927) and Burke-Plummer (1928) models are two asymptotic solutions for pressure drop in case of porous media flow at low and high superficial fluid velocities respectively. The development of the Ergun (1952) model, by adding the Kozeny (1927) and Burke-Plummer (1928) terms together and Osborne Reynolds' (1900) way to express the pressure gradient infer that the fluid flow system in porous media exhibits a smooth transition between the two asymptotic solutions. There are no discontinuities and no sudden changes in slope within the transition region. Yovanovich (2003) presented rules to develop a compact model combining such asymptotic solutions. Development of a compact model simply by adding the asymptotic solutions, as Ergun (1952) did to develop his model, is not the right way. Instead, the behaviour of the asymptotic solutions must be examined and, based on their behaviour, proper rules should be followed to combine the solutions to develop a compact model. For example, consider the parameter, ψ, to have two asymptotes corresponding to very small and very large values of the independent parameter, χ; $\psi \to \psi_0 = C_0 \chi^m$ as $\chi \to 0$, and $\psi \to \psi_\infty = C_\infty \chi^n$ as $\chi \to \infty$ or $\chi \to 1$. If $\psi_0 > \psi_\infty$, the solution, ψ, is concave upwards as $\chi \to 0$, and the asymptotes are combined as $\psi = [\psi_0^j + \psi_\infty^j]^{1/j}$, where j is a fitting parameter. If $\psi_0 < \psi_\infty$, the solution, ψ, is concave downwards as $\chi \to 0$, and the asymptotes are combined as, $1/\psi = [(1/\psi_0)^j + (1/\psi_\infty)^j]^{1/j}$.

In packed beds, 'local' loss occurs between laminar and turbulent flow (Niven, 2002), which is not considered in Ergun (1952) model. The 'local' loss occurs due to expansions, contractions, and changes in flow direction within the packed bed (Niven, 2002). This loss can also be the result of flow separation behind each solid particle. Deviation from laminar flow occurs from local losses, rather than the onset of turbulence (Niven, 2002).

In this paper, local losses besides viscous and kinetic energy losses are considered and combined following the asymptotic behaviour of total pressure loss with the superficial fluid velocity. The proposed model is general, in the sense that the Ergun model can be derived from the model for special cases. New parameters arise in the model. However, a novel way to find the parameters is devised. Finally, a new dimensionless number for fluid flow through porous media has been derived that is analogous to the Reynolds number for fluid flow through hollow media.

8.3 Theoretical Development of the Model

As the velocity approaches zero as a limit, the pressure gradient can be written as (Ergun, 1952)

$$\lim_{u\to 0} \frac{\Delta p}{L} = au \, . \tag{8.2}$$

When the velocity is large enough to achieve completely turbulent flow, where kinetic energy losses constitute the whole resistance, the relationship between the pressure gradient and velocity can be expressed as (Ergun, 1952)

$$\lim_{u\to \infty} \frac{\Delta p}{L} = b\rho u^2 \, . \tag{8.3}$$

Equations (8.2) and (8.3) can be written together as

$$\frac{\Delta p}{L} \to \begin{cases} (\frac{\Delta p}{L})_0 = au, \ u \to 0 \\ (\frac{\Delta p}{L})_\infty = b\rho u^2, \ u \to \infty \end{cases} \tag{8.4}$$

Here, $(\Delta p/L)_0 > (\Delta p/L)_\infty$ as $u \to 0$ and the solution $(\Delta p/L)$ is concave upwards. Hence the correct way of combining the asymptotes, $(\Delta p/L)_0$ and $(\Delta p/L)_\infty$, would not be the direct addition of these terms that was done in Ergun *et al.* (1949), and Ergun (1952). Instead, the following manner (Churchill *et al.*, 1972; Kraus *et al.*, 1983; Churchill, 1988; and Yovanovich, 2003) is used to combine the asymptotes

$$\frac{\Delta p}{L} = [\left(\frac{\Delta p}{L}\right)_0^w + \left(\frac{\Delta p}{L}\right)_\infty^w]^{1/w}, \tag{8.5}$$

where the parameter, w, is a fitting parameter.

The Hagen-Poiseuille equation is applicable for laminar flow through hollow cylindrical pipes. To make the equation fit for porous media at lower velocities, its parameters should be replaced by expressions to retain the insight of the original equation. To this purpose, the superficial fluid velocity or volumetric flux, u, in the Hagen-Poiseuille equation is replaced by the mean tortuous velocity, u_t, which is defined as $\tau u/\phi$. The pipe length, ΔL, is replaced by the actual flow length through a porous bed, τL, and the pipe diameter, D, is expressed in terms of the hydraulic radius, r_H. The diameter of a particle of arbitrary shape and the diameter of the equivalent-volume sphere are redefined incorporating a fitting parameter, λ. The hydraulic radius is expressed in terms of the diameter of the equivalent-volume sphere. Replacement of the parameters in the Hagen-Poiseuille equation yields

$$(\frac{\Delta p}{L})_0 = \frac{72\mu\tau^2 u(1-\phi)^2}{\phi^3 d_e^2}, \tag{8.6}$$

which represents the viscous pressure loss during the fluid flow through porous media.

Similarly, the parameters in the Darcy-Weisbach equation are replaced with analogous porous media parameters to calculate the pressure drop due to turbulence in packed beds and porous media. Substitution with the analogous porous media parameters in the Darcy-Weisbach equation gives Eq. (8.7), representing the pressure loss due to turbulence,

$$(\Delta p_1)_\infty = \frac{3 f_f \rho \tau^3 u^2 L(1-\phi)}{g_c \phi^3 d_e}\,. \tag{8.7}$$

Furthermore, local loss in porous media can be expressed as

$$(\Delta p_2)_\infty = \rho K_L \frac{\tau^2 u^2}{2\phi^2}\,. \tag{8.8}$$

Both local and turbulent losses are proportional to u^2 when all the other parameters are kept constant. Hence, the local losses are additive with the turbulent losses. The total pressure drop due to local and turbulent losses can be written as

$$(\frac{\Delta p}{L})_\infty = \frac{3 f_f \rho \tau^3 u^2 (1-\phi)}{g_c \phi^3 d_e} + \frac{\rho K_L \tau^2 u^2}{2\phi^2 L} \tag{8.9}$$

Substitution of Eqs. (8.6) and (8.9) into Eq. (8.5) yields

$$\frac{\Delta p}{L} = [(\frac{72\mu\tau^2 u(1-\phi)^2}{\phi^3 d_e^2})^w + (\frac{3 f_f \rho \tau^3 u^2 (1-\phi)}{g_c \phi^3 d_e} + \frac{\rho K_L \tau^2 u^2}{2\phi^2 L})^w]^{1/w}\,. \tag{8.10}$$

Eq. (8.10) represents the generalized equation for total pressure drop during flow through porous media. The equation can be written as

$$(\frac{\Delta p}{L})^w = \epsilon^w u^w + (\zeta + \eta)^w u^{2w}\,, \tag{8.11}$$

where

$$\epsilon = \frac{72\mu\tau^2(1-\phi)^2}{\phi^3 d_e^2}\,, \tag{8.12}$$

$$\zeta = \frac{3 f_f \rho \tau^3 (1-\phi)}{g_c \phi^3 d_e}\,, \tag{8.13}$$

$$\eta = \frac{\rho K_L \tau^2 u^2}{2\phi^2 L} . \tag{8.14}$$

8.4 Significance of the Proposed Generalized Model

The proposed generalized model combines viscous and turbulence pressure losses using the proper way of developing compact models, instead of simply adding the pressure losses. In addition, the new model incorporates local losses that occur due to expansions, contractions, changes in flow direction within the packed bed, and flow separation behind each solid particle. For these reasons, the new model is more theoretically sound than the widely used Ergun (1952) model. The new model also has the flexibility to represent different flow phenomena through porous media, due to the large number of possible values of the fitting parameter, w.

8.5 Flow Regimes for Porous Media

We divide the flow regimes for porous media into three regions. One is the laminar flow region, the second is the intermediate flow region, and the third is the turbulent flow region.

The laminar flow region is defined as the region in which pressure loss is proportional to the superficial velocity. For this flow region, Eq. (8.11) becomes

$$\frac{\Delta p}{L} = \epsilon u . \tag{8.15}$$

The intermediate flow regime begins when local losses start to arise. In this flow regime, pressure drop deviates from being proportional to the superficial velocity. Here, the pressure loss occurs due to both viscous and local loss. For this flow regime, Eq. (8.11) becomes

$$(\frac{\Delta p}{L})^w = \epsilon^w u^w + \eta^w u^{2w} . \tag{8.16}$$

Local losses and turbulent loss occur in the turbulent flow region, but viscous loss is negligible here, giving

$$\frac{\Delta p}{L} = (\zeta + \eta)u^2 \,. \tag{8.17}$$

8.6 Calculation of Different Parameters from the Pressure Loss and Superficial Velocity

The fitting parameter, w, can be determined by experiment, making fluid flow through a porous bed and measuring the volumetric fluid flux and pressure drop for different flow regimes. Flow regimes will be identified roughly by plotting $\Delta p/L$ vs. u and drawing asymptotes through the low velocity and high velocity portions. Experimental data at low velocity (or the laminar flow regime) can be taken and, again, $\Delta p/L$ vs. u can be plotted. This will yield a straight line through the origin with slope ϵ.

Then, data for high velocity (or the turbulent flow region) can be used to plot $\Delta p/Lu$ vs. u. This will also yield a straight line that goes through the origin with slope $(\zeta + \eta)$.

Data for the intermediate flow region can be used to calculate the values of ζ and η. The best way to interpret Eq. (8.16) would be to plot $(\Delta p/L)^w/u^{2w}$ as a function of u^{-w}. The resulting plot would be a straight line passing through the point $(0, \eta^w)$ with slope ϵ^w. From the intercept, η^w, the value of η can be determined. From $(\zeta + \eta)$ and η, ζ can be calculated. τ, d_e and K_L can then be determined from ϵ, ζ and η. Once d_e is known, then λ can be determined by d_e.

8.7 Development of an Expression for Modified Reynolds Number

At the onset of turbulent flow, the viscous pressure drop and turbulent pressure drop are equal for flow through a circular pipe. Therefore, an expression for the Reynolds number can be developed by equating the Hagen-Poiseuille and Darcy-Weisbach equations. The intermediate flow regime lies between the laminar and turbulent flow regimes in case of flow through a porous bed. Though the viscous pressure drop cannot be equated to the turbulent pressure drop in this case, we can use the same method to find an appropriate group for the modified Reynolds number. It would be useful to determine such an expression for the modified Reynolds number rather than using the conventional expression for the Reynolds number since the expressions of viscous and turbulent

pressure drops for flow through porous media are different than for flow through circular pipes. Therefore, to develop the new expression for the Reynolds number, we write

$$\frac{72\mu\tau^2(1-\phi)^2u}{\phi^3 d_e^2} \approx \frac{3f_f\rho\tau^3(1-\phi)u^2}{g_c\phi^3 d_e} \ . \tag{8.18}$$

Rearranging Eq. (8.18) yields

$$f_f \approx \frac{24}{\frac{\rho\tau u d_e}{\mu(1-\phi)g_c}} . \tag{8.19}$$

We thus define the modified Reynolds number for porous media as

$$Re_m = \frac{\rho\tau u d_e}{\mu(1-\phi)g_c} . \tag{8.20}$$

8.8 Validation of the Model

The proposed model is a more generalized form of the Ergun model. The model can be reduced to that of Ergun (1952) in the case of not considering local losses, tortuosity, a fitting parameter to define particle shape, and taking a unit value for the fitting parameter, w. Derivation of the Ergun equation from the proposed model (Eq. 8.11) is shown in the Appendix. Though the model is found to be valid theoretically, experimental data is needed to validate the model and the derivation of the expression for modified Reynolds number. In addition, value of the modified Reynolds number for transition from laminar to turbulent flow in porous media can be found from experimental data.

8.9 Conclusions

Viscous, local, and turbulent losses are combined, applying asymptotic analysis to derive a general and more accurate equation for calculating total pressure drop. It is general in the sense that it gives a similar equation to that given by Ergun (1952) if $w = 1$. The intermediate flow regime between laminar and turbulent flows is discussed. The new general equation is reduced for each flow

regime. The diameter of the equivalent volume sphere is redefined. A new way is devised to calculate tortuosity, the diameter of the equivalent volume sphere, and the head-loss coefficient. A new expression is developed for a modified Reynolds number. Determination of the value of this modified Reynolds number at the onset of the intermediate flow regime and turbulent flow regime is a topic for future research.

8.10 Acknowledgement

The authors would like to thank the Natural Sciences and Engineering Research Council of Canada (NSERC); Research & Development Corporation of Newfoundland and Labrador (RDC), funding no. 210992; and Statoil Canada Ltd., funding no. 211162 for providing financial support to accomplish this research under the Statoil Chair in Reservoir Engineering at the Memorial University of Newfoundland, St. John's, NL, Canada.

Bibliography

1. Bear, J. (1972). *Dynamics of fluids in porous media.* New York: Dover publications.
2. Bird, R. B., Stewart, W. E., and Lightfoot, E. N. (1960). *Transport Phenomena.* New York: Wiley Publishing.
3. Blake, F. E. (1922). The resistance of packing to fluid flow. *Transactions of the American Institute of Chemical Engineers, 14*, 415.
4. Burke, S. P., and Plummer, W. B. (1928). Gas Flow through packed columns. *Industrial and Engineering Chemistry, 20*(11), 1196-1200.
5. Carman, P. C. (1937). Fluid flow through granular beds. *Transactions of the Institution of Chemical Engineers (London), 15*,150.
6. Churchill, S.W., and Usagi, R. (1972). A General Expression for the Correlation of Rates of Transfer and Other Phenomena. *American Institute of Chemical Engineers, 18*, 1121-1128.
7. Churchill, S.W. (1988). *Viscous Flows: The Practical Use of Theory*, Boston, MA: Butterworths.
8. Ergun, S., and Orning, A. A. (1949). Fluid flow through randomly packed columns and fluidized beds. *Industrial and Engineering Chemistry, 41*(6), 1179-1184.
9. Ergun, S. (1952), Fluid flow through packed columns. *Chemical Engineering Progress, 48*, 9-94.
10. Kozeny, J. (1927). Ueber kapillare Leitung des Wassers im Boden. *Sitzungsber Akad. Wiss., Wien, 136*(2a), 271-306.
11. Kraus, A.D. and Bar-Cohen, A. (1983). *Thermal Analysis and Control of Electronic Equipment*. New York: Hemisphere Publishing Corporation.
12. Leva, M., Grummer, M. (1947). Pressure drop through packed tubes, part iii, prediction of voids in packed tubes. *Chemical Engineering Progress, 43*, 713-718.
13. Leva, M. (1959). *Fluidization*. New York: McGraw-Hill Book Co.
14. Macdonald, T. F., El-Sayer, M. S., Mow, K., and Dullien, F. A. L., (1979). Flow through porous media- the Ergun equation revisited. *Industrial and Engineering Chemistry Fundamentals*, *18*, 199-208.
15. Niven, R. K. (2002). Physical insight into the Ergun and Wen and Yu equations for fluid flow in packed and fluidised beds. *Chemical Engineering Science*, *57*(3), 527–534.

http://doi.org/10.1016/S0009-2509(01)00371-2

16. Reynolds, O. (1900). *Papers on Mechanical and Physical Subjects*. Cambridge University Press.
17. Yovanovich, M. M. (2003). Asymptotes and asymptotic analysis for development of compact models for microelectronic cooling. *Proceedings of the 19th Annual Semiconductor Thermal Measurement and Management Symposium and Exposition (SEMI-THERM '03), SanJose, Calif, USA*.

Appendix

As the velocity approaches zero as a limit, the pressure gradient can be written as (Ergun, 1952)

$$\lim_{u\to 0} \frac{\Delta p}{L} = au \ . \tag{A 8.1}$$

When the velocity is large enough to yield completely turbulent flow, where kinetic energy losses constitute the whole resistance, the relationship between the pressure gradient and velocity can be expressed as (Ergun, 1952)

$$\lim_{u\to \infty} \frac{\Delta p}{L} = b\rho u^2 \ . \tag{A 8.2}$$

The pressure loss in Eq. (A 8.1) is due to viscous energy losses, while that in Eq. (A 8.2) is due to kinetic energy losses.

Eq. (A 8.1) and (A 8.2) can be written together as

$$\frac{\Delta p}{L} \to \begin{cases} (\frac{\Delta p}{L})_0 = au, \ u \to 0 \\ (\frac{\Delta p}{L})_\infty = b\rho u^2, \ u \to \infty \end{cases} \tag{A 8.3}$$

Here, $(\frac{\Delta p}{L})_0 > (\frac{\Delta p}{L})_\infty$ as $u \to 0$, so the solution, $\frac{\Delta p}{L}$, is concave upwards. The combination of $(\frac{\Delta p}{L})_0$ and $(\frac{\Delta p}{L})_\infty$ using asymptotic analysis yields

$$\frac{\Delta p}{L} = [\left(\frac{\Delta p}{L}\right)_0^w + \left(\frac{\Delta p}{L}\right)_\infty^w]^{1/w} \ , \tag{A 8.4}$$

where the parameter, w, is a fitting parameter. The Hagen-Poiseuille equation for laminar flow through a pipe is

$$(\Delta p)_0 = \frac{32\mu v \Delta L}{D^2}\,. \tag{A 8.5}$$

Replace the fluid velocity, v, by the mean tortuous velocity, u_t, defined as (Bear, 1972; Churchill, 1988)

$$u_t = \tau \frac{u}{\phi}\,, \tag{A 8.6}$$

where u/ϕ is also called as the mean interstitial velocity. The pipe length, ΔL, is replaced by the actual flow length through the porous bed, τL, and the pipe diameter, D, is expressed by the hydraulic radius, the ratio of the volume of voids to their surface area (Leva, 1959; Bird *et al.*, 1960; and Churchill, 1988). Considering a unit bulk volume as the basis, the hydraulic radius can be expressed as

$$r_H = \frac{\phi}{a_b}\,. \tag{A 8.7}$$

Defining a_v as the surface area per unit grain volume, Eq. (A 8.7) can be written as

$$r_H = \frac{\phi}{a_v\,(1-\phi)}\,. \tag{A 8.8}$$

The sphericity is defined as the ratio of the surface area of the equivalent-volume sphere to that of the particle (Leva, 1959). Leva (1959) defined the diameter of a particle of arbitrary shape in terms of sphericity by

$$d_p = \frac{6V_p}{A_p \varphi_p} = \frac{6V_p}{A_{sp}}\,, \tag{A 8.9}$$

where

V_p = volume of a single (non-spherical) particle,

A_{sp} = surface area of the equivalent-volume sphere.

Redefine the diameter of a particle of arbitrary shape by incorporating a fitting parameter λ in Eq. (A 8.9)

$$d_{pm} = \frac{6V_p}{A_p \varphi_p \lambda}. \tag{A 8.10}$$

The value of λ can be determined through experiment where better accuracy is required and can be considered as 1 where simplicity is needed. Rearranging Eq. (A 8.10) yields

$$d_{pm}\varphi_p\lambda = \frac{6}{A_p/V_p} = \frac{6}{a_v}. \tag{A 8.11}$$

The term $d_{pm}\varphi_p\lambda$ is the newly defined diameter of the equivalent-volume sphere. This definition differs slightly from that given by Leva (1959). Representation of this term by d_e gives

$$a_v = \frac{6}{d_e}. \tag{A 8.12}$$

Substitution of $a_v = \frac{6}{d_e}$ into Eq. (A 8.8) gives

$$r_H = \frac{\phi d_e}{6\,(1-\phi)}. \tag{A 8.13}$$

Replacement of v, ΔL, and D by $\tau\frac{u}{\phi}$, τL, and $4r_H$ in Eq. (A 8.5) then yields

$$(\Delta p)_0 = \frac{32\mu\tau^2 uL}{16 r_H^2 \phi}. \tag{A 8.14}$$

Substituting Eq. (A 8.13) into Eq. (A 8.14) yields

$$\left(\frac{\Delta p}{L}\right)_0 = \frac{72\mu\tau^2 u(1-\phi)^2}{\phi^3 d_e^2}\,. \tag{A 8.15}$$

This expression represents the viscous pressure loss during fluid flow through a porous media. The Darcy-Weisbach equation for pressure loss in a circular pipe during turbulent flow is

$$(\Delta p_1)_\infty = \frac{2f_f \rho v^2 \Delta L}{g_c D}\,. \tag{A 8.16}$$

Again, replacing $v, \Delta L,$ and D by $u_t, \tau L$ and $4r_H$, respectively, gives

$$(\Delta p_1)_\infty = \frac{2f_f \rho \tau^3 u^2 L}{4r_H g_c \phi^2}\,. \tag{A 8.17}$$

Substituting Eq. (A 8.13) into Eq. (A 8.17) yields

$$(\Delta p_1)_\infty = \frac{3f_f \rho \tau^3 u^2 L(1-\phi)}{g_c \phi^3 d_e}\,. \tag{A 8.18}$$

This pressure loss is due to turbulence. The head loss through a pipe can be expressed as

$$h_L = K_L \frac{v^2}{2g}\,, \tag{A 8.19}$$

where K_L is the head loss coefficient. Local loss in porous media can be expressed as

$$(\Delta p_2)_\infty = \rho g h_L\,. \tag{A 8.20}$$

Substitution of Eq. (A 8.19) into Eq. (A 8.20) and replacing v with $\tau\frac{u}{\phi}$ gives

$$(\Delta p_2)_\infty = \rho K_L \frac{\tau^2 u^2}{2\phi^2}\,. \tag{A 8.21}$$

The total pressure drop due to local and turbulent losses can be written as

$$(\Delta p)_\infty = (\Delta p_1)_\infty + (\Delta p_2)_\infty \,, \tag{A 8.22}$$

giving

$$(\Delta p)_\infty = \frac{3 f_f \rho \tau^3 u^2 L(1-\phi)}{g_c \phi^3 d_e} + \rho K_L \frac{\tau^2 u^2}{2\phi^2} \,. \tag{A 8.23}$$

Dividing both sides by L gives

$$(\frac{\Delta p}{L})_\infty = \frac{3 f_f \rho \tau^3 u^2 (1-\phi)}{g_c \phi^3 d_e} + \frac{\rho K_L \tau^2 u^2}{2\phi^2 L} \,. \tag{A 8.24}$$

Substitution of Eq. (A 8.15) and (A 8.24) into Eq. (A 8.4) gives

$$\frac{\Delta p}{L} = [(\frac{72\mu\tau^2 u(1-\phi)^2}{\phi^3 d_e^2})^w + (\frac{3 f_f \rho \tau^3 u^2 (1-\phi)}{g_c \phi^3 d_e} + \frac{\rho K_L \tau^2 u^2}{2\phi^2 L})^w]^{1/w} \,. \tag{A 8.25}$$

Eq. (A 8.25) represents the generalized equation for total pressure drop during flow through a porous media. The equation can be written as

$$(\frac{\Delta p}{L})^w = \epsilon^w u^w + (\zeta + \eta)^w u^{2w} \,, \tag{A 8.26}$$

where

$$\epsilon = \frac{72\mu\tau^2(1-\phi)^2}{\phi^3 d_e^2} \,, \tag{A 8.27}$$

$$\zeta = \frac{3 f_f \rho \tau^3 (1-\phi)}{g_c \phi^3 d_e} \,, \tag{A 8.28}$$

$$\eta = \frac{\rho K_L \tau^2 u^2}{2\phi^2 L} . \quad \text{(A 8.29)}$$

Derivation of Ergun equation from Eq. (A 8.26)

Considering the fitting parameter $\lambda = 1$ in Eq. (A 8.10) yields

$$d_{pm} = \frac{6V_p}{A_p \varphi_p} . \quad \text{(A 8.30)}$$

From Eq. (A 8.9) and (A 8.30),

$$d_{pm} = d_p . \quad \text{(A 8.31)}$$

From the definition of the diameter of the equivalent-volume sphere,

$$d_e = d_{pm} \varphi_p \lambda . \quad \text{(A 8.32)}$$

Replacing λ and d_{pm} by 1 and d_p, respectively, in Eq. (A 8.32) gives

$$d_e = d_p \varphi_p . \quad \text{(A 8.33)}$$

Substituting Eq. (A 8.33) and $\tau = 1$ into Eq. (A 8.27) yields

$$\epsilon = \frac{72\mu(1-\phi)^2}{\varphi_p^2 d_p^2 \phi^3} . \quad \text{(A 8.34)}$$

Substituting $\tau = 1$, $g_c = 1$, and Eq. (A 8.33) into Eq. (A 8.28) yields

$$\zeta = \frac{3 f_f \rho(1-\phi)}{\varphi_p d_p \phi^3} . \quad \text{(A 8.35)}$$

Considering $K_L = 0$ in Eq. (A 8.29) gives

$$\eta = 0 \, . \tag{A 8.36}$$

Taking $w = 1$ in Eq. (A 8.26) gives

$$\frac{\Delta p}{L} = \epsilon u + (\zeta + \eta) u^2 \, . \tag{A 8.37}$$

Substitution of Eq. (A 8.34), (A 8.35), and (A 8.36) into Eq. (A 8.37) yields

$$\frac{\Delta p}{L} = \frac{72\mu(1-\phi)^2}{\varphi_p^2 d_p^2 \phi^3} u + \frac{3 f_f \rho (1-\phi)}{\varphi_p d_p \phi^3} u^2 \, . \tag{A 8.38}$$

There is no difference between Eq. (A 8.38) and the Ergun (1952) model, except the numerical coefficients. However, the numerical coefficients in the Ergun (1952) model are not rigid. Different numerical values are found in the literature, such as 150 and 1.75 (Ergun, 1952), 200 and 1.75 (Leva, 1959), and 180 and the range 1.8-4.0 (Macdonald *et al.*, 1979).

Chapter 9

Conclusions and Future Recommendations

9.1 Conclusions

The model of Hossain et al. (2008) is solved numerically using the Caputo, Riemann-Liouville, and Grünwald-Letnikov definitions for the fractional-order derivative. The model is first solved for uniform meshes. Analytical solutions of the model are obtained for the Caputo, Riemann-Liouville, and Grünwald-Letnikov definition of fractional order derivative, and the numerical solutions are validated by comparing with the analytical solution of the model. Error results are analyzed. The error analysis show that the discretization method used in the numerical model is consistent, and $(1-\alpha)$th-order accurate in time. Error values increase with the increase of the fractional order. The numerical solutions found from different definitions of the fractional-order derivative are compared. It is found that the Caputo definition gives the largest value of pressure, and that the Riemann-Liouville definition gives lower values compared to the numerical values found using other definitions. Pressure values from the Grünwald-Letnikov definition lie in between. It is also found that the differences among the solutions increase with the fractional order, α.

The model of Hossain et al. (2008) is also solved numerically using non-uniform meshes. In this case, only the Riemann-Liouville definition for the fractional-order derivative has been used. The L1 algorithm for non-uniform mesh grading is derived. Numerical solutions are obtained for both linear and non-linear cases of the model. Numerical solutions are compared with analytical solutions, and the numerical model is found to be valid. Numerical solutions attained using non-uniform meshes are found to be closer to the analytical solutions than the numerical values found using uniform meshes. A new small-scale reservoir simulator has been developed to capture the memory effect. The simulator is validated comparing the pressure values found as output of the simulator with analytical solutions for different values of fractional order in the linear case and to

manufactured solutions in the non-linear cases. The simulator can be used to investigate the effects of memory on fluid flow through porous media.

A general memory-based mathematical model for flow through porous media is proposed. Memory-based models found in the literature can be derived from this generalized model. The fractional-order differential equation is approximated numerically using uniform meshes in space and non-uniform meshes in time. A small-scale memory-based reservoir simulator, that is called an 'emulator' by Islam et al. (2016), might be developed based on this generalized model.

A new general and more accurate equation for calculating total pressure drop through packed beds and porous media is established. Viscous, local, and turbulent losses are combined applying asymptotic analysis to develop the model. The intermediate flow regime between laminar and turbulent flow is discussed. For each flow regime, the model is reduced. The diameter of the equivalent volume sphere is redefined. Here, a new way is proposed to calculate tortuosity, diameter of the equivalent volume sphere, and the head loss coefficient. The study gives a new expression for a modified Reynolds number.

9.2 Future Recommendations

The simulator developed in this study is of very small scale. This research initiates a first step towards development of a large-scale memory-based reservoir simulator. A lot of research work is still required to develop a complete memory-based reservoir simulator. This simulator would be general and could act as a conventional simulator, as well as incorporating the effects of memory.

Code to solve a generalized memory-based reservoir simulator is not written and validated. A general code for the generalized model can be written and solution for different memory-based equation can be found using such a general code for different cases.

Values of the modified Reynolds number at the onset of the intermediate flow regime and the turbulent flow regime are not determined. Experimental studies are required to determine the

values. Determination of the value of this modified Reynolds number at the onset of the intermediate flow and turbulent flow regimes might be a good topic for future research.